

***In Vitro* Study of the Effects of Topical  
Treatments with Silver Compounds on  
the Inhibition of Demineralisation of  
Hydroxyapatite Discs and Human  
Enamel**

---

2019

**WEI-TE HUANG**

**MSc Oral Biology (QMUL), DDS (Chung Shan Medical University)**

Thesis submitted in fulfilment of the requirements for the degree of Doctor of  
Philosophy in the University of London

Dental Physical Sciences Unit

Institute of Dentistry

Barts and The London School of Medicine and Dentistry

Queen Mary University of London



# Barts and The London

## School of Medicine and Dentistry

### **Statement of Originality**

I, WEI-TE HUANG, confirm that the research included within this thesis is my own work or that where it has been carried out in collaboration with, or supported by others, that this is duly acknowledged below, and my contribution indicated. Previously published material is also acknowledged below.

I attest that I have exercised reasonable care to ensure that the work is original and does not to the best of my knowledge break any UK law, infringe any third party's copyright or other Intellectual Property Right, or contain any confidential material.

I accept that the College has the right to use plagiarism detection software to check the electronic version of the thesis.

I confirm that this thesis has not been previously submitted for the award of a degree by this or any other university.

The copyright of this thesis rests with the author and no quotation from it or information derived from it may be published without the prior written consent of the author.

Signature: WEI-TE HUANG

Date: 30/1/2019

## **Acknowledgements**

This research would not have been possible without the sponsorship from my parents and the caring from the family of my older brother.

I am thankful to my academic supervisors, **Prof. Paul Anderson** and **Dr Saroash Shahid**, for their dedicated and supportive supervision and their patience and invaluable insights to guide me through all the obstacles encountered. Also, I would like to thank Miss **Charlotte Royle**, who provided mental support and constructive advice when required.

A special thanks to **Dr Natalia Karpukhina** for her constant teaching about the MAS-NMR and any priceless technical support provided. I would like to thank **Dr David Gillam** for advising me to validate my experimental methodology, which is crucial for my ISE study.

My PhD journey would not have been so enjoyable without all my fellow students in the Dental Physical Sciences Unit. For all the fun and memorable time we had in the PhD office and at conferences, I thank especially **Tomas Duminis**, **Farah Nabeel Mohammed Tahir Al-Khayyat**, **Huda Al-mandil**, **Alexander Jon Cresswell-Boyes**, **Agron Hoxha**, **Bajram Ferizoli**, **Abdullah Holdar**, **Saja Manna**, **Manpreet Padwal** and **Sherif Elsharkawy**.

I am deeply grateful to my wife, **Chieh En Lai**, for her continued love, encouragement and belief in me. I can never thank her enough for the distress and the depression calmed by her these days. She is the fundamental basis of strength helping me to carry on my PhD.

## Abstract

Despite years of use, the enamel demineralisation inhibitory mechanisms of topical treatments with silver compounds remain obscure. This study aimed to investigate the effects of topical treatments with silver compounds, including  $\text{AgNO}_3$ ,  $\text{AgF}$  and  $\text{Ag}[\text{NH}_3]_2\text{F}$  (silver diammine fluoride; SDF), on demineralisation of hydroxyapatite (HAP) discs and human enamel. Further, the dose-response effects of these silver compounds on demineralisation of human enamel were also investigated.

The dose-response effect of  $\text{Ag}^+$  in solution on demineralisation was investigated using scanning microradiography (SMR). The effects of topical treatments with  $\text{AgNO}_3$ ,  $\text{AgF}$  and  $\text{Ag}[\text{NH}_3]_2\text{F}$  on demineralisation of HAP discs and human enamel were investigated using real-time  $\text{Ca}^{2+}$ ,  $\text{Ag}^+$  and  $\text{F}^-$  ion selective electrodes (ISEs), scanning electron microscopy (SEM), energy dispersive X-ray analysis (EDX), and  $^{31}\text{P}$  and  $^{19}\text{F}$  magic angle spinning-nuclear magnetic resonance (MAS-NMR).

The results from this study suggest that the inhibitory mechanism of topical treatment with  $\text{AgNO}_3$  is associated with the formation of a  $\text{Ag}_3\text{PO}_4$  protective barrier. Whereas, the inhibitory mechanism of topical treatment with  $\text{AgF}$  or  $\text{Ag}[\text{NH}_3]_2\text{F}$  is associated with the  $\text{F}^-$  released from topically treated sample surfaces and the formation of a protective barrier composed of  $\text{Ag}_3\text{PO}_4$ ,  $\text{CaF}_2$  and FHA. Further, the inhibitory efficacy of topical treatment with  $\text{AgNO}_3$  decreased with increasing concentration, whereas, the inhibitory efficacy of topical treatment with  $\text{AgF}$  or  $\text{Ag}[\text{NH}_3]_2\text{F}$  increased with increasing concentration.

## Contents

Statement of Originality.....	I
Acknowledgements.....	II
Abstract.....	III
List of Figures .....	XI
List of Tables .....	XIX
Abbreviations.....	XX
<b>PART I: LITERATURE REVIEW, AIMS AND OBJECTIVES .....</b>	<b>1</b>
<b>Chapter 1 INTRODUCTION OF DENTAL MINERAL .....</b>	<b>2</b>
1.1 Human Tooth Structure .....	2
1.2 Human Enamel.....	3
1.2.1 Composition of Human Enamel .....	3
1.2.2 Mineral Structure of Human Enamel .....	4
1.3 Hydroxyapatite Discs as a Model System for Human enamel .....	6
<b>Chapter 2 DENTAL CARIES AND EROSION .....</b>	<b>7</b>
2.1 Enamel Demineralisation.....	7
2.2 Dental Caries .....	7
2.2.1 Aetiology of Dental Caries.....	8
2.2.2 Chemistry of Dental Caries.....	10
2.2.2.1 Translucent zone .....	12
2.2.2.2 Dark zone .....	12
2.2.2.3 Body of lesion.....	12
2.2.2.4 Surface zone.....	13
2.2.3 Epidemiology of Dental Caries .....	13
2.3 Dental Erosion.....	14
2.3.1 Aetiology of Dental Erosion .....	14
2.3.2 Chemistry of Dental Erosion .....	15
2.3.3 Epidemiology of Dental Erosion.....	18
2.4 Role of Fluoride in Enamel Demineralisation .....	19
<b>Chapter 3 TOPICAL TREATMENTS WITH SILVER COMPOUNDS FOR PROTECTION AGAINST ENAMEL DEMINERALISATION .....</b>	<b>22</b>
3.1 Use of Silver Compounds in Dentistry .....	22
3.2 Topical Treatments with Silver Nitrate for Protection against Enamel Demineralisation .....	23

3.3 Topical Treatments with Silver Fluoride for Protection Against Enamel Demineralisation .....	25
3.4 Topical Treatments with SDF for Protection Against Enamel Demineralisation .....	26
3.4.1. Clinical Effects of Topical Treatments with SDF on Enamel Caries .....	27
3.4.2 Establishment of Standard Protocol for Topical Treatment with SDF .....	28
3.4.3 Cariostatic Mechanisms of SDF .....	29
<b>Chapter 4 AIMS AND OBJECTIVES</b> .....	32
4.1 Aims .....	32
4.2 Objectives .....	32
<b>PART II: INTRODUCTION OF TECHNIQUES USED IN THIS STUDY</b> .....	34
<b>Chapter 5 TECHNIQUES USED IN THIS STUDY</b> .....	35
5.1 Scanning Microradiography .....	35
5.2 Ion Selective Electrode .....	37
5.2.1 Ion Activity and Ion Concentration: Two Different Measures .....	40
5.2.2 Advantages of ISEs .....	40
5.2.3 Limitations of ISEs .....	41
5.2.4 The Effect of Temperature .....	41
5.3 Effect of Data Sampling Frequency on Calculated Error in Gradient .....	42
5.4 Scanning Electron Microscopy .....	46
5.5 Energy-Dispersive X-ray Analysis .....	47
5.6 Magic Angle Spinning – Nuclear Magnetic Resonance .....	48
5.7 Knoop Micro-hardness Test .....	50
5.7.1 Microscopic Photographs .....	50
5.7.2 Knoop Micro-hardness Indentation .....	51
<b>PART III: DEVELOPMENT OF AN ISE METHODOLOGY TO INVESTIGATE THE EFFECTS OF TOPICAL TREATMENTS WITH SILVER COMPOUNDS ON DEMINERALISATION</b> .....	53
<b>Chapter 6 VALIDATION OF A REAL-TIME ISE METHODOLOGY TO QUANTIFY THE INFLUENCE OF INHIBITORS OF DEMINERALISATION KINETICS IN VITRO USING A HYDROXYAPATITE MODEL SYSTEM</b> .....	54
6.1 Introduction .....	54
6.2 Aim .....	56
6.3 Materials and Methods .....	57
6.3.1 Preparation of Samples .....	57
6.3.2 Preparation of Demineralisation Solution .....	57
6.3.3 ISE Calibration .....	58

6.3.4 Demineralisation Study.....	58
6.4 Results.....	61
6.5 Discussion.....	70
6.6 Conclusion.....	72
<b>PART IV: EXPERIMENTAL STUDIES.....</b>	<b>73</b>
<b>Chapter 7 A SMR STUDY OF THE DOSE-RESPONSE EFFECTS OF SILVER IONS IN SOLUTION ON DEMINERALISATION OF HUMAN ENAMEL.....</b>	<b>74</b>
7.1 Introduction.....	74
7.2 Aim.....	76
7.3 Materials and Methods.....	77
7.3.1 Preparation of Enamel Block.....	77
7.3.2 Preparation of the Demineralisation Solution.....	78
7.3.3 SMR Area Scan of the Sample.....	78
7.3.4 Demineralisation Study.....	79
7.4 Results.....	81
7.5 Discussion.....	85
7.6 Conclusion.....	89
<b>Chapter 8 EFFECTS OF TOPICAL TREATMENTS WITH SILVER COMPOUNDS ON DEMINERALISATION OF HAP DISCS.....</b>	<b>90</b>
8.1 Introduction.....	90
8.2 Aims.....	92
8.3 Materials and Methods.....	93
8.3.1 ISE Study.....	93
8.3.2 Digital Photographs.....	96
8.3.3 SEM and EDX Analyses.....	97
8.3.4 <sup>31</sup> P and <sup>19</sup> F MAS-NMR Analyses.....	97
8.4 Results.....	98
8.4.1 Ca <sup>2+</sup> ISE Study.....	98
8.4.1.1. Summary of the Ca <sup>2+</sup> Release from the HAP Discs of Each Treatment Group.	103
8.4.2 Ag <sup>+</sup> ISE study.....	105
8.4.2.1 Mean [Ag <sup>+</sup> ] during the post-treatment 4 h periods of Each Treatment Group	107
8.4.3 F <sup>-</sup> ISE study.....	108
8.4.3.1 Mean [F <sup>-</sup> ] during the post-treatment 4 h periods of Each Treatment Group...	110
8.4.4 Digital Photographs.....	111

8.4.5 SEM Images Analysis .....	112
8.4.6 EDX Analysis .....	114
8.4.7 <sup>31</sup> P MAS-NMR Analysis .....	116
8.4.8 <sup>19</sup> F MAS-NMR Analysis .....	117
<b>Chapter 9 DISCUSSION OF THE EFFECTS OF TOPICAL TREATMENTS WITH SILVER COMPOUNDS ON DEMINERALISATION OF HAP DISCS AND PROPOSED MODELS FOR MECHANISMS .....</b>	<b>121</b>
9.1 Effects of Topical Treatment with De-ionised Water on Demineralisation of HAP Discs	122
9.2 Effects of Topical Treatment with AgNO <sub>3</sub> on Demineralisation of HAP Discs and Proposed Mechanistic Models .....	123
9.2.1 Following Topical Treatment with AgNO <sub>3</sub> .....	123
9.2.2 After Re-immersion of HAP Discs Topically Treated with AgNO <sub>3</sub> into Acid .....	123
9.2.3 After Removal of HAP Discs Topically Treated with AgNO <sub>3</sub> from Acid .....	125
9.2.4 Analysis of the Inhibitory Efficacy of the Topical Treatment with AgNO <sub>3</sub> on Demineralisation of HAP Discs .....	127
9.2.5 Conclusions .....	128
9.3 Effects of Topical Treatments with AgF and Ag[NH <sub>3</sub> ] <sub>2</sub> F on Demineralisation of HAP Discs and Proposed Mechanistic Models.....	129
9.3.1 Following Topical Treatments with AgF and Ag[NH <sub>3</sub> ] <sub>2</sub> F .....	129
9.3.2 After Re-immersion of HAP Discs Topically Treated with AgF, and Ag[NH <sub>3</sub> ] <sub>2</sub> F into Acid .....	130
9.3.3 After Removal of HAP Discs Topically Treated with AgF, and Ag[NH <sub>3</sub> ] <sub>2</sub> F from Acid	134
9.3.4 Analysis of the Inhibitory Efficacy of the Topical Treatments with AgF and Ag[NH <sub>3</sub> ] <sub>2</sub> F on Demineralisation of HAP Discs.....	136
9.3.5 Conclusions .....	137
9.4 Difference Between the Effects of Topical Treatments with Riva-SC and 3.16 M Ag[NH <sub>3</sub> ] <sub>2</sub> F on Demineralisation of HAP Discs.....	138
9.5 Conclusions .....	139
<b>Chapter 10 DOSE-RESPONSE EFFECTS OF TOPICAL TREATMENTS WITH DIFFERENT CONCENTRATIONS OF SILVER COMPOUNDS ON DEMINERALISATION OF HUMAN ENAMEL</b>	<b>140</b>
10.1 Introduction .....	140
10.2 Aims.....	141
10.3 Materials and Methods.....	142
10.3.1 ISE Study.....	143
10.3.2 Digital Photographs.....	145
10.3.3 SEM and EDX Analyses.....	145
10.3.4 <sup>31</sup> P and <sup>19</sup> F MAS-NMR Analyses.....	145



10.3.5 Knoop Micro-Hardness Analysis .....	146
10.4 Results.....	148
10.4.1 Ca <sup>2+</sup> ISE Study .....	148
10.4.1.1 Summary of the Ca <sup>2+</sup> Release from the Enamel Blocks of Each Treatment Group .....	156
10.4.2 Ag <sup>+</sup> ISE Study .....	163
10.4.2.1 Mean [Ag <sup>+</sup> ] during the post-treatment 4 h periods of Each Treatment Group .....	170
10.4.3 F <sup>-</sup> ISE Study .....	173
10.4.3.1 Mean [F <sup>-</sup> ] during the post-treatment 4 h periods of Each Treatment Group ..	178
10.4.4 Digital Photographs.....	181
10.4.5 SEM Images Analysis.....	183
10.4.6 EDX Analysis .....	185
10.4.7 <sup>31</sup> P MAS-NMR Analysis .....	190
10.4.8 <sup>19</sup> F MAS-NMR Analysis .....	191
10.4.9 Microscopic photographs of Human Enamel Sections .....	192
10.4.10 Knoop CSMH profiles of Human Enamel Sections .....	194
<b>Chapter 11 DISCUSSION OF THE EFFECTS OF TOPICAL TREATMENTS WITH SILVER COMPOUNDS ON DEMINERALISATION OF HUMAN ENAMEL AND PROPOSED MODELS FOR MECHANISMS .....</b>	<b>195</b>
11.1 Effects of Topical Treatment with De-ionised Water on Demineralisation of Human Enamel .....	196
11.2 Effects of Topical Treatment with AgNO <sub>3</sub> on Demineralisation of Human Enamel and Proposed Mechanistic Models.....	197
11.2.1 Following Topical Treatment with AgNO <sub>3</sub> .....	197
11.2.2 After Re-immersion of Human Enamel Topically Treated with AgNO <sub>3</sub> into Acid ..	197
11.2.3 After Removal of Human Enamel Topically Treated with AgNO <sub>3</sub> from Acid .....	199
11.2.4 Analysis of the Inhibitory Efficacy of the Topical Treatment with AgNO <sub>3</sub> on Demineralisation of Human Enamel .....	201
11.2.5 Conclusions .....	202
11.3 Effects of Topical Treatments with AgF and Ag[NH <sub>3</sub> ] <sub>2</sub> F on Demineralisation of Human Enamel and Proposed Mechanistic Models.....	202
11.3.1 Following Topical Treatments with AgF and Ag[NH <sub>3</sub> ] <sub>2</sub> F.....	203
11.3.2 After Re-immersion of Human Enamel Topically Treated with AgF and Ag[NH <sub>3</sub> ] <sub>2</sub> F into Acid .....	204

11.3.3 After Removal of Human Enamel Topically Treated with AgF and Ag[NH <sub>3</sub> ] <sub>2</sub> F from Acid .....	208
11.3.4 Analysis of the Inhibitory Efficacy of the Topical Treatments with AgF, Ag[NH <sub>3</sub> ] <sub>2</sub> F and Riva-SC on Demineralisation of Human Enamel .....	210
11.3.5 Conclusions .....	212
11.4 Difference Between the Effects of Topical Treatments with Riva-SC and 3.16 M Ag[NH <sub>3</sub> ] <sub>2</sub> F on Demineralisation of Human enamel.....	213
11.5 Conclusions .....	214
<b>Chapter 12 DISCUSSION OF DOSE-RESPONSE EFFECTS OF TOPICAL TREATMENTS WITH SILVER COMPOUNDS ON DEMINERALISATION OF HUMAN ENAMEL AND PROPOSED MODELS FOR MECHANISMS .....</b>	<b>215</b>
12.1 Dose-response Effects of Topical Treatment with AgNO <sub>3</sub> on Demineralisation of Human Enamel and Proposed Mechanistic Models.....	216
12.1.1 The Dose-response Effects of Ag <sup>+</sup> on the Dose-response Inhibitory Efficacy of the Topical Treatment with AgNO <sub>3</sub> on Enamel Demineralisation.....	218
12.2 Dose-response Effects of Topical Treatments with AgF and Ag[NH <sub>3</sub> ] <sub>2</sub> F on Demineralisation of Human Enamel and Proposed Mechanistic Models .....	221
12.2.1 The Dose-response Effects of Ag <sup>+</sup> on the Dose-response Inhibitory Efficacy of the Topical Treatment with AgF and Ag[NH <sub>3</sub> ] <sub>2</sub> F on Enamel Demineralisation .....	223
12.2.2 The Dose-response Effects of F <sup>-</sup> on the Dose-response Inhibitory Efficacy of the Topical Treatments with AgF and Ag[NH <sub>3</sub> ] <sub>2</sub> F on Enamel Demineralisation.....	225
12.3 Conclusions .....	229
<b>PART V: DISCUSSION, CONCLUSIONS, FUTURE WORK AND CLINICAL RELEVANCE .....</b>	<b>230</b>
<b>Chapter 13 DISCUSSION .....</b>	<b>231</b>
13.1 Comparison of Effects of Topical Treatments with Silver Compounds on Demineralisation of HAP Discs and Human Enamel .....	231
13.1.1 Before Topical Treatments with Silver Compounds .....	231
13.1.2 Following Topical Treatments with Silver Compounds.....	232
13.1.3 After Re-immersion of Topically Treated HAP Discs and Human Enamel into Acids .....	232
13.1.4 After Removal of HAP Discs and Human Enamel Topically Treated with Silver Compounds from Acids.....	234
13.2 Clinical Implications of the Dose-response Effects of Topical Treatments with Silver Compounds on Demineralisation of Human Enamel.....	237
13.2.1 Topical Treatments with Different Concentrations of AgNO <sub>3</sub> on Demineralisation of Human Enamel.....	237
13.2.2 Topical Treatments with Different Concentrations of AgF or Ag[NH <sub>3</sub> ] <sub>2</sub> F on Demineralisation of Human Enamel .....	238

<b>Chapter 14 CONCLUSIONS, FUTURE WORK AND CLINICAL RELEVANCE .....</b>	<b>240</b>
14.1 Conclusions .....	240
14.2 Future Work .....	242
14.3 Clinical Relevance.....	244
<b>PART VI: REFERENCES.....</b>	<b>245</b>
<b>PART VII: APPENDIXES .....</b>	<b>259</b>
Appendix A: Tables of SDF studies.....	260
Appendix B: QMUL Skills Points Record.....	267
Appendix C: Awards .....	268
Appendix D: Conference presentations.....	270
Appendix E: Published paper and papers in preparation .....	278

## List of Figures

<b>Figure 1.1</b> - Structure of tooth (From Douglass, 2003).....	2
<b>Figure 1.2</b> - Hexagonal unit structure of HAP in human enamel (Adapted from Robinson et al., 2000). .....	5
<b>Figure 1.3</b> - Microstructure of enamel showing hierarchical levels (From Yilmaz et al., 2015). .....	6
<b>Figure 2.1</b> – Aetiology of dental caries (Adapted from Selwitz et al., 2007). .....	8
<b>Figure 2.2</b> - Caries balance (Adapted from Garcia-Godoy and Hicks, 2008). .....	9
<b>Figure 2.3</b> - Solubility isotherm of HAP. O: normal intra-oral condition (From Anderson et al., 2001). .....	10
<b>Figure 2.4</b> - Schematic diagrams of enamel caries (Adapted from Robinson et al., 2000). .....	11
<b>Figure 2.5</b> - Causal factors of erosion (Adapted from Magalhaes et al., 2009b).....	15
<b>Figure 2.6</b> - Degree of saturation plotted against pH with respect to HAP and FAP at certain salivary concentration. FAP can still be formed under carious condition while neither HAP or FAP can be formed under erosive pH (Adapted from Meurman and ten Cate, 1996). .....	15
<b>Figure 2.7</b> - (a) Schematic of erosive lesion: O = outer surface; S = sound enamel. (b) Schematic of carious lesion: SL = surface layer; L: lesion; P: prisms (Adapted from Arends and ten Cate, 1981). .....	16
<b>Figure 2.8</b> – Honeycomb erosion lesion (From Wang et al., 2006).....	17
<b>Figure 2.9</b> – Schematic representation of F <sup>-</sup> absorb onto enamel surface, which attract Ca <sup>2+</sup> and PO <sub>4</sub> <sup>3-</sup> , to form an insoluble FAP (or FHA) veneer (From Featherstone, 2008). .....	21
<b>Figure 3.1</b> – Reaction between AgNO <sub>3</sub> and HAP. The PO <sub>4</sub> <sup>3-</sup> released from demineralising enamel can be preserved by the formation of Ag <sub>3</sub> PO <sub>4</sub> (Adapted from Yamaga et al., 1972). .....	24
<b>Figure 3.2</b> – Black staining of Ag[NH <sub>3</sub> ] <sub>2</sub> F treated teeth (From Mei et al., 2016).....	27
<b>Figure 3.3</b> – Reaction between Ag[NH <sub>3</sub> ] <sub>2</sub> F and HAP. The Ca <sup>2+</sup> and PO <sub>4</sub> <sup>3-</sup> released from demineralising enamel can be preserved by the formation of CaF <sub>2</sub> and Ag <sub>3</sub> PO <sub>4</sub> , respectively (Adapted from Yamaga et al., 1972). .....	30
<b>Figure 5.1</b> – Schematic representation of a SMR cell containing a specimen. ....	36
<b>Figure 5.2</b> – Schematic representation of the SMR apparatus. ....	37
<b>Figure 5.3</b> - An ISE calibration curve (From Wroblewski, 2005).....	38
<b>Figure 5.4</b> - Schematic representation of an ISE system (From Harvey, 2016).....	39
<b>Figure 5.5</b> - Temperature effects on the slope of the calibration curve of a single charged ion (Adapted from all-about-pH.com, 2017). .....	42
<b>Figure 5.6</b> - Change in the projected HAP disc mineral mass content in pH 4.0 acetic acid over 24 h with (a) 100 %, (b) 50 %) and (c) 10 % sampling frequency of data. Blue dots: one StdErr away from trendline; Green dots: two StdErr away from trendline; Yellow dots: three StdErr away from trendline (From Lingawi, 2012).....	44
<b>Figure 5.7</b> – Change in the calcium loss from an HAP disc in pH 4.0 acetic acid (a) before (Blue dots) and (b) after (Red dots) topical treatment. The difference between the gradient of the two calcium loss trendlines (0.32 X 10 <sup>-3</sup> ) is detected (Green dots). .....	45

<b>Figure 5.8</b> - Schematic representation of SEM (From Schweitzer, 2014).....	47
<b>Figure 5.9</b> - Schematic representation of EDX (From ACMAL, 2014).....	48
<b>Figure 5.10</b> - Schematic representation of NMR apparatus (From Robert, 1959).....	48
<b>Figure 5.11</b> – Deconvolution of a <sup>19</sup> F MAS-NMR spectra of HAP, and of human enamel powders treated with amine fluoride (From Gerth et al., 2007). .....	50
<b>Figure 5.12</b> – Taking the microscopic photographs through the microscope of the Knoop micro-hardness tester using a camera.....	51
<b>Figure 5.13</b> – Typical microscopic photographs of a tooth with Knoop indentations on a dentine specimen (From Chu and Lo, 2008a).....	51
<b>Figure 5.14</b> – Diagrams of the Knoop indenter (From England, 2013).....	52
<b>Figure 6.1</b> – Half-varnished porous HAP discs.....	57
<b>Figure 6.2</b> – Two setups of the study ISE at room temperature. ....	59
<b>Figure 6.3</b> - Calibration curve of Ca <sup>2+</sup> ISE. LLOD = lower limit of detection. ....	61
<b>Figure 6.4</b> - Typical data collected from one HAP disc with additions of (a) 1.8 ppm Zn <sup>2+</sup> and (b) 107 ppm Zn <sup>2+</sup> groups. ....	63
<b>Figure 6.5</b> - Typical data collected from one HAP disc with additions of (a) 2.3 ppm F and (b) 45.2 ppm F groups. ....	65
<b>Figure 6.6</b> - (a) Log-linear relationship established between mean PRCL <sub>HAP</sub> and [Zn <sup>2+</sup> ]. (b) Log-linear relationship established between mean PRCL <sub>HAP</sub> and [F]. Error bars show the standard errors. ....	68
<b>Figure 6.7</b> – (a) Log-linear relationship established between mean PRML <sub>enamel</sub> and [Zn <sup>2+</sup> ] (Replotted from Mohammed et al., 2015). (b) Log-linear relationship established between mean PRML <sub>enamel</sub> and [F] (Replotted from Mohammed et al., 2014a). Error bars show the standard errors. ....	69
<b>Figure 7.1</b> – The SMR environmental cell containing an enamel block.....	77
<b>Figure 7.2</b> – Area scanning of an enamel block. The coloured scale (on right) represents the projected mineral mass (g*cm <sup>-2</sup> ) in the sample. The white crosses show the three scan points. ....	78
<b>Figure 7.3</b> – Trendlines of the mineral loss per unit area (g*cm <sup>-2</sup> ) measured at the scan point 3 for 0.0 ppm Ag <sup>+</sup> compared to that measured at the same scan point for (a) 0.1 ppm Ag <sup>+</sup> , (b) 9.0 ppm Ag <sup>+</sup> , and (c) 3565.0 ppm Ag <sup>+</sup> .....	81
<b>Figure 7.4</b> – The mean PRML <sub>enamel</sub> plotted against increasing [Ag <sup>+</sup> ] in the demineralisation solution. Error bars show the standard errors. ....	84
<b>Figure 7.5</b> – Comparison between the log-linear dose-response effects of Ag <sup>+</sup> (Blue line) and Zn <sup>2+</sup> (Red line) (From Mohammed et al., 2015) on enamel demineralisation. Error bars show the standard errors. ....	87
<b>Figure 7.6</b> – Schematic representation of the log-linear dependency of the acceleration of enamel demineralisation on [Ag <sup>+</sup> ] showing a decreasing number of Ca <sup>2+</sup> sites can be substituted by Ag <sup>+</sup> with increasing [Ag <sup>+</sup> ]. ....	88
<b>Figure 8.1</b> – Nail-varnished porous HAP discs.....	93
<b>Figure 8.2</b> – a. Schematic representation of setup of the ISE study at 37±0.3 °C; b. Photo of the ISE setup in the study (F ISE was behind Ca <sup>2+</sup> ISE). ....	95
<b>Figure 8.3</b> – Protocol of the ISE study on HAP discs. ....	96
<b>Figure 8.4</b> - Typical Ca <sup>2+</sup> release of DW treatment group.....	98
<b>Figure 8.5</b> - Typical Ca <sup>2+</sup> release of AgNO <sub>3</sub> treatment group.....	99
<b>Figure 8.6</b> – Typical Ca <sup>2+</sup> release of AgF treatment group.....	100

<b>Figure 8.7</b> - Typical $\text{Ca}^{2+}$ release of $\text{Ag}[\text{NH}_3]_2\text{F}$ treatment group. ....	101
<b>Figure 8.8</b> – Typical $\text{Ca}^{2+}$ release of Riva-SC treatment group.....	102
<b>Figure 8.9</b> – The mean $\text{PRCL}_{\text{HAP}}$ of each treatment group. Error bars show the standard errors. Linking line between bars indicate significant differences at $p < 0.05$ between treatment groups. ....	104
<b>Figure 8.10</b> – The mean $\text{Ag}^+$ release from HAP discs under pH 4.0 demineralisation before and after treatments with DW, $\text{AgNO}_3$ , AgF, $\text{Ag}[\text{NH}_3]_2\text{F}$ and Riva-SC. ....	105
<b>Figure 8.11</b> – (a) Mean $R_i$ and (b) mean $R_L$ of the $\text{Ag}^+$ release of each treatment group. ....	106
<b>Figure 8.12</b> – The $[\text{Ag}^+]_{4\text{h}}$ (ppm) of each treatment group. Error bars show the standard errors.....	107
<b>Figure 8.13</b> - The mean $F$ release from HAP discs under pH 4.0 demineralisation before and after treatments with DW, $\text{AgNO}_3$ , AgF, $\text{Ag}[\text{NH}_3]_2\text{F}$ and Riva-SC. ....	108
<b>Figure 8.14</b> – (a) Mean $R_i$ and (b) mean $R_L$ of the $F$ release of each treatment group. ....	109
<b>Figure 8.15</b> - The $[\text{F}]_{4\text{h}}$ (ppm) of each treatment group. Error bars show the standard errors. Linking lines between bars indicate significant differences at $p < 0.05$ between treatment groups. ....	110
<b>Figure 8.16</b> – Digital photographs of HAP discs following different treatments in the ISE study. ....	111
<b>Figure 8.17</b> - Typical SEM images (5.00 kV, 5000 X) of HAP discs in treatment groups of (a) DW, (b) $\text{AgNO}_3$ , (c) AgF, (d) $\text{Ag}[\text{NH}_3]_2\text{F}$ and (e) Riva-SC, after the ISE study.....	113
<b>Figure 8.18</b> – The mean atomic percentage of Ag of each treatment group. Error bars show the standard errors. Linking lines between bars indicate significant differences at $p < 0.05$ between treatment groups. ....	114
<b>Figure 8.19</b> – The mean atomic percentage of F of each treatment group. Error bars show the standard errors. ....	115
<b>Figure 8.20</b> - $^{31}\text{P}$ MAS–NMR spectra of each treatment group before and after pH 4.0 acid challenge.....	116
<b>Figure 8.21</b> – $^{19}\text{F}$ MAS–NMR spectra of each treatment group before and after pH 4.0 acid challenge. (* = sidebands).....	117
<b>Figure 8.22</b> - Deconvoluted $^{19}\text{F}$ spectra of (a) HAP + AgF and (b) pH 4.0 HAP + AgF. ....	118
<b>Figure 8.23</b> – Deconvoluted $^{19}\text{F}$ spectra of (a) HAP + $\text{Ag}[\text{NH}_3]_2\text{F}$ and (b) pH 4.0 HAP + $\text{Ag}[\text{NH}_3]_2\text{F}$ . ....	119
<b>Figure 8.24</b> – Deconvoluted $^{19}\text{F}$ spectra of (a) HAP + Riva-SC and (b) pH 4.0 HAP + Riva-SC. ....	120
<b>Figure 9.1</b> – Schematic representation of an HAP disc topically treated with $\text{AgNO}_3$ . $\text{Ag}_3\text{PO}_4$ is formed on the HAP disc surface and some $\text{Ca}^{2+}$ in the HAP disc is substituted by $\text{Ag}^+$ . ....	123
<b>Figure 9.2</b> - Schematic representation of an HAP disc topically treated with $\text{AgNO}_3$ following re-immersion back into acid. a) $\text{Ag}^+$ loosely attached to HAP disc surfaces is released into solution. b) Gradually, some $\text{Ag}_3\text{PO}_4$ on the HAP disc surface and some $\text{Ag}^+$ in the solution are reduced to black metallic silver. ....	125

<b>Figure 9.3</b> – Schematic representation of an HAP topically treated with AgNO <sub>3</sub> after 4 h demineralisation. Deeper lesions are developed in the Ag <sup>+</sup> substituted HAP, therefore an uneven demineralised HAP disc surface is observed. Further, all the Ag <sub>3</sub> PO <sub>4</sub> is reduced to metallic silver causing black staining. ....	127
<b>Figure 9.4</b> – The effects of topical treatment influencing the inhibitory efficacy. ....	127
<b>Figure 9.5</b> – Schematic representation of an HAP disc topically treated with AgF or Ag[NH <sub>3</sub> ] <sub>2</sub> F. Ag <sub>3</sub> PO <sub>4</sub> , CaF <sub>2</sub> and FHA are formed on the HAP disc surface. ....	129
<b>Figure 9.6</b> - Schematic representation of an HAP disc topically treated with AgF or Ag[NH <sub>3</sub> ] <sub>2</sub> F following re-immersion back into acid. a) Both Ag <sup>+</sup> and F <sup>-</sup> loosely attached to HAP disc surfaces are released into solution. b) Gradually, some Ag <sub>3</sub> PO <sub>4</sub> on the HAP disc surface and some Ag <sup>+</sup> in the solution are reduced to metallic silver, and some CaF <sub>2</sub> on the HAP disc surface is dissolved, providing F <sup>-</sup> for further formation of FHA. ....	133
<b>Figure 9.7</b> - Schematic representation of an HAP topically treated with AgF or Ag[NH <sub>3</sub> ] <sub>2</sub> F after 4 h demineralisation. All the Ag <sub>3</sub> PO <sub>4</sub> is reduced to metallic silver causing black staining and most of the CaF <sub>2</sub> is dissolved which favours further formation of FHA. ....	136
<b>Figure 10.1</b> – Flowchart of the protocol of the study. ....	142
<b>Figure 10.2</b> – Nail-varnished human blocks. ....	143
<b>Figure 10.3</b> – (a) Demineralised lesion of enamel block varnished with blue nail lacquer. (b) Resin-embedded block for micro-hardness test. ....	146
<b>Figure 10.4</b> – Schematic representation of Knoop CSMH. ....	147
<b>Figure 10.5</b> - Typical Ca <sup>2+</sup> release of DW treatment group. ....	148
<b>Figure 10.6</b> - Typical Ca <sup>2+</sup> release of 0.75 M AgNO <sub>3</sub> treatment group. ....	150
<b>Figure 10.7</b> - Typical Ca <sup>2+</sup> release of 2.36 M AgNO <sub>3</sub> treatment group. ....	150
<b>Figure 10.8</b> - Typical Ca <sup>2+</sup> release of 3.16 M AgNO <sub>3</sub> treatment group. ....	150
<b>Figure 10.9</b> - Typical Ca <sup>2+</sup> release of 0.75 M AgF treatment group. ....	152
<b>Figure 10.10</b> - Typical Ca <sup>2+</sup> release of 2.36 M AgF treatment group. ....	152
<b>Figure 10.11</b> - Typical Ca <sup>2+</sup> release of 3.16 M AgF treatment group. ....	152
<b>Figure 10.12</b> - Typical Ca <sup>2+</sup> release of 0.75 M Ag[NH <sub>3</sub> ] <sub>2</sub> F treatment group. ....	154
<b>Figure 10.13</b> - Typical Ca <sup>2+</sup> release of 2.36 M Ag[NH <sub>3</sub> ] <sub>2</sub> F treatment group. ....	154
<b>Figure 10.14</b> - Typical Ca <sup>2+</sup> release of 3.16 M Ag[NH <sub>3</sub> ] <sub>2</sub> F treatment group. ....	154
<b>Figure 10.15</b> – Typical Ca <sup>2+</sup> release of Riva-SC treatment group. ....	155
<b>Figure 10.16</b> - The mean PRCL <sub>enamel</sub> of 3.16 M AgNO <sub>3</sub> , 3.16 M AgF, 3.16 M Ag[NH <sub>3</sub> ] <sub>2</sub> F, Riva-SC and DW treatment groups. Error bars show the standard errors. Linking lines between treatment groups indicate significant differences at p < 0.05 between them. ....	159
<b>Figure 10.17</b> – The mean PRCL <sub>enamel</sub> of 0.75 M, 2.36 M and 3.16 M AgNO <sub>3</sub> treatment groups. ....	160
<b>Figure 10.18</b> - A log-linear dose-response relationship between the mean PRCL <sub>enamel</sub> of AgNO <sub>3</sub> and [AgNO <sub>3</sub> ]. ....	160
<b>Figure 10.19</b> - The mean PRCL <sub>enamel</sub> of 0.75 M, 2.36 M and 3.16 M AgF treatment groups. ....	161
<b>Figure 10.20</b> - A log-linear dose-response relationship between the mean PRCL <sub>enamel</sub> of AgF and [AgF]. ....	161
<b>Figure 10.21</b> - The mean PRCL <sub>enamel</sub> of 0.75 M, 2.36 M and 3.16 M Ag[NH <sub>3</sub> ] <sub>2</sub> F treatment groups. ....	162

<b>Figure 10.22</b> - A log-linear dose-response relationship between the mean $PRCL_{enamel}$ of $Ag[NH_3]_2F$ and $[Ag[NH_3]_2F]$ .....	163
<b>Figure 10.23</b> - The mean $Ag^+$ release from enamel under pH 4.0 demineralisation before and after topical treatments with DW, and 3.16 M silver compounds. ....	164
<b>Figure 10.24</b> - The $Ag^+$ release profiles of 0.75 M, 2.36 M and 3.16 M $AgNO_3$ treatment groups. ....	166
<b>Figure 10.25</b> - The $Ag^+$ release profiles of 0.75 M, 2.36 M and 3.16 M $AgF$ treatment groups. ....	166
<b>Figure 10.26</b> - The $Ag^+$ release profiles of 0.75 M, 2.36 M and 3.16 M $Ag[NH_3]_2F$ treatment groups. ....	166
<b>Figure 10.27</b> - (a) Mean $R_i$ and (b) mean $R_L$ of the $Ag^+$ release of DW and 3.16 M treatment groups. ....	168
<b>Figure 10.28</b> - (a) Mean $R_i$ and (b) mean $R_L$ of the $Ag^+$ release of $AgNO_3$ treatment groups. ....	169
<b>Figure 10.29</b> - (a) Mean $R_i$ and (b) mean $R_L$ of the $Ag^+$ release of $AgF$ treatment groups. ....	169
<b>Figure 10.30</b> - (a) Mean $R_i$ and (b) mean $R_L$ of the $Ag^+$ release of $Ag[NH_3]_2F$ treatment groups. ....	169
<b>Figure 10.31</b> – The $[Ag^+]_{4h}$ (ppm) of 3.16 M $AgNO_3$ , 3.16 M $AgF$ , 3.16 M $Ag[NH_3]_2F$ , Riva-SC and DW treatment groups. Error bars show the standard errors. Linking lines between bars indicate significant differences at $p < 0.05$ between treatment groups. ....	171
<b>Figure 10.32</b> - The $[Ag^+]_{4h}$ (ppm) of 0.75 M, 2.36 M and 3.16 M $AgNO_3$ treatment groups. ....	172
<b>Figure 10.33</b> - The $[Ag^+]_{4h}$ (ppm) of 0.75 M, 2.36 M and 3.16 M $AgF$ treatment groups. ....	172
<b>Figure 10.34</b> - The $[Ag^+]_{4h}$ (ppm) of 0.75 M, 2.36 M and 3.16 M $Ag[NH_3]_2F$ treatment groups. ....	172
<b>Figure 10.35</b> - The mean $F$ release from enamel under pH 4.0 demineralisation before and after topical treatment with DW, and 3.16 M silver compounds.....	173
<b>Figure 10.36</b> - The $F$ release profiles of 0.75 M, 2.36 M and 3.16 M $AgF$ treatment groups. ....	174
<b>Figure 10.37</b> - The $F$ release profiles of 0.75 M, 2.36 M and 3.16 M $Ag[NH_3]_2F$ treatment groups. ....	174
<b>Figure 10.38</b> - (a) Mean $R_i$ and (b) mean $R_L$ of the $F$ release of DW and 3.16 M treatment groups. ....	176
<b>Figure 10.39</b> - (a) Mean $R_i$ and (b) mean $R_L$ of the $F$ release of 0.75 M, 2.36 M and 3.16 M $AgF$ treatment groups. ....	177
<b>Figure 10.40</b> - (a) Mean $R_i$ and (b) mean $R_L$ of the $F$ release of 0.75 M, 2.36 M and 3.16 M $Ag[NH_3]_2F$ treatment groups.....	177
<b>Figure 10.41</b> - The $[F]_{4h}$ (ppm) of 3.16 M $AgNO_3$ , 3.16 M $AgF$ , 3.16 M $Ag[NH_3]_2F$ , Riva-SC and DW treatment groups. Error bars show the standard errors. Linking lines between bars indicate significant differences at $p < 0.05$ between treatment groups. ....	179
<b>Figure 10.42</b> - The $[F]_{4h}$ (ppm) of 0.75 M, 2.36 M and 3.16 M $AgF$ treatment groups. ....	180
<b>Figure 10.43</b> - The $[F]_{4h}$ (ppm) of 0.75 M, 2.36 M and 3.16 M $Ag[NH_3]_2F$ treatment groups. ....	180



<b>Figure 10.44</b> - The colours of enamel treated with DW and Riva-SC following different treatments of the ISE study. ....	181
<b>Figure 10.45</b> - The colours of enamel treated with different concentrations of AgNO <sub>3</sub> , AgF and Ag[NH <sub>3</sub> ] <sub>2</sub> F following different treatments of the ISE study. ....	182
<b>Figure 10.46</b> - Typical SEM images of enamel blocks of (a) DW Tx, (b) 0.75 M AgNO <sub>3</sub> Tx, (c) 2.36 M AgNO <sub>3</sub> Tx and (d) 3.16 M AgNO <sub>3</sub> Tx, (e) 0.75 M AgF Tx, (f) 2.36 M AgF Tx and (g) 3.16 M AgF Tx, (h) 0.75 M Ag[NH <sub>3</sub> ] <sub>2</sub> F Tx, (i) 2.36 M Ag[NH <sub>3</sub> ] <sub>2</sub> F Tx and (j) 3.16 M Ag[NH <sub>3</sub> ] <sub>2</sub> F Tx, and (k) Riva-SC Tx. ....	184
<b>Figure 10.47</b> – The mean atomic percentages of Ag of 3.16 M AgNO <sub>3</sub> , 3.16 M AgF, 3.16 M Ag[NH <sub>3</sub> ] <sub>2</sub> F, Riva-SC and DW treatment groups. Linking lines between bars indicate significant differences at p < 0.05 between treatment groups. ....	185
<b>Figure 10.48</b> - The mean atomic percentages of Ag of AgNO <sub>3</sub> treatment groups. ....	187
<b>Figure 10.49</b> - The mean atomic percentages of Ag of AgF treatment groups. ....	187
<b>Figure 10.50</b> - The mean atomic percentages of Ag of Ag[NH <sub>3</sub> ] <sub>2</sub> F treatment groups. ....	187
<b>Figure 10.51</b> - The mean atomic percentages of F of 3.16 M AgNO <sub>3</sub> , 3.16 M AgF, 3.16 M Ag[NH <sub>3</sub> ] <sub>2</sub> F, Riva-SC and DW treatment groups. Error bars show the standard errors. Linking lines between bars indicate significant differences at p < 0.05 between treatment groups. ....	188
<b>Figure 10.52</b> - The mean atomic percentages of F of AgF treatment groups. ....	189
<b>Figure 10.53</b> - The mean atomic percentages of F of Ag[NH <sub>3</sub> ] <sub>2</sub> F treatment groups. ....	189
<b>Figure 10.54</b> – <sup>31</sup> P MAS-NMR spectra of each treatment group before and after pH 4.0 acid challenge. ....	190
<b>Figure 10.55</b> – <sup>19</sup> F MAS-NMR spectra of each treatment group before and after pH 4.0 acid challenge. ....	191
<b>Figure 10.56</b> - Typical images (40X) of lesions sections of (a) DW Tx, (b) 0.75 M AgNO <sub>3</sub> Tx, (c) 2.36 M AgNO <sub>3</sub> Tx and (d) 3.16 M AgNO <sub>3</sub> Tx, (e) 0.75 M AgF Tx, (f) 2.36 M AgF Tx and (g) 3.16 M AgF Tx, (h) 0.75 M Ag[NH <sub>3</sub> ] <sub>2</sub> F Tx, (i) 2.36 M Ag[NH <sub>3</sub> ] <sub>2</sub> F Tx and (j) 3.16 M Ag[NH <sub>3</sub> ] <sub>2</sub> F Tx, and (k) Riva-SC Tx. ....	193
<b>Figure 10.57</b> – Knoop CSMH of (a) DW Tx, (b ~ d) AgNO <sub>3</sub> Tx, (e ~ g) AgF Tx and (h ~ j) Ag[NH <sub>3</sub> ] <sub>2</sub> F Tx in different concentrations, and (k) Riva-SC Tx. ....	194
<b>Figure 11.1</b> – Schematic representation of an enamel block topically treated with 3.16 M AgNO <sub>3</sub> . Ag <sub>3</sub> PO <sub>4</sub> is formed on the enamel surface and some Ca <sup>2+</sup> in the enamel mineral is substituted by Ag <sup>+</sup> . ....	197
<b>Figure 11.2</b> – Schematic representation of an enamel block topically treated with 3.16 M AgNO <sub>3</sub> following re-immersion back into acid. After immersion of a) Ag <sup>+</sup> loosely attached to enamel surfaces is released into solution. b) Gradually, some Ag <sub>3</sub> PO <sub>4</sub> on the enamel surface and some Ag <sup>+</sup> in the solution are reduced to black metallic silver. ....	199
<b>Figure 11.3</b> – Schematic representation of an enamel block topically treated with AgNO <sub>3</sub> after 4 h demineralisation. Deeper lesions are developed in the substituted enamel, therefore uneven demineralised enamel surface is observed. Further, all the Ag <sub>3</sub> PO <sub>4</sub> is reduced to black metallic silver causing black staining. ....	201
<b>Figure 11.4</b> – Schematic representation of an enamel block topically treated with AgF or Ag[NH <sub>3</sub> ] <sub>2</sub> F. Ag <sub>3</sub> PO <sub>4</sub> , CaF <sub>2</sub> and FHA are formed on the enamel surface. ....	204
<b>Figure 11.5</b> – Schematic representation of an enamel block topically treated with AgF or Ag[NH <sub>3</sub> ] <sub>2</sub> F following re-immersion back into acid. a) Both Ag <sup>+</sup> and F loosely attached	

to enamel surface are released into solution. b) Gradually, some  $\text{Ag}_3\text{PO}_4$  on the enamel surface and some  $\text{Ag}^+$  in the solution are reduced to metallic silver, and some  $\text{CaF}_2$  on the enamel surface is dissolved, providing  $\text{F}^-$  for further formation of FHA... 207

**Figure 11.6** – Schematic representation of an enamel block topically treated with AgF or  $\text{Ag}[\text{NH}_3]_2\text{F}$  after 4 h demineralisation. All the  $\text{Ag}_3\text{PO}_4$  is reduced to metallic silver causing black staining and most of the  $\text{CaF}_2$  is dissolved which favours further formation of FHA. .... 210

**Figure 12.1** – Schematic representation of proposed dose-response inhibitory mechanism of topical treatment with  $\text{AgNO}_3$  on human enamel demineralisation. Following topical treatment with  $\text{AgNO}_3$ , both formation of  $\text{Ag}_3\text{PO}_4$  and  $\text{Ag}^+$  substituted enamel increases with increasing concentration. After acid challenge,  $\text{Ag}_3\text{PO}_4$  is reduced to metallic silver. The enamel surface with more  $\text{Ag}^+$  substituted enamel is more destructed. Further, some metallic silver is lost due to the loss of enamel structure. .... 217

**Figure 12.2** - Comparison of the log-linear relationship between the mean  $\text{PRCL}_{\text{enamel}}$  of  $\text{AgNO}_3$  topical treatment and the  $[\text{Ag}^+]_{4\text{h}}$  (Green line), and the log-linear relationship between the mean  $\text{PRML}_{\text{enamel}}$  of  $\text{Ag}^+$  and the  $[\text{Ag}^+]$  in solution (Grey line). Error bars show the standard errors. .... 219

**Figure 12.3** – The difference between the inhibitory efficacy ( $\text{PRCL}_{\text{enamel}}$ ) of  $\text{AgNO}_3$  (Green dots) observed in ISE study and the theoretical inhibitory efficacy ( $\text{PRML}_{\text{enamel}}$ ) of  $[\text{Ag}^+]_{4\text{h}}$  (Grey dots) obtained from dose-response  $\text{PRML}_{\text{enamel}}$  of  $\text{Ag}^+$  reported in the SMR study. .... 220

**Figure 12.4** – Schematic representation of proposed dose-response inhibitory mechanism of topical treatment with AgF or  $\text{Ag}[\text{NH}_3]_2\text{F}$  on human enamel demineralisation. Following topical treatment with AgF or  $\text{Ag}[\text{NH}_3]_2\text{F}$ , the formation of  $\text{Ag}_3\text{PO}_4$ ,  $\text{CaF}_2$  and FHA increases with increasing concentration. After acid challenge,  $\text{Ag}_3\text{PO}_4$  is reduced to metallic silver and  $\text{CaF}_2$  is dissolved for further formation of FHA. .... 223

**Figure 12.5** - Comparison of the log-linear relationship between the mean  $\text{PRCL}_{\text{enamel}}$  of AgF topical treatment and the  $[\text{Ag}^+]_{4\text{h}}$  (Red line) and the log-linear relationship between the mean  $\text{PRML}_{\text{enamel}}$  of  $\text{Ag}^+$  and the  $[\text{Ag}^+]$  in solution (Grey line). Error bars show the standard errors. .... 224

**Figure 12.6** - Comparison of the log-linear relationship between the mean  $\text{PRCL}_{\text{enamel}}$  of  $\text{Ag}[\text{NH}_3]_2\text{F}$  topical treatment and the  $[\text{Ag}^+]_{4\text{h}}$  (Blue line) and the log-linear relationship between the mean  $\text{PRML}_{\text{enamel}}$  of  $\text{Ag}^+$  and the  $[\text{Ag}^+]$  in solution (Grey line). Error bars show the standard errors. .... 225

**Figure 12.7** - Comparison of the log-linear relationship between the mean  $\text{PRCL}_{\text{enamel}}$  of AgF topical treatment and the  $[\text{F}^-]_{4\text{h}}$  (Red line) and the log-linear relationship between the mean  $\text{PRML}_{\text{enamel}}$  of  $\text{F}^-$  and the  $[\text{F}^-]$  in solution (Purple line). Error bars show the standard errors. .... 226

**Figure 12.8** - Comparison of the log-linear relationship between the mean  $\text{PRCL}_{\text{enamel}}$  of  $\text{Ag}[\text{NH}_3]_2\text{F}$  topical treatment and the  $[\text{F}^-]_{4\text{h}}$  (Blue line) and the log-linear relationship between the mean  $\text{PRML}_{\text{enamel}}$  of  $\text{F}^-$  and the  $[\text{F}^-]$  in solution (Purple line). Error bars show the standard errors. .... 227

**Figure 12.9** - The difference between the inhibitory efficacy ( $\text{PRCL}_{\text{enamel}}$ ) of AgF (Red dots) observed in ISE study and the theoretical inhibitory efficacy ( $\text{PRML}_{\text{enamel}}$ ) of  $[\text{F}^-]_{4\text{h}}$

<i>(Purple dots) obtained from dose-response <math>PRML_{enamel}</math> of F reported in the SMR study.</i>	228
<b>Figure 12.10</b> - <i>The difference between the inhibitory efficacy (<math>PRCL_{enamel}</math>) of <math>Ag[NH_3]_2F</math> (Blue dots) observed in ISE study and the theoretical inhibitory efficacy (<math>PRML_{enamel}</math>) of <math>[F]_{4h}</math> (Purple dots) obtained from dose-response <math>PRML_{enamel}</math> of F reported in the SMR study.</i>	228
<b>Figure 13.1</b> – <i>Mean <math>PRCL_{enamel}</math> and mean <math>PRCL_{HAP}</math> of all treatment groups.</i>	232
<b>Figure 13.2</b> – <i><math>[Ag^+]_{4h}</math> of enamel and HAP disc treatment groups.</i>	233
<b>Figure 13.3</b> - <i><math>[F]_{4h}</math> of enamel and HAP disc treatment groups.</i>	234
<b>Figure 13.4</b> - <i>Mean percentages of Ag detected on HAP disc and human enamel surfaces.</i>	235
<b>Figure 13.5</b> – <i>Mean percentages of F detected on HAP disc and human enamel surfaces.</i>	236
<b>Figure 13.6</b> – <i>Dose-response effects of topical treatments with <math>AgNO_3</math> (Green line), AgF (Red line) and <math>Ag[NH_3]_2F</math> (Blue line) on demineralisation of human enamel.</i>	237

## List of Tables

<b>Table 6.1</b> - $RCL_{HAP}$ before and after $Zn^{2+}$ addition of the Fig. 6.4. ....	63
<b>Table 6.2</b> - $RCL_{HAP}$ before and after $F^-$ addition of the Fig. 6.5.....	65
<b>Table 6.3</b> – The $RCL_{HAP}$ and $PRCL_{HAP}$ of every HAP disc measured at each $[Zn^{2+}]$ . ...	66
<b>Table 6.4</b> - The $RCL_{HAP}$ and $PRCL_{HAP}$ of every HAP disc measured at each $[F^-]$ . ....	67
<b>Table 7.1</b> – The $RML_{enamel}$ and $PRML_{enamel}$ measured at each point for every $[Ag^+]$ in solution. $PRML_{enamel}$ highlighted in red indicate that the $RML_{enamel}$ were not significantly different from the $RML_{enamel}$ measured at 0 ppm $Ag^+$ .....	83
<b>Table 8.1</b> – Compositions of treatment groups.....	94
<b>Table 8.2</b> - The $RCL_{HAP}$ before and after DW topical treatment of the Fig. 8.4.....	98
<b>Table 8.3</b> - The $RCL_{HAP}$ before and after $AgNO_3$ topical treatment of the Fig. 8.5. ....	99
<b>Table 8.4</b> - The $RCL_{HAP}$ before and after $AgF$ topical treatment of the Fig. 8.6. ....	100
<b>Table 8.5</b> - The $RCL_{HAP}$ before and after $Ag[NH_3]_2F$ topical treatment of the Fig. 8.7. ....	101
<b>Table 8.6</b> - The $RCL_{HAP}$ before and after Riva-SC topical treatment of the Fig. 8.8. ....	102
<b>Table 8.7</b> – The $RCL_{HAP}$ and $PRCL_{HAP}$ of every HAP disc in each treatment group... ..	103
<b>Table 8.8</b> – Mean $R_i$ and mean $R_L$ of the $Ag^+$ release following each treatment.....	106
<b>Table 8.9</b> – The mean $[Ag^+]$ during the 4 h demineralisation period after re-immersion of the topically treated HAP samples into acids ( $[Ag^+]_{4h}$ ) of each treatment group.....	107
<b>Table 8.10</b> – Mean $R_i$ and mean $R_L$ of the $F^-$ release following each treatment.....	109
<b>Table 8.11</b> – The mean $[F^-]$ during the 4 h demineralisation period after re-immersion of the topically treated HAP samples into acids ( $[F^-]_{4h}$ ) of each treatment group. ....	110
<b>Table 10.1</b> – Compositions of treatment groups.....	144
<b>Table 10.2</b> – The $RCL_{enamel}$ before and after DW topical treatment of the Fig. 10.5. ....	148
<b>Table 10.3</b> - The $RCL_{enamel}$ before and after $AgNO_3$ topical treatments of the Fig. 10.6 ~ 10.8.....	149
<b>Table 10.4</b> - The $RCL_{enamel}$ before and after $AgF$ topical treatments of the Fig. 10.9 ~ 10.11. ....	151
<b>Table 10.5</b> - The $RCL_{enamel}$ before and after $Ag[NH_3]_2F$ topical treatments of the Fig. 10.12 ~ 10.14.....	153
<b>Table 10.6</b> - The $RCL_{enamel}$ before and after Riva-SC topical treatment of the Fig. 10.15. ....	155
<b>Table 10.7</b> - The $RCL_{enamel}$ and $PRCL_{enamel}$ of every Enamel in each treatment group. ....	157
<b>Table 10.8</b> – Mean $R_i$ and mean $R_L$ of the $Ag^+$ release following each treatment.....	167
<b>Table 10.9</b> – The mean $[Ag^+]$ during the 4 h demineralisation period after re-immersion of the topically treated enamel blocks into acids ( $[Ag^+]_{4h}$ ) of each treatment group. ....	170
<b>Table 10.10</b> – Mean $R_i$ and mean $R_L$ of the $F^-$ release following each treatment.....	175
<b>Table 10.11</b> – The mean $[F^-]$ during the 4 h demineralisation period after re-immersion of the topically treated enamel blocks into acids ( $[F^-]_{4h}$ ) of each treatment group. ....	178

## Abbreviations

AHF	ammonium hexafluorosilicate
APF	acidulated phosphate fluoride
CHX	chlorhexidine
CPP-ACP	casein phosphopeptide amorphous calcium phosphate
CSMH	cross-sectional micro-hardness profiling
DCPD	dicalcium phosphate dihydrate
DMFT	number of permanent teeth decayed, missing and filled teeth
DW	de-ionised water
EDJ	enamel-Dentine junction
EDX	energy-dispersive X-ray analysis
Fig.	figure
FAP	fluorapatite
FHA	fluorohydroxyapatite
GVHD	chronic oral graft versus host disease
HAP	hydroxyapatite
h	hour
Ip	ion product
ISE	ion selective electrode
$K_{sp}$	solubility product constant
$K_a$	acid dissociation constant
LLOD	lower limit of detection
MBC	minimum bactericide concentration
MIC	minimum inhibition concentration
MID	minimal Intervention Dentistry
MAS-NMR	magic angle spinning-nuclear magnetic resonance
min	minute
mM	millimolar
mV	millivoltage
NCOP	non-contact optical profilometry
PRCL	percentage of reduction in the rate of calcium loss
PRML	percentage of reduction in the rate of mineral loss
RCL	rate of calcium loss
RML	rate of mineral loss

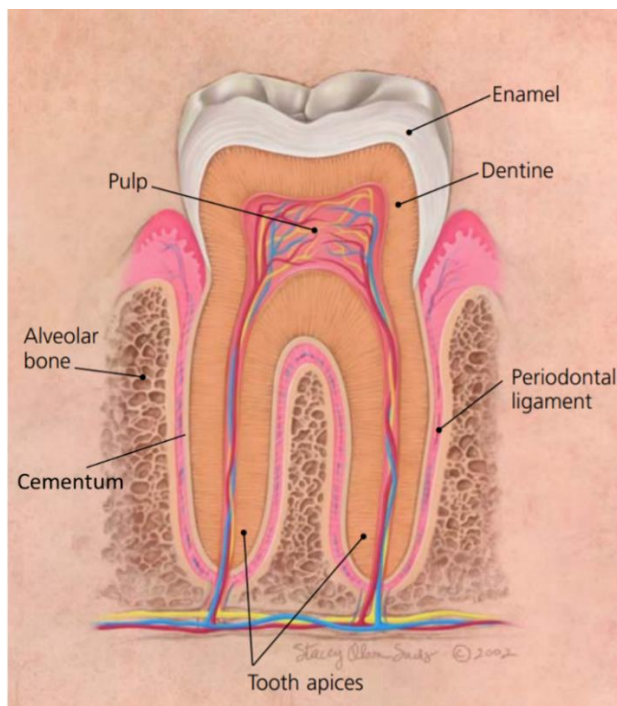
SC	silver capsule of Riva Star (SDI Ltd)
SDF	silver diammine fluoride
SDS	safety data sheet
SE	standard error
SEM	scanning electron microscope
S.m.	Streptococcus mutans
SMR	scanning microradiography
Tx	treatment
WHO	World Health Organization
XRD	X-ray diffraction analysis

# **PART I: LITERATURE REVIEW, AIMS AND OBJECTIVES**

## Chapter 1 INTRODUCTION OF DENTAL MINERAL

### 1.1 Human Tooth Structure

The human tooth is composed of enamel, dentine and cementum as mineralised hard tissues, and dental pulp as soft tissue (**Fig. 1.1**) (Douglass, 2003). In the crown, enamel is the hardest tissue in the human body (He and Swain, 2007), covering a thick dentinal layer comprising the bulk of tooth, and in the root, dentine is surrounded by cementum (Turp and Alt, 1998). Enamel contains the highest apatite mineral (96 wt%), followed by dentine (70 wt%), while cementum (65 wt%) is similar to bone (Driessens, 1980; Curzon and Featherstone, 1983). As enamel is the outermost dental mineral of the tooth exposed to acid challenges, it is discussed in this section.



**Figure 1.1** - Structure of tooth (From Douglass, 2003).



## 1.2 Human Enamel

Enamel is acellular, non-sensitive and cannot be cellularly regenerated once lost. The structure comprises prismatic units with a hierarchical construction (Boyde, 1964). Enamel is thickest at the cusps (2.5 mm) and thinnest at the cervical margins. Due to its high mineral density, the porosity of enamel is extremely low (Berkovitz, 2011).

Incipient caries always starts from enamel, as it is the first surface suffering the acid attacks from organic acids. These acids diffuse through the enamel pores, and selectively dissolve components with higher solubility, and gradually penetrate into underlying dentine. Remineralisation of the demineralised lesion is possible under certain conditions (Featherstone, 2008).

### 1.2.1 Composition of Human Enamel

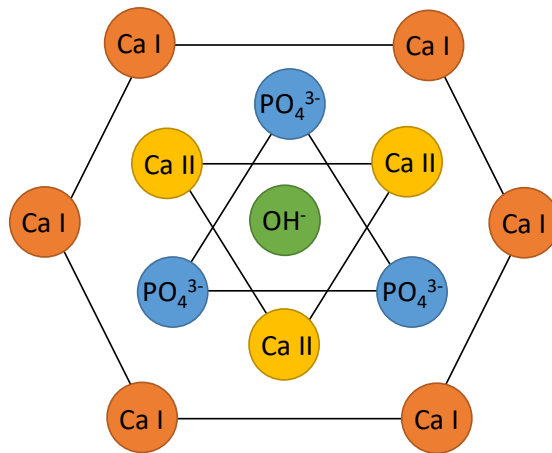
The mineral component of human enamel is a calcium-deficient carbonated hydroxyapatite (LeGeros, 1991; Weatherell, 1975). Mature human enamel is composed of hydroxyapatite (HAP) (92 ~ 96 wt%), water (2 ~ 3 wt%), carbonate (2 ~ 3 wt%), trace elements (sodium, chloride, magnesium, potassium and zinc, 1 wt%), fluoride (0.01 ~ 0.05 wt%) and proteins and lipids (< 1 wt%) (Hicks *et al.*, 2004; LeGeros, 1991). Generally, the concentration of F<sup>-</sup> is highest (thousands of ppm) in the surface and decreases toward EDJ (Enamel-Dentine junction), whereas, the concentration gradients of CO<sub>3</sub><sup>2-</sup> and Mg<sup>2+</sup> are reverse (Robinson *et al.*, 2000). The organic components and water are mainly located in the inter-prismatic regions of enamel (Berkovitz, 2011; Boyde, 1964). As the distributions of these components in enamel are not homogeneous, the response of enamel to physical and chemical challenges varies in different regions (He and Swain, 2008; Simmer *et al.*, 2010; Zhang *et al.*, 2014).

Developmental processes in enamel can profoundly affect the resultant composition by ion substitution. CO<sub>3</sub><sup>2-</sup> can replace OH<sup>-</sup> or PO<sub>4</sub><sup>3-</sup> groups, which depends on the pCO<sub>2</sub> during the amelogenesis. Further, Ca<sup>2+</sup> can also be partially

replaced by  $Mg^{2+}$  up to 0.3 % (Robinson *et al.*, 2000). As both  $CO_3^{2-}$  and  $Mg^{2+}$  are destabilising agents, the regions with higher concentrations of these ions, such as the core of enamel prism (Boyde, 1979), tend to dissolve faster under demineralisation (Robinson *et al.*, 1995). On the other hand,  $F^-$  is a stabilising agent. As FAP (or FHA) has stronger hydrogen bonds within the lattice than HAP, which stabilises the structure of fluoridated enamel, it is more acid-resistant than HAP (Garcia-Godoy and Hicks, 2008; Hicks *et al.*, 2003; Robinson, 2009).  $F^-$  can replace the  $OH^-$  of the enamel during post-eruption maturation, or after contact between enamel and topical fluoride supplements, to form fluorapatite (FAP) or fluorohydroxyapatite (FHA) (Hicks *et al.*, 2003). The incorporation of  $F^-$  into enamel can be up to a depth of 100  $\mu m$  (Arends and Christoffersen, 1990; Lynch, 2013), whose amounts vary with the fluoride supplements that the enamel is exposed to (Schamschula *et al.*, 1982). The difference in the  $F^-$  concentration in the enamel surfaces between non-fluoridated areas and fluoridated areas could be up to 1000 ppm (Weatherell *et al.*, 1977).

### 1.2.2 Mineral Structure of Human Enamel

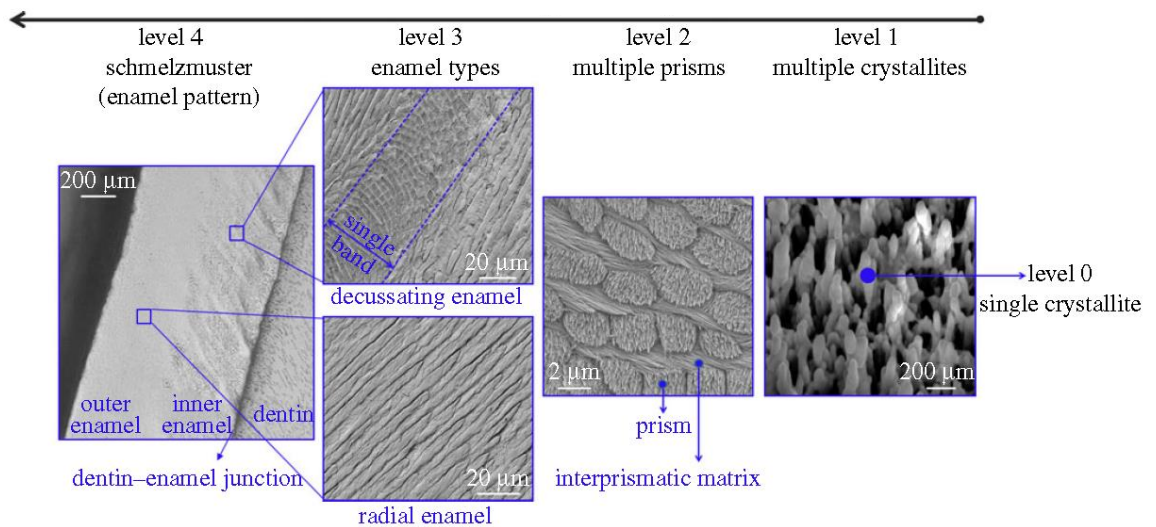
**Fig. 1.2** shows the projected crystal structure of stoichiometric HAP in human enamel viewed down the c-axis  $OH^-$  column (Robinson *et al.*, 2000). The ion arrangement is shown as one  $OH^-$  surrounded by three  $Ca^{2+}$  (Ca II), with three  $PO_4^{3-}$  outside these ions compassing them. These ions are enclosed by six  $Ca^{2+}$  (Ca I) arranged in a hexagon, called the hexagonal HAP unit cell.



**Figure 1.2** - Hexagonal unit structure of HAP in human enamel (Adapted from Robinson *et al.*, 2000).

A hexagonal enamel crystallite (50 nm in width and 25 nm in thickness), composed of millions of hexagonal HAP unit cells (Robinson *et al.*, 2000; Lu *et al.*, 2011), is the basic structural element (level 0) of enamel mineral (Yilmaz *et al.*, 2015). During amelogenesis, hexagonal enamel crystallites are aligned along the c-axis under the guidance of proteins (Berkovitz, 2011; Robinson *et al.*, 2000) and bundled into prisms (5  $\mu\text{m}$  in diameter) and inter-prismatic matrix (level 1). The crystallites in the central part of a rod are aligned with the longitudinal axis of the prism, whereas, those at the sides are aligned in a divergent angle (nearly  $60^\circ$ ) to the longitudinal axis of the prisms (He and Swain, 2007; He and Swain, 2008). The arrangement of multiple prisms (level 2) in cross-section appears as “keyholes”, whereas, in the longitudinal view, the layout is more parallel. These arrangements (level 3) can be categorised as radial enamel in the outer layers and decussating enamel in the inner layers. Finally, different arrangements of enamel constitute the hierarchical structure of enamel (enamel pattern, level 4) to meet the mechanical and physical requirements of mastication in an oral environment (**Fig. 1.3**) (Berkovitz, 2011; Cui and Ge, 2007; Yilmaz *et al.*, 2015).

## Hierarchical order of enamel



**Figure 1.3** - Microstructure of enamel showing hierarchical levels (From Yilmaz *et al.*, 2015).

### 1.3 Hydroxyapatite Discs as a Model System for Human enamel

As hydroxyapatite (HAP) is the main constituent of human enamel (LeGeros, 1991; Busch *et al.*, 2001), compressed HAP discs have been used in many studies to simulate the demineralisation of human enamel (*e.g.*, Anderson *et al.*, 2004a; do Amaral *et al.*, 2016; Jones *et al.*, 2013; Kosoric *et al.*, 2010). HAP discs exhibit similar demineralisation kinetics to that of human enamel and can be used as a model for human enamel in order to understand the formation of *in vivo* dental caries or erosion (Shellis *et al.*, 2010).

The major difference between human enamel mineral and HAP is the presence of about 3 wt% carbonate (Mukundan *et al.*, 1999), which leads to faster dissolution of human enamel than HAP discs (Anderson *et al.*, 2004b; Shellis *et al.*, 2010). Further, HAP discs do not have the complex biological structures (see Section 1.2.2) of human enamel (Anderson *et al.*, 2004b; Yilmaz *et al.*, 2015). However, as HAP discs are easy to obtain and have homogeneous chemical composition and structure, compared to human enamel minerals (Elliott, 1994; Lingawi, 2012), they have been accepted as suitable analogues for dental enamel mineral.

## Chapter 2 DENTAL CARIES AND EROSION

### 2.1 Enamel Demineralisation

Enamel demineralisation results from two dental diseases, dental caries and erosion (Abou Neel *et al.*, 2016). The source of acids in caries is from bacterial metabolism, while erosion is from acids without bacterial involvement (Selwitz *et al.*, 2007; Ren, 2011). The difference between caries and erosion is seen in the structure of each. Caries is characterised by subsurface demineralisation resulting from the exposure to pH 4.5 ~ 6.5 organic acids following fermentation in the plaque. Whereas, erosion is characterised by surface softening resulting from exposure to pH 2.0 ~ 4.0 acidic diet, leading to the destruction of weakened inter-prismatic regions (Arends and ten Cate, 1981).

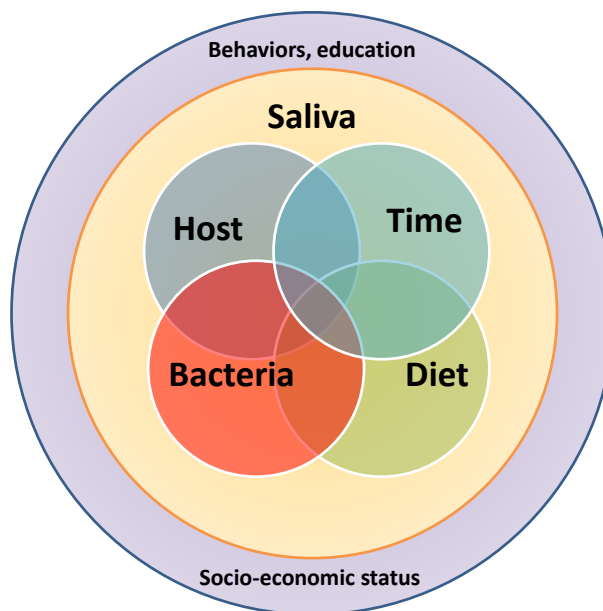
Despite the differences between dental caries and erosion mentioned above, the development of these two dental lesions follows the same chemical reaction (Lussi, 2006a). As the pH decreases, trivalent phosphate ions ( $\text{PO}_4^{3-}$ ) and hydroxyl ions ( $\text{OH}^-$ ) of the enamel HAP will be protonated to divalent phosphate ions ( $\text{HPO}_4^{2-}$ ) and water ( $\text{H}_2\text{O}$ ), respectively. This transformation results in the formation of more soluble dicalcium phosphate dihydrate ( $\text{CaHPO}_4 \cdot 2\text{H}_2\text{O}$ ), so-called brushite, and later causes the weakening of the bonding between  $\text{PO}_4^{3-}$  and  $\text{Ca}^{2+}$ . The consequent  $\text{Ca}^{2+}$  loss from enamel leads to enamel demineralisation (Robinson *et al.*, 1995).

### 2.2 Dental Caries

Dental caries is the most common chronic disease worldwide (Moreira, 2012). It is characterised by localised subsurface destruction of enamel arising from organic acids generated by bacterial metabolism within the biofilm (Newbrun, 1982; Selwitz *et al.*, 2007).

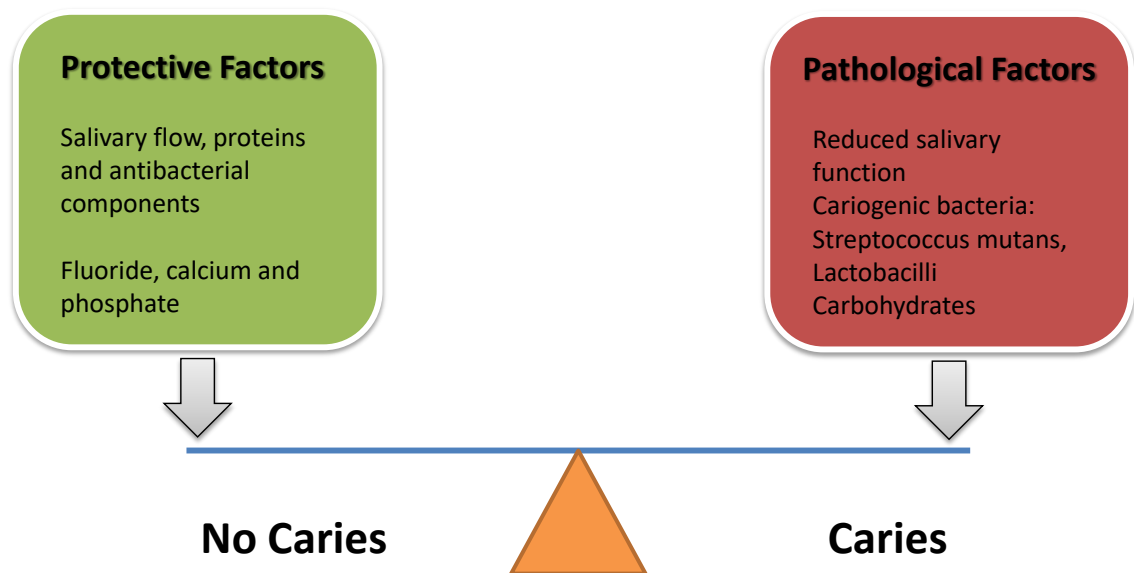
## 2.2.1 Aetiology of Dental Caries

Caries is a multifactorial disease (Hunter, 1988), whose development involves cariogenic microorganisms, environmental triggers and a susceptible host (Anderson, 2002; Marsh, 2009). *Streptococcus mutans* (S.m.), *Streptococcus sobrinus* and *Lactobacillus acidophilus* are the major cariogenic bacteria (Kidd, 2005). They rapidly produce organic acids such as lactic and acetic acids by the fermentation of ingested carbohydrate (Bowen, 2013; Distler and Kroncke, 1980; Sheiham, 2001). Modern refined foods contain a high amount of sugars, especially sucrose, and can promote the production of these organic acids. Therefore, the constant intake of sugary food is a risk factor of dental caries (Marsh, 2009). Defects in tooth structure is also a risk factor, as they make the tooth more susceptible to acid challenge (Selwitz *et al.*, 2007). The progression of caries is associated with time. The longer the time period that the tooth is in acidic conditions, the more destructive the dental lesion will be (Maya *et al.*, 2015) (Fig. 2.1).



*Figure 2.1 – Aetiology of dental caries (Adapted from Selwitz et al., 2007).*

As saliva has sufficient mineral concentrations to keep the fluid saturated with respect to the dental mineral, the integrity of enamel in contact with saliva is maintained (Garcia-Godoy and Hicks, 2008). Further, as the presence of F<sup>-</sup> in saliva is beneficial for the formation of less soluble FAP on the enamel surface (mainly HAP), the dental mineral can be further protected (Robinson, 2009; Miura *et al.*, 1993). Therefore, the presence of saliva is a protective factor of dental caries, and the decrease in secretion of saliva is a risk factor. Other factors such as behaviour, socio-economic status and education level can also affect the risk of dental caries (**Fig. 2.1**) (Fejerskov, 2004; Selwitz *et al.*, 2007).



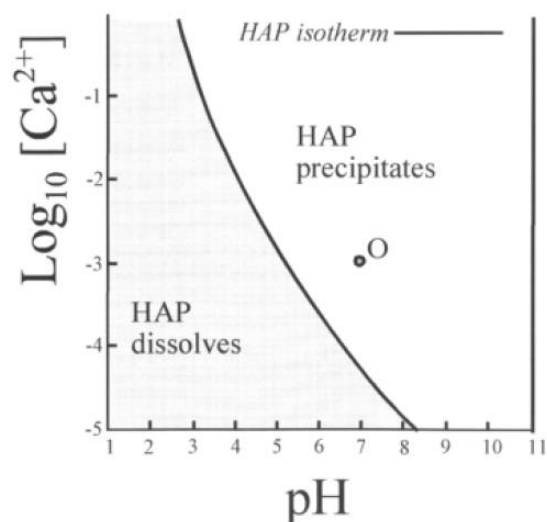
*Figure 2.2 - Caries balance (Adapted from Garcia-Godoy and Hicks, 2008).*

Consequently, a caries balance can be established (**Fig 2.2**) based on the interaction between pathological and protective factors (Featherstone, 2004; Garcia-Godoy and Hicks, 2008). On one side, it is the pathological factors such as acidogenic bacteria, impaired salivary function and frequent carbohydrate consumption, resulting in enamel demineralisation. On the other side, it is the protective factors such as saliva flow, antibacterial effects, fluoride supplements and sufficient mineral concentrations, resulting in enamel remineralisation. The dynamic equilibrium between the pathological and protective factors determines

the final outcome of the carious lesion, which may be progression, reversal, or maintenance (Featherstone, 2004).

### 2.2.2 Chemistry of Dental Caries

The solubility of enamel mineral (mainly HAP,  $\text{Ca}_{10}(\text{PO}_4)_6(\text{OH})_2$ ) increases 10 times with a decrease of 1 pH unit in the solution (Buzalaf *et al.*, 2011). In the oral cavity, whenever the acidity of saliva is below the critical pH of HAP, it becomes under-saturated with respect to enamel mineral, leading to dental demineralisation (Dawes, 2003; Ehrlich *et al.*, 2009). However, whenever the saliva acidity is above the critical pH, remineralisation of the dental mineral occurs (**Fig. 2.3**) (Anderson *et al.*, 2001). Even though the generally recognised critical pH is 5.5, the actual value depends on the concentrations (activities) of  $\text{OH}^-$ ,  $\text{Ca}^{2+}$  and  $\text{PO}_4^{3-}$  in the solution (Anderson *et al.*, 2001; Dawes, 2003). With sufficient supply of  $\text{Ca}^{2+}$ , enamel will not dissolve even under low pH, as long as the ion product (Ip) is equal or greater than the solubility product constant ( $K_{\text{sp}}$ ) of HAP (suggested to be  $\text{p}K_{\text{sp}} = 117.2$ ) (Anderson *et al.*, 2001; Dawes, 2003; Miura *et al.*, 1993).

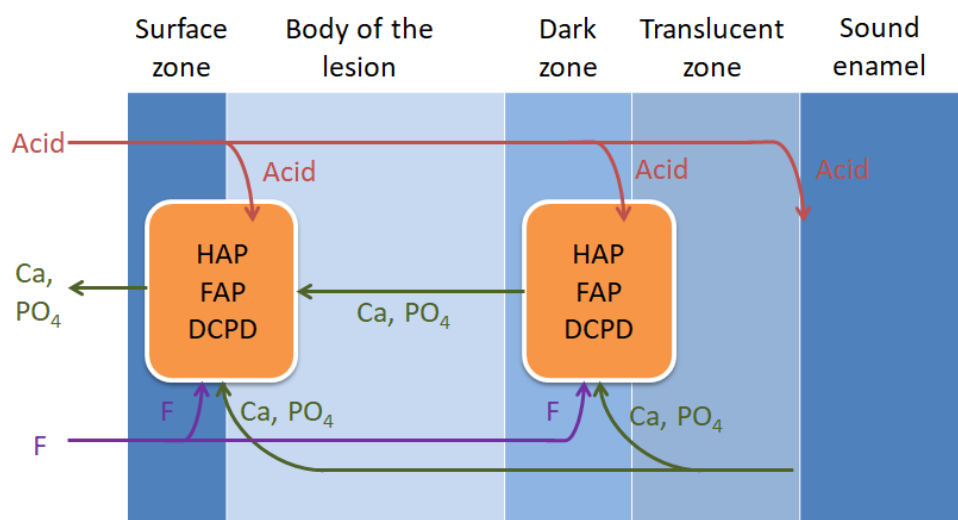


**Figure 2.3** - Solubility isotherm of HAP. O: normal intra-oral condition (From Anderson *et al.*, 2001).



Before bacterially generated organic acids become in contact with the tooth, the acids diffuse through the dental plaque into the defects on the enamel surface, followed by demineralisation of the underlying mineral structure (Rosin-Grget *et al.*, 2013). The carious lesion is usually initiated in the most accessible and soluble periphery and cores of the prisms (Featherstone, 1977). This is due to the loose arrangements of the crystals and the high content of soluble substitutions like  $\text{CO}_3^{2-}$  and  $\text{Mg}^{2+}$  in these areas (Boyde, 1979). Next, the acid then penetrates via cross-striations and pores to the prism body and inter-prismatic area (Featherstone, 2008; Marshall and Lawless, 1981; Robinson *et al.*, 2000).

However, the development of a carious lesion is not only about the advancement of the acid, but also about the diffusion of dissolved  $\text{Ca}^{2+}$  and  $\text{PO}_4^{3-}$  back to the surface region, which induces the formation of a surface zone by mineral re-deposition (Hicks *et al.*, 2004; Moreno and Zahradnik, 1979; Rosin-Grget *et al.*, 2013). There are four zones that can be observed under the inspection of caries using polarising light microscopy; translucent zone, dark zone, body of lesion and surface zone (**Fig 2.4**) (Moreno and Zahradnik, 1979; Robinson *et al.*, 2000; Silverstone, 1981).



**Figure 2.4** - Schematic diagrams of enamel caries (Adapted from Robinson *et al.*, 2000).

### 2.2.2.1 Translucent zone

The translucent zone is the first sign of caries lesion which can be detected by visual examination. It contains few but large pores with 1 ~ 2 % mineral loss. Preliminarily, the organic matrix is decomposed followed by the dissolution of the mineral material, which mostly takes place at inter-crystalline and inter-prismatic regions leading to the formation of channels for ion diffusion (Robinson *et al.*, 2000).

### 2.2.2.2 Dark zone

Dark zone is characterised by the smaller pores in addition to the big ones. There is an increased porosity of 5 ~ 10 % in the area. It has been postulated that those smaller pores are the consequence of slight remineralisation narrowing the large pores. Therefore, it implies that both demineralisation and remineralisation occur at the same time during the process of caries (Robinson *et al.*, 2000).

### 2.2.2.3 Body of lesion

In the body of lesion, there is a higher porosity up to 25 ~ 50 %. It represents the final stage of the enamel demineralisation after the continuous enlargement of pores which ends up with cavitation. The concentrations of  $\text{CO}_3^{2-}$  and  $\text{Mg}^{2+}$  are lower, whilst that of  $\text{F}^-$  is higher in this zone, which facilitates the lateral enlargement of crystallites. This phenomenon further indicates that remineralisation happens during the carious process (Pearce *et al.*, 1995; Robinson *et al.*, 2000).

#### 2.2.2.4 Surface zone

The surface zone remains relatively intact much longer than the other zones under demineralisation, which means that it might be preserved or benefited from the re-deposition process. The porosity of this zone is 1 ~ 2 % which is similar to that of the sound enamel (Anderson *et al.*, 2004a; Robinson *et al.*, 2000). It has been proposed that due to the higher content of F<sup>-</sup> in superficial area of enamel, and the covering of pellicle which retards the mineral loss, the acid may penetrate into the deeper layers of enamel to preferentially dissolve more soluble subsurface substances (Matinlinna, 2015; Robinson *et al.*, 1995).

Subsurface lesions may be attributed to the re-deposition of mineral from the deeper dissolved regions (Moreno and Zahradnik, 1974). Together with components from the plaque, three solid phases including HAP, dicalcium phosphate dihydrate (DCPD), and FAP can achieve an equilibrium with the aqueous phase in the pores, leading to remineralisation at the surface zone (**Fig. 2.4**) (Moreno and Zahradnik, 1974). Supersaturation of oral fluids with respect to FAP ( $pK_{sp} = 121.2$ ) is crucial for the maintenance of the surface zone (Buzalaf *et al.*, 2011; Miura *et al.*, 1993), and more supersaturated the solution with respect to FAP, thicker the surface layer will be (Kidd, 2005). A natural enamel carious lesion has been reported to have a surface layer with a thickness of surface zone in the range of 35 ~ 130  $\mu\text{m}$  (Cochrane *et al.*, 2012).

#### 2.2.3 Epidemiology of Dental Caries

It has been reported that, in 2012, 60 ~ 90 % of children in school and almost 100 % of adults experience dental cavitation worldwide (Moreira, 2012). Further, approximately 92 % of the adults aged 20 to 64 have been reported to have dental decay in the permanent teeth, while 42 % of the children with age 2 to 11 had caries in their deciduous teeth (NIH, 2014). The worldwide average of DMFT (number of permanent teeth decayed, missing and filled teeth) is  $2.11 \pm 1.32$  (Moreira, 2012). Even though there has been a dramatic decline in DMFT number

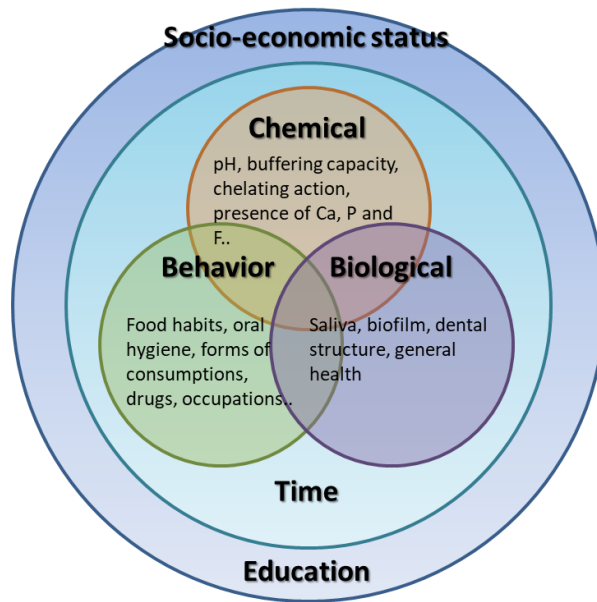
and prevalence for the past several decades (Moreira, 2012), dental caries is still a prevalent oral disease in several countries including USA, UK, China, Brazil, Mexico, Norway, Argentina and Taiwan (Bagramian *et al.*, 2009).

## 2.3 Dental Erosion

Dental erosion is defined as the loss of dental hard tissue through chemical dissolution by acids of non-bacterial origin (Amaechi and Higham, 2005; Lussi, 2006b; Magalhaes *et al.*, 2009a). It is a surface phenomenon showing bulk substance loss, together with a smaller softened surface layer (Magalhaes *et al.*, 2011).

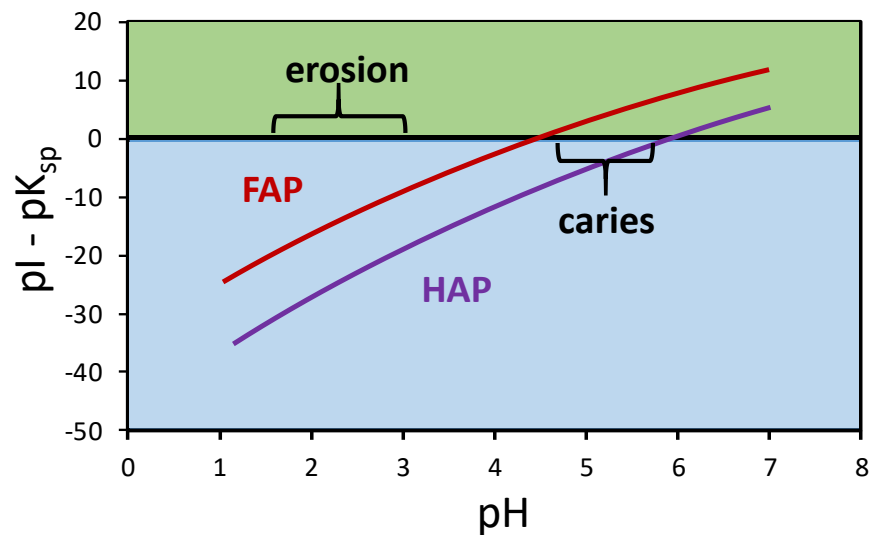
### 2.3.1 Aetiology of Dental Erosion

Dental erosion is a multi-factorial disease, whose development involves the direct interaction between the tooth surface and the erosive solution (Lussi, 2006a). Further, personal habits and lifestyles can affect the development of dental erosion (Lussi, 2006a; Donovan, 2011; Magalhaes *et al.*, 2009b; Gupta *et al.*, 2009). It has been proposed that the determinant factors of the dental erosion progression include chemical, biological and behaviour factors, while physiologic health, educational level and socio-economic status are the modifying factors (**Fig 2.5**) (Donovan, 2011; Magalhaes *et al.*, 2009b; Meurman and ten Cate, 1996). In this section, the chemical factors are discussed.



**Figure 2.5** - Causal factors of erosion (Adapted from Magalhaes et al., 2009b).

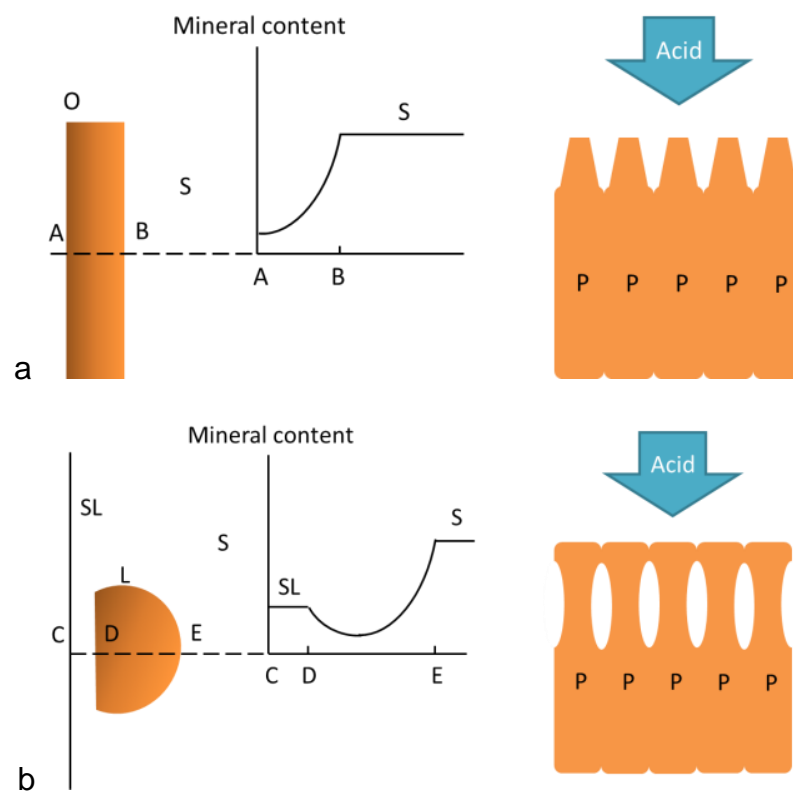
### 2.3.2 Chemistry of Dental Erosion



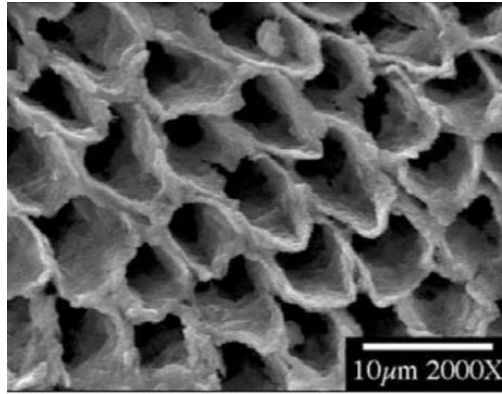
**Figure 2.6** - Degree of saturation plotted against pH with respect to HAP and FAP at certain salivary concentration. FAP can still be formed under carious condition while neither HAP or FAP can be formed under erosive pH (Adapted from Meurman and ten Cate, 1996).

Dental erosion is caused by much lower pH of acids than caries, below the critical pH of FAP (= 4.5) (**Fig. 2.6**) (Magalhaes et al., 2009b; Meurman and ten Cate,

1996). Therefore, as the erosive lesion is developed in a solution under-saturated with respect to both HAP and FAP, no surface layer can be formed in the erosive lesion (**Fig. 2.7**) (Arends and ten Cate, 1981; Larsen, 1974; Larsen, 1990). After erosive acid comes into contact with enamel, the dissociated  $H^+$  dissolves enamel crystals, initially from the enamel sheath area to prism core, and subsequently diffuses to the inter-prismatic area (Donovan, 2011; Lussi, 2006a). This results in a “honeycomb” appearance in prismatic enamel (**Fig. 2.8**) (Lussi, 2006b; Wang *et al.*, 2006).



**Figure 2.7** - (a) Schematic of erosive lesion: O = outer surface; S = sound enamel. (b) Schematic of carious lesion: SL = surface layer; L: lesion; P: prisms (Adapted from Arends and ten Cate, 1981).



**Figure 2.8** – Honeycomb erosion lesion (From Wang *et al.*, 2006).

Erosive acids can be categorised into extrinsic acids such as fresh fruits, fruit juice, soft drinks, acidic mouth rinse, acidic drugs and acidic industrial vapour (Linnett and Seow, 2001; Richards, 2016; Shaw and Smith, 1999; Ren, 2011), and intrinsic acids such as gastric contents (Linnett and Seow, 2001; Shaw and Smith, 1999). Fruits commonly have carboxylic and citric acids, and vinegar has acetic acid, while carbonic and phosphoric acids are usually present in soft drinks (Abou Neel *et al.*, 2016; White *et al.*, 2001). It has been proposed that the pH of extrinsic acids varies between 2.5 ~ 4.0, while that of gastric acid is about 1.2 (Magalhaes *et al.*, 2009b). However, pH is not the only indicator of erosive potential, factors like type of acid, titratable acidity (buffering capacity),  $\text{Ca}^{2+}$ ,  $\text{PO}_4^{3-}$  and  $\text{F}^-$  concentrations, and chelating properties are all elements for erosive potential (Lussi, 2006b; ten Cate and Imfeld, 1996).

Titratable acidity represents the amount of the actual  $\text{H}^+$  concentration available to interact with the dental mineral. The greater titratable acidity is, the harder for saliva to neutralise the pH (Linnett and Seow, 2001; Singh and Jindal, 2010). Different from pH measuring only the dissociated ions in a solution, titratable acidity also measures the erosive potential of bound compounds, giving a more comprehensive view of the potential acidity of a solution (Cairns *et al.*, 2002; Shellis *et al.*, 2014).

After acids dissociate into  $\text{H}^+$  and acid anions, the combination of  $\text{CO}_3^{2-}$  and  $\text{PO}_4^{3-}$  with  $\text{H}^+$  in conjunction with the complexation of  $\text{Ca}^{2+}$  with anions lead to the softening of an enamel surface (Shellis *et al.*, 2014). The strength of acids is determined by the acid dissociation constant ( $K_a$ ), describing how complete the

acids dissociate. Whereas, the strength of anion-calcium interaction is determined by stability constant (K), describing how strong the binding established between anion and calcium (*i.e.*, chelating ability) (Lussi, 2006a; Shellis *et al.*, 2014). Every acid has different strengths of these properties. For acetic acid, it has lower erosive potential than lactic acid, as lactic acid dissociates more readily to release more H<sup>+</sup>, and the lactate-calcium interaction is stronger than acetate-calcium interaction, leading to a stronger chelating effect (Lussi *et al.*, 1993; Shellis *et al.*, 2014).

The other chemical factor associated with erosive potential is the degree of saturation with respect to the enamel mineral. This factor is associated with the concentrations of Ca<sup>2+</sup>, PO<sub>4</sub><sup>3-</sup> and F<sup>-</sup> in the solution. For example, soft drinks enriched with calcium and phosphate salts have been shown to have a protective effect against dental erosion on the teeth (Hara and Zero, 2008; Lussi, 2006b).

### 2.3.3 Epidemiology of Dental Erosion

Dental erosion is a common oral disease and a serious public health issue, which is widespread in developed countries such as United Kingdom, Sweden, Canada and the United States (Higham, 2014; Ren, 2011). Several studies have suggested that preschool children between 2 ~ 5 years old had a prevalence of erosion of 6 ~ 50 %, while school-aged children had a prevalence of 20 ~ 100 %, and adults aged between 18 and 88 years had a prevalence of 4 % ~ 82 % (Lussi, 2006b; Higham, 2014). In the UK, 77 % of 20 ~ 25-year-olds have been reported to have erosion (Abou Neel *et al.*, 2016).

It has been reported that both the prevalence and the incidence of dental erosion, especially in adolescences, has increased recently (Donovan, 2011; Gupta *et al.*, 2009; Linnett and Seow, 2001; Shaw and Smith, 1999), which might arise from the increasing consumption of acidic diets such as soft drinks and fruit juices, and the growing number of people suffering from reflux of gastric content (Donovan, 2011; Lussi, 2006a; ten Cate and Imfeld, 1996). In 2010, a Chinese study reported that dental erosion in 12 to 13-year-old school children is



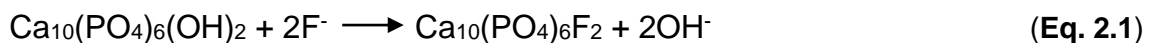
becoming a significant problem, which is in need of an effective solution (Wang *et al.*, 2010).

## 2.4 Role of Fluoride in Enamel Demineralisation

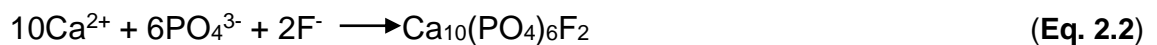
Fluoride was introduced into dentistry almost 80 years ago and is considered to be the major reason for the drastic decline in the caries prevalence for the past decades (Bratthall *et al.*, 1996; ten Cate, 2013). Multiple fluoride supplements have been used for more than 70 years and can be found in various forms, including drinking water (0.5 ~ 1 ppm), dentifrices (100 ~ 1500 ppm), mouthwashes (250 ~ 500 ppm), and gels and varnishes (> 5000 ppm) (Buzalaf *et al.*, 2011; Hellwig and Lennon, 2004; Li *et al.*, 2014; Mohammed *et al.*, 2014a; ten Cate *et al.*, 2008; Twetman *et al.*, 2003).

The inhibitory mechanism of F<sup>-</sup> on demineralisation of HAP involves three modes of interactions (Rosin-Grget *et al.*, 2013):

1) Ionic exchange:



2) Crystal growth:



3) HAP reaction with F<sup>-</sup> resulting in CaF<sub>2</sub> formation:



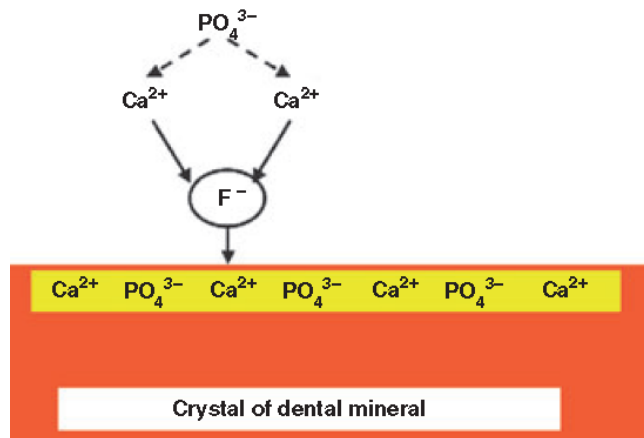
It has been suggested that the **Eq. 2.1** and **Eq. 2.2** take place following long-term exposure to low concentrations of fluoride solution (0.01 ~ 100 ppm), while crystal growth will occur when the solution is supersaturated with FAP ( $K_{sp} = 10^{-121}$ ). Both systemic and topical fluoride sources can lead to these two processes (Cury and

Tenuta, 2009; Rosin-Grget and Lincir, 2001). On the other hand, the formation of  $\text{CaF}_2$  ( $K_{sp} = 3 \times 10^{-10.4}$ ) (**Eq. 2.3**) takes place in solution with higher concentrations of fluoride ( $> 100$  ppm at pH 5.0;  $> 300$  ppm at pH 7.2) (McCann, 1968; ten Cate, 1997), which usually results from topical fluoride sources (Mohammed *et al.*, 2013; Rosin-Grget *et al.*, 2013; ten Cate and Featherstone, 1991). At the higher fluoride concentrations, **Eq. 2.1** and **Eq. 2.2** play minor roles, while **Eq. 2.3** accounts for the major reaction (Rosin-Grget *et al.*, 2013; Yamaga *et al.*, 1972). An *in vitro* study found that, under a pH 4.0 acid challenge, when  $[\text{F}^-]$  was below 45 ppm, FAP (or FHA) was predominantly formed in enamel surface, whereas  $\text{CaF}_2$  was predominantly formed only when the  $[\text{F}^-]$  was above 135 ppm (Mohammed *et al.*, 2013).

Both incorporated fluorides (*e.g.*, fluorapatite; FAP and fluorohydroxyapatite; FHA), and deposited fluorides (*e.g.*,  $\text{CaF}_2$ ), can contribute to the inhibition of enamel demineralisation (Rosin-Grget *et al.*, 2013; ten Cate, 1997; White and Nancollas, 1990). As  $\text{F}^-$  has a better “fit” into the HAP lattice compared to the larger asymmetric  $\text{OH}^-$ , FAP (or FHA) has higher thermal and chemical stability than HAP (Robinson *et al.*, 2004). Therefore, FAP (or FHA) formed in the enamel surface is acid-resistant (Robinson, 2009). As the formation of pure FAP is difficult in a clinical situation, FHA formation is usually more likely (Mei *et al.*, 2018).

On the other hand,  $\text{CaF}_2$  formed on the enamel surface can inhibit the acid attack as a protective barrier (Magalhaes *et al.*, 2011). The formation of  $\text{CaF}_2$  requires slight dissolution of the enamel surface in order to provide the necessary  $\text{Ca}^{2+}$ , followed by the reaction with  $\text{F}^-$  (Buzalaf *et al.*, 2011). The  $\text{CaF}_2$  formed following interaction between fluoride and enamel (mainly HAP) is granular due to the adsorption of  $\text{HPO}_4^{2-}$  around  $\text{CaF}_2$  (Barbier *et al.*, 2010; Rolla, 1988). This granular  $\text{CaF}_2$  is called “ $\text{CaF}_2$ -like globule”, which is less soluble and dissolves more slowly than pure  $\text{CaF}_2$  during acid attacks (White and Nancollas, 1990). Therefore,  $\text{CaF}_2$  (or  $\text{CaF}_2$ -like globule) can also act as a pH-driven reservoir of  $\text{F}^-$ , which favours the formation of FAP (or FHA) (ten Cate, 2013; Vogel, 2011). It has been proposed that under an acid challenge,  $\text{F}^-$  in enamel fluid, dissolved from  $\text{CaF}_2$ , can be adsorbed onto the enamel surface (Featherstone, 1999). These adsorbed  $\text{F}^-$  attract  $\text{Ca}^{2+}$  and  $\text{PO}_4^{3-}$  from oral fluids to form FAP (or FHA), which

protects the mineral of a tooth (**Fig. 2.9**) (Arends and Christoffersen, 1990; Featherstone, 2008).



**Figure 2.9** – Schematic representation of  $\text{F}^-$  absorb onto enamel surface, which attract  $\text{Ca}^{2+}$  and  $\text{PO}_4^{3-}$ , to form an insoluble FAP (or FHA) veneer (From Featherstone, 2008).

## Chapter 3 TOPICAL TREATMENTS WITH SILVER COMPOUNDS FOR PROTECTION AGAINST ENAMEL DEMINERALISATION

### 3.1 Use of Silver Compounds in Dentistry

Minimal Intervention Dentistry (MID) has been advocated since the early 1990s, in order to keep the teeth functional for a whole lifetime. In contrast to traditional clinical treatment, the aim of MID is to reduce the need of tissue cutting and save as much healthy tissue as possible by enhancement of cariostatic effect, and by minimally invasive restoration (Frencken *et al.*, 2012; Murdoch-Kinch and McLean, 2003; Wilson, 2007). Even though fluoride has pronounced remineralisation ability and is still the cornerstone of MID for dental caries management (Hellwig and Lennon, 2004), the fluoride concentration in the oral cavity is not enough to inhibit cariogenic bacterial activities (Tenuta and Cury, 2010). Recently, the use of silver compounds for dental caries has been a growing trend in dentistry due to their anti-bacterial properties and non-invasive ways of applications (Horst *et al.*, 2016; Wilson, 2007). Common silver products used in dentistry include silver nitrate ( $\text{AgNO}_3$ ), silver fluoride ( $\text{AgF}$ ) and SDF ( $\text{Ag}[\text{NH}_3]_2\text{F}$ ) (Peng *et al.*, 2012).  $\text{Ag}[\text{NH}_3]_2\text{F}$  has been the most popular silver compound used in the clinical practice lately, whose treatment is effective in arresting and preventing dental caries both in deciduous and permanent dentitions (Peng *et al.*, 2012; Yamaga *et al.*, 1972).

In terms of cariostatic mechanisms of silver compounds, their anti-bacterial mechanisms have been extensively investigated (Lansdown, 2002; Lansdown, 2006; Russell and Hugo, 1994; Thibodeau *et al.*, 1978). However, even though numerous studies have investigated the effects of silver compounds on dental minerals (Green, 1989; Liu *et al.*, 2012b; Lou *et al.*, 2011; Mei *et al.*, 2017; Miller, 1905; Punyanirun *et al.*, 2018), the inhibitory mechanisms of topical treatments with  $\text{AgNO}_3$ ,  $\text{AgF}$  and  $\text{Ag}[\text{NH}_3]_2\text{F}$  on demineralisation of dental mineral remain obscure.

In clinical practice, treatments with silver compounds are topically applying the silver compounds on the lesions using a micro-brush for a certain application time (Horst *et al.*, 2016). Therefore, to investigate the effects of the topical treatments with silver compounds on demineralisation of dental mineral *in vitro*, a *real-time* methodology able to allow “as if clinical” topical treatments with silver compounds on dental mineral, *i.e.*, following a clinical protocol, needs to be developed.

### 3.2 Topical Treatments with Silver Nitrate for Protection against Enamel Demineralisation

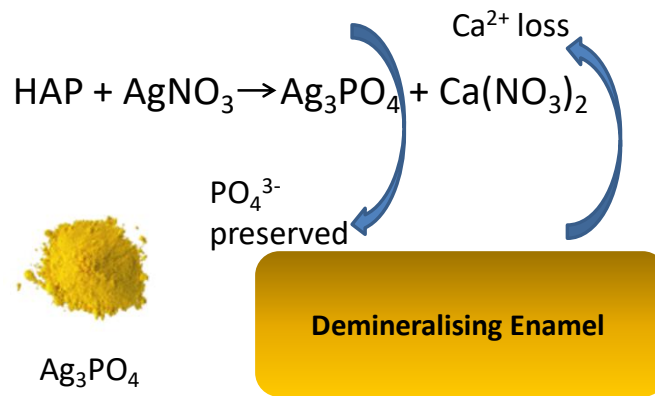
Since the 1840s, silver nitrate ( $\text{AgNO}_3$ ) (pH 4.2) has been used to reduce the prevalence of caries in deciduous dentition (Peng *et al.*, 2012; Lou *et al.*, 2011). Other applications of  $\text{AgNO}_3$  include caries prevention in permanent dentition, and as a desensitising agent. In 1917, Howe developed ammoniacal silver nitrate ( $\text{Ag}[\text{NH}_3]_2\text{NO}_3$ , so-called Howe’s solution), and this has been subsequently used in caries management (Rosenblatt *et al.*, 2009).

$\text{AgNO}_3$  was one of the first silver compounds topically applied to manage dental caries due to its antibacterial property. It has been concluded that the major antibacterial component of silver compounds was the  $\text{Ag}^+$  (Thibodeau *et al.*, 1978). 10 ~ 40 ppm of  $\text{Ag}^+$  has been shown to be able to destroy most of the pathogens (Lansdown, 2006). Further, it was found that 20 ppm  $\text{Ag}^+$  is lethal to *Streptococcus mutans* (S.m.) after contact of 3 to 4 h, while 200 ppm  $\text{Ag}^+$  is instantaneously lethal to S.m. (Thibodeau *et al.*, 1978).

Even though the antibacterial property of  $\text{AgNO}_3$  is well-understood, its effects on dental mineral are still unclear. The interaction between  $\text{AgNO}_3$  and enamel mineral has been suggested to be (Yamaga *et al.*, 1972):



and shown diagrammatically in **Fig 3.1**:



**Figure 3.1** – Reaction between  $\text{AgNO}_3$  and HAP. The  $\text{PO}_4^{3-}$  released from demineralising enamel can be preserved by the formation of  $\text{Ag}_3\text{PO}_4$  (Adapted from Yamaga *et al.*, 1972).

As the  $\text{Ag}_3\text{PO}_4$  (yellow) is insoluble (solubility =  $6.5 \times 10^{-4}$  g/100 mL) (Lewis, 1920) (Eq 3.1 and Fig. 3.1), it has been proposed that the formation of a “protective barrier” composed of insoluble  $\text{Ag}_3\text{PO}_4$  following treatment with  $\text{AgNO}_3$  can inhibit the demineralisation of dental mineral (Lou *et al.*, 2011; Yamaga *et al.*, 1972). On the other hand, the formation of soluble  $\text{Ca}(\text{NO}_3)_2$  (solubility = 121.2 g/100 mL) has been proposed to result in the loss of  $\text{Ca}^{2+}$  from the treated dental mineral (Yamaga *et al.*, 1972).

A study found that following mixing HAP powders with  $\text{AgNO}_3$ , the colour of the mixture changed from white to yellow immediately due to the formation of yellow  $\text{Ag}_3\text{PO}_4$  particles (Lou *et al.*, 2011). Gradually, these yellow particles turned black due to the chemical reduction of yellow  $\text{Ag}_3\text{PO}_4$  to black metallic silver. The formation of black metallic silver is the cause of the black staining of lesions topically treated with silver compounds, which is the major disadvantage of silver compound treatments (Peng *et al.*, 2012). However, even though  $\text{Ag}_3\text{PO}_4$  was confirmed to be formed in the mixture of HAP powders with  $\text{AgNO}_3$ , the formation of  $\text{Ag}_3\text{PO}_4$  following the topical treatment with  $\text{AgNO}_3$  on enamel mineral using a micro-brush has not been confirmed. Further, any protective effect of the  $\text{Ag}_3\text{PO}_4$  has not been investigated.

Other than the previously proposed protective effect from  $\text{AgNO}_3$  treatment (Yamaga *et al.*, 1972), a study found that the  $\text{Ca}^{2+}$  in HAP could be substituted by  $\text{Ag}^+$  after immersion of HAP in  $\text{AgNO}_3$  (Ling Feng *et al.*, 1998). Moreover, it has been reported that the solubility of the  $\text{Ag}^+$  substituted HAP disc under pH

4.2 acid attack increased with increasing incorporation of Ag<sup>+</sup> in the HAP (Singh *et al.*, 2011). This indicates that Ag<sup>+</sup> substituted HAP was more susceptible to acid challenge than HAP. Further studies are required to see whether a similar dose-response effect of Ag<sup>+</sup> can also occur, influencing the demineralisation of human enamel.

### **3.3 Topical Treatments with Silver Fluoride for Protection Against Enamel Demineralisation**

Since the 1970s, silver fluoride (AgF) (pH 11.0) has been used to treat dental caries. AgF is a colourless solution comprising silver and fluoride. The applications of AgF can disturb the growth and metabolism of the bacteria in the biofilm (Shah *et al.*, 2014). A series of clinical trials were carried out using 40 wt% (3.16 M) AgF followed by topical application of 10 wt% SnF<sub>2</sub> as a reducing agent in an Australian school (Craig *et al.*, 1981; Craig *et al.*, 1987; Green, 1989). It was shown that this combination treatment was more effective than the treatment with 10 wt% SnF<sub>2</sub> alone, which could arrest proximal and occlusal caries in deciduous dentitions and prevent the development of caries in first permanent molars. It has been suggested that the application of AgF can facilitate the formation of both insoluble Ag<sub>3</sub>PO<sub>4</sub> and CaF<sub>2</sub> (solubility = 0.0015 g/ 100 mL), and therefore the loss of both PO<sub>4</sub><sup>3-</sup> and Ca<sup>2+</sup> from enamel mineral can be inhibited (Peng *et al.*, 2012; Yamaga *et al.*, 1972). However, no study has been carried out to confirm this theoretical cariostatic mechanism.

Unfortunately, many studies claiming to examine the effects of AgF, are actually using Ag[NH<sub>3</sub>]<sub>2</sub>F (Peng *et al.*, 2012; Rosenblatt *et al.*, 2009).

### 3.4 Topical Treatments with SDF for Protection Against Enamel Demineralisation

As the storage of topical AgF agent for a long period is not easy due to photosensitivity of Ag<sup>+</sup> (Liu *et al.*, 2012c; Zhao *et al.*, 2017a), Ag[NH<sub>3</sub>]<sub>2</sub>F (Silver Diammine Fluoride, SDF) was developed. The ammonia in SDF helps to stabilise Ag<sup>+</sup> in the solution by forming a silverdiammine complex, [Ag(NH<sub>3</sub>)<sub>2</sub>]<sup>+</sup>, through reversible reaction (Liu *et al.*, 2012b). Ag[NH<sub>3</sub>]<sub>2</sub>F is also a colourless solution comprising silver and fluoride but less alkaline (pH ~ 10.0) (Mei *et al.*, 2013a).

Since the 1970s, Ag[NH<sub>3</sub>]<sub>2</sub>F has been accepted as a therapeutic agent for anti-caries function by the central Pharmaceutical Council of the Ministry of Health and Welfare in Japan (Yamaga *et al.*, 1972). However, the applications of Ag[NH<sub>3</sub>]<sub>2</sub>F are not common in western countries (Gao *et al.*, 2016). Recently, Ag[NH<sub>3</sub>]<sub>2</sub>F has drawn attention from dental researchers due to its profound effectiveness in preventing and arresting dental caries, and its non-invasive method of application (Frencken *et al.*, 2012; Mei *et al.*, 2017). In 2015, Ag[NH<sub>3</sub>]<sub>2</sub>F entered the US market shortly after being approved for clinical use by United State Food and Drug Administration (FDA) in 2014 (Horst *et al.*, 2016). In 2016, a Current Dental Terminology (CDT) code was approved for Ag[NH<sub>3</sub>]<sub>2</sub>F to be used in arresting dental caries (Horst *et al.*, 2016).

Ag[NH<sub>3</sub>]<sub>2</sub>F has been regarded as an efficient, affordable, effective and safe therapeutic agent across ages, whose application for caries control conforms to the World Health Organization's Millennium Goals, and the US Institute of Medicine's criteria for 21<sup>st</sup> Century medical care (Horst *et al.*, 2016). Further, the low cost and the simplicity of Ag[NH<sub>3</sub>]<sub>2</sub>F treatment on dental caries make it appropriate to be used in children from low-income families living in underprivileged and remote areas (Chu and Lo, 2008b; Contreras *et al.*, 2017; Fung *et al.*, 2013). In terms of caries in permanent teeth of adults, Ag[NH<sub>3</sub>]<sub>2</sub>F can also be used for patients who cannot tolerate conventional treatments, or for patients with extreme risks of caries such as salivary dysfunction (Horst *et al.*, 2016).



It has been proposed that the use of  $\text{Ag}[\text{NH}_3]_2\text{F}$  is more effective in controlling carious lesions than other minimally invasive topical treatments such as fluoride varnish (Crystal and Niederman, 2016). However, similar to other silver compound treatments, the major disadvantage of topical treatment with  $\text{Ag}[\text{NH}_3]_2\text{F}$  is the black staining of the treated lesion (**Fig. 3.2**) (Horst *et al.*, 2016; Mei *et al.*, 2016). A new  $\text{Ag}[\text{NH}_3]_2\text{F}$  product, which is claimed to be able to treat lesions without the black staining has been issued by Riva Star (SDI Ltd, Australia). The product comprises a silver capsule containing 3.16 M  $\text{Ag}[\text{NH}_3]_2\text{F}$ , and a green capsule containing saturated solution of potassium iodine (SSKI). The concept is that the application of SSKI following treatment with  $\text{Ag}[\text{NH}_3]_2\text{F}$  will remove excessive  $\text{Ag}^+$  by forming white  $\text{AgI}$ , thereby eliminating the possibility of black staining (Ngo *et al.*, 2002).



**Figure 3.2** – Black staining of  $\text{Ag}[\text{NH}_3]_2\text{F}$  treated teeth (From Mei *et al.*, 2016).

### 3.4.1. Clinical Effects of Topical Treatments with SDF on Enamel Caries

Many  $\text{Ag}[\text{NH}_3]_2\text{F}$  studies have been carried out to investigate its effectiveness in clinical practice (Contreras *et al.*, 2017). These studies cover a wide range from coronal caries in primary teeth and permanent teeth, to root caries (**Appendix A**). In this section, clinical studies of  $\text{Ag}[\text{NH}_3]_2\text{F}$  topical treatments on coronal caries are discussed.

Amongst all the different concentrations of Ag[NH<sub>3</sub>]<sub>2</sub>F available, including 12 wt% (0.75 M), 38 wt% (2.36 M) and 50.9 wt% (3.16 M) Ag[NH<sub>3</sub>]<sub>2</sub>F (Fung *et al.*, 2013; SDI, 2016a), 38 wt% is the most commonly used (Horst *et al.*, 2016). An annual application of 38 wt% Ag[NH<sub>3</sub>]<sub>2</sub>F has been reported to be able to prevent pit and fissure caries in permanent 1<sup>st</sup> molars (Liu *et al.*, 2012a). Further, Llodra *et al.* found that a biannual 38 wt% Ag[NH<sub>3</sub>]<sub>2</sub>F application could reduce and prevent caries in both deciduous teeth and permanent 1<sup>st</sup> molars (Llodra *et al.*, 2005). Recently, a randomised controlled trial (RCT) concluded that the topical application of 38 wt% Ag[NH<sub>3</sub>]<sub>2</sub>F is effective and safe in arresting cavities in preschool children (Milgrom *et al.*, 2018). Chu *et al.* reported a case about application of 38 wt% Ag[NH<sub>3</sub>]<sub>2</sub>F on rampant caries in permanent dentition (Chu *et al.*, 2014); A 14-year-old boy with chronic oral graft versus host disease (GVHD) was in need of treatment of multiple cavitated caries. After topical application of 38 wt% Ag[NH<sub>3</sub>]<sub>2</sub>F followed by restoration with temporary dental material, the prognosis was good without any pain perceived.

However, despite the fact that there are multiple concentrations of Ag[NH<sub>3</sub>]<sub>2</sub>F products on the market, the dose-response effects of these products have not been investigated. Further, even though the compositions of all the commercial Ag[NH<sub>3</sub>]<sub>2</sub>F products were provided in their safety data sheets (SDS), the manufacture processes of the products are market secrets. Therefore, studies can be done to compare the effects of the topical treatments with these products with the effects of the same concentration of laboratory-prepared Ag[NH<sub>3</sub>]<sub>2</sub>F on the demineralisation of dental mineral.

### 3.4.2 Establishment of Standard Protocol for Topical Treatment with SDF

Several studies have shown that Ag[NH<sub>3</sub>]<sub>2</sub>F is more effective in caries arrest at 38 wt% (2.36 M) than 12 wt% (0.75 M) (Fung *et al.*, 2016; Fung *et al.*, 2018). Furthermore, randomised controlled trials (RCTs) have found that biannual application of 38 wt% Ag[NH<sub>3</sub>]<sub>2</sub>F application is more effective than annual and consecutive three weekly Ag[NH<sub>3</sub>]<sub>2</sub>F applications in caries arrest (Duangthip *et*

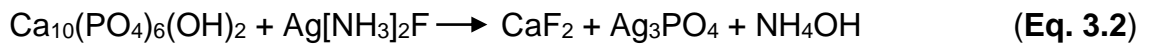
*al.*, 2016; Fung *et al.*, 2016; Fung *et al.*, 2018; Yee *et al.*, 2009; Zhi *et al.*, 2012). Therefore, based on the current evidence (Duangthip *et al.*, 2017; Fung *et al.*, 2016; Fung *et al.*, 2018), the biannual application of 38 wt% Ag[NH<sub>3</sub>]<sub>2</sub>F is the most effective protocol.

For Ag[NH<sub>3</sub>]<sub>2</sub>F application, application times from 10 sec to 3 min have been used in most of the clinical studies. In 2016, University of California San Francisco (UCSF) proposed that the application time of Ag[NH<sub>3</sub>]<sub>2</sub>F should be more than 1 min for the optimal effectiveness (Horst *et al.*, 2016). They also recommended that Ag[NH<sub>3</sub>]<sub>2</sub>F treated lesion should be rinsed. However, concerns have been expressed about losing effectiveness by rinsing (Horst, 2018). Another review suggested that a 30 ~ 60 sec Ag[NH<sub>3</sub>]<sub>2</sub>F application followed by air-drying provides the best results for caries arrest (Crystal and Niederman, 2016). Lately, in 2017, American Academy of Paediatric Dentistry (AAPD) announced a guideline of using 1 min 38 wt% Ag[NH<sub>3</sub>]<sub>2</sub>F application followed by gentle air-drying in arresting carious primary teeth. Further, they expected similar cariostatic effectiveness of Ag[NH<sub>3</sub>]<sub>2</sub>F could be exerted on carious permanent teeth through the same protocol (Crystal *et al.*, 2017). Therefore, 1 min application followed by air-drying should be the best procedure for Ag[NH<sub>3</sub>]<sub>2</sub>F treatment.

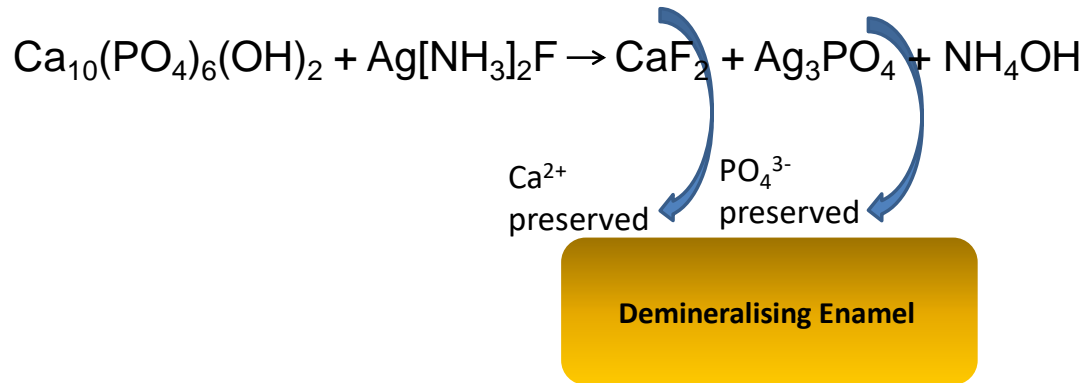
### 3.4.3 Cariostatic Mechanisms of SDF

Even though several possible cariostatic mechanisms of Ag[NH<sub>3</sub>]<sub>2</sub>F have been suggested (Mei *et al.*, 2018; Zhao *et al.*, 2017a), to date, its cariostatic mechanism is still unclear (Mei *et al.*, 2017). It has been proposed that as fluoride in Ag[NH<sub>3</sub>]<sub>2</sub>F inhibits mineral loss, and silver in Ag[NH<sub>3</sub>]<sub>2</sub>F inhibits activities of cariogenic bacteria, the development of dental caries can be arrested (Rosenblatt *et al.*, 2009). Actions of Ag[NH<sub>3</sub>]<sub>2</sub>F on dental mineral, cariogenic bacteria and dentinal organic content (**Appendix A**) have all been studied, and the action of Ag[NH<sub>3</sub>]<sub>2</sub>F on enamel mineral is discussed in this section.

The interaction between Ag[NH<sub>3</sub>]<sub>2</sub>F and enamel mineral has been suggested to be (Yamaga *et al.*, 1972):



and shown diagrammatically in **Fig 3.3**:



**Figure 3.3** –. Reaction between  $\text{Ag}[\text{NH}_3]_2\text{F}$  and HAP. The  $\text{Ca}^{2+}$  and  $\text{PO}_4^{3-}$  released from demineralising enamel can be preserved by the formation of  $\text{CaF}_2$  and  $\text{Ag}_3\text{PO}_4$ , respectively (Adapted from Yamaga *et al.*, 1972).

As both insoluble  $\text{CaF}_2$  (solubility =  $1.6 \times 10^{-3}$  g/100 mL) and  $\text{Ag}_3\text{PO}_4$  (solubility =  $6.5 \times 10^{-4}$  g/100 mL) are formed following  $\text{Ag}[\text{NH}_3]_2\text{F}$  application (**Eq. 3.2**), it has been proposed that both  $\text{Ca}^{2+}$  and  $\text{PO}_4^{3-}$  released from dental mineral, can be preserved by the formation of a protective barrier composed of insoluble  $\text{CaF}_2$  and  $\text{Ag}_3\text{PO}_4$  (**Fig. 3.3**). Furthermore, the formed  $\text{CaF}_2$  has been proposed to act as a reservoir of  $\text{F}^-$  for the formation of acid-resistant FAP (or FHA) (Yamaga *et al.*, 1972).

It has been reported that  $\text{CaF}_2$  and  $\text{Ag}_3\text{PO}_4$  were formed in enamel powders mixed with  $\text{Ag}[\text{NH}_3]_2\text{F}$  (Zhao *et al.*, 2017a). Further, an study found that the mineral density of incipient enamel caries in permanent premolars treated with  $\text{Ag}[\text{NH}_3]_2\text{F}$  was increased (Punyanirun *et al.*, 2018). These findings suggest the ability of  $\text{Ag}[\text{NH}_3]_2\text{F}$  application in preserving both  $\text{Ca}^{2+}$  and  $\text{PO}_4^{3-}$  of the treated dental mineral. However, it has been proposed that  $\text{Ag}_3\text{PO}_4$  can be dissolved in ammonium (Firsching, 1961), which may affect the  $\text{Ag}_3\text{PO}_4$  formation following  $\text{Ag}[\text{NH}_3]_2\text{F}$  topical treatment. Further, a study reported that following mixing HAP powders with  $\text{Ag}[\text{NH}_3]_2\text{F}$ , metallic silver rather than  $\text{Ag}_3\text{PO}_4$  was found, and the  $\text{CaF}_2$ -like globules disappeared after rinsing with water (Lou *et al.*, 2011). Therefore, the formation of  $\text{Ag}_3\text{PO}_4$  and the cariostatic efficacy of the formed  $\text{CaF}_2$  are questionable.

Recently, an *in vitro* study was carried out using calcium phosphate ( $\text{Ca}_3(\text{PO}_4)_2$ ) incubated with low concentrations of  $\text{Ag}[\text{NH}_3]_2\text{F}$  ( $2.36 \times 10^{-3} \sim 2.36 \times 10^{-2}$  M), taking into account the salivary dilution after application (Mei *et al.*, 2017). After incubation at  $37^\circ\text{C}$  for 24 h, fluorohydroxyapatite (FHA, a partially fluoride-substituted HAP) was found using X-ray diffraction (XRD). As a result, they proposed that acid-resistant FHA formation should be a more reasonable explanation for the cariostatic efficacy of treatment with  $\text{Ag}[\text{NH}_3]_2\text{F}$  (Mei *et al.*, 2017).

However,  $\text{Ca}_3(\text{PO}_4)_2$  is stoichiometrically different from HAP and enamel mineral, and XRD is not a suitable technique to differentiate FHA from HAP due to the crystallographic similarity between these two compounds. Therefore, further studies are required to confirm the formation of FHA following topical treatment with  $\text{Ag}[\text{NH}_3]_2\text{F}$  on enamel mineral.  $^{19}\text{F}$  MAS-NMR is one of the few techniques capable of differentiating FHA from HAP, which can be used to identify FHA following  $\text{Ag}[\text{NH}_3]_2\text{F}$  topical treatment on dental mineral (Elsharkawy *et al.*, 2018; Mohammed *et al.*, 2013; White *et al.*, 1994).

## Chapter 4 AIMS AND OBJECTIVES

### 4.1 Aims

1. To develop a real-time methodology to investigate the effects of topical treatments with silver compounds on dental mineral.
2. To investigate the dose-response effects of  $\text{Ag}^+$  in solution on demineralisation of human enamel.
3. To understand the inhibitory mechanisms of topical treatments with silver compounds, including silver nitrate ( $\text{AgNO}_3$ ), silver fluoride ( $\text{AgF}$ ) and SDF ( $\text{Ag}[\text{NH}_3]_2\text{F}$ ), on demineralisation of hydroxyapatite (HAP) discs and human enamel.
4. To investigate the dose-response effects of topical treatments with  $\text{AgNO}_3$ ,  $\text{AgF}$  and  $\text{Ag}[\text{NH}_3]_2\text{F}$  on demineralisation of human enamel.
5. To compare the inhibitory efficacy and effects of topical treatment with a commercial  $\text{Ag}[\text{NH}_3]_2\text{F}$  product with laboratory-prepared  $\text{Ag}[\text{NH}_3]_2\text{F}$  on demineralisation of HAP discs and human enamel.

### 4.2 Objectives

1. Real-time  $\text{Ca}^{2+}$  ion selective electrodes (ISEs) will be used to monitor calcium loss of hydroxyapatite (HAP) discs before and after treatments with increasing  $\text{F}^-$  and  $\text{Zn}^{2+}$  concentrations in order to validate the technique by comparison with the previously reported dose-response studies of demineralisation inhibition using Scanning Microradiography (SMR) (Chapter 6).
2. Real-time scanning microradiograph (SMR) will be used to monitor mineral loss of human enamel under acid challenge in a demineralisation solution containing an increasing concentration of  $\text{Ag}^+$  (Chapter 7).

3.  $\text{Ca}^{2+}$ ,  $\text{Ag}^+$  and  $\text{F}^-$  ISEs, scanning electron microscopy (SEM), energy dispersive X-ray analysis (EDX) and  $^{31}\text{P}$  and  $^{19}\text{F}$  MAS-NMR will be used to investigate the effects of topical treatments with 3.16 M  $\text{AgNO}_3$ , 3.16 M  $\text{AgF}$  and 3.16 M  $\text{Ag}[\text{NH}_3]_2\text{F}$  on the demineralisation of HAP discs and human enamel (Chapter 8 and 10). Also, a Knoop micro-hardness tester will be used to investigate the effects of topical treatments with 3.16 M  $\text{AgNO}_3$ , 3.16 M  $\text{AgF}$  and 3.16 M  $\text{Ag}[\text{NH}_3]_2\text{F}$  on demineralisation of human enamel (Chapter 10).

4.  $\text{Ca}^{2+}$ ,  $\text{Ag}^+$  and  $\text{F}^-$  ISEs, SEM, EDX,  $^{31}\text{P}$  and  $^{19}\text{F}$  MAS-NMR and Knoop micro-hardness tester will be used to investigate the effects of topical treatments with 0.75 M, 2.36 M and 3.16 M of  $\text{AgNO}_3$ ,  $\text{AgF}$  and  $\text{Ag}[\text{NH}_3]_2\text{F}$  on the demineralisation of human enamel (Chapter 10).

5.  $\text{Ca}^{2+}$ ,  $\text{Ag}^+$  and  $\text{F}^-$  ISEs, SEM, EDX and  $^{31}\text{P}$  and  $^{19}\text{F}$  MAS-NMR will be used to investigate the effects of topical treatment with Silver Capsule of Riva Star (SDI Ltd, Australia) on the demineralisation of HAP discs and human enamel (Chapter 8). Also, a Knoop micro-hardness tester will be used to investigate the effects of topical treatment with Silver Capsule of Riva Star on demineralisation of human enamel (Chapter 10).

**PART II: INTRODUCTION OF  
TECHNIQUES USED IN THIS  
STUDY**



## Chapter 5 TECHNIQUES USED IN THIS STUDY

### 5.1 Scanning Microradiography

Scanning microradiography (SMR) is an X-ray attenuation technique, which can monitor the mineral mass of the specimen in real-time (Anderson and Elliott, 1993; Elliott *et al.*, 1994). During the experiment, the specimen is contained in a SMR cell, which is mounted on the SMR stage. Next, the intensity of a 15 µm X-ray beam attenuated by passing through the specimen, is continually measured. The attenuated X-ray intensity is detected, and therefore the mineral mass of the specimen can be calculated by the computer system (**Eq. 5.1**) (Anderson and Elliott, 1993). The SMR cell allows the creation of strictly controlled condition for specific study. For example, by circulating acid through the SMR cell containing enamel or HAP sections (**Fig. 5.1**), many different demineralisation studies have been carried out (*e.g.*, Anderson *et al.*, 1998; Anderson *et al.*, 2004a; Kosoric *et al.*, 2010; Mohammed *et al.*, 2014a; Mohammed *et al.*, 2015).

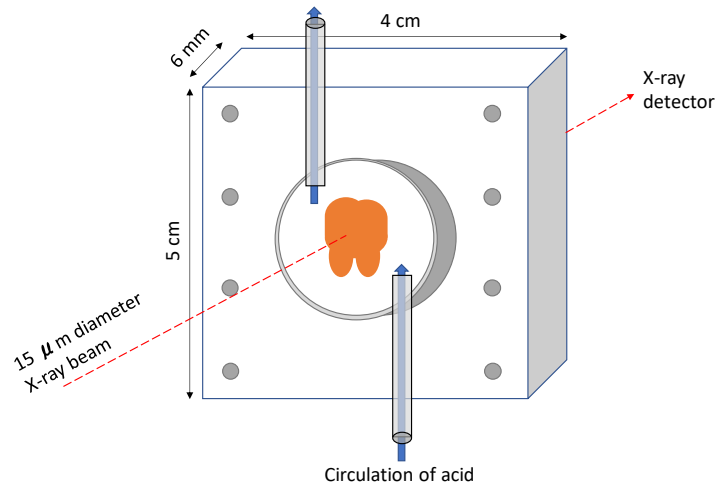
$$I = I_0 \times e^{-\mu_m M} \quad (\text{Eq. 5.1})$$

$I$  = transmitted X-ray intensity

$I_0$  = incident X-ray intensity

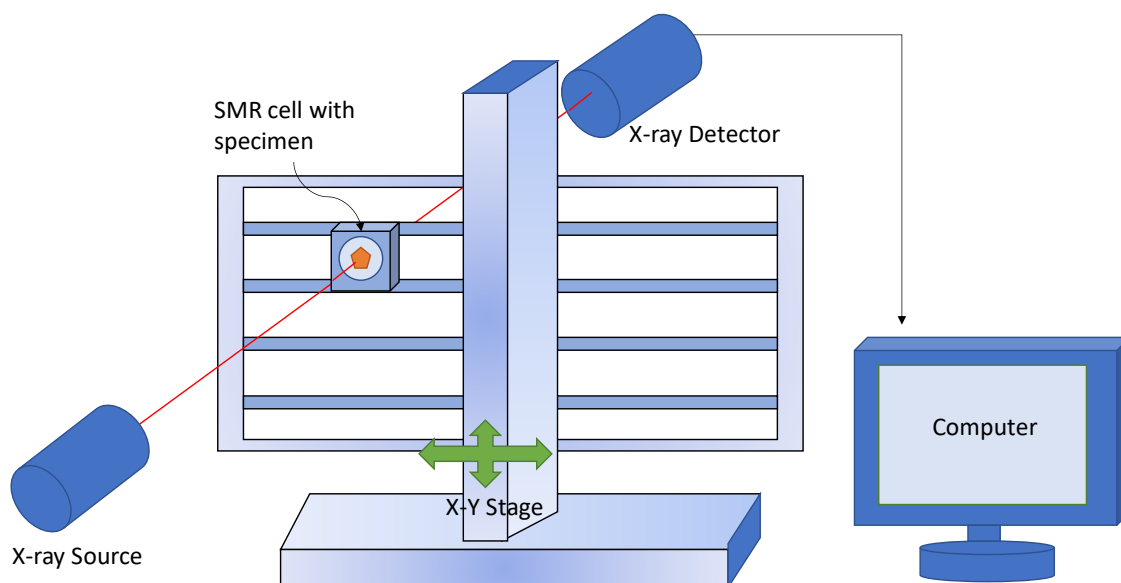
$\mu_m$  = mass absorption coefficient

$M$  = mass per unit area of the specimen (g/cm<sup>2</sup>)



**Figure 5.1** – Schematic representation of a SMR cell containing a specimen.

The SMR apparatus includes SMR cells, SMR stages, an X-ray generator, an X-ray detector and a computer (Anderson and Elliott, 1993). SMR cells are transparent boxes (4 cm X 5 cm X 6 mm) made of polymethyl methacrylate (**Fig. 5.1**). In the centre of each SMR cell, there is a circular chamber, which contains the specimen. The SMR cell is mounted on the SMR stage with screws. The SMR apparatus has X and Y stages which allow the cell to move up to 600 mm horizontally in X-axis and up to 200 mm vertically in Y-axis. The X-ray generator includes a PANalytical® X-ray tube to produce a stable 15 μm X-ray beam using a 15 μm aperture made up of 90 % gold and 10 % platinum. The attenuated X-ray beam after passing through the specimen is then detected by the X-ray detector coupled with a digital spectrometer. Subsequently, the received signal is processed with a digital converter into a sequence of digital values, and the mineral mass of the tested specimen can be obtained (**Fig. 5.2**) (Anderson and Elliott, 1993).



**Figure 5.2** – Schematic representation of the SMR apparatus.

## 5.2 Ion Selective Electrode

An ion selective electrode (ISE) is a potentiometric sensor used as an analytic tool for the concentration (or activity) measurement of a selected free ion in solution (Rundle, 2000). The scientific applications of ISEs are diverse, including pollution monitoring, analysis of agriculture composition, measurement of salt contents in meat, examination of fluoridation of water, detection of corrosive effects in canned foods, determining the constituents of dairy products or preservatives, and laboratory research (Frant, 1994; Oesch *et al.*, 1986). In dentistry, ISEs have been used for the measurement of  $\text{Ca}^{2+}$  activity in oral fluids to evaluate the  $\text{Ca}^{2+}$  concentrations in saliva, dental plaque and plaque fluid (Carey and Vogel, 2000).  $\text{F}^-$  ISEs have been used for the detection of  $\text{F}^-$  concentration in mineral and drinking water, mouthwashes, toothpastes, tea, food, and urine, in order to measure the  $\text{F}^-$  concentrations, which is useful to prevent fluorosis development in humans (Adejumo *et al.*, 2009; Bratovic and Odobasic, 2011; Frant and Ross, 1968; Itota *et al.*, 2004; Kiliçel and Dağ, 2014; Malde *et al.*, 2001; Ruiz-Payana *et al.*, 2005; Villa *et al.*, 2010).

In this study,  $\text{Ag}^+$  ISEs were used to monitor the concentration of  $\text{Ag}^+$  in the solution.  $\text{Ag}^+$  ISEs have not previously been used in dental research.

ISEs can deliver real-time information about the concentration variation of specific ions in complex samples by automatically measuring electronic voltages between two electrodes continuously. The relationship between ion concentration and the voltage reading is defined by the “Nernst equation” which states that this voltage is proportional to the logarithm of the concentration (or activity) (**Eq 5.2**) (Covington and Kenneth, 1979). Therefore, the ISE readings recorded can be converted into concentration units (**Fig 5.3**).

$$\text{Nernst equation: } E = E^0 + \left(\frac{2.303RT}{nF}\right) \times \text{Log}(A) \quad (\text{Eq 5.2})$$

E = total potential in mV

$E^0$  = constant of a given ISE/reference pair

2.303 = conversion factor

R = gas constant (8.314joules/degree/mole)

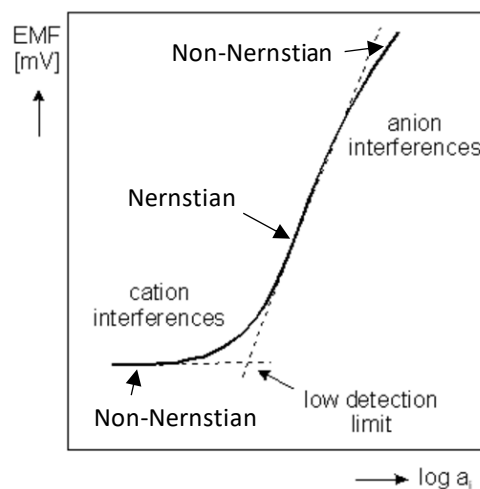
T = absolute temperature (Kelvin)

n = the ionic charge

F = Faraday constant (96500 coulombs)

A = activity (effective ions) of the measured ion

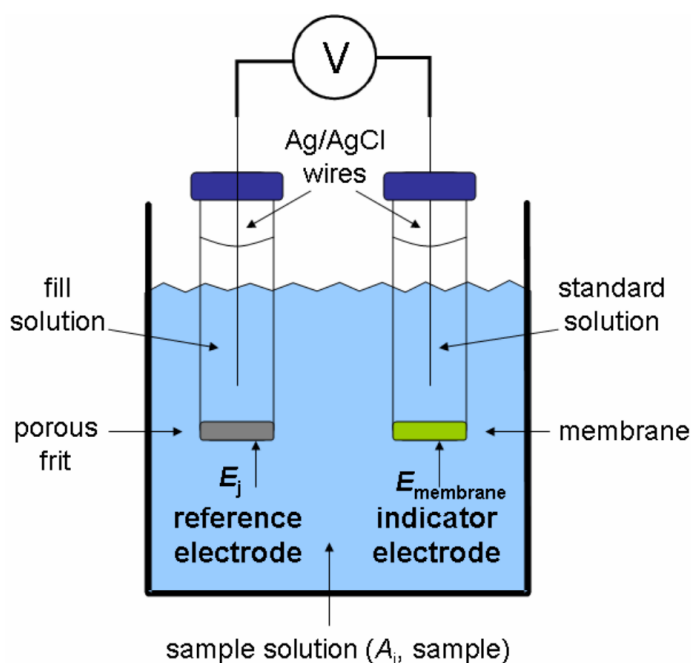
Slope =  $2.303RT/nF$  (e.g., at 25 °C; Slope of  $\text{Ca}^{2+} \approx 29.5 \text{ mV/dec}$ ,  $\text{Ag}^+ \approx 59.1 \text{ mV/dec}$ ,  $\text{F}^- \approx -59.1 \text{ mV/dec}$ )



**Figure 5.3** - An ISE calibration curve (From Wroblewski, 2005).

Overall, there are four types of conventional sensing ISEs including glass body electrode, solid state (crystalline membrane), liquid ion exchange (polymer membrane) and gas sensing type (Chen *et al.*, 2011; Lakshminarayanaiah, 2012; Buhlmann and Chen, 2012; Srinivasan and Rechnitz, 1969; Yim *et al.*, 1993). The basic ISE system comprises an indicator electrode, a reference electrode and a voltmeter (Rundle, 2000). The crucial part of the system required for the selectivity of the specific ion is the membrane of the indicator electrode which only allows that one specific ion to pass through (Wilson and Walker, 2000).

In a potentiometric electrochemical cell, one half-cell provides a known reference potential and the potential of the other half-cell indicates the target ion concentration in the solution (**Fig 5.4**) (Harvey, 2016). Since the potential of the reference electrode is constant, it is the indicator electrode which possesses the analytical information. Therefore, by measuring the disparity of the indicator and reference electrode potentials the concentration (M) of the target ion in the solution can be measured (Rundle, 2000).



**Figure 5.4** - Schematic representation of an ISE system (From Harvey, 2016).

### 5.2.1 Ion Activity and Ion Concentration: Two Different Measures

The measurement of the ISE relies on the equilibrium of the concentrations of ions permitted across an ion-selective ISE membrane, and is directly associated with the total number of ions in dilute solution. However, in a solution with high concentrations of ions (both positively- and negatively-charged), the mobility of individual ions is reduced due to inter-ionic interactions. This leads to lower measured ISE readings (in mV), resulting in a lowered measurement of the target ion concentration (Rundle, 2000). The effective concentration measured by ISEs is the “activity” of the ion. Consequently, the calibration curve (**Fig. 5.3**) at higher concentrations curves away from linearity due to the disparity between the measured activity and the actual concentration. Therefore, it is more correct to state that the measured voltage is proportional to the logarithm of the activity of the target ion. The activity coefficient is the ratio of the ion activity divided by the ion concentration. This decreases with increasing ion concentration, and is determined by the total effect of all the ions in the solution (Ionic Strength, IS), calculated using **Eq 5.3** (Rundle, 2000).

$$IS = 0.5 \times \sum c_i z_i^2 \quad (\text{Eq 5.3})$$

$c_i$  = concentration in Moles

$z_i$  = valence

### 5.2.2 Advantages of ISEs

The use of ISE systems has several advantages. First, the apparatus is relatively inexpensive and simple to use compared to other analytic techniques. Secondly, the electrodes are robust which are suitable to use in nature or laboratory. In addition, the operation and reading of an ISE system is independent of the colour or turbidity of the test solution. Moreover, ISEs are able to measure both cations and anions (even though not all ions are measurable). Normally, the precision

level is of the order of  $\pm 2$  or 3 % (Rundle, 2000). Continuous monitoring of the concentration variation in real-time is also possible. Many studies can only observe the sample before and after the intervention, whereas, real-time monitoring of the ion concentration is not interrupted by the topical treatments of the specimen, which is the most important feature of the ISE system with regard to this project.

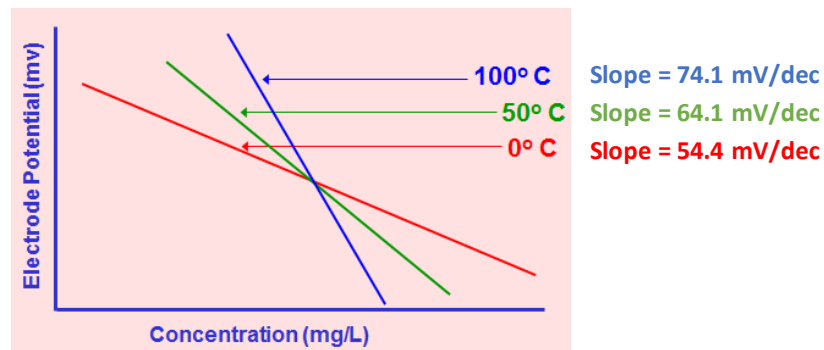
### 5.2.3 Limitations of ISEs

1. ISEs can only detect dissolved ions in aqueous solutions, so insoluble compounds cannot be analysed using ISEs (Christian, 2004).
2. The membranes may not be so specific to the target ion and may be slightly permeable to other ions existing in the test solution. There is no ideal membrane with the complete selective ability to rule out other ions' interference, and the capacity depends on the selectivity coefficient ( $k$ ) (Wroblewski, 2005).
3. Operating ISEs above the higher limit of detection or below the lower limit of detection, *i.e.*, out of the linearity range, will have the potential for error (Skoog *et al.*, 1996). Generally, the range for linear (Nernstian) calibration curve is within  $0.1 \sim 10^{-5}$  M (Rundle, 2000).
4. ISEs have a temperature range. Crystal-membrane types can be used in the range of  $0^{\circ}\text{C}$  to  $80^{\circ}\text{C}$ , whilst the range of PVC-membrane types is from  $0^{\circ}\text{C}$  to  $50^{\circ}\text{C}$  (Rundle, 2000). Outside of these ranges, the membranes might be damaged resulting in errors of readings.

### 5.2.4 The Effect of Temperature

As temperature is one of the factors in the Nernst equation, it can affect ISE readings recorded during the study (Koryta and Štulík, 1983). The increase in temperature leads to a decrease in ISE reading. From the slope of the Nernst equation, it can be seen that the higher the temperature, the steeper the tendency

of the calibration line (**Fig 5.5**). Therefore, experiments should be conducted at the same temperature as that is used in the calibration (all-about-pH.com, 2017). According to the Nernst equation (**Eq. 5.2**), the change in the slope per degree is about 0.2 mV/dec.



**Figure 5.5** - Temperature effects on the slope of the calibration curve of a single charged ion (Adapted from all-about-pH.com, 2017).

### 5.3 Effect of Data Sampling Frequency on Calculated Error in Gradient

In the SMR results, the projected mineral mass of the specimen is plotted against the time period of the study. In the ISE results, the calcium loss of the specimen is plotted against over a time period of the ISE study. Subsequently, the trend of the change in the mineral mass or in the calcium loss can be illustrated by a trendline of these data. The more points in the data plot, the more accurate the trendline gradient will be to represent the change.

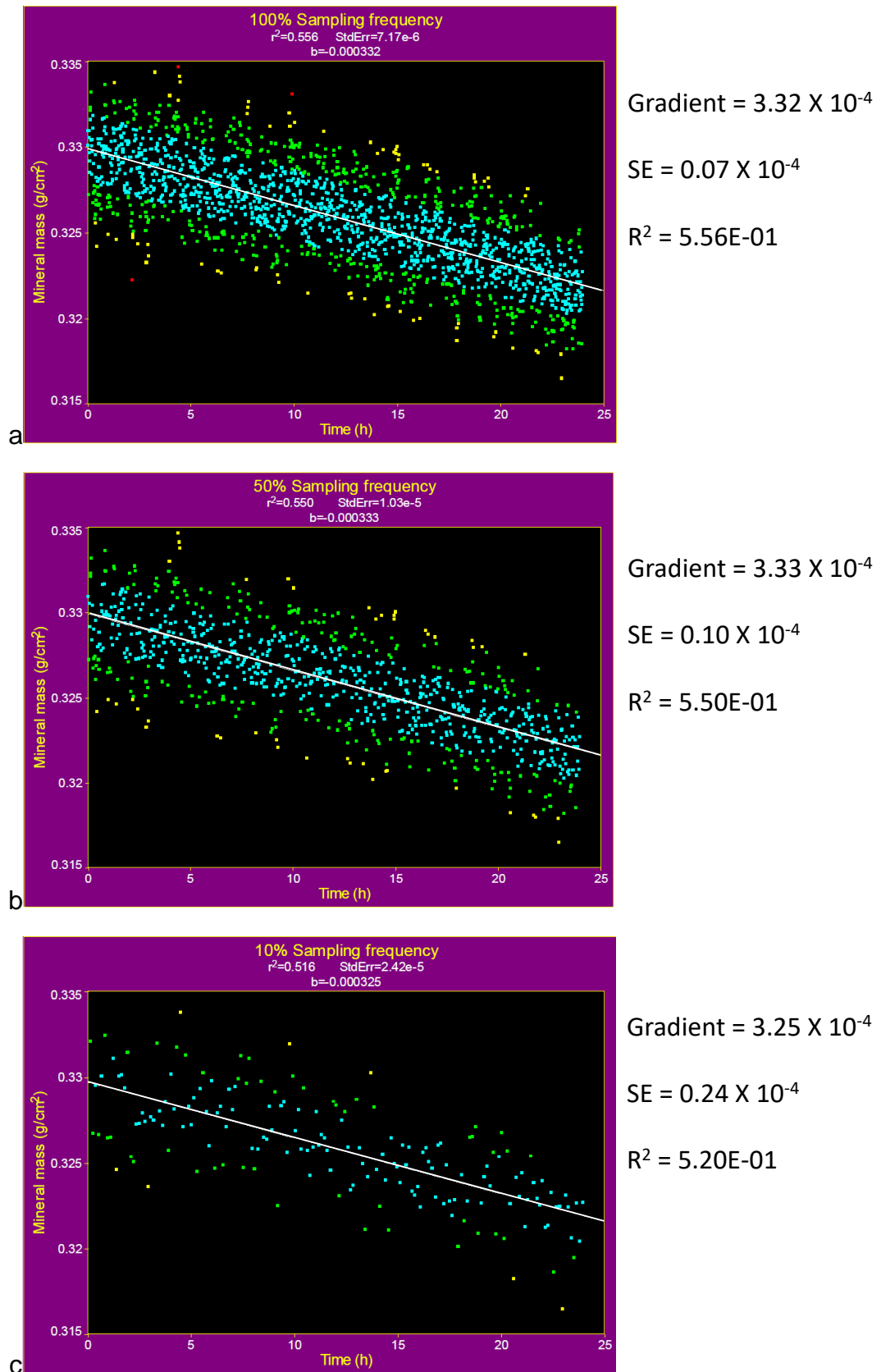
For example, **Fig. 5.6a ~ c** shows the change in the projected HAP disc mineral mass content in acetic acid over 24 h with 100 %, 50 % and 10 % of sampling data (Lingawi, 2012). The standard error of the trendline increases as the number of points decreases. Further, the percentage increase in the standard error is equal to the square root of the percentage decrease in the data point number. For instance, the standard error of the 100 % sampling frequency ( $= 0.07 \times 10^{-4}$ ) increases by the square root of 2 ( $= 100 \% \text{ divided by } 50 \%$ ) to the standard error of the 50 % sampling frequency ( $= 0.10 \times 10^{-4}$ ). Therefore, as real-time SMR



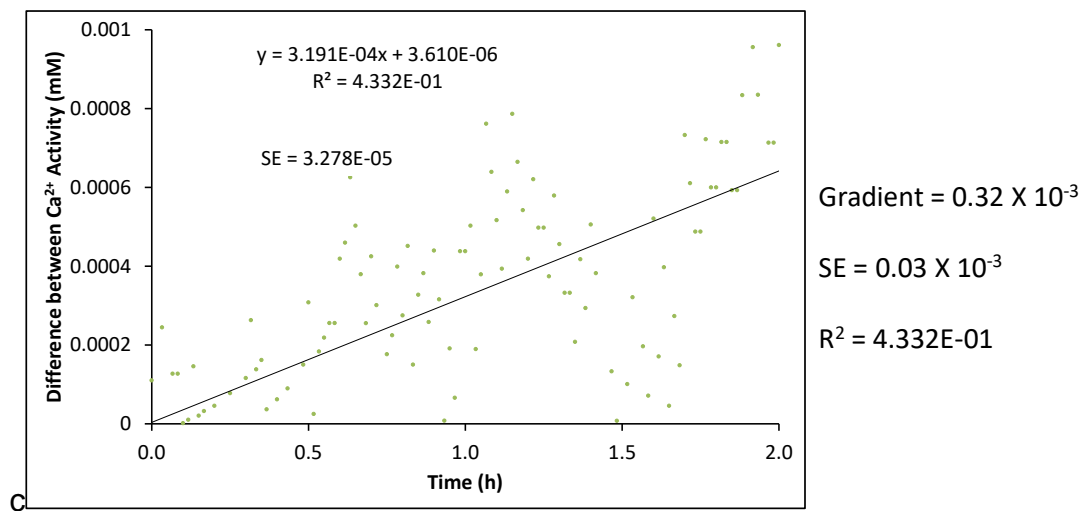
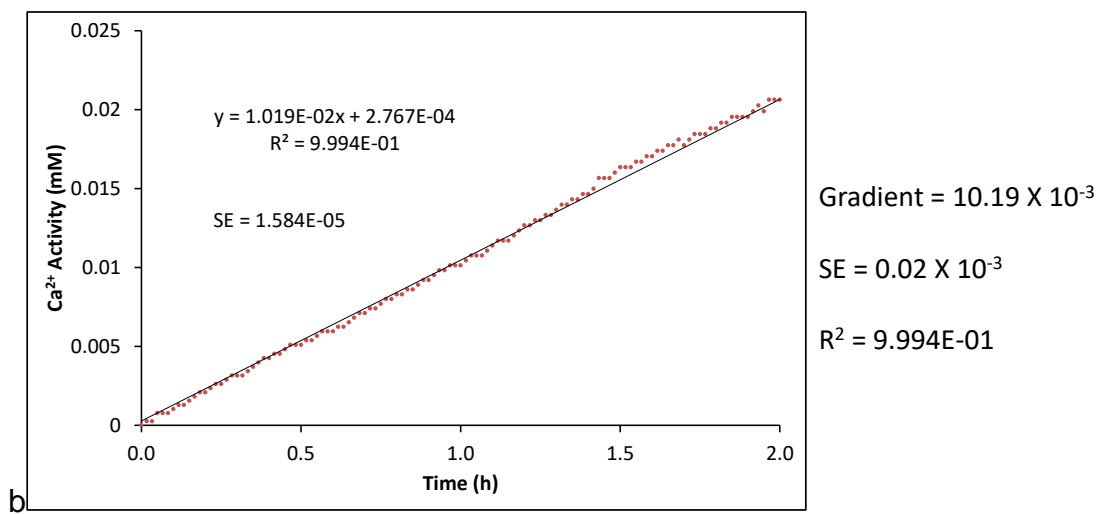
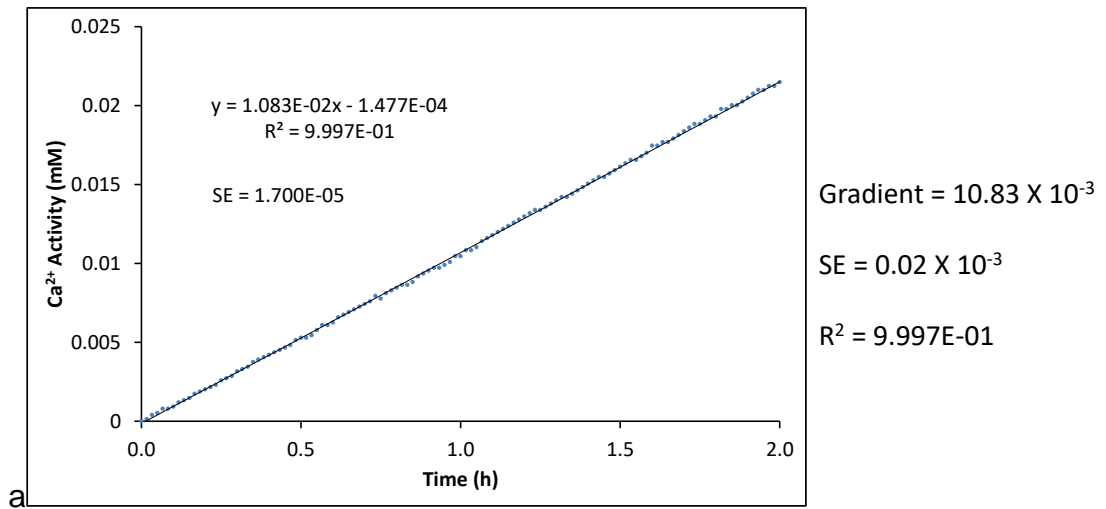
monitoring collects numerous data points, the gradient of change in the mineral mass of the specimen can be calculated with a low error value using SigmaPlot 10.0 (Systat Software, California, USA). This applies equally to ISE data collecting constant direction of change.

**Fig. 5.7a** shows the ISE measured calcium loss from an HAP disc in pH 4.0 acetic acid, and **Fig. 5.7b** shows the calcium loss from the same HAP disc which is topically treated and re-immersed back into acetic acid. The gradients of the changes in the calcium loss before and after treatment are similar. However, the difference between the two calcium loss ISE data are still significant due to the numerous data points collected (**Fig. 5.7c**).

For both SMR and ISE data, the error is improved by a factor of  $\sqrt{N}$ , when N is the number of measurements.



**Figure 5.6** - Change in the projected HAP disc mineral mass content in pH 4.0 acetic acid over 24 h with (a) 100 %, (b) 50 %) and (c) 10 % sampling frequency of data. Blue dots: one StdErr away from trendline; Green dots: two StdErr away from trendline; Yellow dots: three StdErr away from trendline (From Lingawi, 2012).

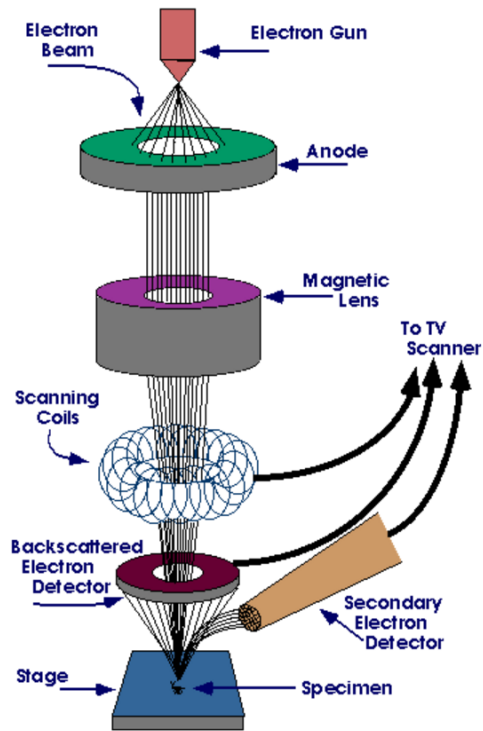


**Figure 5.7** – Change in the calcium loss from an HAP disc in pH 4.0 acetic acid (a) before (Blue dots) and (b) after (Red dots) topical treatment. The difference between the gradient of the two calcium loss trendlines ( $0.32 \times 10^{-3}$ ) is detected (Green dots).

## 5.4 Scanning Electron Microscopy

Scanning electron microscopy (SEM) is a non-destructive technique used to obtain a magnified image through interactions between thermo-ionically emitted electrons (electron beam) and the assessed sample surface (Vernon-Parry, 2000). Before being inspected by SEM, non-conductive samples must be coated with an electrically conductive thin film (either gold or carbon in the order of 20 nm thickness) to enable their imaging (Nixon, 1969).

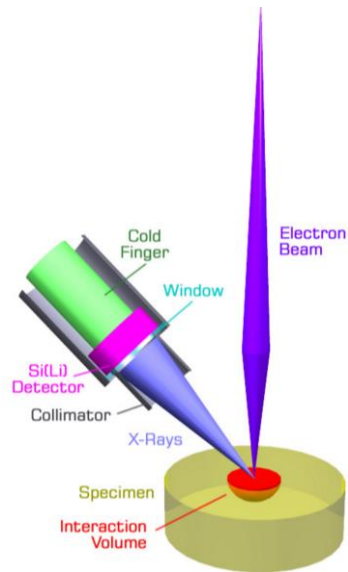
After electrons are emitted from the electron gun with significant amounts of kinetic energy, several electromagnetic condenser lenses focus the electron beam into a fine probe. Next, this energy is dissipated as a variety of signals produced by electron-sample interactions when the incident electrons are decelerated in the solid sample (Schweitzer, 2014; Swepp, 2017; Vernon-Parry, 2000). The interactions between electrons and samples in a variety of ways, which produce secondary electrons (that produce SEM images) and characteristic X-rays (that are used for elemental analysis like energy-dispersive X-ray analysis, EDX) (Vernon-Parry, 2000). Production of secondary and low energy electrons are the main interactions for generation of topographic information as they can only escape from a very shallow, near-surface layer of the sample, and provide the highest spatial resolution (Vernon-Parry, 2000) (**Fig. 5.8**).



*Figure 5.8 - Schematic representation of SEM (From Schweitzer, 2014).*

## 5.5 Energy-Dispersive X-ray Analysis

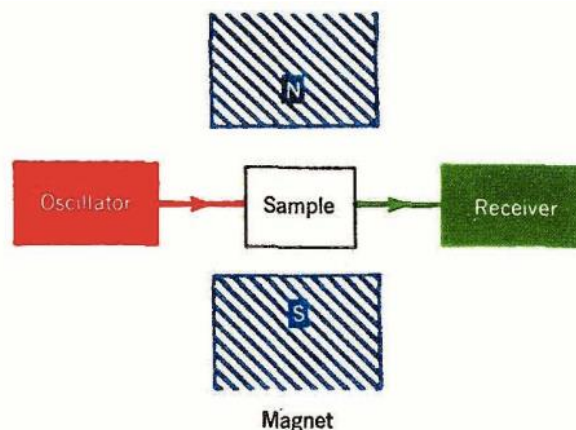
Energy Dispersive X-ray analysis (EDX) is a technique used for elemental analysis. As a focused beam of electrons bombards the sample to excite an electron in an inner shell, ejecting it from the shell, an electron from an outer, higher-energy shell then fills the electron-hole of the inner, lower-energy shell, and the emitted characteristic X-ray can be detected (**Fig 5.9**). As the magnitude of the signal is proportional to the energy of the X-ray, EDX spectrum can be illustrated as X-ray counts versus energy. That provides a means of rapidly evaluating the elemental constituents of a specimen and gives accurate quantitative analysis. Qualitative analysis involves the identification of the peaks in the spectrum to determine the elements present in the excited volume of the sample. Quantitative analysis (determination of the concentrations of the elements present) entails measuring line intensities for each element in the sample (ACMAL, 2014; Peter, 2005; Middleton, 1999).



*Figure 5.9 - Schematic representation of EDX (From ACMAL, 2014).*

## 5.6 Magic Angle Spinning – Nuclear Magnetic Resonance

Nuclear magnetic resonance (NMR) is a non-destructive characteristic tool which can be used to determine the physical and chemical properties of atoms or molecules. Information including structure, reaction state and environment of the molecules can be obtained by interpreting the NMR spectrograms (Iggo, 2011).



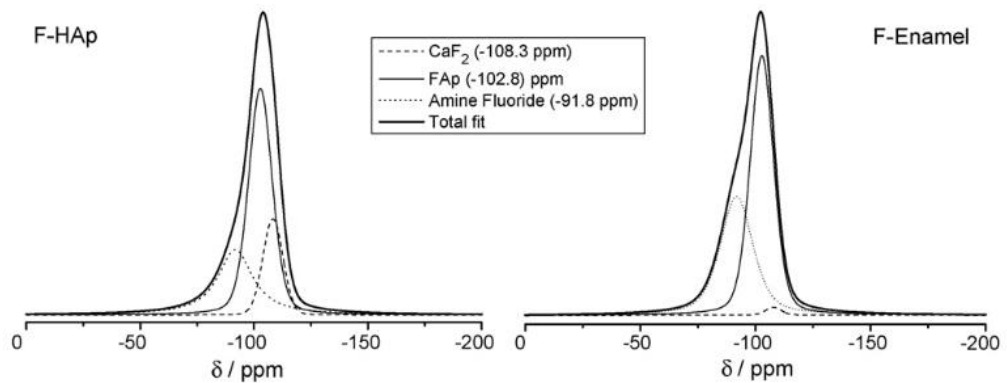
*Figure 5.10 - Schematic representation of NMR apparatus (From Robert, 1959).*

The apparatus comprises a magnet, a radio-frequency oscillator and a receiver (**Fig 5.10**). Under the particular magnetic field ( $B_0$ ), which defines the resonance frequency (or Larmor frequency;  $\nu$ ), the sample put in the magnet pole gap can absorb certain energy ( $\Delta E$ ). After the “relaxation”, energy is emitted at a certain radio-frequency which can be detected and recorded by the receiver (Robert, 1959). The resonance frequency ( $\nu$ ) is characteristic of a given nucleus of the inspected sample, which is affected by its chemical environment, called chemical shielding. Chemical shielding is associated with the interaction of the electrons surrounding the nucleus with the applied magnetic field ( $B_0$ ), whose magnitude can be measured as the “chemical shift ( $\delta$ )” of the resonance line from that of a reference compound (**Eq. 5.4**) (Iggo, 2011). The characterisation of the sample is then achieved by measuring the positions of peaks of chemical shifts observed in NMR spectra, as they represent specific forms or states of the target nuclei (Robert, 1959). In contrast to aqueous phase NMR, solid-state NMR spectroscopy is affected by local nuclear interactions which result in broad spectra masking the chemical shift peaks. To overcome this problem in solid-state NMR, the sample is spun at high speed at a magic angle ( $54.74^\circ$ ) with respect to the magnet field in solid-state NMR. This is magic angle spinning (MAS), which averages the interactions, and consequently the peaks become narrower, and distinguishable spectra with better resolution are produced (Alia *et al.*, 2009; Iggo, 2011).

$$\delta = (\nu_{\text{observed}} - \nu_{\text{reference}}) / \nu_{\text{reference}} \quad (\text{Eq. 5.4})$$

However, not all nuclei are magnetically active. Only nuclei with odd numbers of protons and/or neutrons such as  $^{31}\text{P}$  and  $^{19}\text{F}$  can be applied in NMR characterisation (Iggo, 2011; Shoolery, 1954). Both  $^{31}\text{P}$  and  $^{19}\text{F}$  MAS-NMR have been used in dental research for decades.  $^{31}\text{P}$  MAS-NMR can identify numerous apatite species (Tsai and Chan, 2011), and  $^{19}\text{F}$  MAS-NMR is capable of differentiating FAP and FHA from HAP, and can distinguish between FAP, FHA and  $\text{CaF}_2$  (Elsharkawy *et al.*, 2018; Mohammed *et al.*, 2013; White *et al.*, 1994).

Sometimes chemical shift peaks overlap with each other, which leads to a combined asymmetric peak. In this case, deconvolution of the spectrum, *e.g.*, using DmFit (France), is required to identify each compound contributing to the peak (**Fig. 5.11**) (Gerth *et al.*, 2007).



**Figure 5.11** – Deconvolution of a  $^{19}\text{F}$  MAS-NMR spectra of HAP, and of human enamel powders treated with amine fluoride (From Gerth *et al.*, 2007).

## 5.7 Knoop Micro-hardness Test

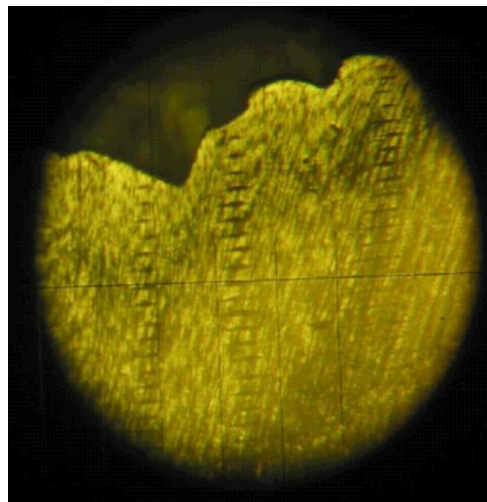
### 5.7.1 Microscopic Photographs

The microscope of the Knoop micro-hardness tester can be used to monitor the morphology of lesion sections. By attaching a camera to the microscope (**Fig. 5.12**), these microscopic photographs of the lesion sections (**Fig. 5.13**) can be obtained.





**Figure 5.12** – Taking the microscopic photographs through the microscope of the Knoop micro-hardness tester using a camera.

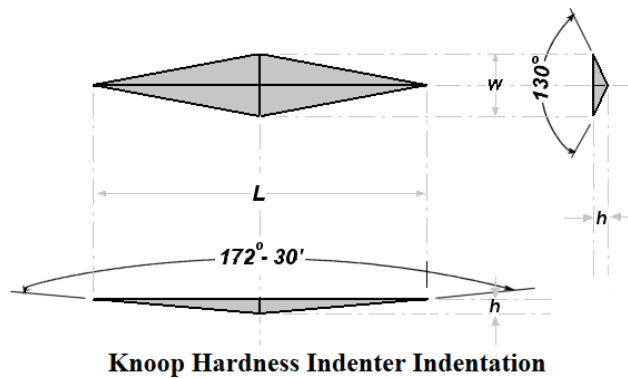


**Figure 5.13** – Typical microscopic photographs of a tooth with Knoop indentations on a dentine specimen (From Chu and Lo, 2008a).

### 5.7.2 Knoop Micro-hardness Indentation

Micro-hardness testing refers to static indentations made with loads not exceeding 1 kgf. The indenter of the Knoop micro-hardness tester is a rhombic-

based pyramidal-shaped diamond with edge angles of  $172^{\circ} 30'$  and  $130^{\circ} 0'$  (**Fig 5.14**) (Davidson *et al.*, 1974; England, 2013). The hardness assessment is conducted by forcing the indenter into the surface of the sample with a test force of between 1 gf and 1 kgf and then to measure the length of the indentation diagonal with a light microscope. Calculation of the Knoop hardness (KHN) is carried out via **Eq 5.5** (ASTM, 2012; England, 2013).



*Figure 5.14 – Diagrams of the Knoop indenter (From England, 2013).*

$$\text{KHN} = \frac{F}{A} = \frac{F}{CL^2} \quad (\text{Eq 5.5})$$

F = applied load in kgf

A = the unrecovered projected area of the indentation ( $\text{mm}^2$ )

L = measured the length of the long diagonal of indentation (mm)

C = 0.07028 = Constant of indenter relating projected area of the indentation to the square of the length of the long diagonal.

**PART III: DEVELOPMENT OF  
AN ISE METHODOLOGY TO  
INVESTIGATE THE EFFECTS  
OF TOPICAL TREATMENTS  
WITH SILVER COMPOUNDS ON  
DEMINERALISATION**

## Chapter 6 VALIDATION OF A REAL-TIME ISE METHODOLOGY TO QUANTIFY THE INFLUENCE OF INHIBITORS OF DEMINERALISATION KINETICS IN VITRO USING A HYDROXYAPATITE MODEL SYSTEM

### 6.1 Introduction

Numerous techniques have been used to investigate caries progression, such as profilometry, scanning electron microscopy, microradiography and micro-indentation (Arends *et al.*, 1987; Shellis *et al.*, 2010). However, in addition to these static methodologies, *real-time* techniques have also been developed to monitor the dissolution process by periodic measurements of tissue loss or inspection of surface morphology (Shellis *et al.*, 2010).

For example, scanning micro-radiography (SMR) allows continuous observation of demineralisation *in vitro* and has been used in several dental researches (e.g., Kosoric *et al.*, 2010; Mohammed *et al.*, 2015; Shah *et al.*, 2011). However, SMR is very technique sensitive and requires extensive protocols to ensure accurate measurement. As silver compounds are reduced to metallic silver over time due to the photosensitivity of Ag<sup>+</sup> (Lin *et al.*, 2015), the effect of topical treatments with silver compounds may be affected by application time. Therefore, the real-time SMR technique could not be applied in this study, as it requires time-consuming sample preparations following the topical treatments of the specimens. Thus, a novel real-time methodology allowing efficient topical treatment of the specimen was needed to investigate the effects of topical treatments with silver compounds on demineralisation.

Ion selective electrodes (ISEs) are potentiometric sensors which can be used as analytic tools for measuring the effective concentration of selected ions in a solution and have been used in the dental area for many years (Bjorvatn and Morch, 1979; Covington and Kenneth, 1979). As dental caries and dental erosion are associated with Ca<sup>2+</sup> loss from dental hard tissues

(Abou Neel *et al.*, 2016), the  $\text{Ca}^{2+}$  release from dental mineral can be regarded as a proxy for demineralisation. Therefore, the use of real-time  $\text{Ca}^{2+}$  ISE has the potential for demineralisation studies. Furthermore, real-time  $\text{Ca}^{2+}$  ISE study allows topical treatments of specimens *during* the experiment in an efficient way, which is required for the investigation of the effects of topical treatments with silver compounds on demineralisation. However, even though real-time ISEs have been used in many research areas other than dentistry (Chumbimuni-Torres *et al.*, 2009; Kim *et al.*, 2005; Zeitchek and Anthony, 2013), cariostatic demineralisation studies using real-time  $\text{Ca}^{2+}$  ISE have not been reported

The inhibitory effects of  $\text{F}^-$  and of  $\text{Zn}^{2+}$  on enamel demineralisation *in vitro* have been studied previously using SMR (Mohammed *et al.*, 2014a; Mohammed *et al.*, 2015). The results showed a log-linear relationship between mean percentage reduction in the rate of enamel mineral loss ( $\text{PRML}_{\text{enamel}}$ ) with increasing  $\text{F}^-$  concentration, and with increasing  $\text{Zn}^{2+}$  concentration. If similar results of the SMR studies can be replicated using real-time ISE, the technique can be validated to be used for quantifying the influence of inhibitors of demineralisation kinetics *in vitro*.

## 6.2 Aim

The aim was to validate the use of  $\text{Ca}^{2+}$  ISEs for real-time monitoring of calcium loss of hydroxyapatite (HAP) discs by replicating the previous SMR studies exactly but using  $\text{Ca}^{2+}$  ISE. HAP discs were used in the present corroboration study to avoid the interference from inhomogeneities in human enamel such as individual variations in composition and biological structures (Section 1.2.1 and Section 1.2.2).

## 6.3 Materials and Methods

### 6.3.1 Preparation of Samples



*Figure 6.1 – Half-varnished porous HAP discs.*

Forty-eight porous HAP circular discs (20% porosity, 12 mm in diameter, 2 mm in thickness; Plasma Biotel Ltd, UK) were varnished with red nail lacquer (KIKO, Italy) to expose only the upper face to the demineralisation solution (**Fig 6.1**). The varnished discs were then allocated into sixteen groups ( $n = 3$  each) of increasing  $[Zn^{2+}]$  or increasing  $[F^-]$  as previously described (Mohammed *et al.*, 2014a; Mohammed *et al.*, 2015).

### 6.3.2 Preparation of Demineralisation Solution

A 0.1 M  $CH_3COOH$  (Sigma-Aldrich, UK) demineralisation solution buffered by adding 1.0 M KOH (Sigma-Aldrich, UK) drop by drop up to pH 4.0 was prepared, as used previously (Mohammed *et al.*, 2014a; Mohammed *et al.*, 2015).

### 6.3.3 ISE Calibration

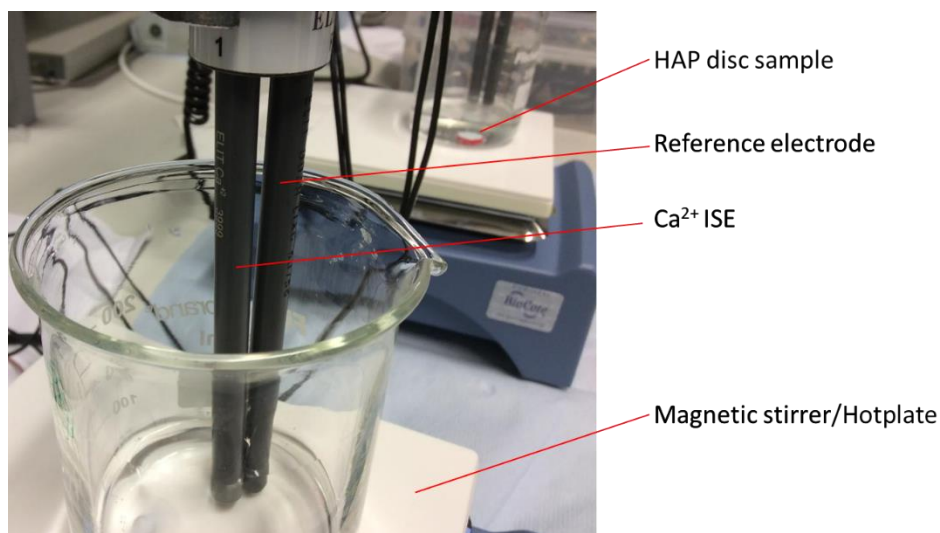
A  $\text{Ca}^{2+}$  ISE paired with a double-junction lithium acetate reference electrode (ELIT 003n), was connected to an 8 channel ion analyser (attached to a computer) to record the mV output at specified time intervals. All ISE equipment used were products of Nico2000 (Nico2000 Ltd, UK).

ISEs are pH sensitive, so the ISE calibration solution was prepared with the demineralisation solution in the same pH as used in the main study. A 1 mM  $\text{Ca}^{2+}$  standard solution was made by adding 0.147 g  $\text{CaCl}_2 \cdot 2\text{H}_2\text{O}$  into the demineralisation solution and made up to 1 L. The  $\text{Ca}^{2+}$  ISE was immersed in 50 mL of demineralisation solution, and standard calcium solution was added drop-wise to gradually increase the  $[\text{Ca}^{2+}]$  up to about 0.5 mM. The calibration was performed at  $23.0 \pm 1.0$  °C using a temperature stabilised stirrer (Stuart UC152D/KIT, UK). Subsequently, the activity coefficients for each  $[\text{Ca}^{2+}]$  were calculated with an ionic speciation program, Chemist (MicroMath, Missouri, USA). Next, the calibration curve was obtained by plotting the logarithm of calcium activity (mM) against ISE readings in mV.

### 6.3.4 Demineralisation Study

Each varnished HAP disc was immersed into 50 mL demineralisation solution ( $23.0 \pm 1.0$  °C) for 1 h. The solution was continuously stirred using a magnetic stirrer (Stuart UC152D/KIT, UK). The  $\text{Ca}^{2+}$  ISE was used to monitor the increase in  $\text{Ca}^{2+}$  activity as demineralisation progressed, at intervals of 1 min (**Fig 6.2**).





**Figure 6.2** – Two setups of the study ISE at room temperature.

Then, 1 mL zinc acetate or sodium fluoride were added to the solutions to obtain concentrations of 0.1, 0.4, 1.8, 9.0, 36.0, 107.0, 356.0 or 1782.0 ppm  $Zn^{2+}$ , and 0.1, 0.5, 2.3, 11.3, 45.2, 135.7, 452.5 or 2262.4 ppm  $F^-$  in each group for zinc and fluoride experiments, respectively, *i.e.*, similar to those used in the previous studies (Mohammed *et al.*, 2014a; Mohammed *et al.*, 2015). Each disc was then demineralised for another 1 h, and the  $Ca^{2+}$  activity was monitored at 1 min intervals as before. The temperature was maintained at  $23.0 \pm 1.0$  °C as in the previously reported studies (Mohammed *et al.*, 2014a; Mohammed *et al.*, 2015).

The  $Ca^{2+}$  ISE readings (mV) were converted to concentration units (mM) using the calibration curve, and the  $Ca^{2+}$  activity was plotted as a function of time (h) for each  $Zn^{2+}$  or  $F^-$  addition. The activity of  $Ca^{2+}$  (mM) was plotted as a function of time (h) for each group, and the percentage reduction in the rate of calcium loss of HAP ( $PRCL_{HAP}$ ) for each  $Zn^{2+}$  and  $F^-$  addition was calculated in a way similar to  $PRML_{enamel}$ , which was the ratio between the rate of  $Ca^{2+}$  release after the topical treatment ( $R_a$ ) to the rate of  $Ca^{2+}$  release before the topical treatment ( $R_b$ ) (**Eq. 6.1**). Thereafter,  $PRCL_{HAP}$  could be used in the same way as  $PRML_{enamel}$  and was plotted as a function of  $[Zn^{2+}]$  and  $[F^-]$ , similar to the previous studies (Mohammed *et al.*, 2014a; Mohammed *et al.*, 2015).

$$\text{PRCL} = \left(1 - \frac{R_a}{R_b}\right) \times 100\% \quad (\text{Eq. 6.1})$$

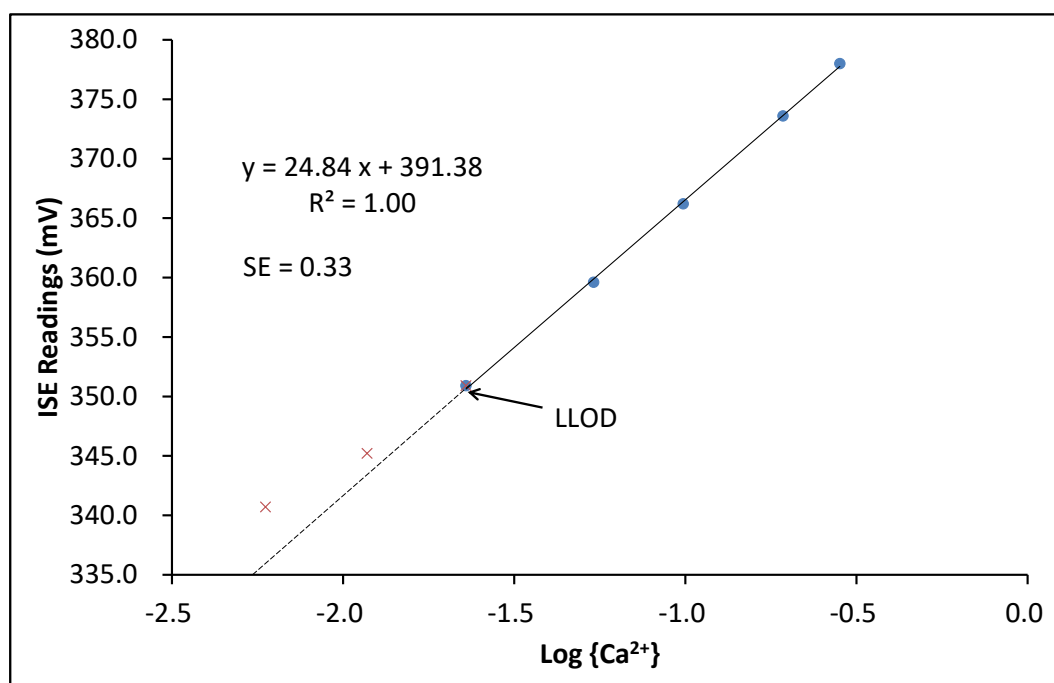
PRCL = Percentage reduction in the rate of calcium loss

$R_a$  = The rate of  $\text{Ca}^{2+}$  release after the topical treatment

$R_b$  = The rate of  $\text{Ca}^{2+}$  release before the topical treatment

## 6.4 Results

The calibration plot of the  $\text{Ca}^{2+}$  ISE (**Fig. 6.3**) shows a linear relationship between mV and log activity ( $R^2 = 1.00$ ) for  $\text{Ca}^{2+}$  activity greater than 0.023 mM (lower limit of detection, LLOD). A linear regression line was used to convert ISE mV to mM. Values below the linear Nernstian response region of the calibration curve were not used. The error of the gradient was calculated using SigmaPlot 10.0 (Systat Software, California, USA).



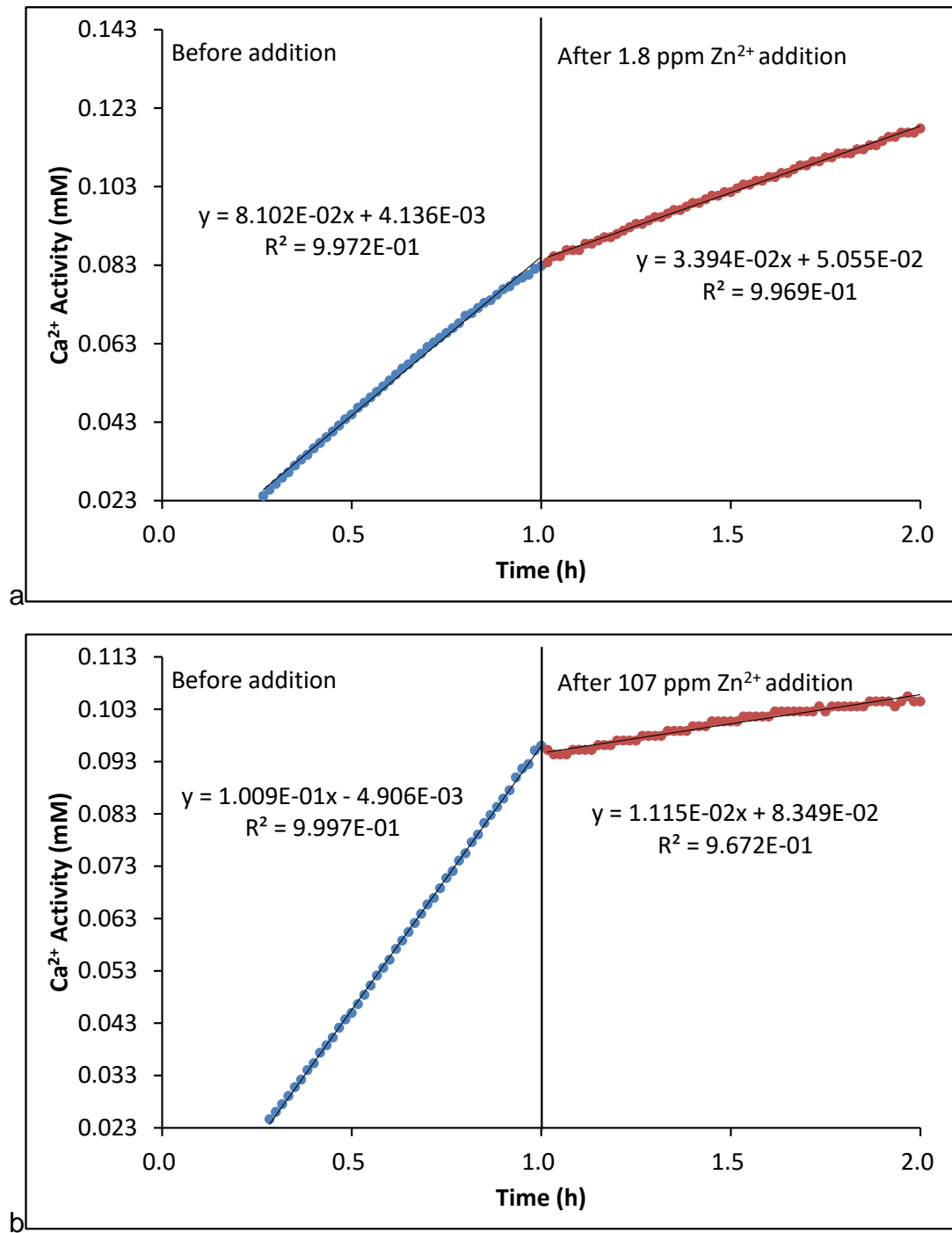
**Figure 6.3** - Calibration curve of  $\text{Ca}^{2+}$  ISE. LLOD = lower limit of detection.

**Fig. 6.4a** shows a typical plot of  $\text{Ca}^{2+}$  release from a demineralising HAP disc before and after addition of 1.8 ppm  $\text{Zn}^{2+}$ . The  $\text{Ca}^{2+}$  release was approximately linear both before and after the addition of  $\text{Zn}^{2+}$ . The rate of the  $\text{Ca}^{2+}$  release was  $\approx 0.081$  mM/h before and  $\approx 0.034$  mM/h after the addition of  $\text{Zn}^{2+}$ .

**Fig. 6.4b** shows a typical plot of  $\text{Ca}^{2+}$  release from a demineralising HAP disc before and after addition of 107.0 ppm  $\text{Zn}^{2+}$ . The  $\text{Ca}^{2+}$  release was approximately linear both before and after the addition of  $\text{Zn}^{2+}$ . The rate of the  $\text{Ca}^{2+}$  release was  $\approx 0.101$  mM/h before and  $\approx 0.011$  mM/h after the addition of  $\text{Zn}^{2+}$ . The reduction in the rate of  $\text{Ca}^{2+}$  release after addition of 107.0 ppm  $\text{Zn}^{2+}$  was more than that after the addition of 1.8 ppm  $\text{Zn}^{2+}$ .

Similar plots were obtained for all  $\text{Zn}^{2+}$  additions, with a reduction in the rate of  $\text{Ca}^{2+}$  release increased with increasing  $[\text{Zn}^{2+}]$  in the solutions.

**Table 6.1** shows the rates of calcium loss of HAP discs ( $\text{RCL}_{\text{HAP}}$ ) +/- standard error (SE) before and after addition of 1.8 ppm and 107 ppm  $\text{Zn}^{2+}$  of the **Fig. 6.4**. Errors of gradients were calculated using SigmaPlot 10.0 (Systat Software, California, USA). In each treatment group, the  $R_a$  was significantly different ( $p$  value  $< 0.05$ ) from the  $R_b$ .



**Figure 6.4** - Typical data collected from one HAP disc with additions of (a) 1.8 ppm  $Zn^{2+}$  and (b) 107 ppm  $Zn^{2+}$  groups.

**Table 6.1** -  $RCL_{HAP}$  before and after  $Zn^{2+}$  addition of the **Fig. 6.4**.

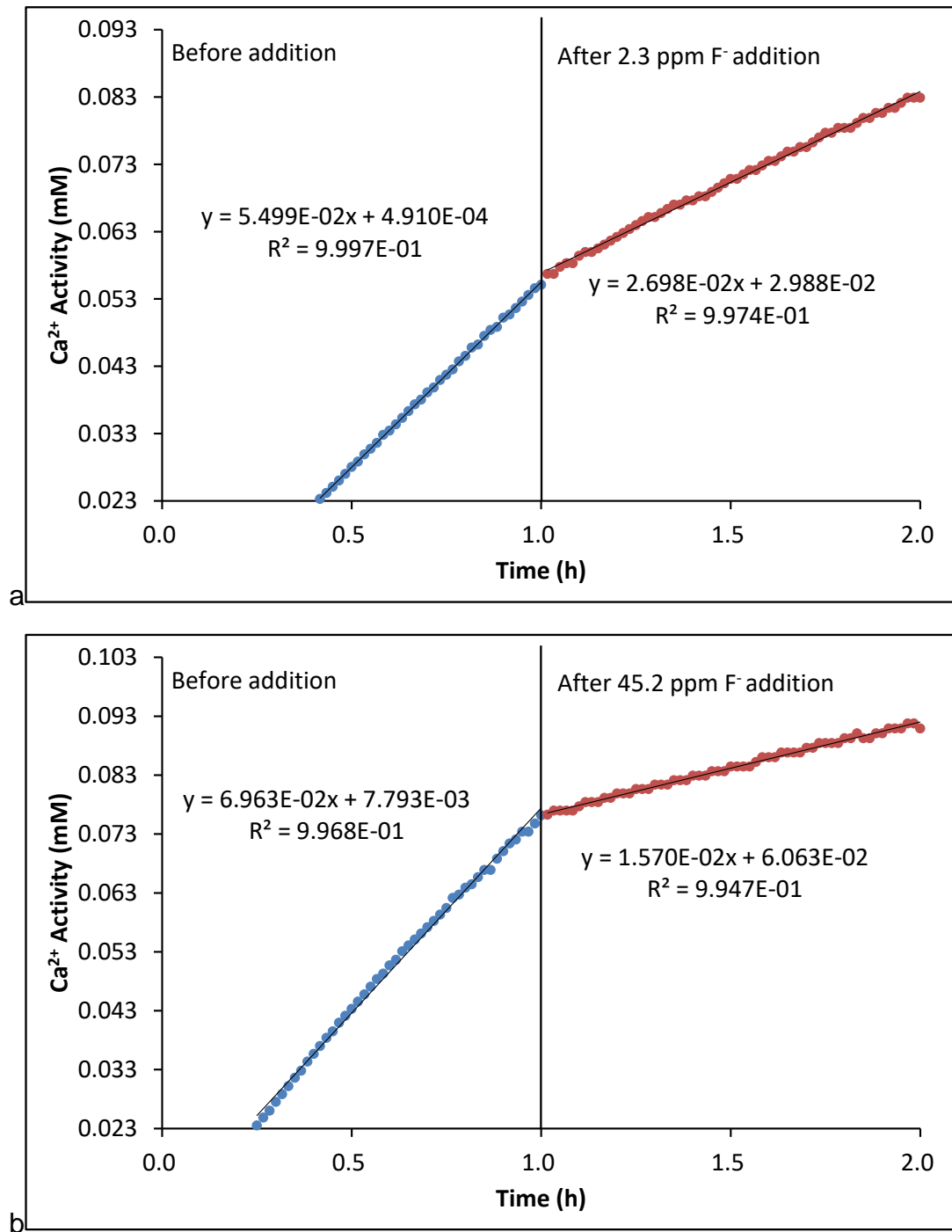
Treatment	$R_{b+/-SE}$ ( $\times 10^{-3}$ mM/h)	$R_{a+/-SE}$ ( $\times 10^{-3}$ mM/h)	p value
1.8 ppm $Zn^{2+}$	$81.02 \pm 0.70$	$33.94 \pm 0.20$	< 0.01
107 ppm $Zn^{2+}$	$100.90 \pm 0.30$	$11.15 \pm 0.30$	< 0.01

**Fig. 6.5a** shows a typical plot of  $\text{Ca}^{2+}$  release from a demineralising HAP disc before and after addition of 2.3 ppm  $\text{F}^-$ . The  $\text{Ca}^{2+}$  release was approximately linear both before and after the addition of  $\text{F}^-$ . The rate of the  $\text{Ca}^{2+}$  release was  $\approx 0.055$  mM/h before and  $\approx 0.027$  mM/h after addition of  $\text{F}^-$ .

**Fig. 6.5b** shows a typical plot of  $\text{Ca}^{2+}$  release from a demineralising HAP disc before and after addition of 45.2 ppm  $\text{F}^-$ . The  $\text{Ca}^{2+}$  release was approximately linear both before and after the addition of  $\text{F}^-$ . The rate of the  $\text{Ca}^{2+}$  release was  $\approx 0.070$  mM/h before and  $\approx 0.016$  mM/h after addition of  $\text{F}^-$ . The reduction in the rate of  $\text{Ca}^{2+}$  release after addition of 45.2 ppm  $\text{F}^-$  was more than that after the addition of 2.3 ppm  $\text{F}^-$ .

Similar plots were obtained for all  $\text{F}^-$  additions, with a reduction in the rate of  $\text{Ca}^{2+}$  release increased with increasing  $[\text{F}^-]$  in the solutions.

**Table 6.2** shows the  $\text{RCL}_{\text{HAP}} \pm \text{SE}$  before and after addition of 2.3 ppm and 45.2 ppm  $\text{F}^-$  of the **Fig. 6.5**. Errors of gradients were calculated using SigmaPlot 10.0 (Systat Software, California, USA). In each treatment group, the  $R_a$  was significantly different ( $p$  value  $< 0.05$ ) from the  $R_b$ .



**Figure 6.5** - Typical data collected from one HAP disc with additions of (a) 2.3 ppm F<sup>-</sup> and (b) 45.2 ppm F<sup>-</sup> groups.

**Table 6.2** -  $R_{CL_{HAP}}$  before and after F<sup>-</sup> addition of the Fig. 6.5.

Treatment	$R_b \pm SE$ (X 10 <sup>-3</sup> mM/h)	$R_a \pm SE$ (X 10 <sup>-3</sup> mM/h)	p value
2.3 ppm F <sup>-</sup>	54.99 ± 0.20	26.98 ± 0.20	< 0.01
45.2 ppm F <sup>-</sup>	69.63 ± 0.60	15.70 ± 0.10	< 0.01

**Table 6.3** and **Table 6.4** show the  $R_{CL_{HAP}} \pm SE$  ( $\times 10^{-3}$  mM/h) and the  $PR_{CL_{HAP}}$  measured at increasing  $[Zn^{2+}]$  and  $[F^{-}]$  in the solution. Every  $R_a$  ( $R_{CL_{HAP}}$ ) measured at each  $[Zn^{2+}]$  and  $[F^{-}]$  was significantly different ( $p < 0.05$ ) from the  $R_b$  ( $R_{CL_{HAP}}$ ).

The mean  $PR_{CL_{HAP}}$  (%) in both  $Zn^{2+}$  and  $F^{-}$  experiments show that inhibitory efficacy on demineralisation of HAP discs increased with increasing  $[Zn^{2+}]$  and  $[F^{-}]$ . Complete inhibition was achieved at 356 ppm  $Zn^{2+}$  and at 452.5 ppm  $F^{-}$ , respectively.

**Table 6.3** – The  $R_{CL_{HAP}}$  and  $PR_{CL_{HAP}}$  of every HAP disc measured at each  $[Zn^{2+}]$ .

$[Zn^{2+}]$	HAP Disc	$R_b \pm SE$ ( $\times 10^{-3}$ mM/h)	$R_a \pm SE$ ( $\times 10^{-3}$ mM/h)	$PR_{CL_{HAP}}$ (%)
0.1 ppm	1	37.63 $\pm$ 0.20	2.39 $\pm$ 0.88	36.5
	2	139.10 $\pm$ 0.30	110.50 $\pm$ 0.70	20.6
	3	97.54 $\pm$ 0.40	72.38 $\pm$ 0.40	25.8
	Average	91.42 $\pm$ 29.45	68.93 $\pm$ 25.06	27.6 $\pm$ 4.7
0.4 ppm	1	73.26 $\pm$ 0.70	36.40 $\pm$ 0.40	50.3
	2	74.17 $\pm$ 1.80	44.60 $\pm$ 1.50	39.9
	3	85.4 $\pm$ 0.30	51.5 $\pm$ 0.60	39.7
	Average	77.62 $\pm$ 3.90	44.17 $\pm$ 4.36	43.3 $\pm$ 3.5
1.8 ppm	1	52.83 $\pm$ 0.10	27.91 $\pm$ 0.30	47.2
	2	81.02 $\pm$ 0.70	33.94 $\pm$ 0.20	58.1
	3	29.07 $\pm$ 0.80	10.40 $\pm$ 0.50	64.2
	Average	54.31 $\pm$ 15.01	24.09 $\pm$ 7.06	56.5 $\pm$ 5.0
9 ppm	1	55.45 $\pm$ 0.50	15.65 $\pm$ 0.10	71.8
	2	66.85 $\pm$ 0.60	14.82 $\pm$ 0.20	77.8
	3	94.99 $\pm$ 0.50	27.02 $\pm$ 0.60	71.6
	Average	72.41 $\pm$ 11.75	19.16 $\pm$ 3.94	73.7 $\pm$ 2.1
36 ppm	1	46.55 $\pm$ 0.40	9.73 $\pm$ 0.10	79.1
	2	68.58 $\pm$ 0.20	18.42 $\pm$ 0.20	73.1
	3	46.20 $\pm$ 0.20	10.49 $\pm$ 0.08	77.3
	Average	53.78 $\pm$ 7.40	12.88 $\pm$ 2.78	76.5 $\pm$ 1.8
107 ppm	1	66.15 $\pm$ 0.50	2.76 $\pm$ 0.2	95.8
	2	100.90 $\pm$ 0.30	11.15 $\pm$ 0.30	88.9
	3	61.76 $\pm$ 0.70	14.32 $\pm$ 0.50	76.8
	Average	76.27 $\pm$ 12.38	9.41 $\pm$ 3.45	87.2 $\pm$ 5.6
356 ppm	1	44.17 $\pm$ 0.50	-1.44 $\pm$ 1.50	103.2
	2	149.50 $\pm$ 0.50	0.80 $\pm$ 1.20	94.8
	3	96.19 $\pm$ 0.50	-2.85 $\pm$ 0.70	103.0
	Average	96.62 $\pm$ 30.41	1.17 $\pm$ 3.34	<b>100.0 <math>\pm</math> 2.8</b>
1782 ppm	1	103.10 $\pm$ 0.10	-10.40 $\pm$ 1.20	110.1
	2	118.10 $\pm$ 0.30	2.33 $\pm$ 1.10	98.1
	3	111.50 $\pm$ 0.60	2.60 $\pm$ 1.20	97.7
	Average	110.90 $\pm$ 4.34	-1.82 $\pm$ 4.29	<b>100.0 <math>\pm</math> 4.1</b>

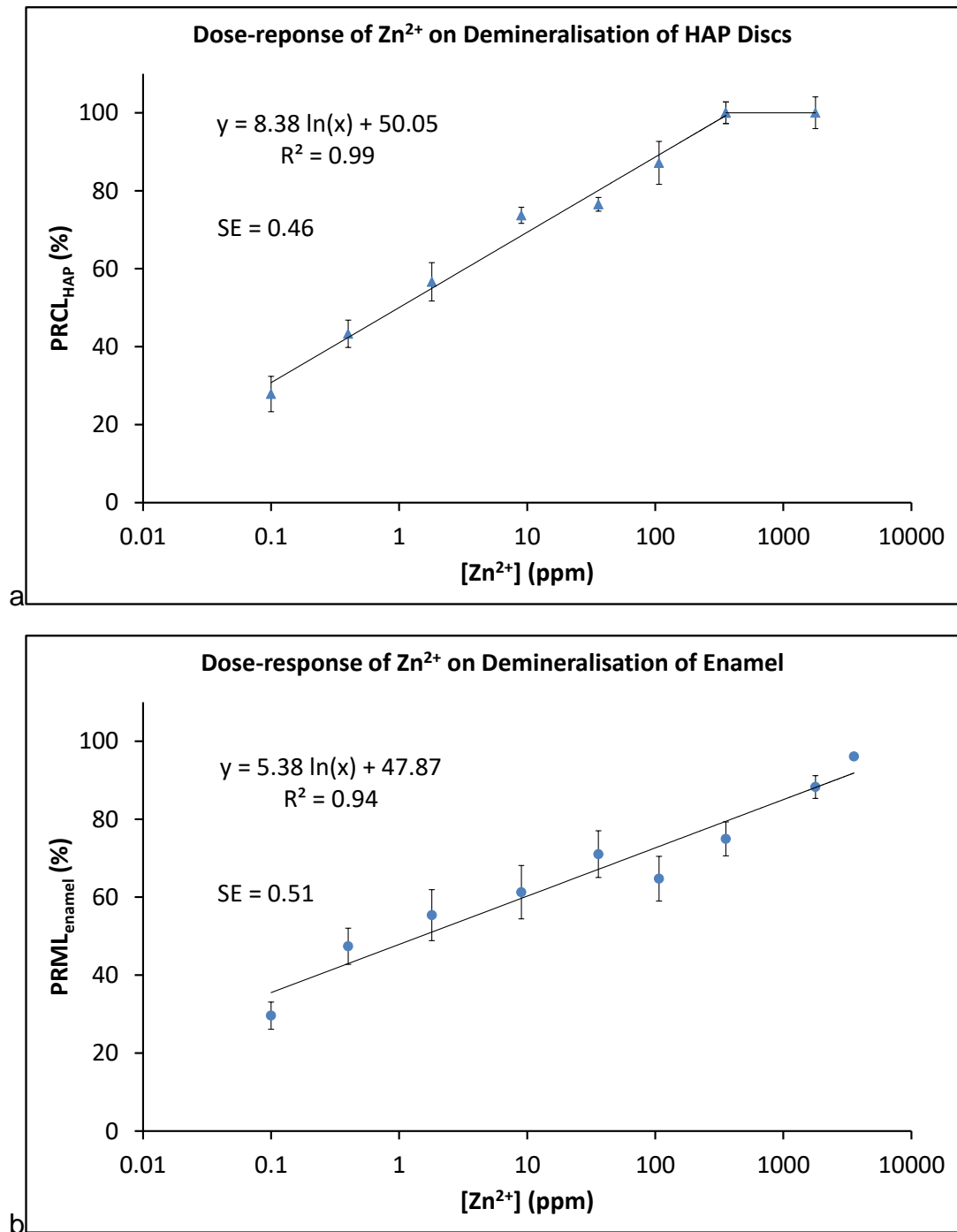


**Table 6.4** - The  $RCL_{HAP}$  and  $PRCL_{HAP}$  of every HAP disc measured at each  $[F^-]$ .

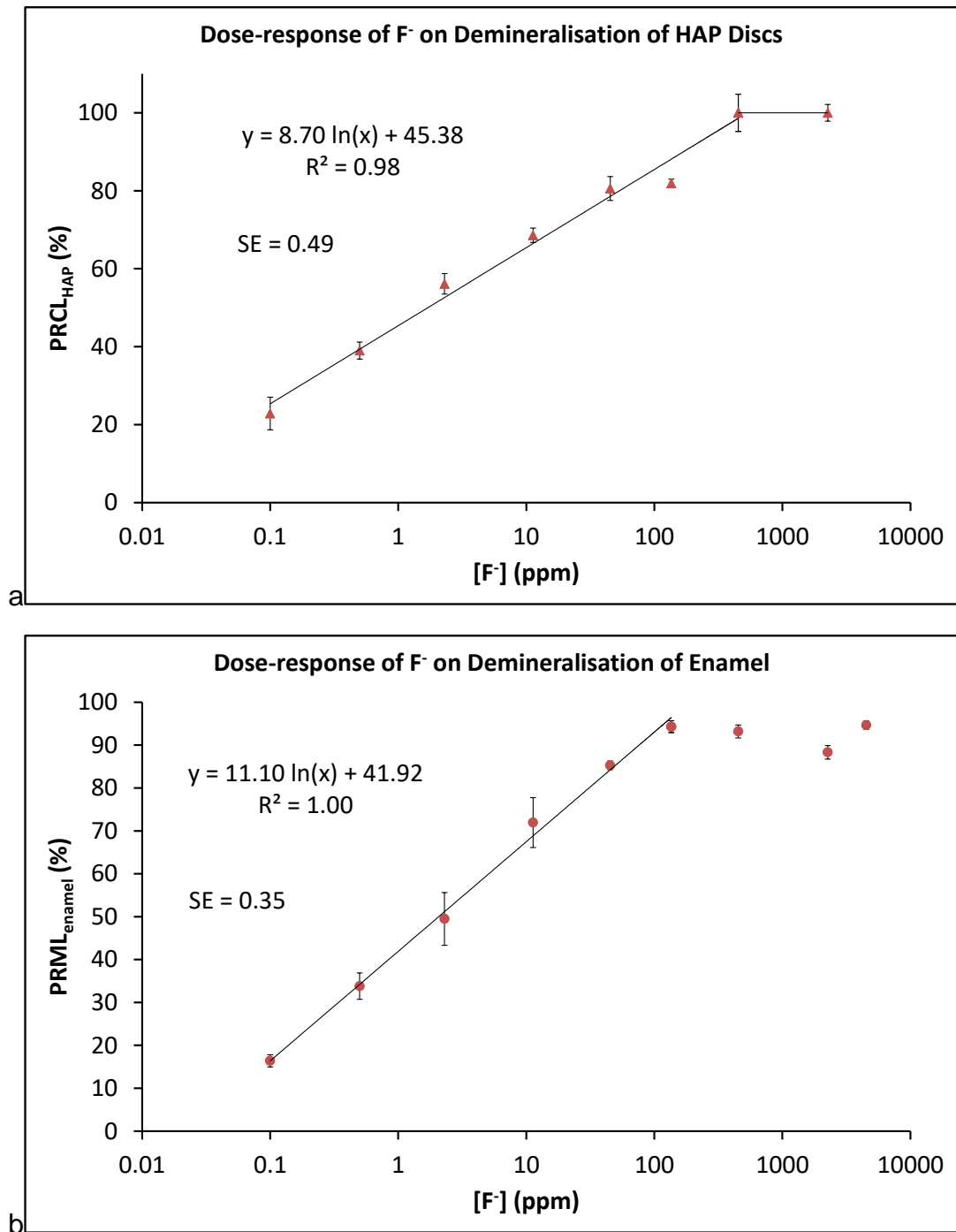
$[F^-]$	HAP Disc	$R_b \pm SE$ ( $\times 10^{-3}$ mM/h)	$R_a \pm SE$ ( $\times 10^{-3}$ mM/h)	$PRCL_{HAP}$ (%)
0.1 ppm	1	74.69 $\pm$ 0.20	62.54 $\pm$ 0.30	16.3
	2	113.50 $\pm$ 0.90	78.74 $\pm$ 0.10	30.6
	3	52.50 $\pm$ 0.20	41.19 $\pm$ 0.40	21.5
	Average	80.23 $\pm$ 17.83	60.82 $\pm$ 10.87	22.8 $\pm$ 4.2
0.5 ppm	1	114.10 $\pm$ 0.20	73.70 $\pm$ 0.20	35.4
	2	58.64 $\pm$ 0.10	33.41 $\pm$ 0.20	43.0
	3	61.73 $\pm$ 0.20	37.93 $\pm$ 0.20	38.6
	Average	78.16 $\pm$ 17.99	48.35 $\pm$ 12.74	39.0 $\pm$ 2.2
2.3 ppm	1	71.77 $\pm$ 0.30	30.40 $\pm$ 0.30	57.6
	2	54.99 $\pm$ 0.20	26.98 $\pm$ 0.20	51.0
	3	71.23 $\pm$ 0.40	28.69 $\pm$ 0.10	59.7
	Average	66.00 $\pm$ 5.10	28.69 $\pm$ 0.99	56.1 $\pm$ 2.7
11.3 ppm	1	45.09 $\pm$ 0.20	13.50 $\pm$ 0.15	70.1
	2	117.70 $\pm$ 0.60	34.42 $\pm$ 0.20	70.8
	3	82.92 $\pm$ 0.60	29.15 $\pm$ 0.20	64.8
	Average	81.92 $\pm$ 21.00	25.69 $\pm$ 6.28	68.6 $\pm$ 1.9
45.2 ppm	1	65.57 $\pm$ 0.20	11.48 $\pm$ 0.10	82.5
	2	77.03 $\pm$ 0.50	13.71 $\pm$ 0.10	82.2
	3	69.63 $\pm$ 0.60	15.70 $\pm$ 0.10	77.5
	Average	70.74 $\pm$ 3.35	13.63 $\pm$ 1.22	80.7 $\pm$ 1.2
135.7 ppm	1	43.88 $\pm$ 0.20	7.65 $\pm$ 0.01	82.6
	2	110.40 $\pm$ 0.50	22.25 $\pm$ 0.30	79.8
	3	100.40 $\pm$ 0.60	16.69 $\pm$ 0.40	83.2
	Average	84.89 $\pm$ 20.71	15.56 $\pm$ 4.26	81.9 $\pm$ 1.0
452.5 ppm	1	51.75 $\pm$ 0.10	3.32 $\pm$ 1.50	93.6
	2	75.12 $\pm$ 0.40	-7.01 $\pm$ 1.20	109.3
	3	80.33 $\pm$ 0.60	-4.92 $\pm$ 1.40	106.1
	Average	69.07 $\pm$ 8.79	-2.87 $\pm$ 3.15	<b>100.0 <math>\pm</math> 4.8</b>
2262.4 ppm	1	66.00 $\pm$ 0.10	-15.95 $\pm$ 1.40	124.2
	2	67.13 $\pm$ 0.10	-11.58 $\pm$ 2.20	117.3
	3	73.16 $\pm$ 0.50	-16.95 $\pm$ 2.60	123.2
	Average	68.76 $\pm$ 2.22	-14.83 $\pm$ 1.65	<b>100.0 <math>\pm</math> 2.2</b>

**Fig. 6.6a** and **Fig. 6.7a** show the mean  $PRCL_{HAP}$  plotted as the logarithm of  $[Zn^{2+}]$  and  $[F^-]$ , both showing a log-linear relationship. Both  $PRCL_{HAP}$  of  $Zn^{2+}$  and  $F^-$  increased with increasing concentrations. The  $PRCL_{HAP}$  of  $Zn^{2+}$  reached 100 % at 356.0 ppm, and the  $PRCL_{HAP}$  of  $F^-$  reached 100 % at 452.5 ppm.

**Fig. 6.6b** and **Fig. 6.7b** show the log-linear relationships between mean  $PRML_{enamel}$  of  $Zn^{2+}$  and  $F^-$  and their concentrations reported by Mohammed *et al.* (2014a & 2015), which are similar to those reported in this study.



**Figure 6.6** - (a) Log-linear relationship established between mean  $PRCL_{HAP}$  and  $[Zn^{2+}]$ . (b) Log-linear relationship established between mean  $PRML_{enamel}$  and  $[Zn^{2+}]$  (Replotted from Mohammed et al., 2015). Error bars show the standard errors.



**Figure 6.7** – (a) Log-linear relationship established between mean  $PRCL_{HAP}$  and  $[F]$ . (b) Log-linear relationship established between mean  $PRML_{enamel}$  and  $[F]$  (Replotted from Mohammed et al., 2014a). Error bars show the standard errors.

## 6.5 Discussion

The release of  $\text{Ca}^{2+}$ , used in this study as a proxy for demineralisation, was linear during real-time monitoring both before, and after the additions of  $\text{Zn}^{2+}$  and  $\text{F}^-$  (**Fig. 6.4** and **Fig. 6.5**) for all inhibitor concentrations used. This is similar to the data reported in the previous SMR studies, although over a different time-scale (Mohammed *et al.*, 2014a; Mohammed *et al.*, 2015). This suggests that the cariostatic influence is immediate (within the time-frame of the methodology), with no accumulation of inhibitor action. The changes in slope immediately after inhibitor addition show the changes in rates of calcium loss by the effects of  $\text{Zn}^{2+}$  and  $\text{F}^-$ . The log-linear relationships between mean  $\text{PRCL}_{\text{HAP}}$  and inhibitor concentrations (**Fig. 6.6a** and **Fig. 6.7a**) are similar to those previously reported by Mohammed *et al.* (2014a & 2015) (**Fig. 6.6b** and **Fig. 6.7b**), confirming the validity of the ISE methodology. Further, although the underlying reasons for the log-linear dose-response remain uncertain, the fact that this is repeatable using both methodologies suggests that the log-linear dose-response is a function of the chemistry of the interaction between these inhibitor ions and the inhibition of demineralisation. It has been proposed that the log-linear dependency of inhibition of demineralisation on  $\text{Zn}^{2+}$  and  $\text{F}^-$  may be due to the availability of fewer  $\text{PO}_4^{3-}$  and  $\text{Ca}^{2+}$  sites with increasing  $[\text{Zn}^{2+}]$  and  $[\text{F}^-]$ , and therefore more and more  $\text{Zn}^{2+}$  and  $\text{F}^-$  are competing for a smaller number of these unoccupied sites on the HAP crystal surfaces (Mohammed *et al.*, 2014a; Mohammed *et al.*, 2015).

In this study, HAP discs were utilised to simulate the demineralisation of human enamel under carious simulating condition, with or without the additions of inhibitors. The demineralisation process of HAP disc under carious or erosive challenge has been extensively investigated using different real-time monitoring techniques (Anderson *et al.*, 2004a; do Amaral *et al.*, 2016; Jones *et al.*, 2013; Kosoric *et al.*, 2010). Anderson *et al.* found that the mineral loss of HAP is linear with time for over 100 h using scanning micro-radiography (SMR) (Anderson *et al.*, 2004a). As the rate of mineral mass loss is constant, the process should be controlled by the reaction taking place at the advancing front. Similarly, it has been reported that both dissolution rates of enamel and HAP were constant, while the former was faster than the latter due to structural and compositional

differences between them (Berkovitz, 2011; Bollet-Quivogne *et al.*, 2005; Shellis *et al.*, 2010) (Section 1.3). This indicated that the demineralisation process of HAP is qualitatively similar to enamel but is quantitatively different. Consequently, the preliminary demineralisation research using HAP is useful to understand a simplified reaction occurring between the solution and dental mineral, even though the confirmatory work on the dental hard tissue is still necessary. In the present study, mean  $PRCL_{HAP}$  reached 100 % for  $[Zn^{2+}]$  above 356.0 ppm and for  $[F^-]$  above 452.5 ppm.

As ISE measures the activity of  $Ca^{2+}$ , representing the quantity of ion concentration corrected for interionic interactions, the data can be directly related to the chemical reactions occurring during the process (Rundle, 2000). This real-time  $Ca^{2+}$  ISE methodology can be used in studies of  $Ca^{2+}$  loss such as teeth, bones or dental materials, which make it a potential analytic tool to be utilised in a broader scale (Jeffcoat, 1998; Kumar *et al.*, 2013; Tezel *et al.*, 2011). For examples,  $Ca^{2+}$  loss from teeth and bones can be investigated to study dental caries, dental erosion or osteoporosis (Jeffcoat, 1998; Kumar *et al.*, 2013; Tezel *et al.*, 2011). Further, the  $Ca^{2+}$  release from some  $Ca^{2+}$ -containing dental materials such as casein phosphopeptide amorphous calcium phosphate (CPP-ACP) can be investigated to study its therapeutic effect on enamel demineralisation (Somasundaram *et al.*, 2013).

This study reproduced the results of Mohammed *et al.* (2014a & 2015) demonstrating a similar log-relationship established between mean  $PRCL_{HAP}$  and inhibitor concentration, which validated the use of real-time ISE as an effective *in vitro* method for monitoring demineralisation kinetics. Further, even though the real-time  $Ca^{2+}$  ISE system monitors the demineralisation indirectly from the solution, whereas, SMR monitors the demineralisation directly from the mineral mass of the specimen, the results showed that the values of PRCL and PRML (*i.e.*, from the two different techniques) are similar.

## 6.6 Conclusion

In conclusion, the demineralisation of dental mineral can be monitored by continuously recording the concentration of  $\text{Ca}^{2+}$  in the solution in contact with the dental mineral using real-time  $\text{Ca}^{2+}$  ISE measurements.

The technique can detect very small changes in rate because a large number of data points are measured before and after treatment.

# **PART IV: EXPERIMENTAL STUDIES**

## Chapter 7 A SMR STUDY OF THE DOSE-RESPONSE EFFECTS OF SILVER IONS IN SOLUTION ON DEMINERALISATION OF HUMAN ENAMEL

### 7.1 Introduction

The understanding of the effects of  $\text{Ag}^+$  (in solution) on demineralisation is crucial for the interpretation of the effects of topical treatments with silver compounds on demineralisation. It has been reported that following immersion of hydroxyapatite (HAP) in  $\text{AgNO}_3$ ,  $\text{Ag}^+$  can substitute for the  $\text{Ca}^{2+}$  in HAP, forming “ $\text{Ca}_{10-x}\text{Ag}_x(\text{PO}_4)_6(\text{OH})_2$ ” (Ling Feng *et al.*, 1998; Singh *et al.*, 2011). Further, the susceptibility of the  $\text{Ag}^+$  substituted HAP to acid attack has been reported to increase with increasing incorporation of  $\text{Ag}^+$  in the HAP (Singh *et al.*, 2011). Therefore, the  $\text{Ag}^+$  has an accelerating effect on demineralisation of HAP by the formation of a  $\text{Ag}^+$  substituted HAP. The chemical formula of  $\text{Ag}^+$  substituted HAP,  $\text{Ca}_{10-x}\text{Ag}_x(\text{PO}_4)_6(\text{OH})_2$ , proposed in the previous study (Singh *et al.*, 2011) does not have a balance in charge, as it requires two one-charged  $\text{Ag}^+$  to replace one two-charged  $\text{Ca}^{2+}$ . Therefore, the correct stoichiometry for a  $\text{Ag}^+$  substituted HAP should be  $\text{Ca}_{10-x}\text{Ag}_{2x}(\text{PO}_4)_6(\text{OH})_2$ . Further studies are required to confirm the stoichiometry.

The reaction between  $\text{Ag}^+$  and human enamel, mainly composed of HAP (Hicks *et al.*, 2004), should be similar to that of HAP. This suggests that the demineralisation of human enamel would *increase* with increasing concentration of  $\text{Ag}^+$  in solution in contact with the human enamel, as reported by Singh *et al.* (2011). However, as human enamel has composition gradients and a hierarchical structure which are different from synthetic HAP discs (Section 1.3) (Robinson *et al.*, 2000; Robinson, 2009; Yilmaz *et al.*, 2015), a confirmatory study is still needed.

Scanning microradiography (SMR) is a real-time technique which can monitor the mineral loss of a demineralising specimen in controlled conditions based on the attenuation of X-ray beams (Anderson and Elliott, 1993). Further, SMR has



been used in previous studies investigating the dose-response of other metal ions on demineralisation of human enamel (e.g.,  $Zn^{2+}$ ) (Mohammed *et al.*, 2015).

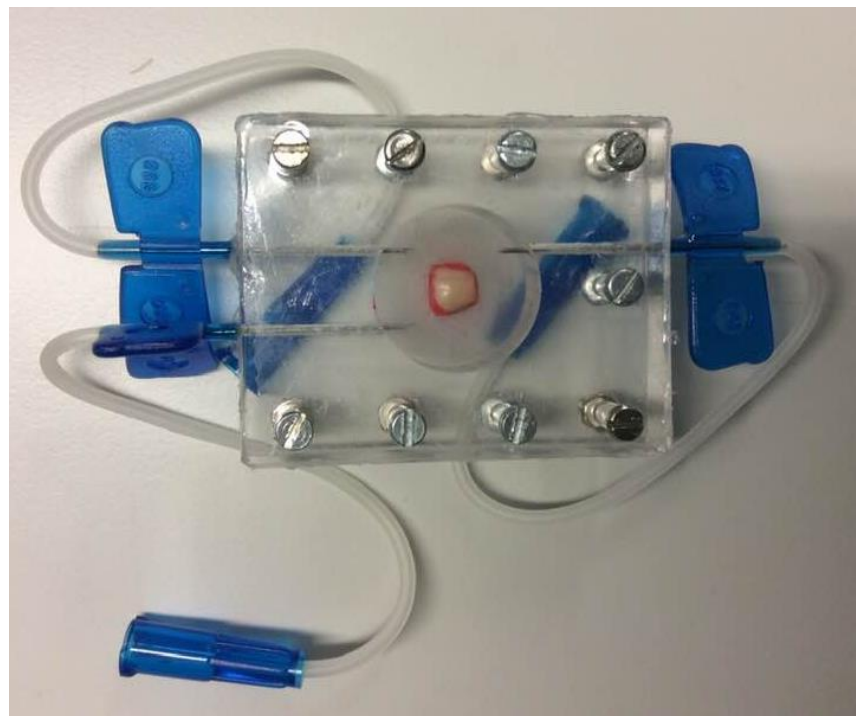
## 7.2 Aim

The aim of this *in vitro* study was to investigate the dose-response effects of Ag<sup>+</sup> in solution on demineralisation of a human enamel block using SMR.

## 7.3 Materials and Methods

### 7.3.1 Preparation of Enamel Block

An enamel block (5 mm X 5 mm with ~ 2mm in thickness) was sectioned from a caries-free permanent molar (QMREC 2011/99) using a cutting machine (Struers Accutom-5; USA). The dentine was polished away (300 LVAC, Kemet) with carbide papers with roughness up to P4000 under copious water cooling. Subsequently, the cut internal surface was coated with red nail lacquer (KIKO, Italy), and was put into a SMR environmental cell (volume = 2 cm<sup>3</sup>), leaving only the natural surface exposed (**Fig 7.1**).

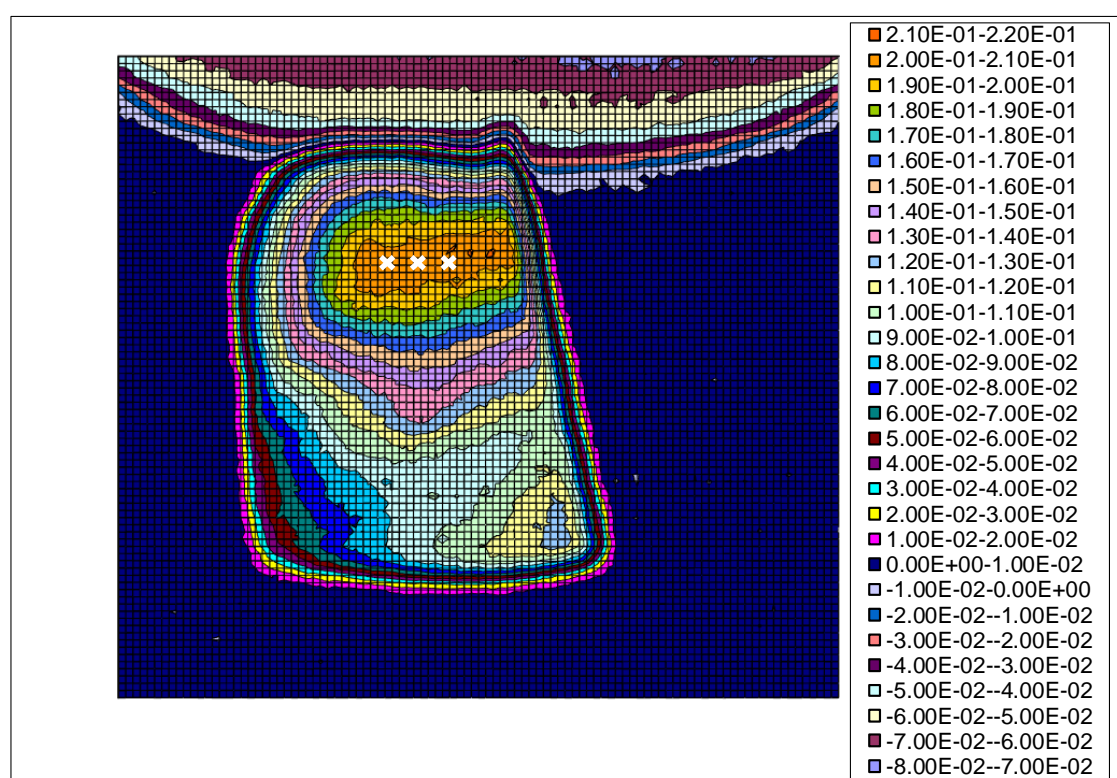


*Figure 7.1 – The SMR environmental cell containing an enamel block.*

### 7.3.2 Preparation of the Demineralisation Solution

A 1 L, 0.1 M CH<sub>3</sub>COOH (Sigma-Aldrich, UK) demineralising solution buffered by adding 1.0 M KOH (Sigma-Aldrich, UK) drop by drop to pH 4.0 was prepared, as described in Section 6.3.2.

### 7.3.3 SMR Area Scan of the Sample



**Figure 7.2** – Area scanning of an enamel block. The coloured scale (on right) represents the projected mineral mass (g\*cm<sup>2</sup>) in the sample. The white crosses show the three scan points.

After the SMR cell containing the enamel sample was mounted on the SMR scanning stage, an SMR area scan of the enamel sample was performed. This provided an indication of the different projected mineral density levels of the sample and its exact location on the SMR stage (**Fig. 7.2**). Three scan points on the horizontal line, 0.5 mm apart, were chosen in the area with similar projected

mineral mass. The mineral masses of these points were then monitored throughout the demineralisation period.

### 7.3.4 Demineralisation Study

Throughout the demineralisation study, the demineralisation solution was circulated at 0.788 mL/min, during which the X-ray beam was targeted at the three selected scan points. Subsequently, AgNO<sub>3</sub> (Sigma-Aldrich, UK) was added to the demineralisation solution to obtain concentrations of 0.0 ppm Ag<sup>+</sup>, 0.1 ppm Ag<sup>+</sup>, 9.0 ppm Ag<sup>+</sup> and 3565.0 ppm Ag<sup>+</sup>. These four concentrations were chosen from the range of concentrations used in the previous SMR study investigating the dose-response of Zn<sup>2+</sup> on enamel demineralisation (Mohammed *et al.*, 2015). Further, the range of [Ag<sup>+</sup>] in saliva following topical treatment with Ag[NH<sub>3</sub>]<sub>2</sub>F has been reported to be between 2.36 X 10<sup>-3</sup> M and 2.36 X 10<sup>-2</sup> M (= 254.9 ppm and 2548.8 ppm Ag<sup>+</sup>) (Mei *et al.*, 2017), which was covered by the [Ag<sup>+</sup>] range in the present study.

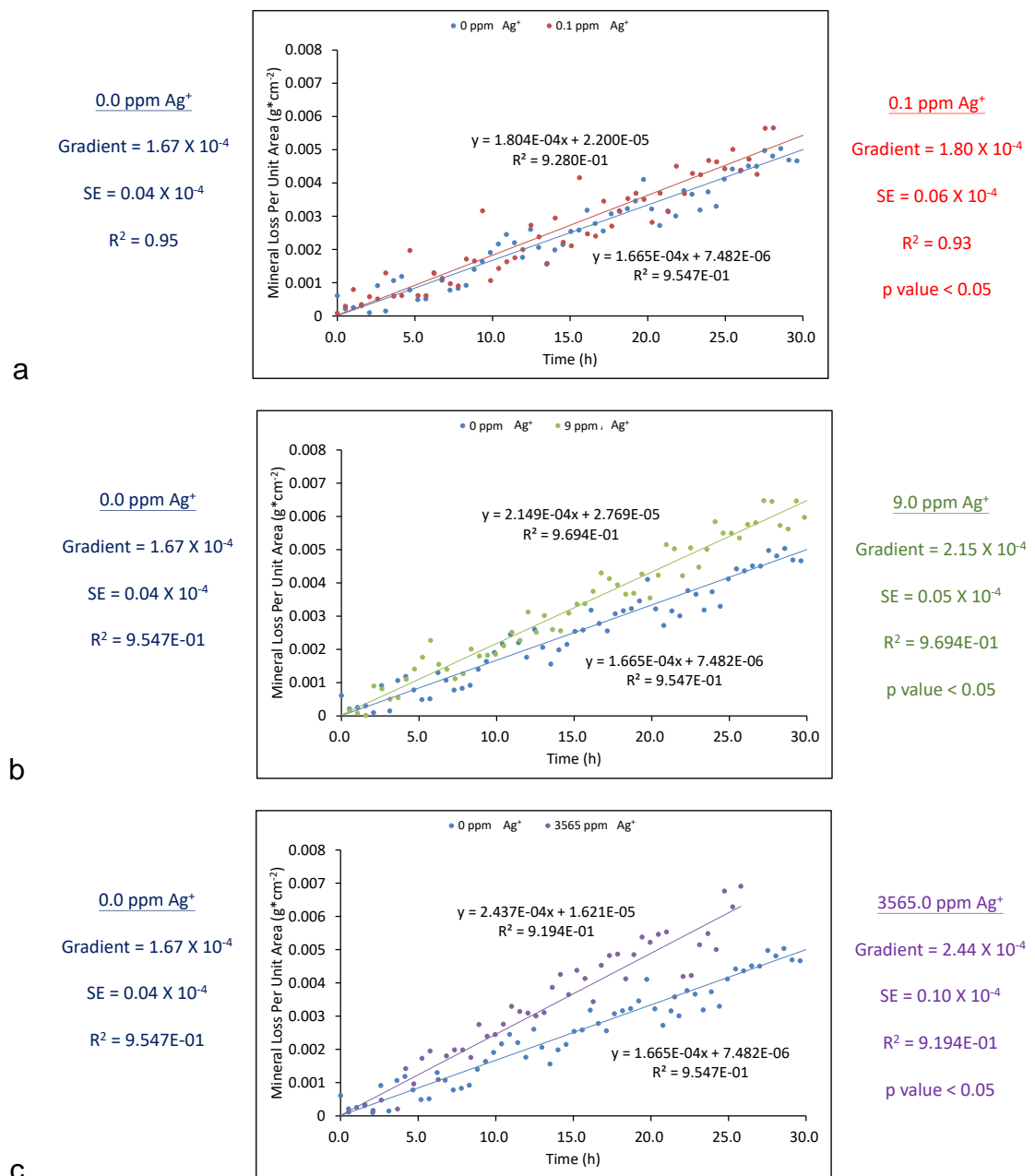
Initially, demineralisation solution (without Ag<sup>+</sup>) was circulated through the SMR cell for a period around 30 h, whilst the mineral mass measurements of the three scan points were continuously monitored at 30 min intervals. After the initial demineralisation period, the SMR cell was circulated with the demineralisation solution containing 0.1 ppm Ag<sup>+</sup>, 9.0 ppm Ag<sup>+</sup> and 3565.0 ppm Ag<sup>+</sup> for a period around 30 h, respectively, whilst the mineral mass measurements of the three scan points were monitored throughout all the demineralisation periods. The study was carried out at 23.0±1.0 °C, as described in the previous Zn<sup>2+</sup> study (Mohammed *et al.*, 2015).

After the study, the mineral loss per unit area (g\*cm<sup>-2</sup>) of each point measured at each [Ag<sup>+</sup>] was plotted as a function of time (h), and the rates of enamel mineral loss (RML<sub>enamel</sub>) recorded at 0.1 ppm Ag<sup>+</sup>, 9.0 ppm Ag<sup>+</sup> and 3565.0 ppm Ag<sup>+</sup> were compared with that recorded during the initial demineralisation (without Ag<sup>+</sup>) for every scan point. Next, the percentage reduction in the rate of mineral loss of enamel (PRML<sub>enamel</sub>) at each [Ag<sup>+</sup>] was calculated as the ratio of the RML<sub>enamel</sub> at

that  $[Ag^+]$  to the  $RML_{enamel}$  without  $Ag^+$  to assess the inhibitory efficacy of the  $Ag^+$ . A positive value of  $PRML_{enamel}$  indicates the inhibition of enamel demineralisation, whereas, the negative value of  $PRML_{enamel}$  indicates the acceleration of enamel demineralisation.

## 7.4 Results

**Fig. 7.3** shows the trendlines of the mineral loss per unit area ( $g^*cm^{-2}$ ) measured at the scan point 3 for 0.0 ppm  $Ag^+$  compared to that measured at the same scan point for (a) 0.1 ppm  $Ag^+$ , (b) 9.0 ppm  $Ag^+$ , and (c) 3565.0 ppm  $Ag^+$ . The trendline observed for every  $[Ag^+]$  was linear with time. Further, the  $RML_{enamel}$  ( $g^*cm^{-2}h^{-1}$ ) increased with increasing  $[Ag^+]$  in the solution.



**Figure 7.3** – Trendlines of the mineral loss per unit area ( $g^*cm^{-2}$ ) measured at the scan point 3 for 0.0 ppm  $Ag^+$  compared to that measured at the same scan point for (a) 0.1 ppm  $Ag^+$ , (b) 9.0 ppm  $Ag^+$ , and (c) 3565.0 ppm  $Ag^+$ .

**Table 7.1** shows the  $RML_{\text{enamel}} \pm SE$  ( $\times 10^{-4} \text{ g} \cdot \text{cm}^{-2} \cdot \text{h}^{-1}$ ) and  $PRML_{\text{enamel}}$  (%) measured at different scan points for increasing  $[Ag^+]$  in the solution. The error of the gradient was calculated using SigmaPlot 10.0 (Systat Software, California, USA).  $PRML_{\text{enamel}}$  highlighted in red indicate that the  $RML_{\text{enamel}}$  measured at that  $[Ag^+]$  were not significantly different ( $p > 0.05$ ) from the  $RML_{\text{enamel}}$  measured at 0 ppm  $Ag^+$ .

After an increase of  $[Ag^+]$  in the solution to 0.1 ppm, changes in the  $RML_{\text{enamel}}$  measured at the three scan points were not consistent with each other. The  $RML_{\text{enamel}}$  measured at the scan point 1 and 2 were inhibited, whereas that of the scan point 3 was increased. After the following increase of  $[Ag^+]$  in the solution to 9.0 ppm and 3565.0 ppm, all the  $RML_{\text{enamel}}$  measured at every scan point were increased.

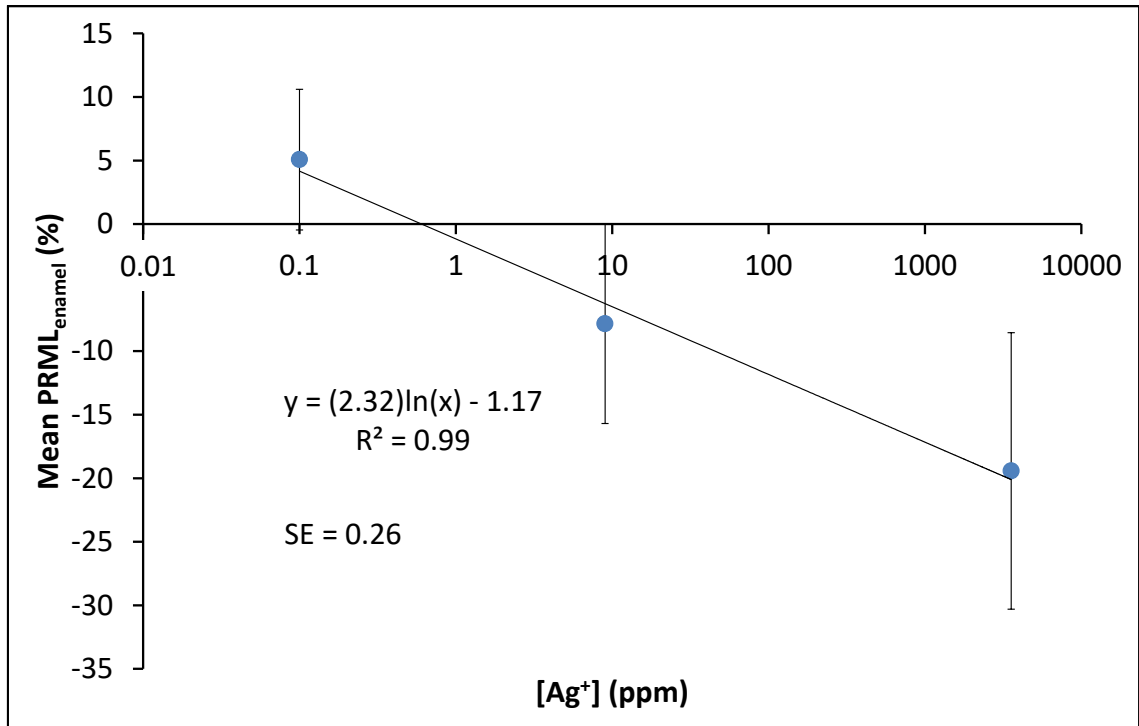
The mean  $PRML_{\text{enamel}}$  (%) shows that minor inhibitory efficacy on enamel demineralisation was observed for 0.1 ppm  $Ag^+$ . However, this inhibitory efficacy disappeared with increasing  $[Ag^+]$ , as the enamel demineralisation was accelerated with increasing  $[Ag^+]$  from 9.0 ppm to 3565.0 ppm  $Ag^+$ .



**Table 7.1** – The  $RML_{enamel}$  and  $PRML_{enamel}$  measured at each point for every  $[Ag^+]$  in solution.  $PRML_{enamel}$  highlighted in red indicate that the  $RML_{enamel}$  were not significantly different from the  $RML_{enamel}$  measured at 0 ppm  $Ag^+$ .

Scan Point		0 ppm $Ag^+$	0.1 ppm $Ag^+$	9 ppm $Ag^+$	3565 ppm $Ag^+$
1	$RML_{enamel} \pm SE$ ( $X 10^{-4} g^*cm^{-2}*h^{-1}$ )	$2.5 \pm 0.0$	$2.2 \pm 0.1$	$2.5 \pm 0.1$	$2.7 \pm 0.0$
	$PRML_{enamel}$ (%)	0.0	12.0	0.0	-8.0
2	$RML_{enamel} \pm SE$ ( $X 10^{-4} g^*cm^{-2}*h^{-1}$ )	$1.1 \pm 0.0$	$1.0 \pm 0.1$	$1.1 \pm 0.1$	$1.2 \pm 0.0$
	$PRML_{enamel}$ (%)	0.0	9.1	0.0	-9.1
3	$RML_{enamel} \pm SE$ ( $X 10^{-4} g^*cm^{-2}*h^{-1}$ )	$1.7 \pm 0.0$	$1.8 \pm 0.1$	$2.1 \pm 0.1$	$2.4 \pm 0.1$
	$PRML_{enamel}$ (%)	0.0	-5.9	-23.5	-41.2
Average	Mean $RML_{enamel}$ ( $X 10^{-4} g^*cm^{-2}*h^{-1}$ )	$1.8 \pm 0.4$	$1.7 \pm 0.4$	$1.9 \pm 0.4$	$2.1 \pm 0.5$
	Mean $PRML_{enamel}$ (%)	$0.0 \pm 0.0$	$5.1 \pm 5.5$	$-7.8 \pm 7.8$	$-19.4 \pm 10.9$

**Fig. 7.4** shows a log-linear relationship ( $R^2 = 0.99$ ) between the mean  $PRML_{enamel}$  and the  $[Ag^+]$  in the solution. This log-linear dependency indicates that enamel exhibited increasingly faster demineralisation at a higher  $[Ag^+]$ .



**Figure 7.4** – The mean  $PRML_{enamel}$  plotted against increasing  $[Ag^+]$  in the demineralisation solution. Error bars show the standard errors.

## 7.5 Discussion

This *in vitro* study investigated the effects of increasing  $[Ag^+]$  on the demineralisation of human enamel using SMR. Three concentrations (0.1 ppm, 9.0 ppm and 3565.0 ppm) of  $Ag^+$  and a control (0 ppm) were selected in the present study, mirroring the concentrations used in the previous SMR study investigating the dose-response effects of  $Zn^{2+}$  on enamel demineralisation (Mohammed *et al.*, 2015). This enabled the comparison of the dose-response effects of these two metal ions on the enamel demineralisation under the same condition.

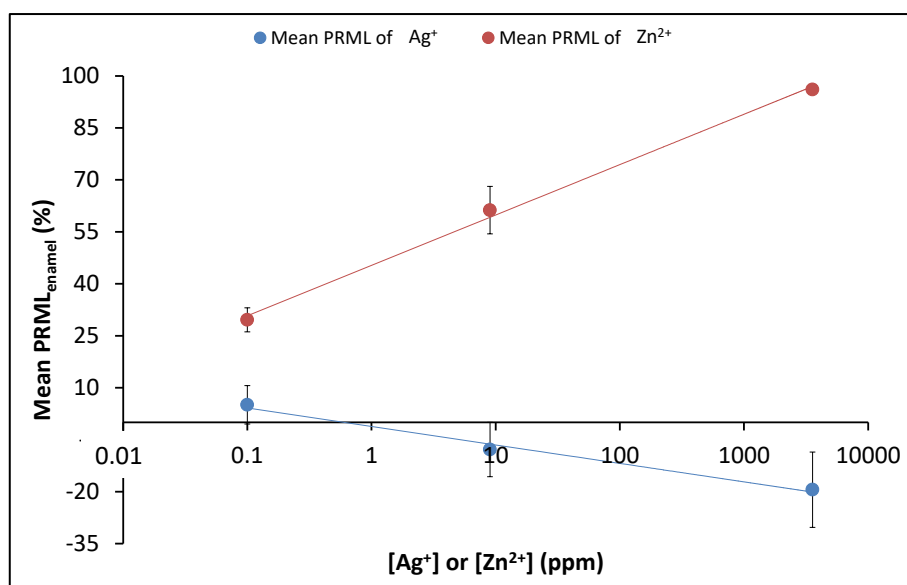
As human enamel has variations in compositions, which would, therefore, result in a difference in solubility (Robinson *et al.*, 1995), demineralisation studies using different specimens in control and experimental groups require a large number of enamel samples to ensure the reproducibility. In this study, the rates of enamel demineralisation measured at each scan point for 0.1 ppm, 9.0 ppm and 3565.0 ppm of  $[Ag^+]$  were compared with the rates of enamel initial demineralisation (without  $Ag^+$ ) measured at the same scan point with similar mineral mass on the same enamel sample. Therefore, numerous samples were not necessary as each scan point acted as its own control.

In the present study, all the trends in mineral loss from demineralising enamel observed were linear with time (**Fig. 7.3**), which is consistent with previous SMR studies (Anderson *et al.*, 1998; Anderson *et al.*, 2004a; Mohammed *et al.*, 2014a; Mohammed *et al.*, 2015). Even though the mean  $RML_{enamel}$  values measured at three scan points for each  $[Ag^+]$  were different, the change of mean  $PRML_{enamel}$  with increasing  $[Ag^+]$  measured at each scan point showed a similar trend (**Table 7.1**). The effects of 0.1 ppm  $Ag^+$  on demineralisation of enamel were not consistent between scan points, as the mean  $RML_{enamel}$  of scan points 1 and 2 were decreased, whereas, the mean  $RML_{enamel}$  of the scan point 3 was increased after the addition of  $Ag^+$  (**Table 7.1**). This may be due to that the effect of  $Ag^+$  was not strong enough at this low  $[Ag^+]$  to show a consistent effect on all the scan points of the enamel. Following the increase of  $[Ag^+]$  to 9.0 ppm and then further to 3565.0 ppm, the mean  $RML_{enamel}$  at all scan points kept increasing (**Table 7.1**).

The increase in mean  $RML_{\text{enamel}}$  may be due to the substitution of  $Ca^{2+}$  by  $Ag^+$ , forming  $Ag^+$  substituted enamel, which has a higher susceptibility to acid challenge than that of enamel (Singh *et al.*, 2011). The increased susceptibility of the  $Ag^+$  substituted enamel to acid challenge may result from the difference between the charges of  $Ag^+$  and  $Ca^{2+}$ , which made  $Ag^+$  unable to facilitate proper bonding with other ions, and thereby destabilised the HAP lattice. Therefore, the increase in mean  $RML_{\text{enamel}}$  following the increase of  $[Ag^+]$  to 9.0 ppm and to 3565.0 ppm indicates that the formation of  $Ag^+$  substituted enamel dominated the dose-response effects of  $Ag^+$  on enamel demineralisation at these  $[Ag^+]$ .

The change in the mean  $PRML_{\text{enamel}}$  (from  $5.1 \pm 5.5$  % to  $-7.8 \pm 7.8$  %) following  $[Ag^+]$  increased from 0.1 ppm to 9.0 ppm (an increase of 8.9 ppm  $Ag^+$ ), was comparable to that (from  $-7.8 \pm 7.8$  % to  $-19.4 \pm 10.9$  %) following  $[Ag^+]$  increased from 9.0 ppm to 3565.0 ppm (an increase of 3556.0 ppm  $Ag^+$ ) (**Table 7.1**). This indicates that  $Ag^+$  exhibited a greater change in accelerating enamel demineralisation at lower  $[Ag^+]$  compared to higher  $[Ag^+]$ , which led to a log-linear relationship observed between the mean  $PRML_{\text{enamel}}$  and the  $[Ag^+]$  (**Fig. 7.4**).

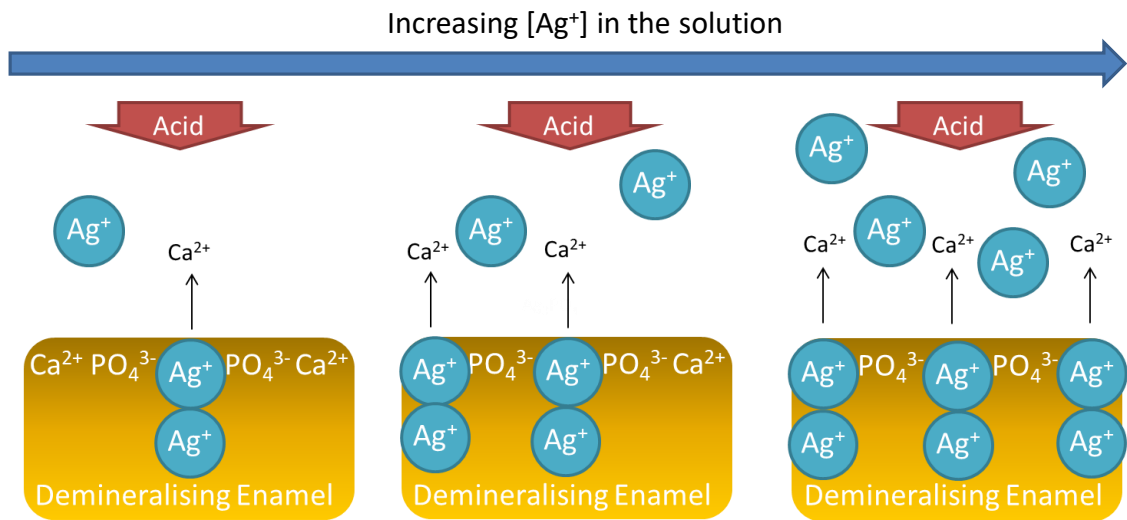
In a previous SMR study of the dose-response effects of  $Zn^{2+}$  on enamel demineralisation, a log-linear relationship was also found between the mean  $PRML_{\text{enamel}}$  and  $[Zn^{2+}]$ . More noticeably, the inhibitory efficacy of  $Zn^{2+}$  *increased* with increasing  $[Zn^{2+}]$  (**Fig. 7.5**) (Mohammed *et al.*, 2015). The difference between the effects of  $Ag^+$  and  $Zn^{2+}$  on the enamel demineralisation may be due to the ability of the ion in substituting for the  $Ca^{2+}$  in HAP. So far, no substitution of  $Ca^{2+}$  in HAP with  $Zn^{2+}$  has been reported. It has been proposed that all attempts to produce  $Zn^{2+}$  substituted apatite resulted in a mixture of phase such as  $Zn_3(PO_4)_2 \cdot 4H_2O$  (McConnell and Foreman, 1966; Mohammed *et al.*, 2014b).



**Figure 7.5** – Comparison between the log-linear dose-response effects of Ag<sup>+</sup> (Blue line) and Zn<sup>2+</sup> (Red line) (From Mohammed *et al.*, 2015) on enamel demineralisation. Error bars show the standard errors.

The log-linear dependency of the inhibition of enamel demineralisation on [Zn<sup>2+</sup>] was suggested to be due to the occupation of the PO<sub>4</sub><sup>3-</sup> sites on enamel surfaces (Mohammed *et al.*, 2015). As the number of the PO<sub>4</sub><sup>3-</sup> sites unoccupied with Zn<sup>2+</sup> is decreased with increasing [Zn<sup>2+</sup>], the increase in the inhibitory efficacy is decreased with increasing [Zn<sup>2+</sup>], as more and more Zn<sup>2+</sup> are competing for a smaller number of the unoccupied sites on the enamel surface. Whereas, the log-linear dependency of acceleration of enamel demineralisation on [Ag<sup>+</sup>] may be due to the number of the Ca<sup>2+</sup> sites on the enamel surfaces able to be substituted by Ag<sup>+</sup>, decreased with increasing [Ag<sup>+</sup>], which led to less change in the mean PRML<sub>enamel</sub> exhibited at higher [Ag<sup>+</sup>] range. This is shown schematically in **Fig. 7.6**.

Therefore, Ag<sup>+</sup> accelerates the enamel demineralisation. Thus, the cariostatic effects of AgNO<sub>3</sub> topical treatment on carious enamel must be due to the antibacterial properties of Ag<sup>+</sup> (Lansdown, 2002; Lansdown, 2006; Russell and Hugo, 1994; Thibodeau *et al.*, 1978) (Section 3.2). Further, as the accelerating effect on enamel demineralisation of Ag<sup>+</sup> increases with increasing concentration, the concentration of AgNO<sub>3</sub> topically applied on the enamel should not be too high, in order to obtain an optimal therapeutic outcome.



**Figure 7.6** – Schematic representation of the log-linear dependency of the acceleration of enamel demineralisation on  $[Ag^+]$  showing a decreasing number of  $Ca^{2+}$  sites can be substituted by  $Ag^+$  with increasing  $[Ag^+]$ .

## 7.6 Conclusion

There is a negative dose-response effect of  $\text{Ag}^+$  in solution on the demineralisation inhibition of human enamel. Further, there is a log-linear relationship between the inhibitory efficacy and the  $[\text{Ag}^+]$ .

## Chapter 8 EFFECTS OF TOPICAL TREATMENTS WITH SILVER COMPOUNDS ON DEMINERALISATION OF HAP DISCS

### 8.1 Introduction

Silver nitrate ( $\text{AgNO}_3$ ), silver fluoride ( $\text{AgF}$ ) and silver diammine fluoride (SDF,  $\text{Ag}[\text{NH}_3]_2\text{F}$ ) have been used for the management of dental caries for many decades (Peng *et al.*, 2012) (Chapter 3). Currently,  $\text{Ag}[\text{NH}_3]_2\text{F}$  is the most popular silver compound used in clinical practice (Horst *et al.*, 2016). Different concentrations of  $\text{Ag}[\text{NH}_3]_2\text{F}$  are used in commercial products, with 3.16 M (Silver Capsule of Riva Star, SDI Ltd, Australia) the highest concentration available (Fung *et al.*, 2013; SDI, 2016a).

The inhibitory mechanisms of these silver compound topical treatments on dental mineral demineralisation remain obscure (Mei *et al.*, 2017; Zhao *et al.*, 2017a). Therefore, real-time  $\text{Ca}^{2+}$  ISEs were used in this study to measure the reduction in the rate of  $\text{Ca}^{2+}$  release following topical treatments with 3.16 M  $\text{AgNO}_3$ , 3.16 M  $\text{AgF}$  and 3.16 M  $\text{Ag}[\text{NH}_3]_2\text{F}$ , as an assessment of the caries inhibition efficacy (Huang *et al.*, 2018). Furthermore,  $\text{Ag}^+$  and  $\text{F}^-$  ISEs are also available (Section 5.2), which can be used to investigate the interactions of  $\text{F}^-$  and  $\text{Ag}^+$  with dental mineral following treatments with silver compounds.  $\text{NaF}$  was not used to assess the inhibitory efficacy of the topical treatment with fluoride in the present study as the highest concentration of  $\text{NaF}$  agent is only about 0.95 M.

$^{31}\text{P}$  and  $^{19}\text{F}$  Magic Angle Spinning–Nuclear Magnetic Resonance (MAS–NMR) characterisation studies have been used in dental research to identify apatite species (Tsai and Chan, 2011), and to differentiate between FAP, fluorhydroxyapatite (FHA),  $\text{CaF}_2$  and HAP (Mohammed *et al.*, 2013; White *et al.*, 1994; White *et al.*, 1988). Therefore, they can be used to detect any phosphorous and fluorine reaction products formed after the interactions between silver compounds and dental mineral.



Photographs of the dental mineral samples (e.g., HAP discs) topically treated with silver compounds can also be used to monitor discolouration. As  $\text{Ag}_3\text{PO}_4$  is yellow (Lewis, 1920), which is chemically reduced to black metallic silver after exposure to light and/or heat (Lou *et al.*, 2011), colour changes of lesions following the silver compound topical treatments can indicate  $\text{Ag}_3\text{PO}_4$  formation.

## 8.2 Aims

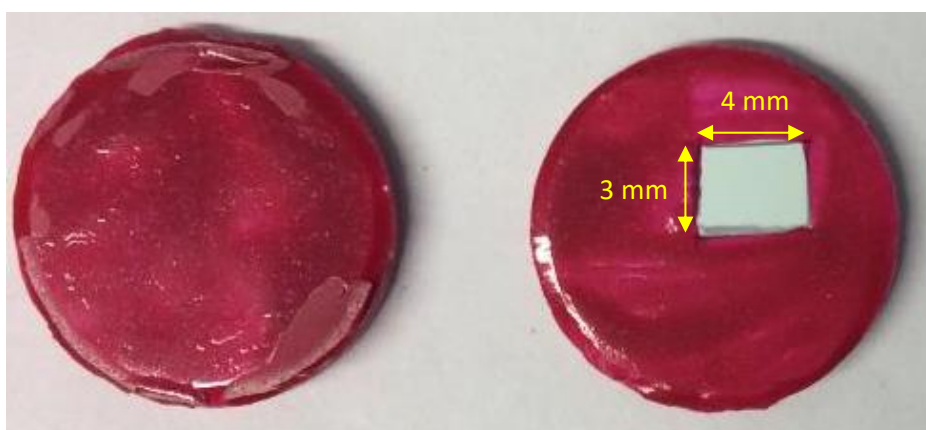
The first aim was to understand the inhibitory mechanisms of  $\text{AgNO}_3$ ,  $\text{AgF}$  and  $\text{Ag}[\text{NH}_3]_2\text{F}$  topical treatments on the demineralisation of HAP discs. This was achieved by investigating the effects of topical treatments with  $\text{AgNO}_3$ ,  $\text{AgF}$  and  $\text{Ag}[\text{NH}_3]_2\text{F}$  on the demineralisation of HAP discs, using:  $\text{Ca}^{2+}$ ,  $\text{Ag}^+$  and  $\text{F}^-$  ion selective electrodes (ISEs), digital camera, scanning electron microscopy (SEM), energy dispersive X-ray analysis (EDX). Further,  $^{31}\text{P}$  and  $^{19}\text{F}$  MAS-NMR were also used to identify any phosphorous and fluoride reaction products formed following the interactions between silver compounds and HAP powders.

The second aim was to compare the inhibitory efficacy and the effects of topical treatment with a commercial  $\text{Ag}[\text{NH}_3]_2\text{F}$  product with laboratory-prepared  $\text{Ag}[\text{NH}_3]_2\text{F}$  on demineralisation of HAP discs. This was achieved by investigating the effects of topical treatment with Silver Capsule of Riva Star, on the demineralisation inhibition of HAP discs, using the techniques mentioned above.

## 8.3 Materials and Methods

ISE study, digital imaging, and SEM and EDX analyses were conducted using HAP discs typically treated with  $\text{AgNO}_3$ ,  $\text{AgF}$  and  $\text{Ag}[\text{NH}_3]_2\text{F}$ , which underwent demineralisation.  $^{31}\text{P}$  and  $^{19}\text{F}$  MAS-NMR analyses were conducted on HAP powders mixed with these silver compounds, with and without acid challenge. As the amounts of reaction products formed in these mixed powders were large, the changes in the proportions of the reaction products before and after acid challenge can be monitored.

### 8.3.1 ISE Study



*Figure 8.1 – Nail-varnished porous HAP discs.*

Fifteen porous HAP discs (20% porosity, 12 mm in diameter, 2 mm in thickness; Plasma Biototal Ltd, UK) were varnished with red nail lacquer (KIKO, Italy) to leave only a 3 mm X 4 mm window on each sample exposed (**Fig. 8.1**). The window sizes were standardised to control the area exposed to acid challenge. The varnished discs were then allocated into five treatment groups ( $n = 3$  each) (shown in **Table 8.1**). The demineralisation solution was made using 0.1 M  $\text{CH}_3\text{COOH}$  buffered to pH 4.0, using KOH, as described in Section 6.3.2.

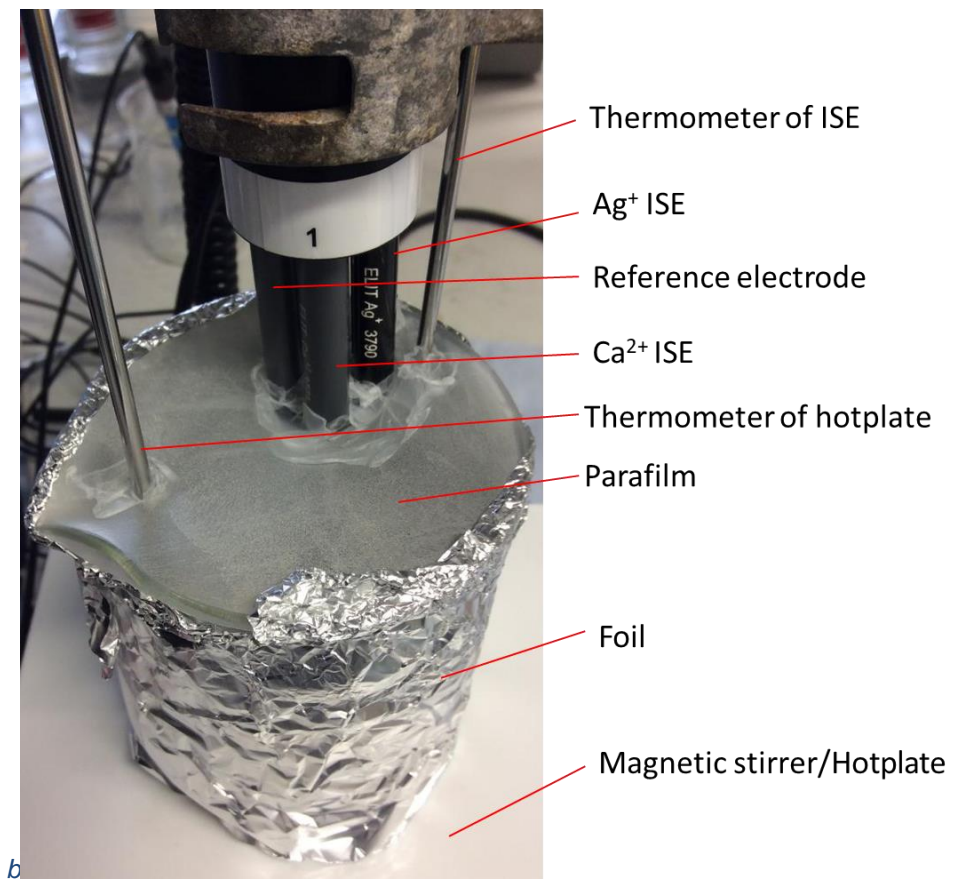
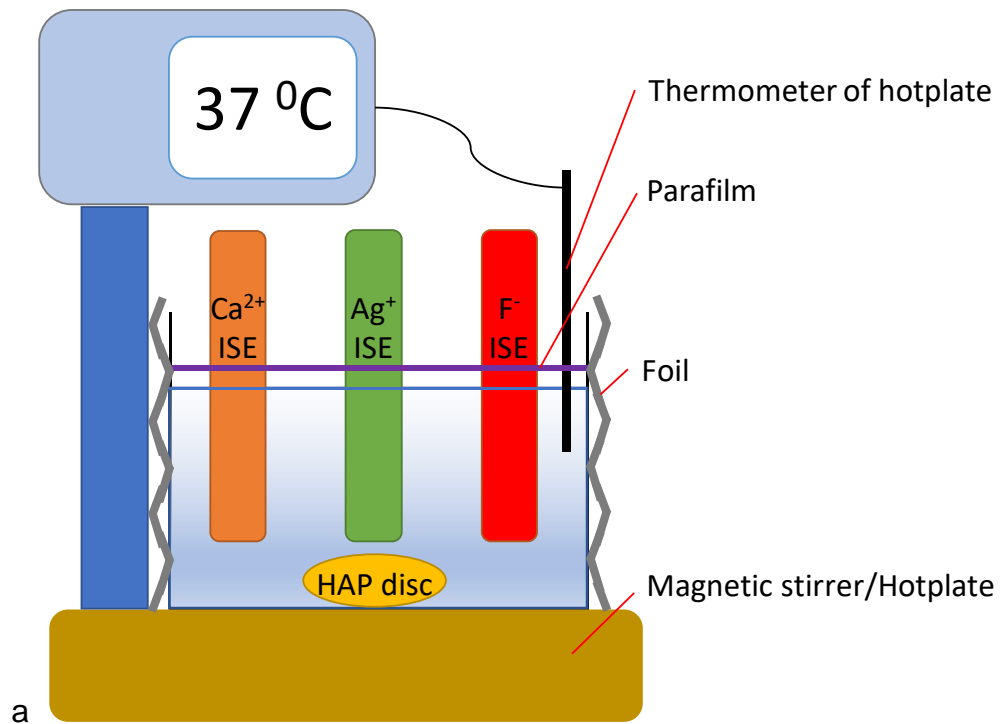
**Table 8.1** – Compositions of treatment groups.

Group names	Compositions	*Preparation
DW Tx	De-ionised water	From Triplered Ltd (UK)
AgNO <sub>3</sub> Tx	3.16 M AgNO <sub>3</sub>	1.07 g AgNO <sub>3</sub> + 2 mL DW
AgF Tx	3.16 M AgF	0.80 g AgF + 2 mL DW
Ag[NH <sub>3</sub> ] <sub>2</sub> F Tx	3.16 M SDF	0.80 g AgF + 1 mL DW + 1 mL 30 wt% NH <sub>4</sub> OH
Riva-SC Tx	Silver Capsule (3.16 M SDF)	Riva Star of SDI Ltd (Australia)

\* = all chemicals shown in preparation are from Sigma-Aldrich, UK

Calibrations of Ca<sup>2+</sup>, F<sup>-</sup> and Ag<sup>+</sup> ISEs were conducted before the experiment, as described in Section 6.3.3, but at 37±0.3 °C (LLOD of Ca<sup>2+</sup>: 0.023 mM, LLOD of F<sup>-</sup>: 0.001 mM, LLOD of Ag<sup>+</sup>: 0.001 mM). Further, the activity coefficient of each ion was calculated with an ionic speciation program (Chemist, MicroMath, USA) (activity coefficient of Ca<sup>2+</sup> ≈ 0.6, F<sup>-</sup> ≈ 1, Ag<sup>+</sup> ≈ 1).

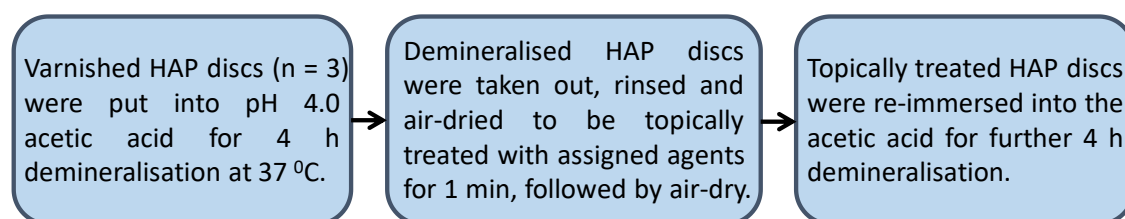
In the ISE study, the top of the beaker was covered by parafilm and the beaker was surrounded by foil to minimise evaporation and avoid the exposure to light. The thermometer of the hotplate of the stirrer was used to heat up and maintain the solution at 37±0.3 °C, and the thermometer of the ISE was used to monitor the temperature. The stirring speed was set at the lowest to avoid too much agitation during the experiments. Ca<sup>2+</sup>, Ag<sup>+</sup> and F<sup>-</sup> ISEs were used to simultaneously monitor the activities of Ca<sup>2+</sup>, F<sup>-</sup> and Ag<sup>+</sup> as demineralisation progressed, at intervals of 1 min (**Fig. 8.2a** and **b**).



**Figure 8.2** – a. Schematic representation of setup of the ISE study at  $37 \pm 0.3$  °C; b. Photo of the ISE setup in the study (F<sup>-</sup> ISE was behind Ca<sup>2+</sup> ISE).

The protocol used in the ISE study is shown as a flowchart (**Fig. 8.3**). Firstly, each varnished HAP disc was immersed in 50 mL of demineralisation solution at  $37 \pm 0.3$  °C for 4 h using a temperature stabilised stirrer (Stuart UC152D/KIT, UK). After 4 h demineralisation, the demineralised HAP discs were taken out, rinsed with DW, air-dried, and topically treated with the pre-assigned application agent for 1 min using a micro-brush (Centrix, USA), followed by air-drying. This protocol was as similar to the clinical procedures recommended by Crystal and Niederman (2016) as could be achieved in the present *in vitro* study. Each disc was then further demineralised for another 4 h, and the ion activities of  $\text{Ca}^{2+}$ ,  $\text{Ag}^+$  and  $\text{F}^-$  were monitored at 1 min intervals using ISEs as before.

Finally, the activity of  $\text{Ca}^{2+}$  (mM) was plotted as a function of time (h) for each group, and the percentage reduction in the rate of calcium loss of HAP ( $\text{PRCL}_{\text{HAP}}$ ) for each treatment was calculated, as described in Section 6.3.4. The activities of  $\text{F}^-$  and  $\text{Ag}^+$  were similarly plotted as a function of time.



**Figure 8.3** – Protocol of the ISE study on HAP discs.

### 8.3.2 Digital Photographs

Digital photographs of the HAP discs in each treatment group were taken using a digital camera (Olympus TG-5, Japan) after the first 4 h demineralisation, after topical treatments, and after further 4 h demineralisation, in order to monitor the colour changes at each step.

### 8.3.3 SEM and EDX Analyses

After the ISE study, each HAP disc was removed from the acid. They were then carbon-coated in order to be imaged with SEM and elementally analysed with EDX. SEM (FEI Inspect-F, USA) was operated at a high voltage of 5.00 kV and 5000 X magnification. Both SEM and EDX analyses were conducted in the middle area of the exposed window to avoid any interference from the nail varnish at the margin of the window.

### 8.3.4 $^{31}\text{P}$ and $^{19}\text{F}$ MAS-NMR Analyses

HAP powders were treated with silver compounds and acid challenged using procedures similar to those used in the ISE study.

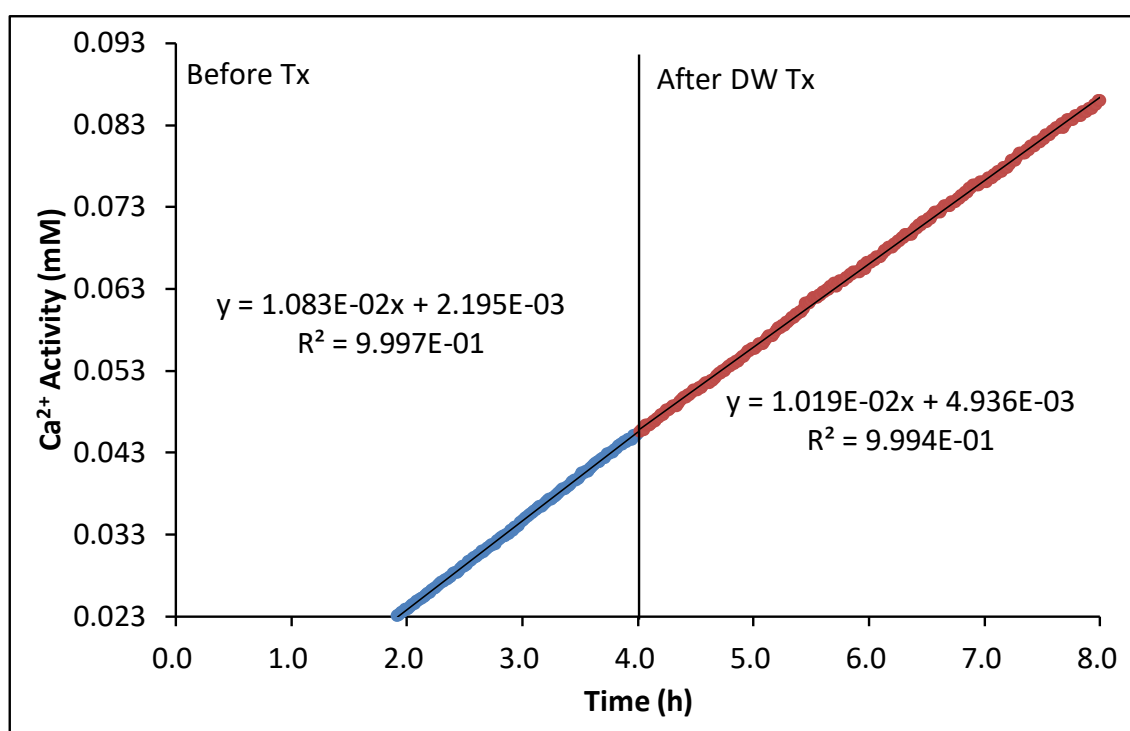
1.0 g un-sintered HAP powders (CAPTAL ® 'R', Plasma Biotol Ltd, UK) were mixed with 2.5 mL of either DW (HAP + DW), 3.16 M  $\text{AgNO}_3$  (HAP +  $\text{AgNO}_3$ ), 3.16 M  $\text{AgF}$  (HAP +  $\text{AgF}$ ), 3.16 M  $\text{Ag}[\text{NH}_3]_2\text{F}$  (HAP +  $\text{Ag}[\text{NH}_3]_2\text{F}$ ), or Silver Capsule of Riva Star (HAP + Riva-SC). Thereafter, the samples were collected after 1 min centrifugation (3000 rpm) (MICROSPIN 24S; Sorvall). Next, half of the collected samples were immersed in 5.0 mL demineralisation solution (pH 4.0) as used in the ISE study for 4 h, followed by 1 min centrifugation (3000 rpm) to prepare the acid challenged samples. All the collected samples were then put into a desiccator for 24 h for drying.

After desiccation, samples were analysed with  $^{31}\text{P}$  MAS-NMR and  $^{19}\text{F}$  MAS-NMR (600 MHz Bruker, Coventry, UK). Solid-state  $^{31}\text{P}$  MAS-NMR analysis was carried out using a 14.1 Tesla spectrometer at a Larmor frequency of 242.94 Mega-hertz (MHz) for a 16 min scan with a recycle delay of 1 min. Solid-state  $^{19}\text{F}$  MAS-NMR analysis was carried out using a 14.1 Tesla spectrometer at a Larmor frequency of 564.66 MHz for a 1 h scan with a recycle delay of 30 s. All scans were obtained under magic angle spinning conditions of 20 kHz.

## 8.4 Results

### 8.4.1 Ca<sup>2+</sup> ISE Study

**Fig. 8.4** shows a typical plot of Ca<sup>2+</sup> release from a HAP disc of the DW treatment group. The Ca<sup>2+</sup> release was linear with time, both before and after treatment. The rate of Ca<sup>2+</sup> release was decreased following the DW treatment (**Table 8.2**). All three samples of the DW treatment group showed a similar linear Ca<sup>2+</sup> release, both before and after treatment, and a similar reduction in the rate of Ca<sup>2+</sup> release following the treatments. Errors of gradients were calculated using SigmaPlot 10.0 (Systat Software, California, USA).



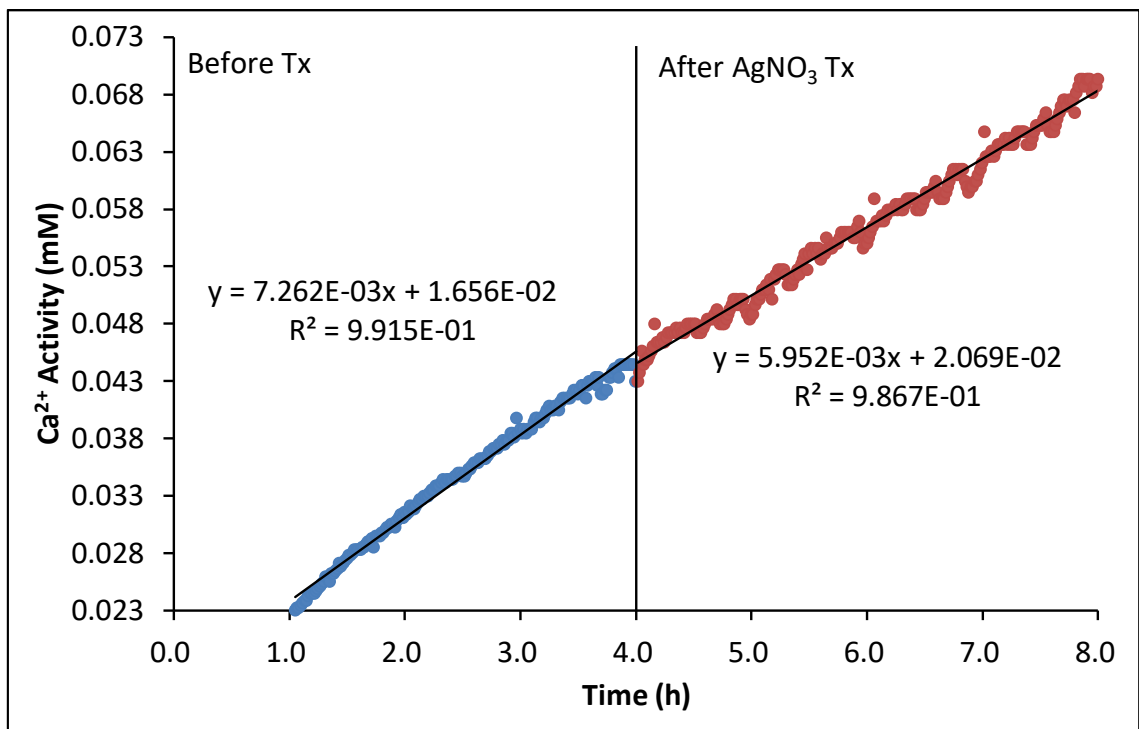
**Figure 8.4** - Typical Ca<sup>2+</sup> release of DW treatment group.

**Table 8.2** - The  $RCL_{HAP}$  before and after DW topical treatment of the **Fig. 8.4**.

Treatment	$R_b \pm SE$ ( $\times 10^{-3}$ mM/h)	$R_a \pm SE$ ( $\times 10^{-3}$ mM/h)	p value
DW Tx	$10.83 \pm 0.17$	$10.19 \pm 0.16$	< 0.01



**Fig. 8.5** shows a typical plot of  $\text{Ca}^{2+}$  release from a HAP disc of the  $\text{AgNO}_3$  treatment group. The  $\text{Ca}^{2+}$  release was linear with time, both before and after treatment. The rate of  $\text{Ca}^{2+}$  release was decreased following the  $\text{AgNO}_3$  treatment (**Table 8.3**). All three samples of the  $\text{AgNO}_3$  treatment group showed a similar linear  $\text{Ca}^{2+}$  release, both before and after treatment, and a similar reduction in the rate of  $\text{Ca}^{2+}$  release following the treatments.

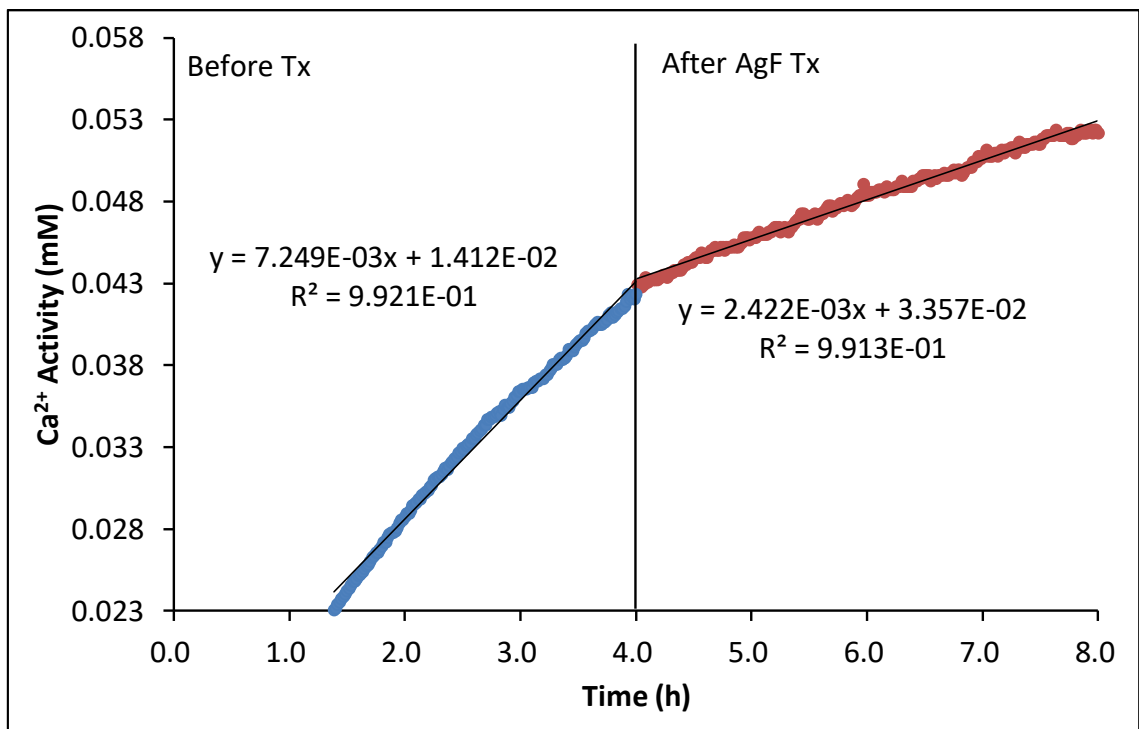


**Figure 8.5** - Typical  $\text{Ca}^{2+}$  release of  $\text{AgNO}_3$  treatment group.

**Table 8.3** - The  $R_{\text{CLHAP}}$  before and after  $\text{AgNO}_3$  topical treatment of the **Fig. 8.5**.

Treatment	$R_b \pm \text{SE}$ ( $\times 10^{-3}$ mM/h)	$R_a \pm \text{SE}$ ( $\times 10^{-3}$ mM/h)	p value
$\text{AgNO}_3$ Tx	$7.26 \pm 0.51$	$5.95 \pm 0.45$	< 0.01

**Fig. 8.6** shows a typical plot of  $\text{Ca}^{2+}$  release from a HAP disc of the AgF treatment group. The  $\text{Ca}^{2+}$  release was linear with time, both before and after treatment. The rate of  $\text{Ca}^{2+}$  release was decreased following the AgF treatment (**Table 8.4**). All three samples of the AgF treatment group showed a similar linear  $\text{Ca}^{2+}$  release, both before and after treatment, and a similar reduction in the rate of  $\text{Ca}^{2+}$  release following the treatments.

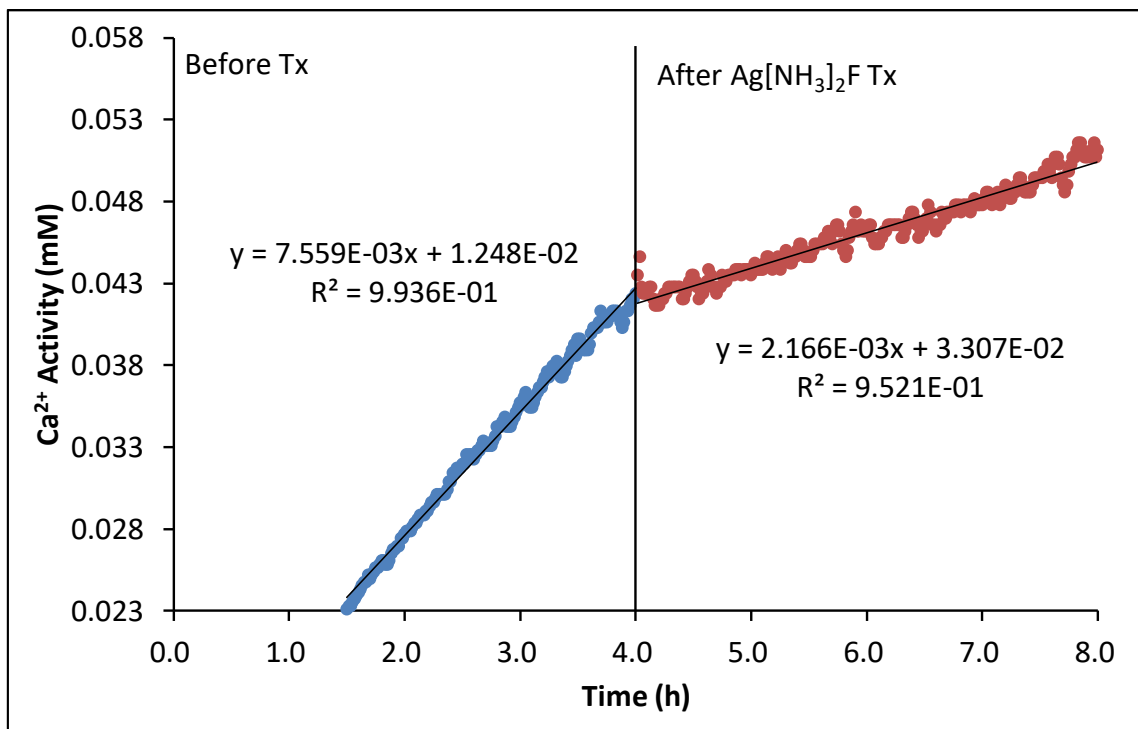


**Figure 8.6** – Typical  $\text{Ca}^{2+}$  release of AgF treatment group.

**Table 8.4** - The  $RCL_{\text{HAP}}$  before and after AgF topical treatment of the **Fig. 8.6**.

Treatment	$R_b \pm \text{SE}$ ( $\times 10^{-3}$ mM/h)	$R_a \pm \text{SE}$ ( $\times 10^{-3}$ mM/h)	p value
AgF Tx	$7.25 \pm 0.52$	$2.42 \pm 0.15$	< 0.01

**Fig. 8.7** shows a typical plot of  $\text{Ca}^{2+}$  release from a HAP disc of the  $\text{Ag}[\text{NH}_3]_2\text{F}$  treatment group. The  $\text{Ca}^{2+}$  release was linear with time, both before and after treatment. The rate of  $\text{Ca}^{2+}$  release was decreased following the  $\text{Ag}[\text{NH}_3]_2\text{F}$  treatment (**Table 8.5**). All three samples of the  $\text{Ag}[\text{NH}_3]_2\text{F}$  treatment group showed a similar linear  $\text{Ca}^{2+}$  release, both before and after treatment, and a similar reduction in the rate of  $\text{Ca}^{2+}$  release following the treatments.

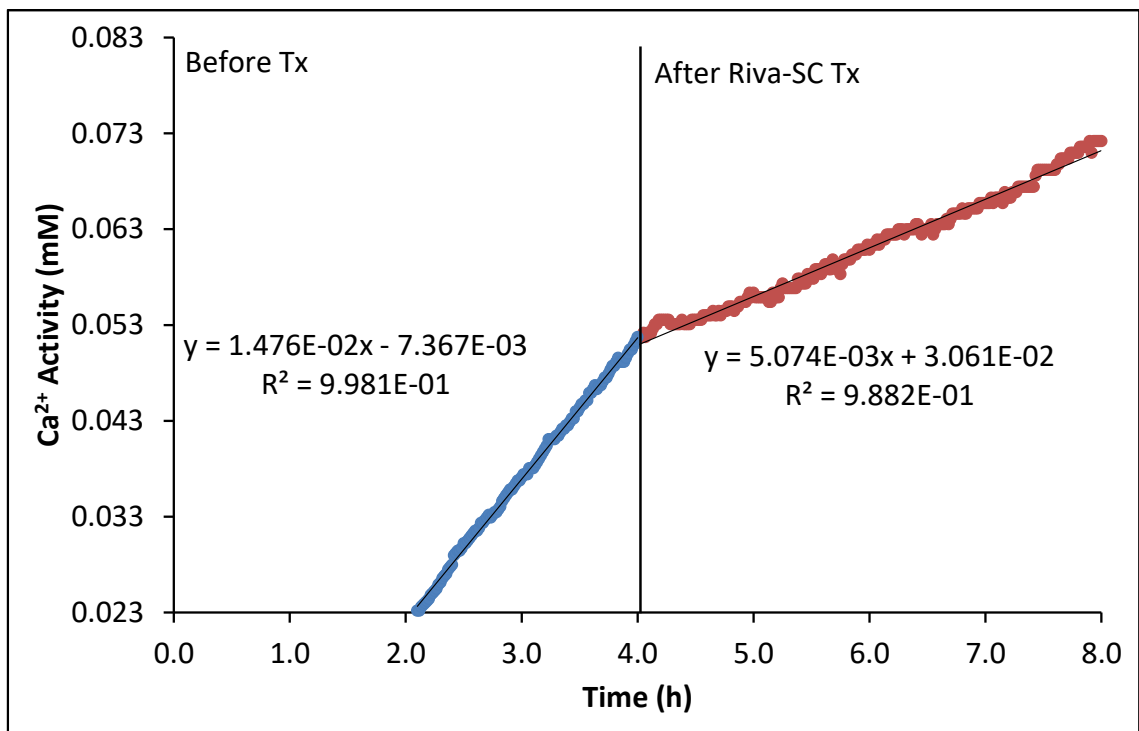


**Figure 8.7** - Typical  $\text{Ca}^{2+}$  release of  $\text{Ag}[\text{NH}_3]_2\text{F}$  treatment group.

**Table 8.5** - The  $R_{\text{CL}_{\text{HAP}}}$  before and after  $\text{Ag}[\text{NH}_3]_2\text{F}$  topical treatment of the **Fig. 8.7**.

Treatment	$R_{\text{b}} \pm \text{SE}$ ( $\times 10^{-3}$ mM/h)	$R_{\text{a}} \pm \text{SE}$ ( $\times 10^{-3}$ mM/h)	p value
$\text{Ag}[\text{NH}_3]_2\text{F}$ Tx	$7.56 \pm 0.50$	$2.17 \pm 0.31$	< 0.01

**Fig. 8.8** shows a typical plot of  $\text{Ca}^{2+}$  release from a HAP disc of the Riva-SC treatment group. The  $\text{Ca}^{2+}$  release was linear with time, both before and after treatment. The rate of  $\text{Ca}^{2+}$  release was decreased following the Riva-SC treatment (**Table 8.6**). All three samples of the Riva-SC treatment group showed a similar linear  $\text{Ca}^{2+}$  release, both before and after treatment, and a similar reduction in the rate of  $\text{Ca}^{2+}$  release following the treatments.



**Figure 8.8** – Typical  $\text{Ca}^{2+}$  release of Riva-SC treatment group.

**Table 8.6** - The  $RCL_{\text{HAP}}$  before and after Riva-SC topical treatment of the **Fig. 8.8**.

Treatment	$R_b \pm \text{SE}$ ( $\times 10^{-3}$ mM/h)	$R_a \pm \text{SE}$ ( $\times 10^{-3}$ mM/h)	p value
Riva-SC Tx	$14.76 \pm 0.61$	$5.07 \pm 0.36$	< 0.01

#### 8.4.1.1. Summary of the Ca<sup>2+</sup> Release from the HAP Discs of Each Treatment Group

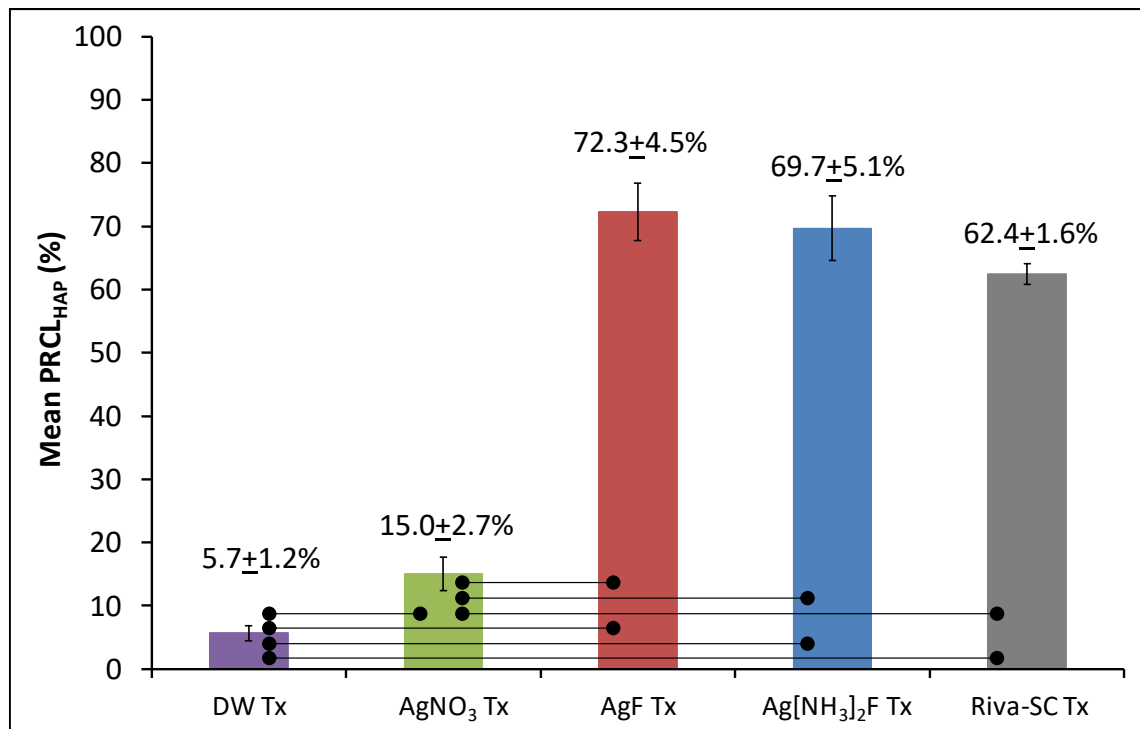
**Table 8.7** shows the rates of calcium loss of HAP ( $R_{CL_{HAP}}$ ) before and after treatments, and the percentages reduction in the rates of calcium loss of HAP ( $PR_{CL_{HAP}}$ ) of every HAP disc in each treatment group. Every  $R_a$  ( $R_{CL_{HAP}}$ ) measured was significantly different ( $p < 0.05$ ) from the  $R_b$  ( $R_{CL_{HAP}}$ ) of the same HAP disc sample.

The mean  $R_{CL_{HAP}}$  before treatments were similar ( $\approx 0.010$  mM/h), whereas, the mean  $R_{CL_{HAP}}$  following treatments were different. The mean  $R_{CL_{HAP}}$  following topical treatments with fluoride-containing silver compounds like AgF, Ag[NH<sub>3</sub>]<sub>2</sub>F and Riva-SC, were much lower than those following topical treatments with AgNO<sub>3</sub> and DW.

**Table 8.7** – The  $R_{CL_{HAP}}$  and  $PR_{CL_{HAP}}$  of every HAP disc in each treatment group.

Tx Group	HAP Disc	$R_b \pm SE$ (X 10 <sup>-3</sup> mM/h)	$R_a \pm SE$ (X 10 <sup>-3</sup> mM/h)	$PR_{CL_{HAP}}$ (%)
DW Tx	1	12.32 ± 0.20	11.90 ± 0.28	3.4
	2	10.83 ± 0.17	10.19 ± 0.16	5.9
	3	8.24 ± 0.20	7.61 ± 0.20	7.6
	Average	10.46 ± 1.19	9.90 ± 1.25	5.7 ± 1.2
AgNO <sub>3</sub> Tx	1	11.58 ± 0.20	10.46 ± 0.50	9.7
	2	12.70 ± 0.30	10.50 ± 0.60	17.3
	3	7.26 ± 0.51	5.95 ± 0.45	18.0
	Average	10.51 ± 1.66	8.97 ± 1.51	15.0 ± 2.7
AgF Tx	1	9.19 ± 0.52	2.85 ± 0.77	69.0
	2	11.51 ± 0.60	2.16 ± 0.30	81.2
	3	7.25 ± 0.52	2.42 ± 0.15	66.6
	Average	9.32 ± 0.23	2.48 ± 0.20	72.3 ± 4.5
Ag[NH <sub>3</sub> ] <sub>2</sub> F Tx	1	7.56 ± 0.50	2.17 ± 0.31	71.3
	2	7.26 ± 0.50	1.62 ± 0.70	77.7
	3	15.25 ± 0.50	6.07 ± 0.60	60.2
	Average	10.02 ± 2.62	3.29 ± 1.40	69.7 ± 5.1
Riva-SC Tx	1	10.04 ± 0.50	4.04 ± 0.30	61.2
	2	19.34 ± 0.60	7.64 ± 0.20	60.5
	3	14.76 ± 0.61	5.07 ± 0.36	65.7
	Average	14.83 ± 2.58	5.58 ± 1.11	62.4 ± 1.6

**Fig. 8.9** shows the mean  $PRCL_{HAP}$  of each treatment group. The mean  $PRCL_{HAP}$  of AgF,  $Ag[NH_3]_2F$  and Riva-SC treatment groups were much higher than that of  $AgNO_3$  treatment group, while the mean  $PRCL_{HAP}$  of DW treatment group was the lowest. There were no significant differences between the mean  $PRCL_{HAP}$  of AgF,  $Ag[NH_3]_2F$  and Riva-SC treatment groups.



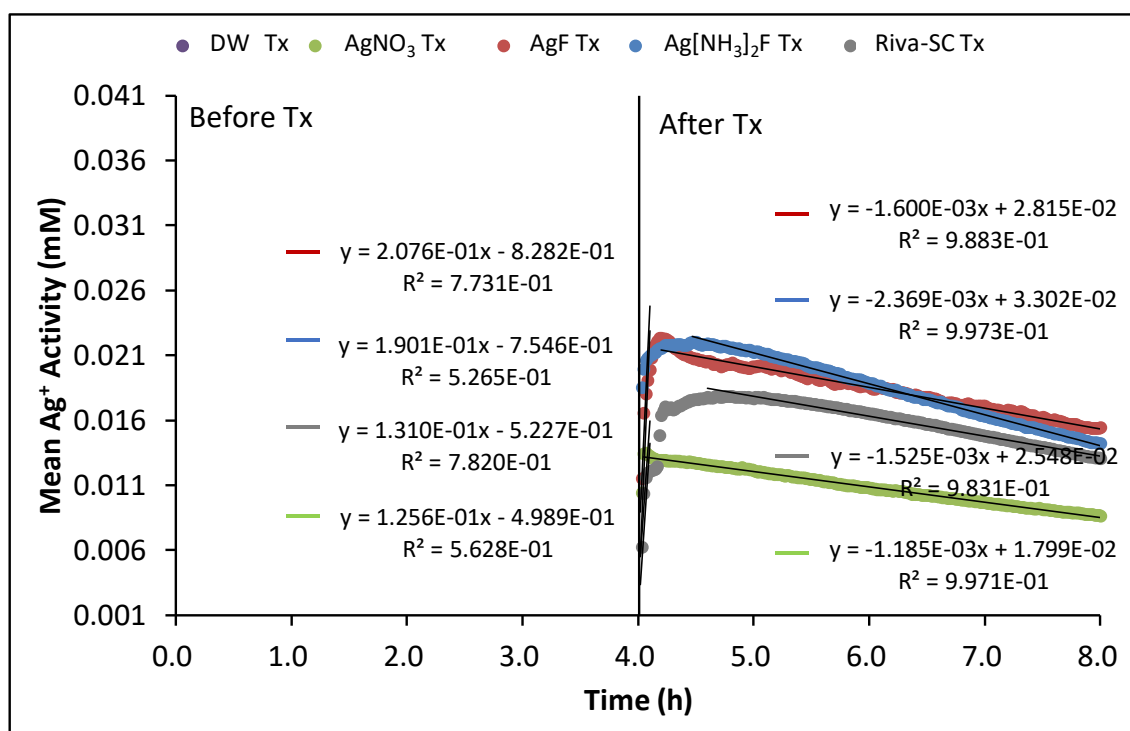
**Figure 8.9** – The mean  $PRCL_{HAP}$  of each treatment group. Error bars show the standard errors. Linking line between bars indicate significant differences at  $p < 0.05$  between treatment groups.

### 8.4.2 Ag<sup>+</sup> ISE study

The Ag<sup>+</sup> release profiles of each treatment group were plotted from the mean activities of Ag<sup>+</sup> released from the three HAP discs of each treatment group (**Fig. 8.10**). After re-immersion of HAP discs topically treated with AgNO<sub>3</sub>, AgF, Ag[NH<sub>3</sub>]<sub>2</sub>F and Riva-SC into acids, all the mean activities of Ag<sup>+</sup> in the solution increased rapidly from zero and then subsequently decreased continually.

Even though the Ag<sup>+</sup> release profiles are not linear, the approximate rates of the changes in the mean Ag<sup>+</sup> activities can be extrapolated by the slopes of the trendlines of initial increase and later decrease in Ag<sup>+</sup> activities.

No Ag<sup>+</sup> release was observed in the DW treatment group.

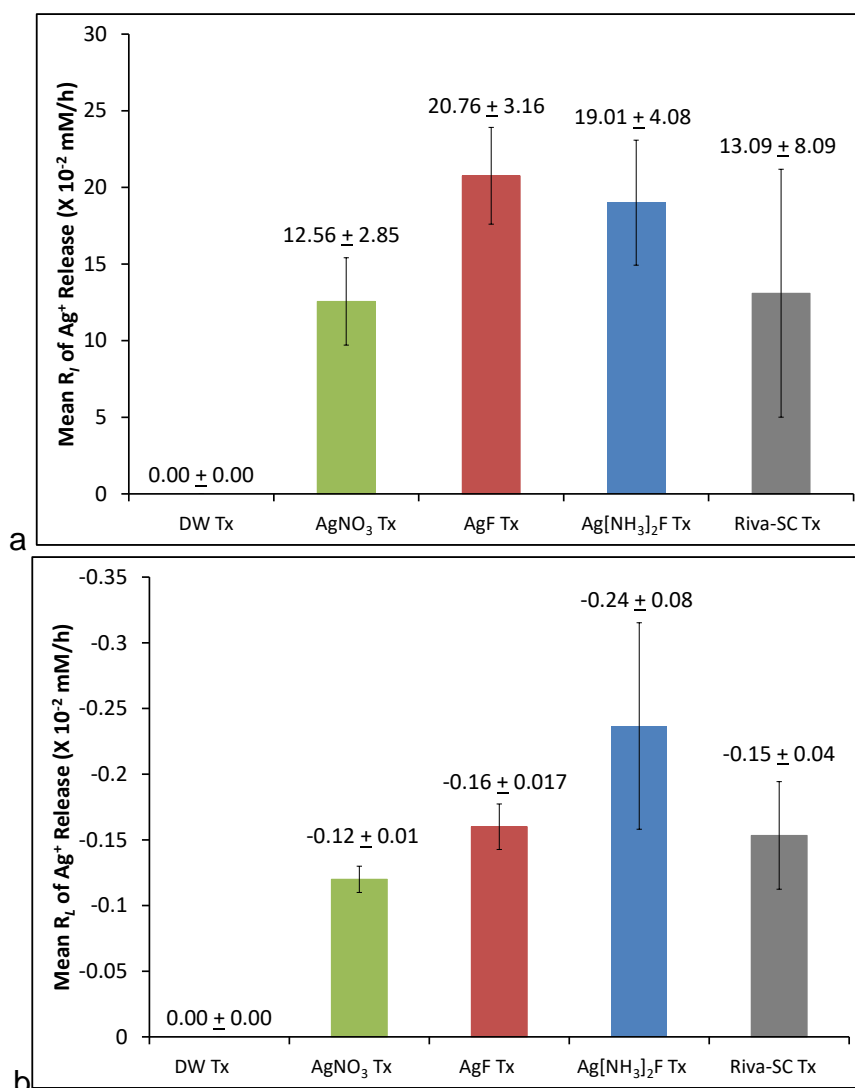


**Figure 8.10** – The mean Ag<sup>+</sup> release from HAP discs under pH 4.0 demineralisation before and after treatments with DW, AgNO<sub>3</sub>, AgF, Ag[NH<sub>3</sub>]<sub>2</sub>F and Riva-SC.

**Table 8.8** shows the mean initial rates ( $R_i$ ) of increase in the  $\text{Ag}^+$  activities and the mean later rates ( $R_L$ ) of decrease in the  $\text{Ag}^+$  activities following topical treatments with silver compounds. However, there were no significant differences in  $R_i$  and  $R_L$  between each treatment group (**Fig. 8.11**).

**Table 8.8** – Mean  $R_i$  and mean  $R_L$  of the  $\text{Ag}^+$  release following each treatment.

Tx Group	Mean $R_i$ ± SE (X $10^{-2}$ mM/h)	Mean $R_L$ ± SE (X $10^{-2}$ mM/h)
DW Tx	0.00 ± 0.00	0.00 ± 0.00
$\text{AgNO}_3$ Tx	12.56 ± 2.85	-0.12 ± 0.01
AgF Tx	20.76 ± 3.16	-0.16 ± 0.02
$\text{Ag}[\text{NH}_3]_2\text{F}$ Tx	19.01 ± 4.08	-0.24 ± 0.08
Riva-SC Tx	13.10 ± 8.09	-0.15 ± 0.04



**Figure 8.11** – (a) Mean  $R_i$  and (b) mean  $R_L$  of the  $\text{Ag}^+$  release of each treatment group.



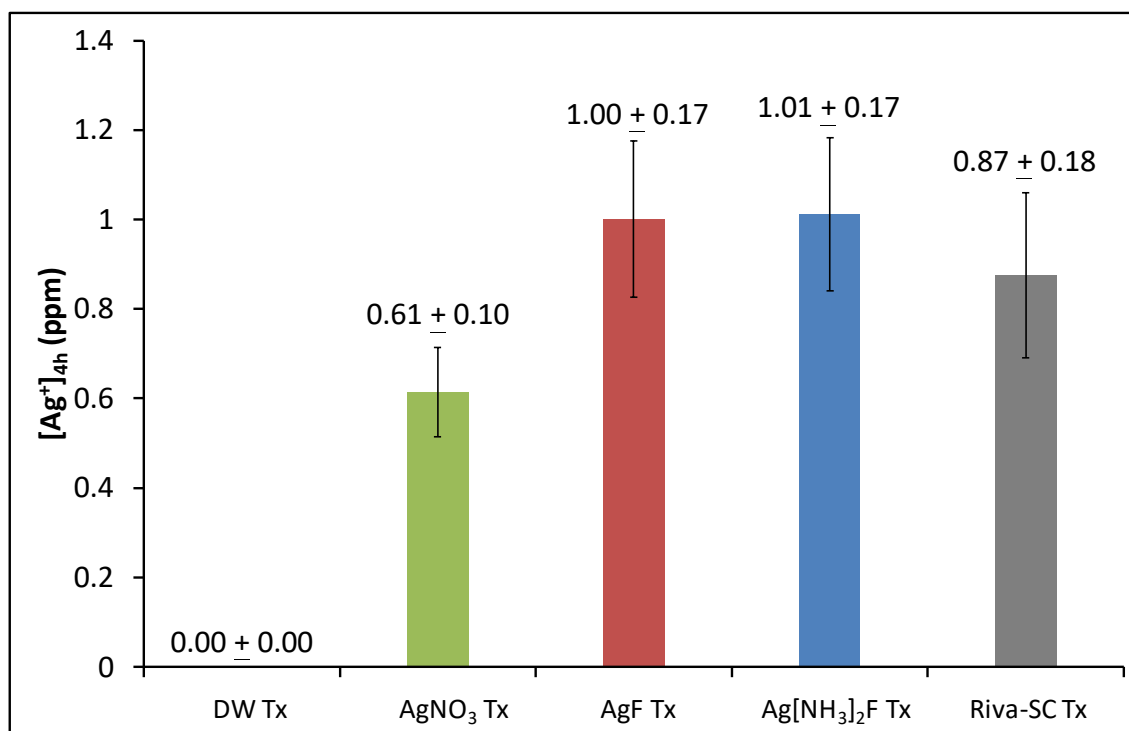
### 8.4.2.1 Mean $[Ag^+]$ during the post-treatment 4 h periods of Each Treatment Group

The mean  $[Ag^+]$  during the 4 h demineralisation period after re-immersion of the topically treated HAP samples into acid ( $[Ag^+]_{4h}$ ) (**Table 8.9**) of each treatment group was calculated, in order to compare the effects of  $Ag^+$  in the acid on the demineralisation of the HAP discs.

**Fig. 8.12** shows the  $[Ag^+]_{4h}$  of each treatment group. There were no significant differences between the  $[Ag^+]_{4h}$  of  $AgNO_3$ ,  $AgF$ ,  $Ag[NH_3]_2F$  and Riva-SC treatment groups.

**Table 8.9** – The mean  $[Ag^+]$  during the 4 h demineralisation period after re-immersion of the topically treated HAP samples into acids ( $[Ag^+]_{4h}$ ) of each treatment group.

Tx Groups	$[Ag^+]_{4h}$	
DW Tx	$0.0 \pm 0.0 \times 10^{-3}$ mM	$0.00 \pm 0.00$ ppm
$AgNO_3$ Tx	$5.7 \pm 0.9 \times 10^{-3}$ mM	$0.61 \pm 0.10$ ppm
$AgF$ Tx	$9.3 \pm 1.6 \times 10^{-3}$ mM	$1.00 \pm 0.17$ ppm
$Ag[NH_3]_2F$ Tx	$9.4 \pm 1.6 \times 10^{-3}$ mM	$1.01 \pm 0.17$ ppm
Riva-SC Tx	$8.1 \pm 1.7 \times 10^{-3}$ mM	$0.87 \pm 0.18$ ppm



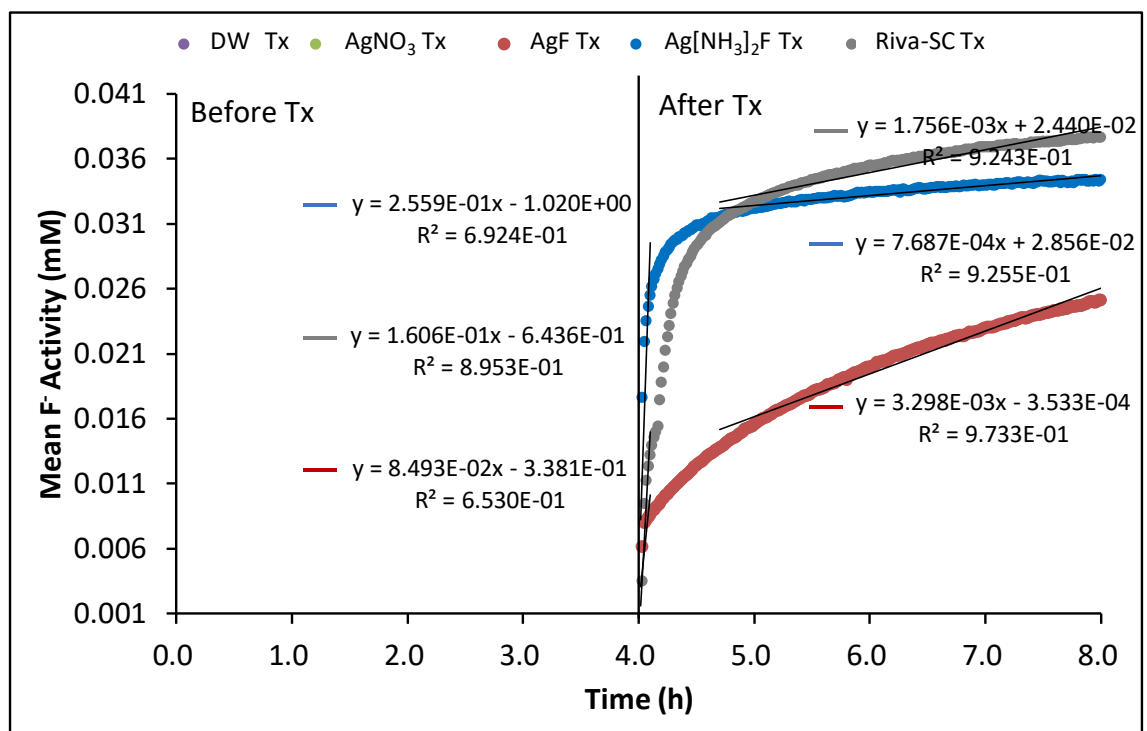
**Figure 8.12** – The  $[Ag^+]_{4h}$  (ppm) of each treatment group. Error bars show the standard errors.

### 8.4.3 F<sup>-</sup> ISE study

The F<sup>-</sup> release profiles of each treatment group were plotted from the mean activities of F<sup>-</sup> released from the three HAP discs of each treatment group (**Fig. 8.13**). After re-immersion of HAP discs topically treated with AgF, Ag[NH<sub>3</sub>]<sub>2</sub>F and Riva-SC into acids, there was a rapid increase in all the mean activities of F<sup>-</sup> from zero, which slowed with time.

Even though the F<sup>-</sup> release profiles are not linear, the approximate rates of the changes in the mean F<sup>-</sup> activities can be extrapolated by the slopes of trendlines of initial increase and later increase in F<sup>-</sup> activities.

No F<sup>-</sup> release was observed in DW and AgNO<sub>3</sub> treatment groups.

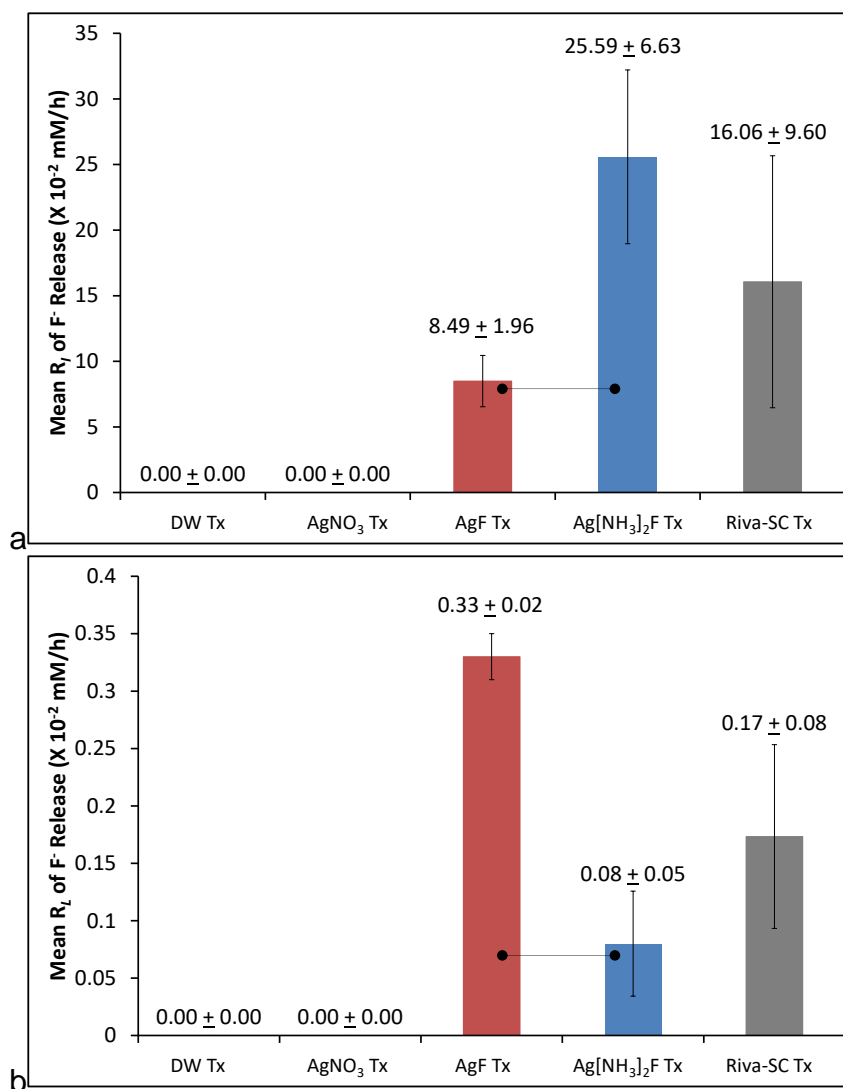


**Figure 8.13** - The mean F<sup>-</sup> release from HAP discs under pH 4.0 demineralisation before and after treatments with DW, AgNO<sub>3</sub>, AgF, Ag[NH<sub>3</sub>]<sub>2</sub>F and Riva-SC.

**Table 8.10** shows the mean  $R_I$  and the mean  $R_L$  of increase in the  $F^-$  activities following silver compounds topical treatments. The mean  $R_I$  of  $Ag[NH_3]_2F$  treatment group was significantly faster than the mean  $R_I$  of  $AgF$  treatment group, but the mean  $R_L$  of  $Ag[NH_3]_2F$  treatment group was significantly slower than the mean  $R_L$  of  $AgF$  treatment group. The mean  $R_I$  and  $R_L$  of Riva-SC treatment group were not significantly different from other treatment groups (**Fig. 8.14**).

**Table 8.10** – Mean  $R_I$  and mean  $R_L$  of the  $F^-$  release following each treatment.

Tx Group	Mean $R_I$ ± SE (X $10^{-2}$ mM/h)	Mean $R_L$ ± SE (X $10^{-2}$ mM/h)
DW Tx	0.00 ± 0.00	0.00 ± 0.00
$AgNO_3$ Tx	0.00 ± 0.00	0.00 ± 0.00
$AgF$ Tx	8.49 ± 1.96	0.33 ± 0.02
$Ag[NH_3]_2F$ Tx	25.59 ± 6.63	0.08 ± 0.05
Riva-SC Tx	16.06 ± 9.60	0.17 ± 0.08



**Figure 8.14** – (a) Mean  $R_I$  and (b) mean  $R_L$  of the  $F^-$  release of each treatment group.

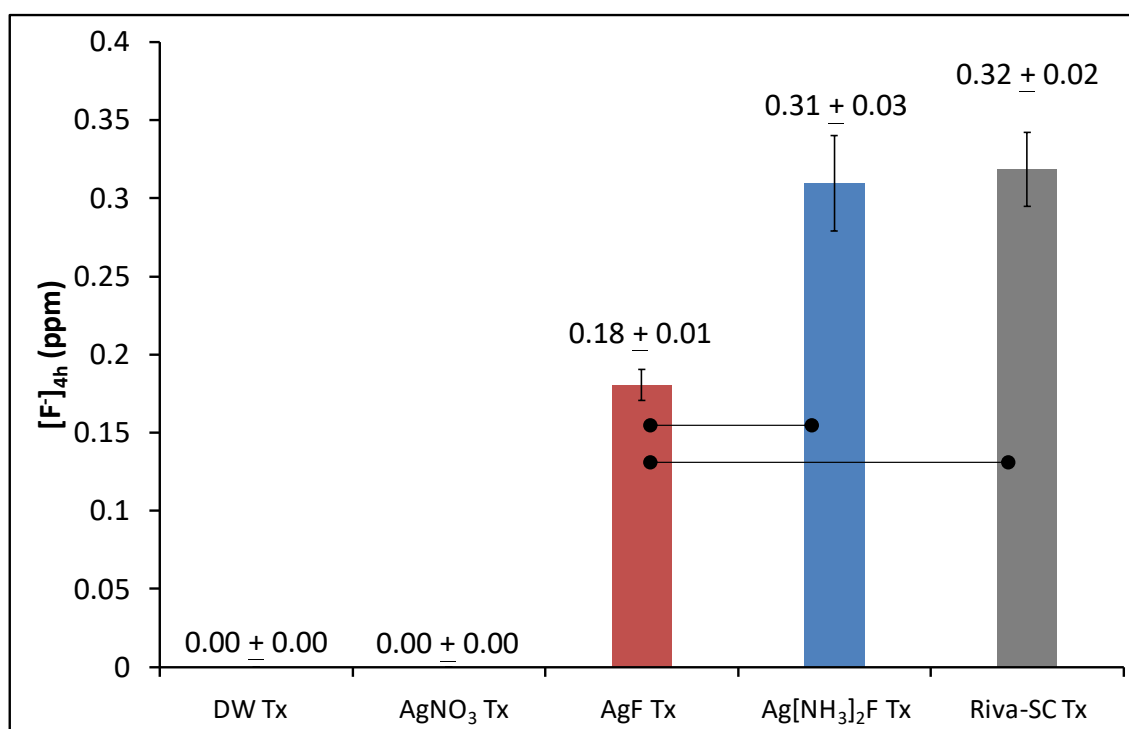
### 8.4.3.1 Mean $[F^-]$ during the post-treatment 4 h periods of Each Treatment Group

The mean  $[F^-]$  during the 4 h demineralisation period after re-immersion of the topically treated HAP samples into acid ( $[F^-]_{4h}$ ) (**Table 8.11**) of each treatment group was calculated, in order to compare the effects of  $F^-$  in the acid on the demineralisation of the HAP discs.

**Fig. 8.15** shows the  $[F^-]_{4h}$  of each treatment group. The  $[F^-]_{4h}$  of  $Ag[NH_3]_2F$  and Riva-SC treatment groups were higher than the  $[F^-]_{4h}$  of AgF treatment group. There was no significant difference between the  $[F^-]_{4h}$  of  $Ag[NH_3]_2F$  and Riva-SC treatment groups.

**Table 8.11** – The mean  $[F^-]$  during the 4 h demineralisation period after re-immersion of the topically treated HAP samples into acids ( $[F^-]_{4h}$ ) of each treatment group.








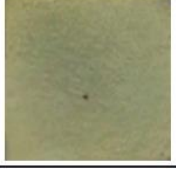







Tx Groups	$[F^-]_{4h}$	
DW Tx	$0.0 \pm 0.0 \times 10^{-3}$ mM	$0.00 \pm 0.00$ ppm
$AgNO_3$ Tx	$0.0 \pm 0.0 \times 10^{-3}$ mM	$0.00 \pm 0.00$ ppm
AgF Tx	$9.5 \pm 0.5 \times 10^{-3}$ mM	$0.18 \pm 0.01$ ppm
$Ag[NH_3]_2F$ Tx	$16.3 \pm 1.6 \times 10^{-3}$ mM	$0.31 \pm 0.03$ ppm
Riva-SC Tx	$16.8 \pm 1.2 \times 10^{-3}$ mM	$0.32 \pm 0.02$ ppm



**Figure 8.15** - The  $[F^-]_{4h}$  (ppm) of each treatment group. Error bars show the standard errors. Linking lines between bars indicate significant differences at  $p < 0.05$  between treatment groups.

#### 8.4.4 Digital Photographs

Following topical treatments with AgNO<sub>3</sub>, AgF, Ag[NH<sub>3</sub>]<sub>2</sub>F and Riva-SC, yellow staining was observed on the HAP disc surfaces, which then turned to black staining after further 4 h demineralisation (**Fig. 8.16**). No staining was observed on the HAP discs topically treated with DW.

	After the first 4 h demin.	After topical treatment	After further 4 h demin.
DW Tx			
AgNO <sub>3</sub> Tx			
AgF Tx			
Ag[NH <sub>3</sub> ] <sub>2</sub> F Tx			
Riva-SC Tx			

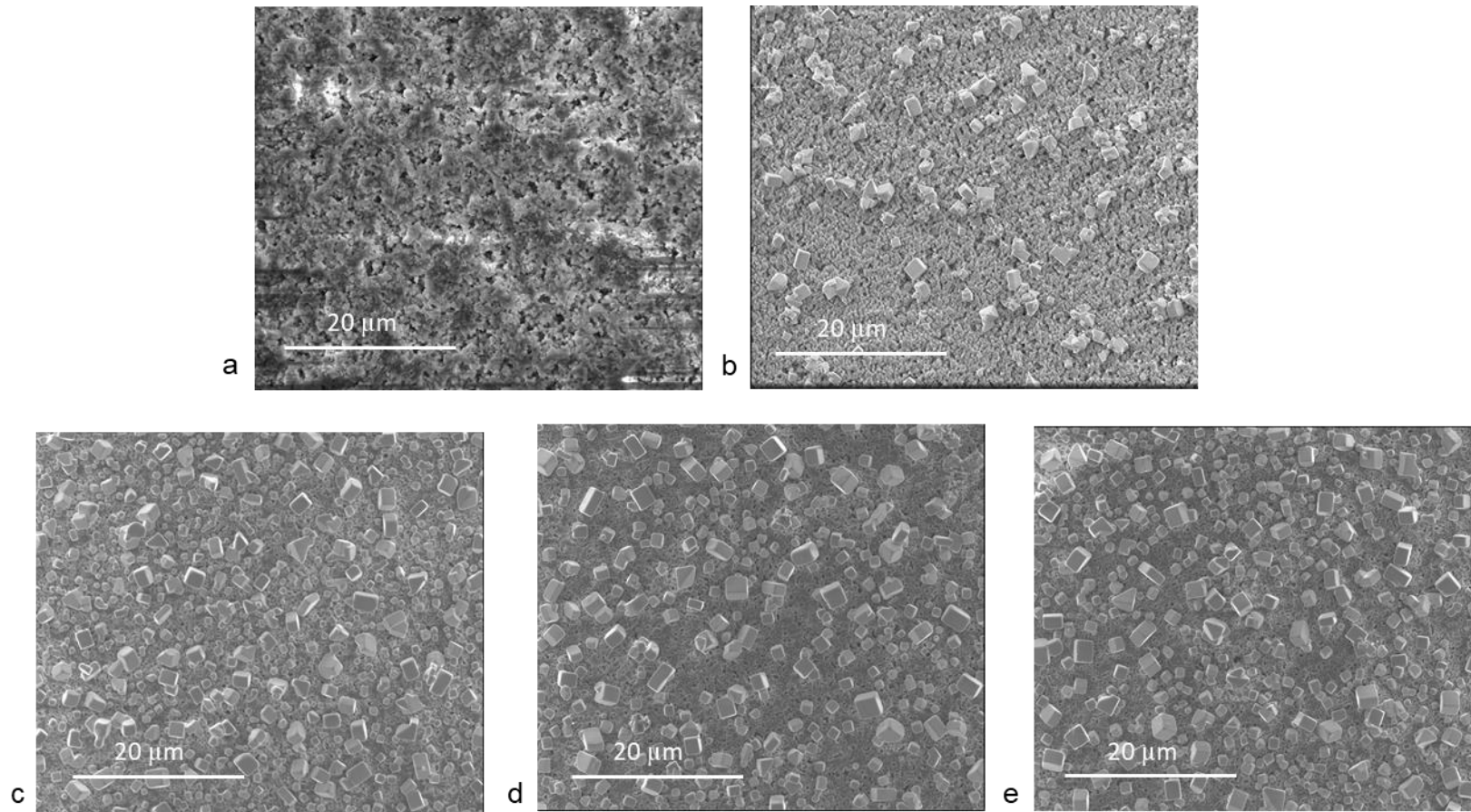
*Figure 8.16 – Digital photographs of HAP discs following different treatments in the ISE study.*

#### 8.4.5 SEM Images Analysis

**Fig. 8.17a ~ e** shows typical SEM images of HAP disc surfaces topically treated with application agents after demineralisation. The HAP disc surfaces treated with AgF, Ag[NH<sub>3</sub>]<sub>2</sub>F or Riva-SC were less uneven than that treated with AgNO<sub>3</sub>, while the HAP disc surfaces treated with DW were the most uneven and porous.

There were numerous cubic particles (~ 3 μm) deposited on HAP disc surfaces topically treated with silver compounds (**Fig. 8.17b ~ e**). Further, there were granular particles (~ 1 μm) deposited on HAP disc surfaces topically treated with AgF, Ag[NH<sub>3</sub>]<sub>2</sub>F or Riva-SC (**Fig. 8.17c, d, and e**).

All particles deposited on the HAP disc surfaces were of similar sizes and were distributed evenly across the surfaces. Further, the HAP disc surfaces treated with AgF, Ag[NH<sub>3</sub>]<sub>2</sub>F or Riva-SC (**Fig. 8.17c, d, and e**) were more densely covered by the deposited particles than that treated with AgNO<sub>3</sub> (**Fig. 8.17b**) due to the additional deposition of granular particles.

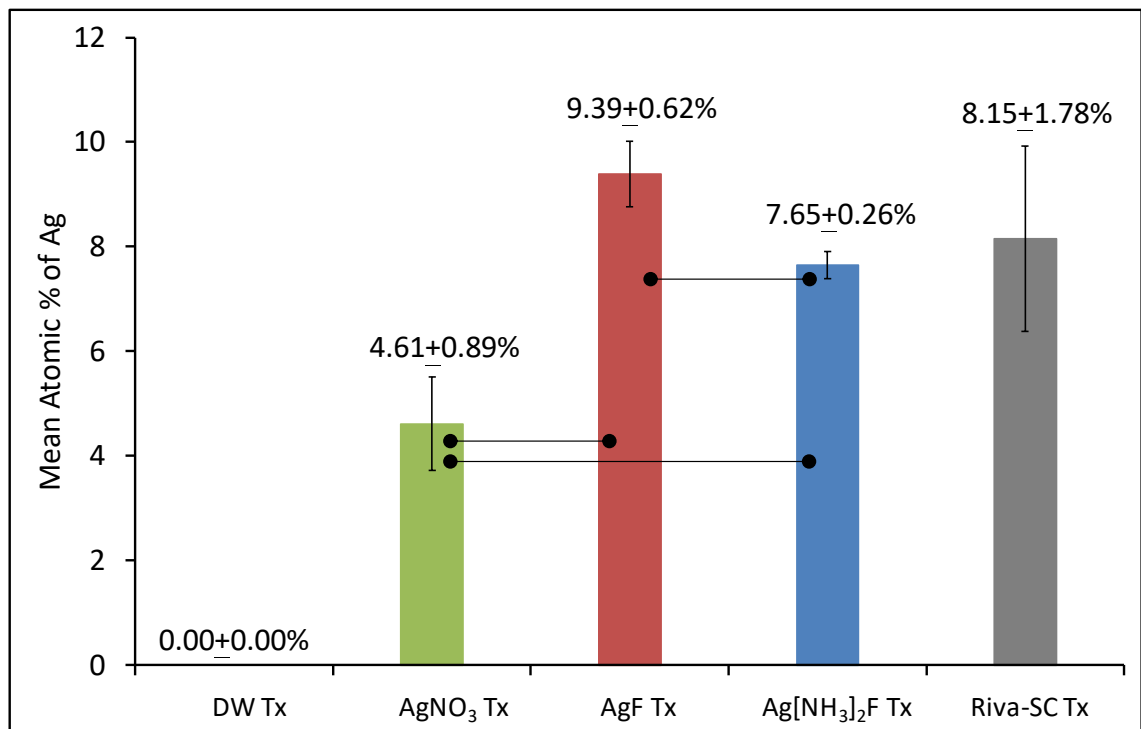


**Figure 8.17** - Typical SEM images (5.00 kV, 5000 X) of HAP discs in treatment groups of (a) DW, (b) AgNO<sub>3</sub>, (c) AgF, (d) Ag[NH<sub>3</sub>]<sub>2</sub>F and (e) Riva-SC, after the ISE study.

### 8.4.6 EDX Analysis

EDX analysis showed that elemental Ag (**Fig. 8.18**) was present on the HAP disc surfaces topically treated with AgNO<sub>3</sub>, AgF, Ag[NH<sub>3</sub>]<sub>2</sub>F and Riva-SC after demineralisation. The mean atomic percentage of Ag detected in AgF treatment group was higher than that of the Ag[NH<sub>3</sub>]<sub>2</sub>F treatment group, both of which were higher than 3.16 M AgNO<sub>3</sub> treatment group. There were no significant differences between the mean atomic Ag % of Riva-SC and other treatment groups.

No Ag was detected on the HAP surfaces topically treated with DW.

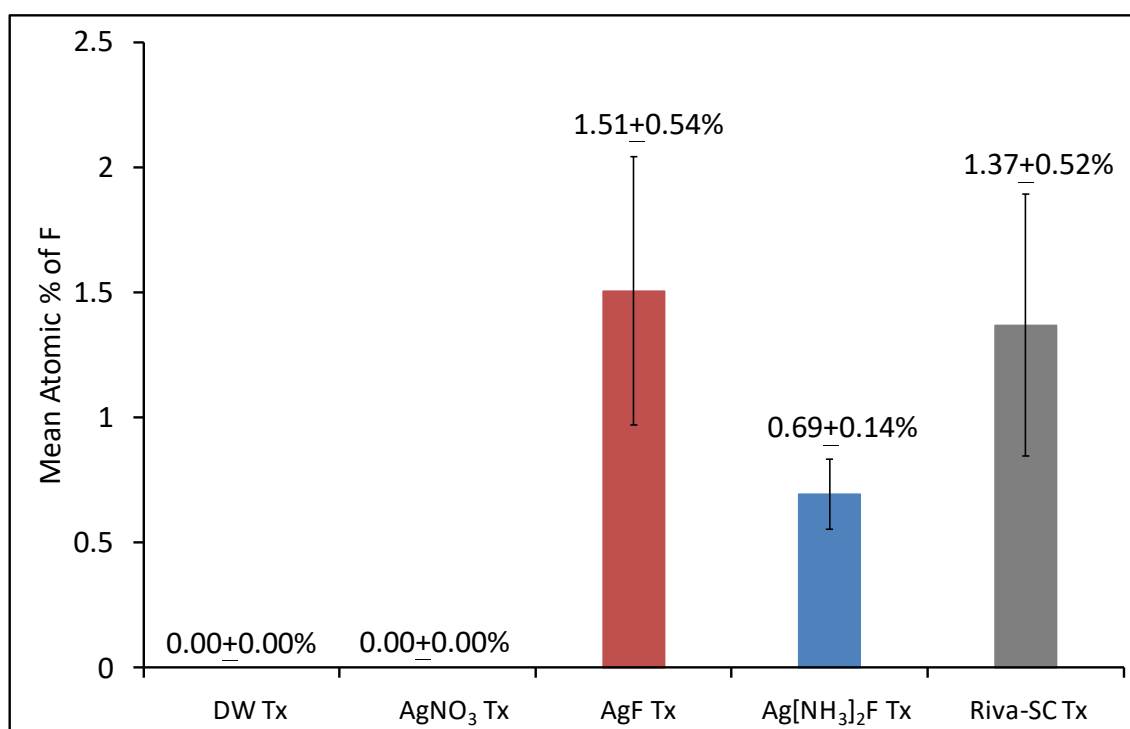


**Figure 8.18** – The mean atomic percentage of Ag of each treatment group. Error bars show the standard errors. Linking lines between bars indicate significant differences at  $p < 0.05$  between treatment groups.



Elemental F (**Fig. 8.19**) was present on the HAP surfaces topically treated with AgF, Ag[NH<sub>3</sub>]<sub>2</sub>F and Riva-SC after demineralisation. The mean percentage of F detected in the treatment group of AgF was slightly higher than those detected in the Ag[NH<sub>3</sub>]<sub>2</sub>F and Riva-SC treatment groups. However, there were no significant differences between the mean atomic F % of these treatment groups.

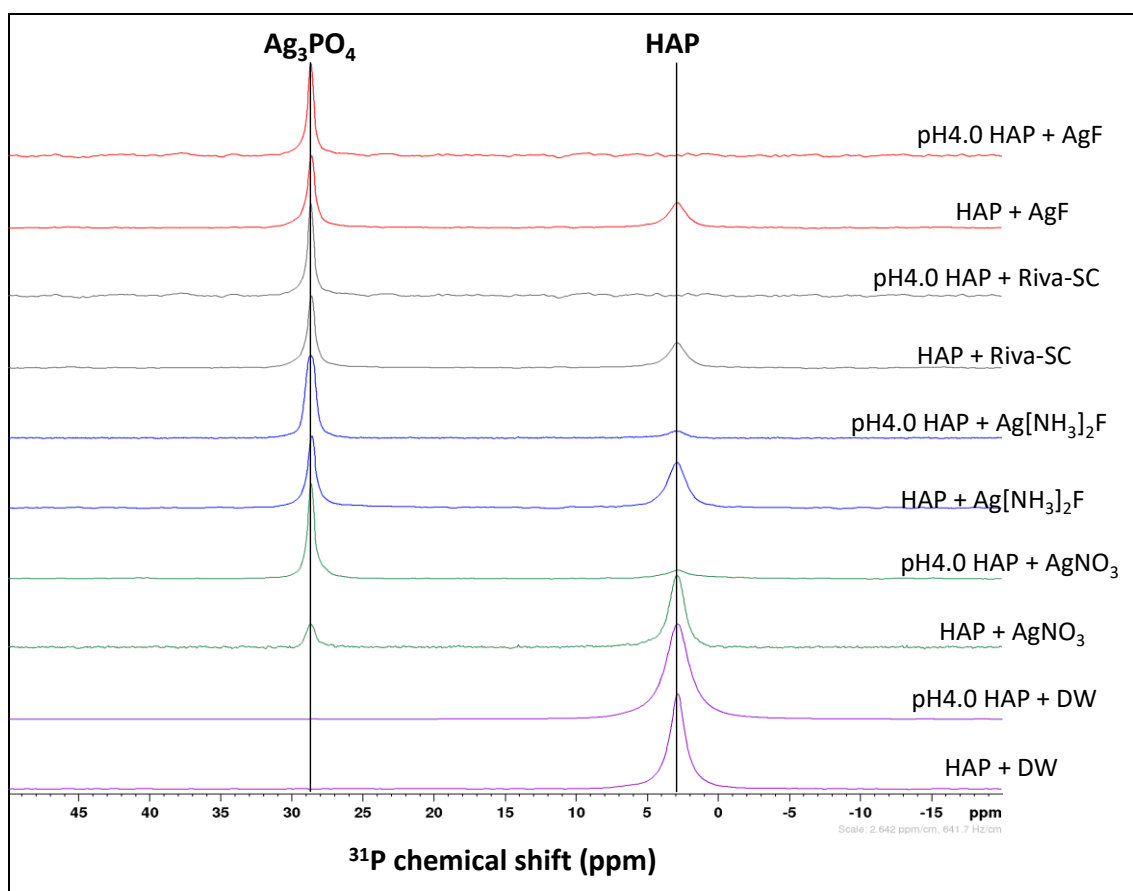
No F was detected on the HAP surfaces topically treated with DW and AgNO<sub>3</sub>.



**Figure 8.19** – The mean atomic percentage of F of each treatment group. Error bars show the standard errors.

### 8.4.7 $^{31}\text{P}$ MAS-NMR Analysis

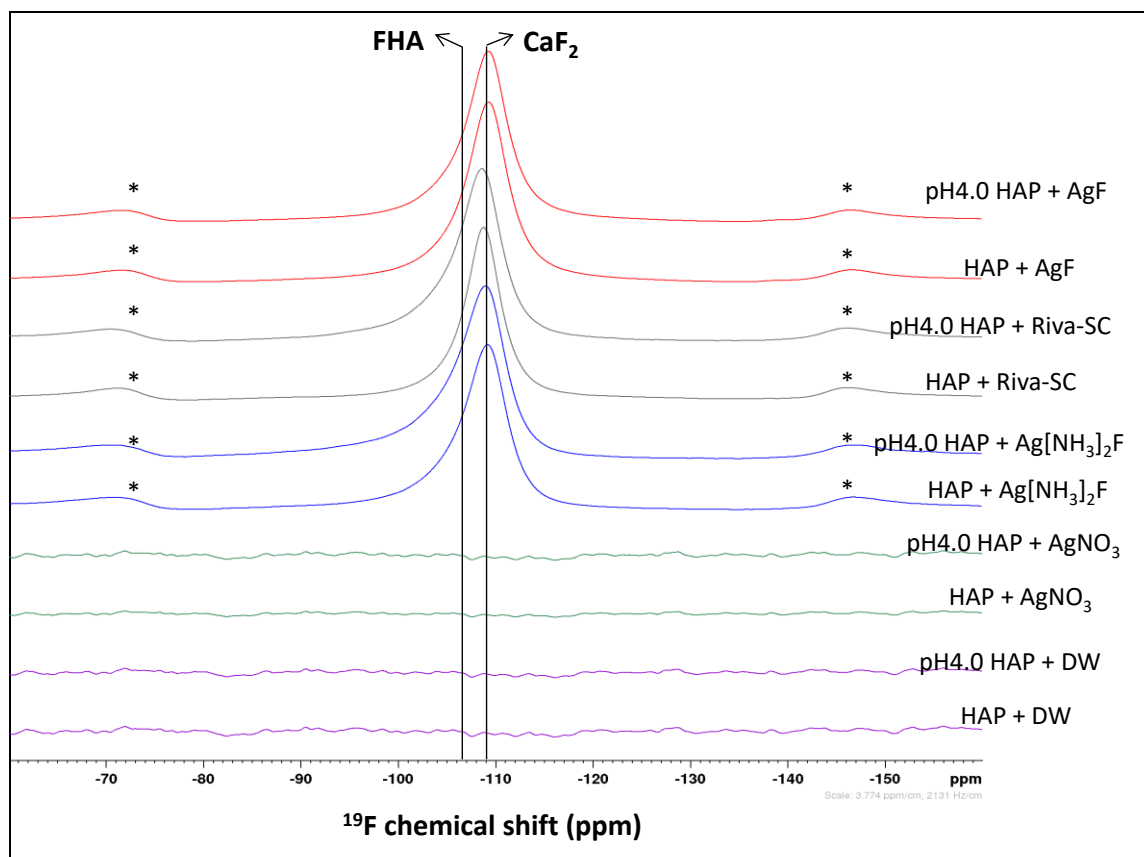
The  $^{31}\text{P}$  MAS-NMR spectra (**Fig. 8.20**) showed that chemical shift peaks of HAP (2.9 ppm) and  $\text{Ag}_3\text{PO}_4$  (28.8 ppm) were detected in HAP powders mixed with  $\text{AgNO}_3$ , AgF,  $\text{Ag}[\text{NH}_3]_2\text{F}$  or Riva-SC. Furthermore, after acid challenge, the proportions of  $\text{Ag}_3\text{PO}_4$  in all silver compound treatment groups increased, whereas the proportions of HAP decreased.



**Figure 8.20** -  $^{31}\text{P}$  MAS-NMR spectra of each treatment group before and after pH 4.0 acid challenge.

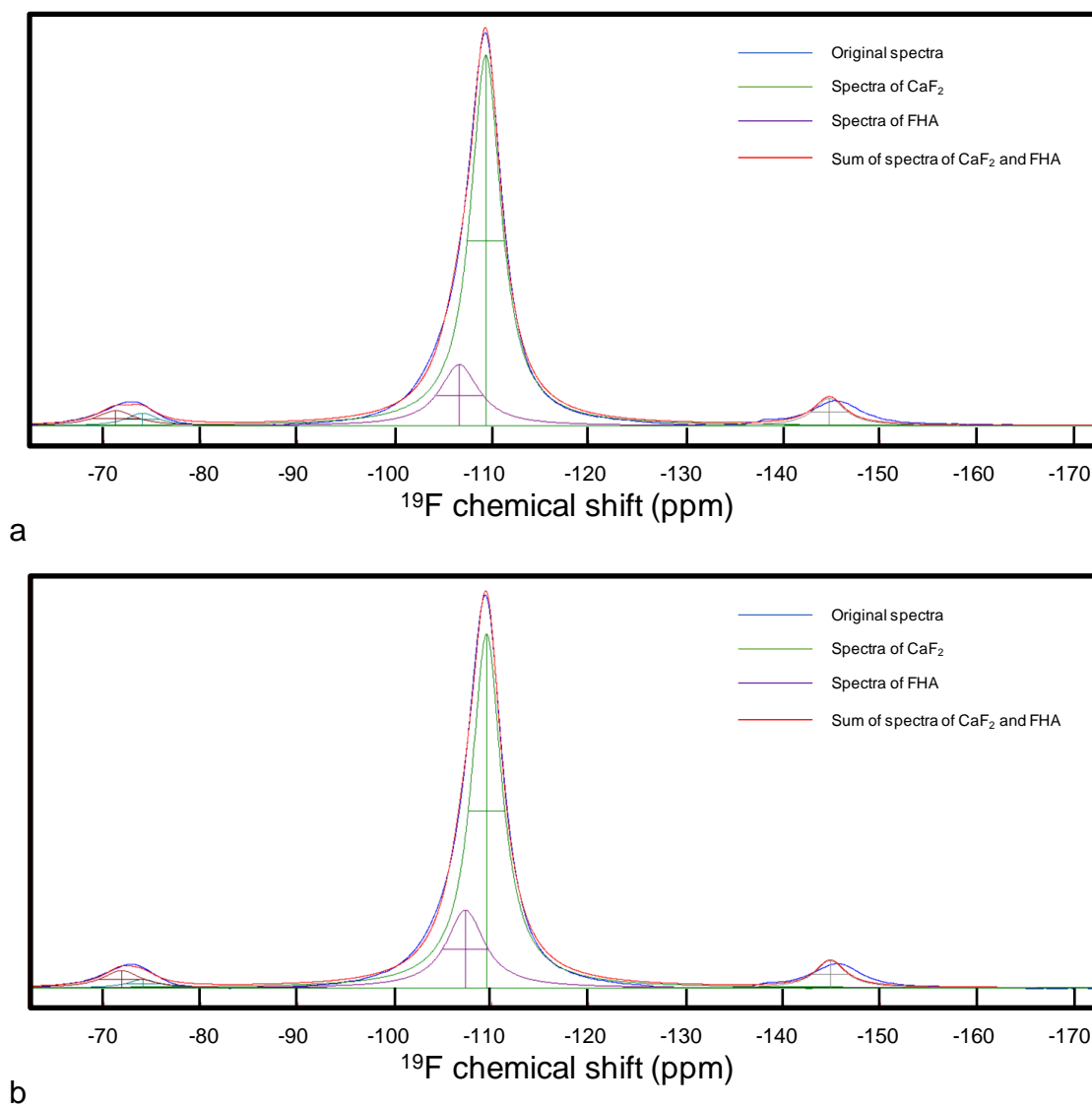
### 8.4.8 $^{19}\text{F}$ MAS-NMR Analysis

The  $^{19}\text{F}$  MAS-NMR spectra (**Fig. 8.21**) showed that no fluoride compounds were detected in HAP powders mixed with DW or  $\text{AgNO}_3$ . However, both  $\text{CaF}_2$  (-109.1 ppm) and FHA (fluorohydroxyapatite) (-106.6 ppm) were detected in HAP powders mixed with  $\text{AgF}$ ,  $\text{Ag}[\text{NH}_3]_2\text{F}$  or Riva-SC. As FHA has a relatively lower content of fluoride than FAP, its chemical shift (-106.6 ppm) is at the upfield side of the FAP (-103.6 ppm).

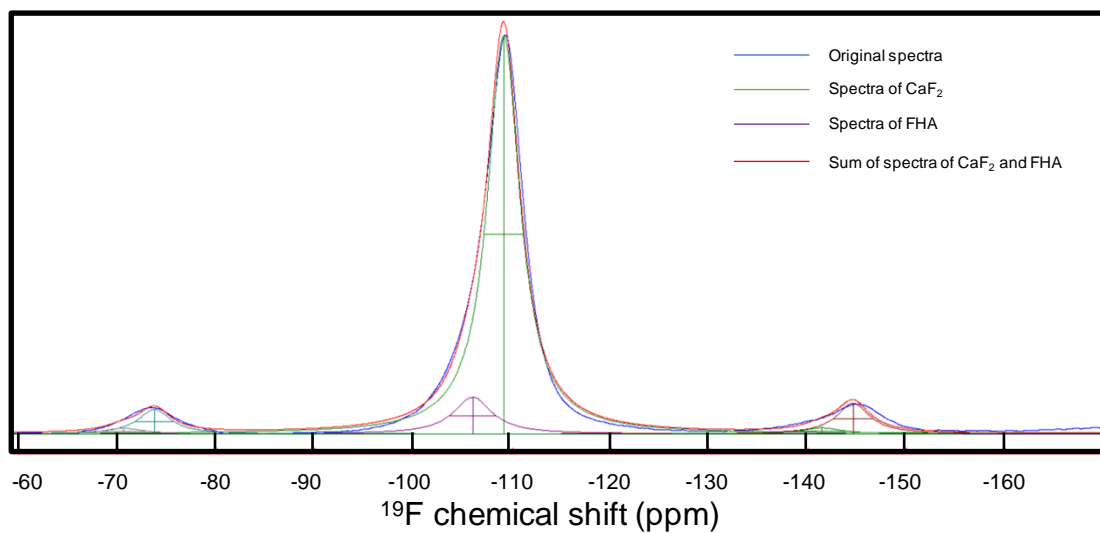


**Figure 8.21** –  $^{19}\text{F}$  MAS-NMR spectra of each treatment group before and after pH 4.0 acid challenge. (\* = sidebands)

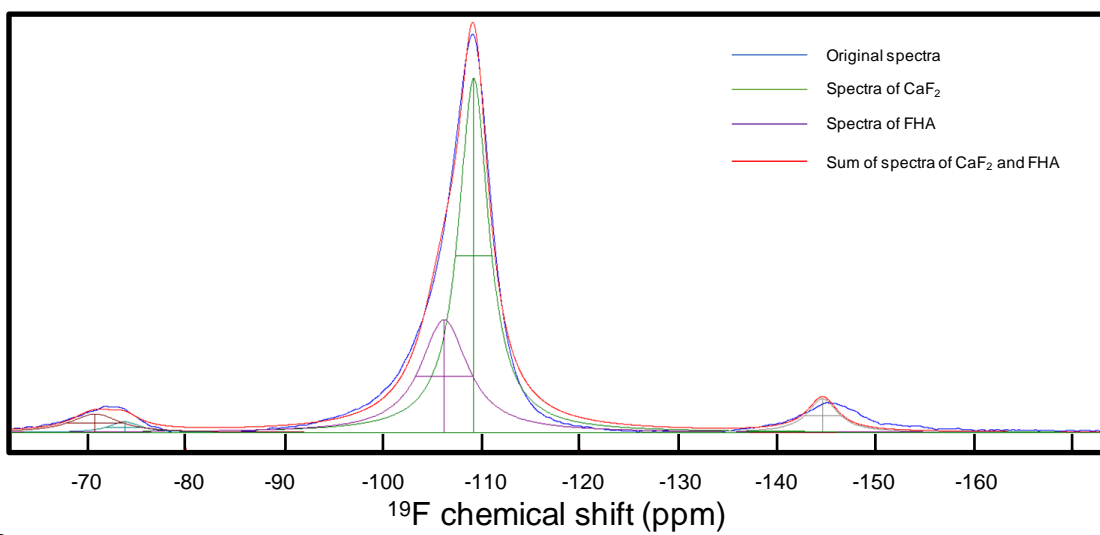
As the chemical shift peaks of  $\text{CaF}_2$  and FHA were too close and overlapped with each other, deconvolution was required using DmFit (France) (Section 5.6). **Fig. 8.22 ~ Fig. 8.24** show that, after the acid challenge, the proportions of FHA in the HAP powders mixed with AgF,  $\text{Ag}[\text{NH}_3]_2\text{F}$  and Riva-SC increased, whereas the proportions of  $\text{CaF}_2$  decreased.



**Figure 8.22** - Deconvoluted  $^{19}\text{F}$  spectra of (a) HAP + AgF and (b) pH 4.0 HAP + AgF.

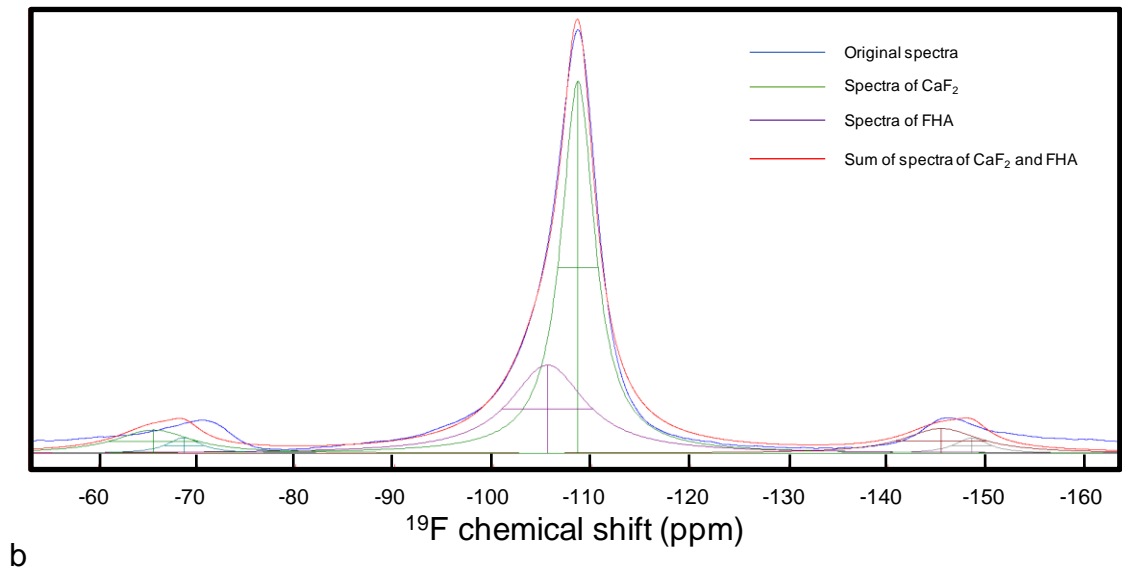
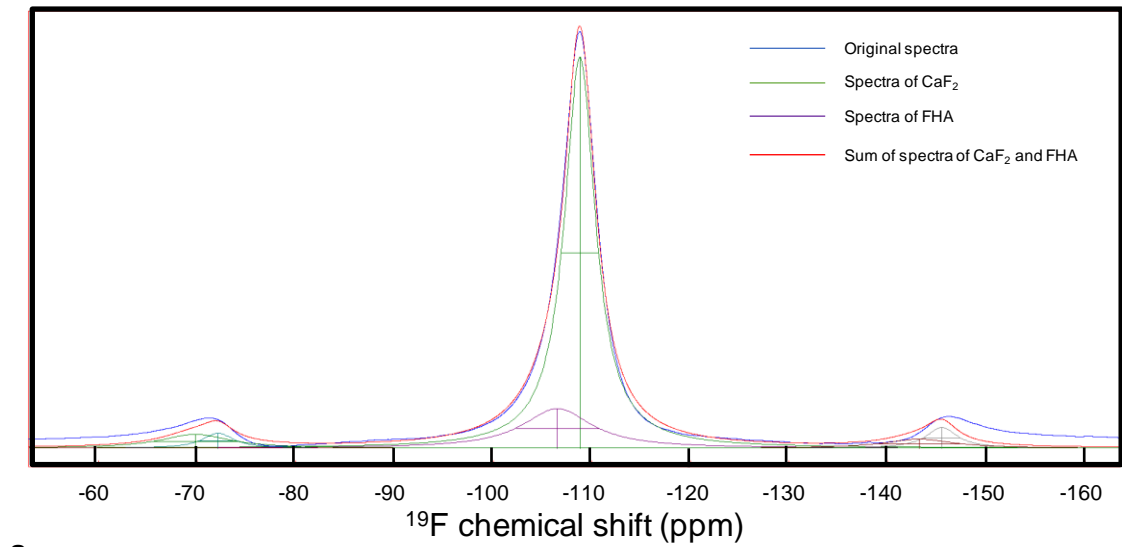


a



b

**Figure 8.23**– Deconvoluted  $^{19}\text{F}$  spectra of (a) HAP +  $\text{Ag}[\text{NH}_3]_2\text{F}$  and (b) pH 4.0 HAP +  $\text{Ag}[\text{NH}_3]_2\text{F}$ .



**Figure 8.24** – Deconvoluted  $^{19}\text{F}$  spectra of (a) HAP + Riva-SC and (b) pH 4.0 HAP + Riva-SC.

## Chapter 9 DISCUSSION OF THE EFFECTS OF TOPICAL TREATMENTS WITH SILVER COMPOUNDS ON DEMINERALISATION OF HAP DISCS AND PROPOSED MODELS FOR MECHANISMS

The linear  $\text{Ca}^{2+}$  release with time from demineralising HAP discs under acid challenge (**Fig. 8.4 ~ Fig. 8.8**) observed in the ISE study was consistent with previously reported results of mineral loss from HAP and enamel during demineralisation using real-time scanning microradiography (SMR) (Anderson *et al.*, 1998; Anderson *et al.*, 2004b; Hassanali *et al.*, 2017). However, SMR could not be used in this study as it does not allow topical treatments of specimens during the experiment due to the time-consuming sample preparation procedure (Section 6.1).

After demineralisation, uneven HAP disc surfaces were observed (**Fig. 8.17a ~ e**), which demonstrated the aggressive destruction from the acid attack. The surface roughness of HAP discs has been reported to increase after pH 4.0 demineralisation using non-contact optical profilometry (Baysan and Anderson, 2009).

## 9.1 Effects of Topical Treatment with De-ionised Water on Demineralisation of HAP Discs

In the ISE study, following the topical treatment with de-ionised water (DW) on HAP discs, a small inhibitory efficacy ( $5.7 \pm 1.2$  %) was observed (**Fig. 8.9**). This might be due to the removal of softened HAP surfaces during the topical applications using a micro-brush, which exposed the intact HAP layers beneath. Further, the physical forces of the topical treatment may smooth the HAP surfaces. Therefore, after re-immersion of the topically treated HAP discs back into acid, the demineralisation was initiated on an intact and smoothed HAP surface, which led to a slower  $\text{Ca}^{2+}$  release from the demineralising HAP discs. It has been suggested that eroded dental surfaces are more vulnerable to physical abrasion effects than sound dental surfaces (Shellis and Addy, 2014). Therefore, demineralisation of HAP discs can be slightly inhibited by the abrasion effects following using a micro-brush during the topical treatments.

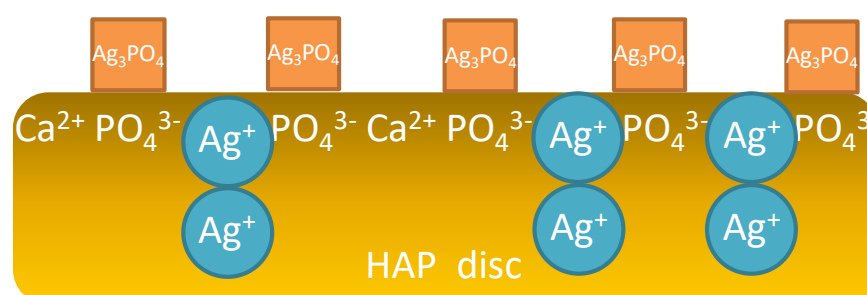
In this study, the inhibitory efficacy of the topical treatments was based on the ratios between the slope values of "4 h"  $\text{Ca}^{2+}$  release trend-lines before and after the treatments. However, the ratios between the slope values of shorter time periods (e.g. 2 h or 3 h) for  $\text{Ca}^{2+}$  release trend-lines before and after the treatments may be different from the present result, leading to different inhibitory efficacy. Therefore, the time period chosen for the  $\text{Ca}^{2+}$  release can affect the interpretation of the results, which may lead to different conclusions. This is a limitation of the current study.



## 9.2 Effects of Topical Treatment with AgNO<sub>3</sub> on Demineralisation of HAP Discs and Proposed Mechanistic Models

### 9.2.1 Following Topical Treatment with AgNO<sub>3</sub>

In the ISE study, immediately following topical treatment with AgNO<sub>3</sub> on HAP discs, yellow staining was observed on the HAP disc surfaces (**Fig. 8.16**), which indicated the formation of yellow Ag<sub>3</sub>PO<sub>4</sub> (Lewis, 1920). This was consistent with the formation of Ag<sub>3</sub>PO<sub>4</sub> in the HAP powders mixed with AgNO<sub>3</sub>, detected with <sup>31</sup>P MAS-NMR (**Fig. 8.20**). It has been proposed that Ag<sup>+</sup> can substitute for Ca<sup>2+</sup> in the HAP lattice (Ling Feng *et al.*, 1998; Singh *et al.*, 2011) (Section 3.2). Therefore, some Ag<sup>+</sup> substituted HAP could also be formed following the topical treatment with AgNO<sub>3</sub>. This is shown schematically in **Fig. 9.1**.



**Figure 9.1** – Schematic representation of an HAP disc topically treated with AgNO<sub>3</sub>. Ag<sub>3</sub>PO<sub>4</sub> is formed on the HAP disc surface and some Ca<sup>2+</sup> in the HAP disc is substituted by Ag<sup>+</sup>.

### 9.2.2 After Re-immersion of HAP Discs Topically Treated with AgNO<sub>3</sub> into Acid

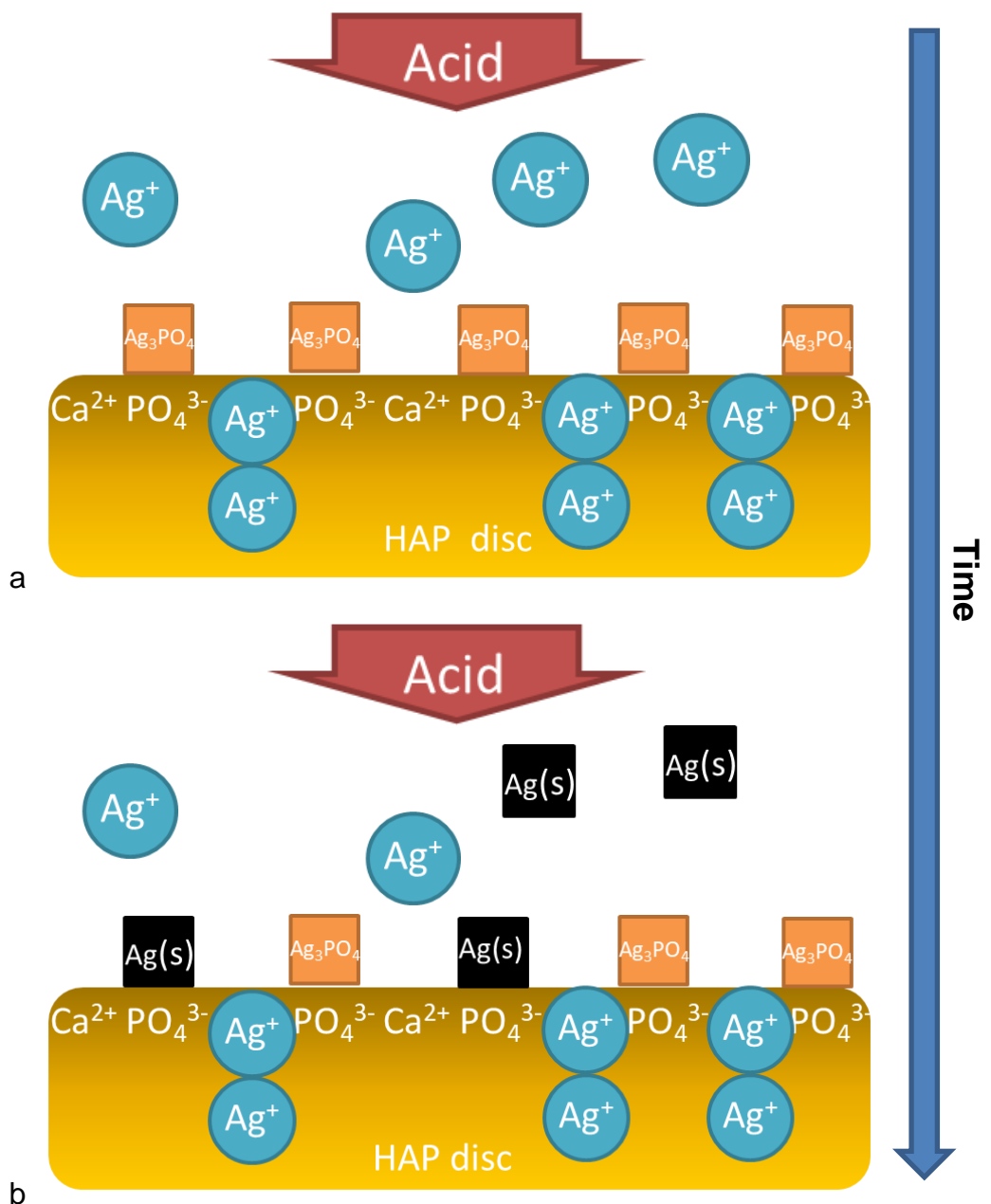
After re-immersing the HAP discs topically treated with AgNO<sub>3</sub> back into acid, the ISE data showed that there was a small immediate reduction by 15.0±2.7 % in the rate of Ca<sup>2+</sup> release (**Fig. 8.5** and **Fig. 8.9**). <sup>31</sup>P MAS-NMR spectra showed that in the HAP powders treated with AgNO<sub>3</sub>, after acid challenge, the proportion of Ag<sub>3</sub>PO<sub>4</sub> increased and the proportion of HAP decreased (**Fig. 8.20**). This may

be due to the acidic demineralisation of HAP by the acid, providing more  $\text{PO}_4^{3-}$  for further  $\text{Ag}_3\text{PO}_4$  formation, which indicates that  $\text{Ag}_3\text{PO}_4$  has higher acid-resistance than HAP. Therefore, the inhibition of  $\text{Ca}^{2+}$  release from demineralising HAP discs following the topical treatment with  $\text{AgNO}_3$  may be associated with the formation of a “protective barrier” composed of  $\text{Ag}_3\text{PO}_4$ . This experimental result confirmed the theoretical inhibitory mechanism of  $\text{AgNO}_3$  on HAP demineralisation, proposed by Yamaga *et al.* (1972) (Section 3.2). Gradually, yellow  $\text{Ag}_3\text{PO}_4$  on the treated HAP discs was reduced to black metallic silver due to the photosensitivity of  $\text{Ag}^+$ , as described by Liu *et al.* (2012c). Even though foil was used in the present study to limit the exposure to light, it has been reported that  $\text{Ag}_3\text{PO}_4$  will be reduced to metallic silver in both light and dark conditions (Lou *et al.*, 2011).

However, the mean  $\text{PRCL}_{\text{HAP}}$  following topical treatment with  $\text{AgNO}_3$  ( $15.0 \pm 2.7$  %) is not much higher than that following topical treatment with DW ( $5.7 \pm 1.2$  %) (**Fig. 8.9**), implying that the inhibitory efficacy of the topical treatment with  $\text{AgNO}_3$  is low. The low inhibitory efficacy of the topical treatment may be due to the formation of  $\text{Ag}^+$  substituted HAP, which has been proposed to be more susceptible to acid challenge than HAP (Singh *et al.*, 2011).

The  $\text{Ag}^+$  released from the HAP discs topically treated with  $\text{AgNO}_3$  was detected with  $\text{Ag}^+$  ISEs after the re-immersion of the HAP discs back into acid (**Fig. 8.10**). The initial increase in the mean  $\text{Ag}^+$  activity could result from the release of  $\text{Ag}^+$  loosely attached to the HAP disc surfaces, whereas, the later decrease in the mean  $\text{Ag}^+$  activity could result from the chemical reduction of  $\text{Ag}^+$ . These very small metallic silver particles will be dispersed in the solution due to the agitation of the magnetic stirrer.

**Fig. 9.2a** shows that, after re-immersing the HAP discs topically treated with  $\text{AgNO}_3$  back into acid,  $\text{Ag}^+$  loosely attached to the HAP disc surfaces is released into solution. Further, the  $\text{Ag}_3\text{PO}_4$  protective barrier protects the HAP disc from demineralisation. **Fig. 9.2b** shows that some  $\text{Ag}^+$  in the solution and some  $\text{Ag}_3\text{PO}_4$  on the HAP disc surface are gradually reduced to black metallic silver. Further, the metallic silver reduced from the  $\text{Ag}^+$  in the solution will be dispersed in the solution.



**Figure 9.2** - Schematic representation of an HAP disc topically treated with AgNO<sub>3</sub> following re-immersion back into acid. a) Ag<sup>+</sup> loosely attached to HAP disc surfaces is released into solution. b) Gradually, some Ag<sub>3</sub>PO<sub>4</sub> on the HAP disc surface and some Ag<sup>+</sup> in the solution are reduced to black metallic silver.

### 9.2.3 After Removal of HAP Discs Topically Treated with AgNO<sub>3</sub> from Acid

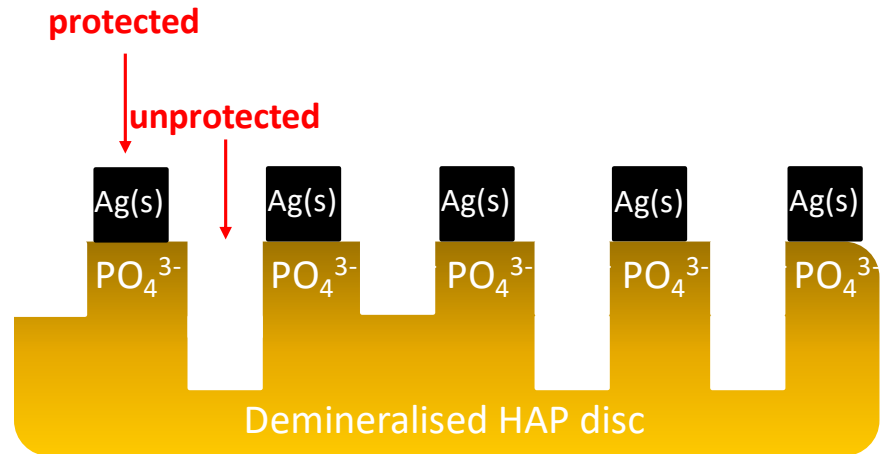
After removing the HAP discs topically treated with AgNO<sub>3</sub> from acid, SEM images showed that the HAP disc surfaces were less uneven than the surfaces

topically treated with DW (**Fig. 8.17a** and **b**), which demonstrated the inhibitory efficacy of topical treatment with AgNO<sub>3</sub>. Deeper lesions observed on the HAP disc surfaces may be due to the loss of Ag<sup>+</sup> substituted HAP, which has a higher susceptibility to acidic demineralisation.

Cubic particles were observed on the HAP disc surfaces topically treated with AgNO<sub>3</sub> (**Fig. 8.17b**). These cubic particles may be Ag<sub>3</sub>PO<sub>4</sub> or metallic silver, as a previous study has reported that yellow cubic Ag<sub>3</sub>PO<sub>4</sub> were found in the HAP powders mixed with AgNO<sub>3</sub>, which gradually reduced to black cubic metallic silver (Lou *et al.*, 2011). In the present study, as only black staining was observed on the HAP disc surfaces topically treated with AgNO<sub>3</sub> (**Fig. 8.16**), most of the Ag<sub>3</sub>PO<sub>4</sub> has been reduced to metallic silver over the post-treatment 4 h demineralisation period.

**Fig. 8.5** shows that, during the post-treatment 4 h demineralisation period, the inhibited Ca<sup>2+</sup> release from demineralising HAP disc following the topical treatment with AgNO<sub>3</sub> was linear with time, even though Ag<sub>3</sub>PO<sub>4</sub> in the protective barrier was gradually reduced to metallic silver. This indicates that the inhibitory efficacy of the topical treatment with AgNO<sub>3</sub> was not subsequently affected by the chemical reduction of Ag<sub>3</sub>PO<sub>4</sub> in the protective barrier to metallic silver. Therefore, the metallic silver particles reduced from Ag<sub>3</sub>PO<sub>4</sub> particles continued to play the same protective role as the Ag<sub>3</sub>PO<sub>4</sub> particles in the protective barrier during demineralisation.

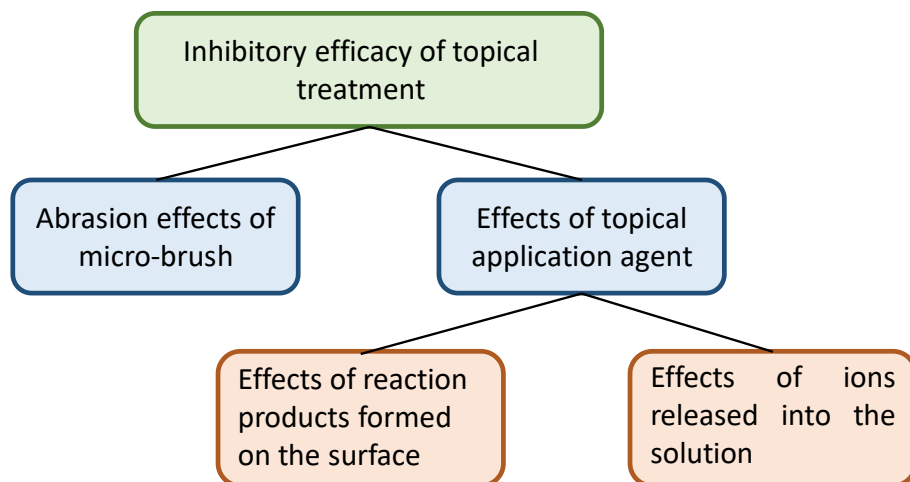
**Fig. 9.3** shows that after removing the HAP discs topically treated with AgNO<sub>3</sub> from acid, deeper lesions developed in the Ag<sup>+</sup> substituted HAP are observed, and therefore the demineralised HAP disc surface is very uneven. Further, all the Ag<sub>3</sub>PO<sub>4</sub> on the HAP disc surfaces is reduced to metallic silver causing black staining. The HAP disc surface covered by the metallic silver is protected during the demineralisation.



**Figure 9.3** – Schematic representation of an HAP topically treated with  $\text{AgNO}_3$  after 4 h demineralisation. Deeper lesions are developed in the  $\text{Ag}^+$  substituted HAP, therefore an uneven demineralised HAP disc surface is observed. Further, all the  $\text{Ag}_3\text{PO}_4$  is reduced to metallic silver causing black staining.

#### 9.2.4 Analysis of the Inhibitory Efficacy of the Topical Treatment with $\text{AgNO}_3$ on Demineralisation of HAP Discs

As discussed in topical treatment with DW (Section 9.1), demineralisation of HAP discs can be inhibited merely by the abrasion effects from using a micro-brush during the topical treatment ( $\text{PRCL}_{\text{HAP}} = 5.7 \pm 1.2 \%$ ). Therefore, the inhibitory efficacy ( $\text{PRCL}_{\text{HAP}} = 15.0 \pm 2.7 \%$ ) observed following the topical treatment with  $\text{AgNO}_3$  on the demineralisation of HAP discs was partially be attributed to the abrasion effects of the micro-brush.



**Figure 9.4** – The effects of topical treatment influencing the inhibitory efficacy.

The rest of the inhibitory efficacy should be associated with the effects of topically applied AgNO<sub>3</sub>. The effects of topically applied AgNO<sub>3</sub> include the effects of the reaction products deposited on the HAP disc surfaces and the effects of the ions released from the topically treated HAP discs (**Fig. 9.4**). As discussed previously (Section 9.2.2), Ag<sub>3</sub>PO<sub>4</sub> particles were formed as a protective barrier on the HAP discs topically treated with AgNO<sub>3</sub>, which contributed to the inhibitory efficacy. Whereas, as the Ag<sup>+</sup> in the solution released from the topically treated HAP discs accelerated the demineralisation due to the formation of Ag<sup>+</sup> substituted HAP (Singh *et al.*, 2011), the inhibitory efficacy was compromised. However, as the [Ag<sup>+</sup>]<sub>4h</sub> in the solution was only 0.61±0.10 ppm (**Table 8.9**), the accelerating effect of Ag<sup>+</sup> should be small. According to the log-linear dose-response of Ag<sup>+</sup> on demineralisation of enamel reported in Chapter 7 (**Fig. 7.4**), the effect of the Ag<sup>+</sup> at 0.61 ppm is negligible.

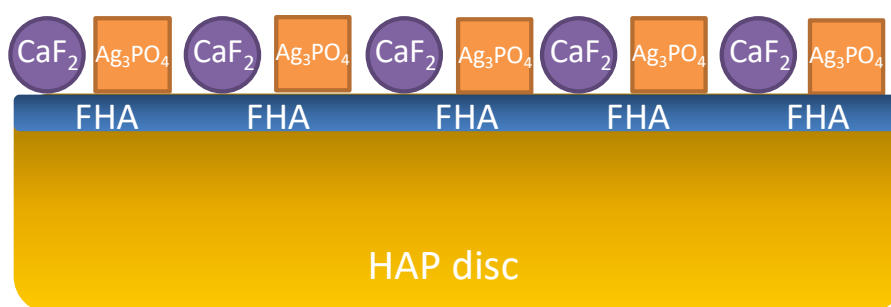
### 9.2.5 Conclusions

In conclusion, Sections 9.2.1, 9.2.2, 9.2.3 and 9.2.4 show that the inhibitory efficacy of topical treatment with AgNO<sub>3</sub> on demineralisation of HAP discs is associated with the formation of a protective barrier composed of Ag<sub>3</sub>PO<sub>4</sub> (gradually reduced to metallic silver), and the abrasion effects of topical treatment.

## 9.3 Effects of Topical Treatments with AgF and Ag[NH<sub>3</sub>]<sub>2</sub>F on Demineralisation of HAP Discs and Proposed Mechanistic Models

### 9.3.1 Following Topical Treatments with AgF and Ag[NH<sub>3</sub>]<sub>2</sub>F

In the ISE study, immediately following topical treatments with AgF and Ag[NH<sub>3</sub>]<sub>2</sub>F on HAP discs, yellow staining was observed on the HAP disc surfaces (**Fig. 8.16**), which indicated the formation of yellow Ag<sub>3</sub>PO<sub>4</sub> (Lewis, 1920). This was consistent with the formation of Ag<sub>3</sub>PO<sub>4</sub> in the HAP powders mixed with AgF and Ag[NH<sub>3</sub>]<sub>2</sub>F detected with <sup>31</sup>P MAS-NMR (**Fig. 8.20**). Further, the formation of CaF<sub>2</sub> and fluorohydroxyapatite (FHA) in the HAP powders mixed with AgF and Ag[NH<sub>3</sub>]<sub>2</sub>F was also detected with <sup>19</sup>F MAS-NMR (**Fig. 8.21**). Therefore, the Ca<sup>2+</sup> lost from HAP discs due to the formation of Ag<sup>+</sup> substituted HAP (Ling Feng *et al.*, 1998; Singh *et al.*, 2011) will be preserved as CaF<sub>2</sub>, and unstable Ag<sup>+</sup> substituted HAP will be replaced by more stable FHA (Robinson, 2009). Thus, HAP discs topically treated with AgF and Ag[NH<sub>3</sub>]<sub>2</sub>F should be better protected against demineralisation than those topically treated with AgNO<sub>3</sub> due to the additional CaF<sub>2</sub> deposits covering the HAP disc surfaces, and, the formation of acid-resistant FHA. This is shown schematically in **Fig 9.5**.



**Figure 9.5** – Schematic representation of an HAP disc topically treated with AgF or Ag[NH<sub>3</sub>]<sub>2</sub>F. Ag<sub>3</sub>PO<sub>4</sub>, CaF<sub>2</sub> and FHA are formed on the HAP disc surface.

### 9.3.2 After Re-immersion of HAP Discs Topically Treated with AgF, and Ag[NH<sub>3</sub>]<sub>2</sub>F into Acid

After re-immersing the HAP discs topically treated with AgF and Ag[NH<sub>3</sub>]<sub>2</sub>F back into acid, the ISE data showed that there was an immediate reduction in the rate of Ca<sup>2+</sup> release (**Fig. 8.6** and **Fig. 8.7**). The mean PRCL<sub>HAP</sub> of the AgF and Ag[NH<sub>3</sub>]<sub>2</sub>F treatment groups (72.3±4.5 % and 69.7±5.1 %) were much higher than that of the AgNO<sub>3</sub> treatment group (15.0±2.7 %) (**Fig. 8.9**), showing that the inhibitory efficacy of F<sup>-</sup> was greater than that of Ag<sup>+</sup>.

<sup>31</sup>P MAS-NMR spectra showed that in the HAP powders mixed with AgF, and Ag[NH<sub>3</sub>]<sub>2</sub>F, the proportions of Ag<sub>3</sub>PO<sub>4</sub> increased, and the proportions of HAP decreased after acid challenge (**Fig. 8.20**). This indicates that the Ag<sub>3</sub>PO<sub>4</sub> has higher acid-resistant than HAP (as discussed in Section 9.2.2). Furthermore, <sup>19</sup>F MAS-NMR spectra showed that in the HAP powders mixed with AgF and Ag[NH<sub>3</sub>]<sub>2</sub>F, the proportions of CaF<sub>2</sub> decreased and the proportions of FHA increased after acid challenge (**Fig. 8.22** and **Fig. 8.23**). This may be due to the acidic demineralisation of CaF<sub>2</sub>, providing F<sup>-</sup> for further formation of FHA. Both CaF<sub>2</sub> and FHA have been proposed to be able to inhibit the demineralisation of HAP (Rosin-Grget *et al.*, 2013; ten Cate, 1997; White and Nancollas, 1990) (Section 2.4). Therefore, the inhibition of Ca<sup>2+</sup> release from demineralising HAP discs following the topical treatments with AgF and Ag[NH<sub>3</sub>]<sub>2</sub>F could be associated with the formation of a protective barrier composed of Ag<sub>3</sub>PO<sub>4</sub>, CaF<sub>2</sub> and FHA. This experimental result confirmed the theoretical inhibitory mechanism of Ag[NH<sub>3</sub>]<sub>2</sub>F on HAP demineralisation, proposed by Yamaga *et al.* (1972) (Section 3.4.3). Gradually, yellow Ag<sub>3</sub>PO<sub>4</sub> on the treated HAP discs was reduced to black metallic silver due to the photosensitivity of Ag<sup>+</sup> (Liu *et al.*, 2012c).

The Ag<sup>+</sup> released from the HAP discs topically treated with AgF and Ag[NH<sub>3</sub>]<sub>2</sub>F was detected with Ag<sup>+</sup> ISEs after the re-immersion of the HAP discs back into acid (**Fig. 8.10**). As mentioned in AgNO<sub>3</sub> treatment group (Section 9.2.2), the initial increase in the mean Ag<sup>+</sup> activity could result from the release of Ag<sup>+</sup> loosely attached to the HAP disc surfaces, whereas, the later decrease in the mean Ag<sup>+</sup> activity could result from chemical reduction of Ag<sup>+</sup>. These very small metallic



silver particles will be dispersed in the solution due to the agitation of the magnetic stirrer.

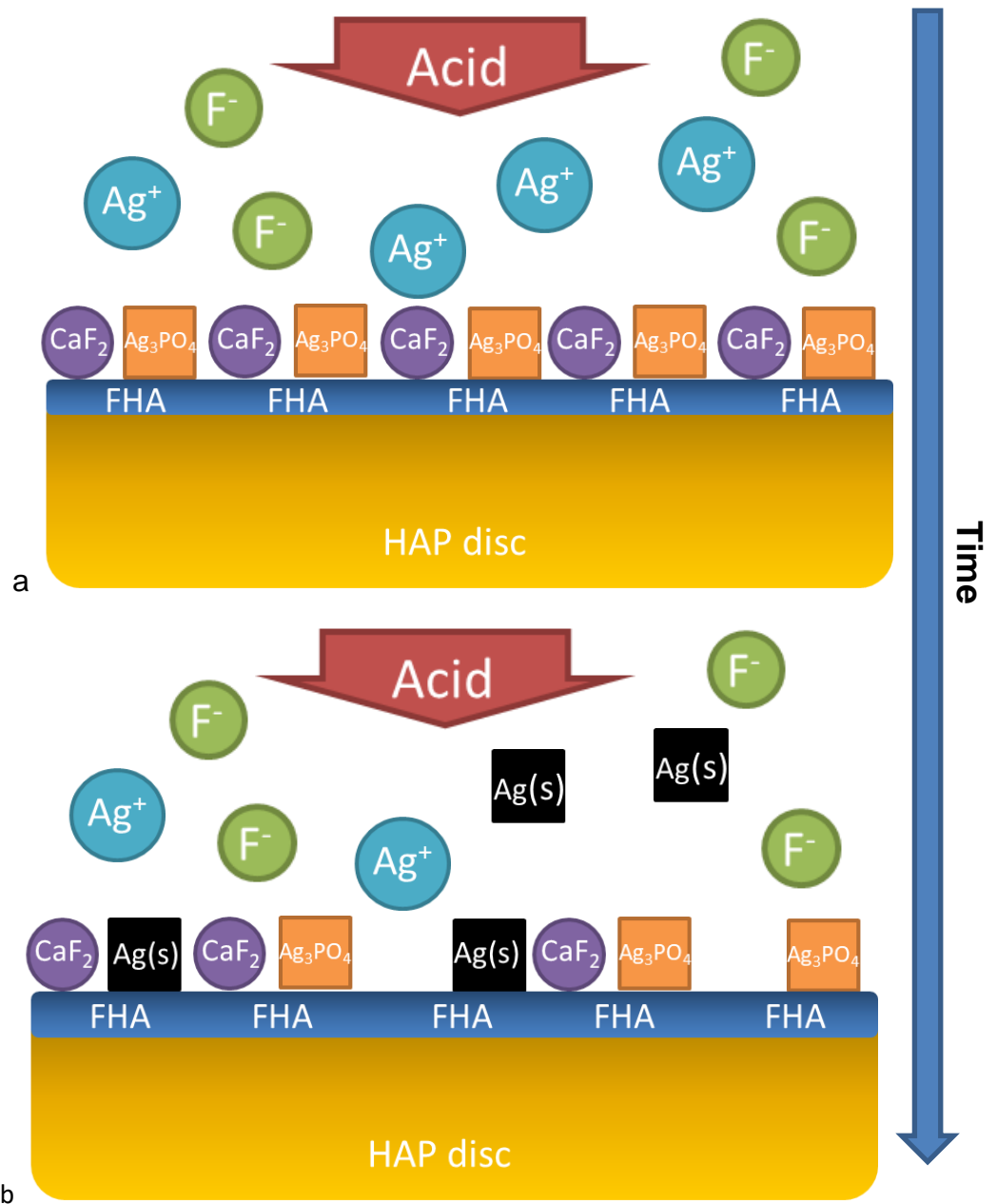
**Fig. 8.11a** and **b** shows that there were no significant differences in the initial increase rate of  $\text{Ag}^+$  activities and the later decrease rate of  $\text{Ag}^+$  activities between AgF and  $\text{Ag}[\text{NH}_3]_2\text{F}$  treatment groups. This indicates the hindrance of the chemical reduction of  $\text{Ag}^+$  by the formation of  $\text{Ag}[\text{NH}_3]_2^+$  following the  $\text{Ag}[\text{NH}_3]_2\text{F}$  topical treatment (Liu *et al.*, 2012b) was not obvious. Similar  $\text{Ag}^+$  release profiles explain why there were no significant differences between the  $[\text{Ag}^+]_{4\text{h}}$  of AgF and  $\text{Ag}[\text{NH}_3]_2\text{F}$  treatment groups (**Fig. 8.12**). Therefore, the effects of  $\text{Ag}^+$  in the solution on both AgF and  $\text{Ag}[\text{NH}_3]_2\text{F}$  topically treated HAP discs should be similar.

The  $\text{F}^-$  released from the HAP discs topically treated with AgF and  $\text{Ag}[\text{NH}_3]_2\text{F}$  was detected with  $\text{F}^-$  ISEs after the re-immersion of the HAP discs back into acid (**Fig. 8.13**). The initial increase in the mean  $\text{F}^-$  activity could result from the release of  $\text{F}^-$  loosely attached to the HAP disc surfaces (Arends and Christoffersen, 1990; Dijkman *et al.*, 1982), whereas, the later increase in the mean  $\text{F}^-$  activity could result from the slow dissolution of  $\text{CaF}_2$ -like globules (Buzalaf *et al.*, 2011; White and Nancollas, 1990; Rolla, 1988). It has been proposed that  $\text{CaF}_2$ -like globule ( $\text{CaF}_2$  with the adsorption of  $\text{HPO}_4^{2-}$ ), which has lower solubility than pure  $\text{CaF}_2$ , can act as a pH-driven  $\text{F}^-$  reservoir, favouring the formation of FHA (ten Cate, 2013; Vogel, 2011) (Section 2.4).

**Fig. 8.14a** and **b** shows that the initial increase rate of  $\text{F}^-$  activity following  $\text{Ag}[\text{NH}_3]_2\text{F}$  topical treatment was significantly faster than that following AgF topical treatment. However, the later increase rate of  $\text{F}^-$  activity following  $\text{Ag}[\text{NH}_3]_2\text{F}$  topical treatments was significantly slower than that following AgF topical treatment. This may be due to that the proportion of  $\text{CaF}_2$  without the adsorption of  $\text{HPO}_4^{2-}$ , which has higher solubility, formed following  $\text{Ag}[\text{NH}_3]_2\text{F}$  topical treatment was higher than that following AgF topical treatment, leading to faster initial  $\text{F}^-$  release. Further, the proportion of  $\text{CaF}_2$  with the adsorption of  $\text{HPO}_4^{2-}$  ( $\text{CaF}_2$ -like globule) formed following  $\text{Ag}[\text{NH}_3]_2\text{F}$  topical treatment was lower than that following AgF topical treatment, leading slower later  $\text{F}^-$  release. The much faster initial  $\text{F}^-$  release following  $\text{Ag}[\text{NH}_3]_2\text{F}$  topical treatment resulted in significantly higher  $[\text{F}^-]_{4\text{h}}$  detected following  $\text{Ag}[\text{NH}_3]_2\text{F}$  topical treatment than

that following AgF topical treatment (**Fig. 8.15**). Therefore, the effects of F<sup>-</sup> in the solution on Ag[NH<sub>3</sub>]<sub>2</sub>F topically treated HAP discs should be higher than those on AgF topically treated HAP discs. Less CaF<sub>2</sub>-like globules formed following Ag[NH<sub>3</sub>]<sub>2</sub>F topical treatment may be due to the interference of the adsorption of HPO<sub>4</sub><sup>2-</sup> around CaF<sub>2</sub> surfaces. The most likely interference factor could be the ammonium (NH<sub>4</sub><sup>+</sup>) dissolved from the Ag[NH<sub>3</sub>]<sub>2</sub>F. However, further studies are required to confirm the extrapolation.

**Fig. 9.6a** shows that, after re-immersing the HAP discs topically treated with AgF or Ag[NH<sub>3</sub>]<sub>2</sub>F back into acid, both Ag<sup>+</sup> and F<sup>-</sup> loosely attached to HAP disc surface are released into solution. Further, the protective barrier composed of Ag<sub>3</sub>PO<sub>4</sub>, CaF<sub>2</sub> and FHA protects the HAP disc from demineralisation. **Fig. 9.6b** shows that some Ag<sup>+</sup> in the solution and some Ag<sub>3</sub>PO<sub>4</sub> on the HAP disc surface are gradually reduced to metallic silver. Further, some CaF<sub>2</sub> on the HAP disc surface is gradually dissolved, providing F<sup>-</sup> for further formation of FHA.



**Figure 9.6** - Schematic representation of an HAP disc topically treated with  $\text{AgF}$  or  $\text{Ag}[\text{NH}_3]_2\text{F}$  following re-immersion back into acid. a) Both  $\text{Ag}^+$  and  $\text{F}^-$  loosely attached to HAP disc surfaces are released into solution. b) Gradually, some  $\text{Ag}_3\text{PO}_4$  on the HAP disc surface and some  $\text{Ag}^+$  in the solution are reduced to metallic silver, and some  $\text{CaF}_2$  on the HAP disc surface is dissolved, providing  $\text{F}^-$  for further formation of FHA.

### 9.3.3 After Removal of HAP Discs Topically Treated with AgF, and Ag[NH<sub>3</sub>]<sub>2</sub>F from Acid

After removing the HAP discs topically treated with AgF and Ag[NH<sub>3</sub>]<sub>2</sub>F from acid, SEM images showed that the HAP disc surfaces were less uneven than those topically treated with AgNO<sub>3</sub> (**Fig. 8.17b ~ d**), which demonstrated that the inhibitory efficacy of F<sup>-</sup> was greater than that of Ag<sup>+</sup>.

Cubic and granular particles were observed on the HAP disc surfaces topically treated with AgF and Ag[NH<sub>3</sub>]<sub>2</sub>F (**Fig. 8.17c and 8.17d**). As only black staining was observed on the HAP disc surfaces (**Fig. 8.16**), the cubic particles were mostly cubic metallic silver reduced from Ag<sub>3</sub>PO<sub>4</sub> (as discussed in Section 9.2.3). On the other hand, the granular particles should be CaF<sub>2</sub>-like globules (Rolla and Saxegaard, 1990; Buzalaf *et al.*, 2011) (Section 2.4). A previous study also reported that cubic metallic silver and CaF<sub>2</sub>-like globules were found in the HAP powders (2.5 mg) mixed with Ag[NH<sub>3</sub>]<sub>2</sub>F (0.5 mL) (Lou *et al.*, 2011). However, they did not find Ag<sub>3</sub>PO<sub>4</sub> following mixing with Ag[NH<sub>3</sub>]<sub>2</sub>F. This may be due to higher amounts of the HAP powder (1.0 g) and the Ag[NH<sub>3</sub>]<sub>2</sub>F (2.5 mL) used in this study, leading to more formation of Ag<sub>3</sub>PO<sub>4</sub>. Further, they identified CaF<sub>2</sub>-like globules which disappeared after water rinsing. However, as no rinsing procedure was conducted after the topical treatment in the present study, CaF<sub>2</sub>-like globules were observed on the HAP disc surfaces.

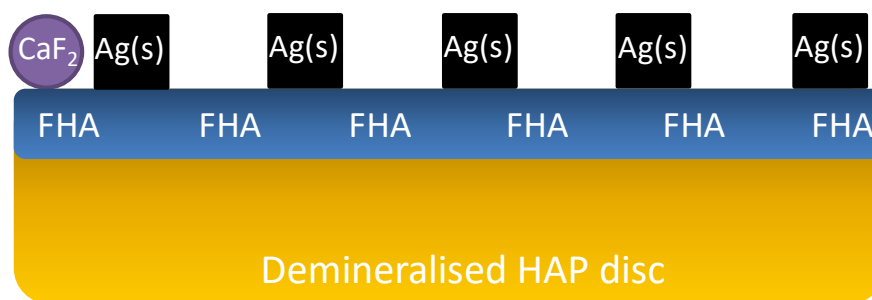
The mean atomic percentage of Ag detected on the HAP disc surfaces topically treated with AgF was significantly higher than that of AgNO<sub>3</sub> (**Fig. 8.18**). This indicates that the participation of F<sup>-</sup> increased the formation of silver compounds deposited on the surfaces. A previous study found that as the formation of CaF<sub>2</sub> requires slight dissolution of enamel, it results in the PO<sub>4</sub><sup>3-</sup> release from the dissociation of enamel mineral (mainly HAP) (Mohammed *et al.*, 2013). Therefore, in the present study, as CaF<sub>2</sub> was formed following topical treatments with AgF (**Fig. 8.21**), PO<sub>4</sub><sup>3-</sup> released from the dissociation of HAP discs led to more formation of Ag<sub>3</sub>PO<sub>4</sub> on the surfaces. The mean atomic percentage of Ag detected on the HAP disc surfaces topically treated with Ag[NH<sub>3</sub>]<sub>2</sub>F was

significantly lower than that of AgF (**Fig. 8.18**), which may be due to that  $\text{Ag}_3\text{PO}_4$  can be dissolved in ammonium (Firsching, 1961) (Section 3.4.3).

The mean atomic percentages of F detected on the HAP discs topically treated with AgF and  $\text{Ag}[\text{NH}_3]_2\text{F}$  were small ( $< 2\%$ ) (**Fig. 8.19**). This indicates that most of the  $\text{CaF}_2$  was dissolved during the post-treatment 4 h demineralisation period. The mean atomic percentage of F detected on the HAP discs topically treated with AgF was slightly higher than that of  $\text{Ag}[\text{NH}_3]_2\text{F}$  treatment group (**Fig. 8.19**). The lower mean atomic percentages of F detected on the  $\text{Ag}[\text{NH}_3]_2\text{F}$  topically treated HAP discs should be due to the faster initial  $\text{F}^-$  release (**Fig. 8.14a**), as discussed in Section 9.3.2.

**Fig. 8.6** and **Fig. 8.7** show that, during the post-treatment 4 h demineralisation period, the inhibited  $\text{Ca}^{2+}$  release from demineralising HAP disc following the topical treatments with AgF and  $\text{Ag}[\text{NH}_3]_2\text{F}$  was linear with time, even though  $\text{Ag}_3\text{PO}_4$  in the protective barrier was gradually reduced to metallic silver and the  $\text{CaF}_2$  in the protective barrier was gradually dissolved. This indicates that the inhibitory efficacy of topical treatments with these fluoride-containing silver compounds was not subsequently affected by the chemical reduction of  $\text{Ag}_3\text{PO}_4$  to metallic silver and the dissolution of  $\text{CaF}_2$ . As mentioned in Section 9.2.3, the metallic silver particles reduced from  $\text{Ag}_3\text{PO}_4$  particles continue to play the same protective role as the  $\text{Ag}_3\text{PO}_4$  particles in the protective barrier. Therefore, the further FHA formation due to the supply of  $\text{F}^-$  from  $\text{CaF}_2$  dissolution should compensate for the protective effect lost from the dissolution of  $\text{CaF}_2$  in the protective barrier.

**Fig. 9.7** shows that after removing the HAP discs topically treated with AgF, or  $\text{Ag}[\text{NH}_3]_2\text{F}$  from acid, all the  $\text{Ag}_3\text{PO}_4$  on the HAP disc is reduced to metallic silver causing black staining. Further, most of the  $\text{CaF}_2$  is dissolved, which favours further formation of FHA. The HAP disc surface covered by the metallic silver,  $\text{CaF}_2$  and FHA is protected during the demineralisation.



**Figure 9.7** - Schematic representation of an HAP topically treated with AgF or Ag[NH<sub>3</sub>]<sub>2</sub>F after 4 h demineralisation. All the Ag<sub>3</sub>PO<sub>4</sub> is reduced to metallic silver causing black staining and most of the CaF<sub>2</sub> is dissolved which favours further formation of FHA.

### 9.3.4 Analysis of the Inhibitory Efficacy of the Topical Treatments with AgF and Ag[NH<sub>3</sub>]<sub>2</sub>F on Demineralisation of HAP Discs

As discussed in Section 9.2.4, the inhibitory efficacy of the topical treatment on demineralisation of HAP discs can be influenced by the abrasion effects from using a micro-brush during the topical treatment and the effects of topical application agent (**Fig. 9.4**). Therefore, the abrasion effects of the topical treatment (PRCL<sub>HAP</sub> = 5.7±1.2 %) contributed to the inhibitory efficacy of topical treatments with AgF (PRCL<sub>HAP</sub> = 72.3±4.5 %) and Ag[NH<sub>3</sub>]<sub>2</sub>F (PRCL<sub>HAP</sub> = 69.7±5.1 %).

The effects of topical application agent include the effects of the reaction products deposited on the HAP disc surfaces and the effects of the ions released from the topically treated HAP discs (**Fig. 9.4**). Therefore, the protective barrier, composed of Ag<sub>3</sub>PO<sub>4</sub>, CaF<sub>2</sub> and FHA, formed on the HAP disc surfaces topically treated with AgF and Ag[NH<sub>3</sub>]<sub>2</sub>F (Section 9.3.2) also contributed to the inhibitory efficacy.

After re-immersing the treated HAP discs back into acids, both Ag<sup>+</sup> and F<sup>-</sup> were released (**Fig. 8.10** and **Fig. 8.13**). Ag<sup>+</sup> in solution accelerates the demineralisation of HAP (Singh *et al.*, 2011). According to the log-linear dose-response of Ag<sup>+</sup> on demineralisation of enamel (**Fig. 7.4**), the effects of the Ag<sup>+</sup> at 1.00 ppm, [Ag<sup>+</sup>]<sub>4h</sub> of AgF, and 1.01 ppm, [Ag<sup>+</sup>]<sub>4h</sub> of Ag[NH<sub>3</sub>]<sub>2</sub>F (**Table 8.9**), will accelerate the demineralisation both by 1.2 % (PRML<sub>enamel</sub>). On the other hand, F<sup>-</sup> in solution inhibits the demineralisation of HAP (White and Nancollas, 1990).

According to the log-linear dose-response of  $F^-$  on demineralisation of enamel (**Fig. 6.7b**) (Mohammed *et al.*, 2014a), the effects of the  $F^-$  at 0.18 ppm,  $[F^-]_{4h}$  of AgF, and 0.31 ppm,  $[F^-]_{4h}$  of  $Ag[NH_3]_2F$  (**Table 8.11**), will inhibit the demineralisation by 22.9 % and 28.9 % ( $PRML_{enamel}$ ), respectively.

Even though the inhibitory efficacy ( $PRML_{enamel}$ ) resulting from the  $F^-$  in solution following AgF topical treatment is lower than that following  $Ag[NH_3]_2F$  topical treatment, the  $PRCL_{HAP}$  of topical treatments with AgF and  $Ag[NH_3]_2F$  were similar (**Fig. 8.9**). Therefore, the inhibitory efficacy from the protective barrier formed on the HAP disc surfaces topically treated with AgF was higher than that formed on the HAP disc surfaces topically treated with  $Ag[NH_3]_2F$ . This is consistent with higher amounts of silver and fluoride compounds detected on the AgF topically treated HAP discs (**Fig. 8.18** and **Fig. 8.19**),

### 9.3.5 Conclusions

In conclusion, Sections 9.3.1, 9.3.2, 9.3.3 and 9.3.4 show that the inhibitory efficacy of topical treatments with AgF and  $Ag[NH_3]_2F$  on demineralisation of HAP discs is associated with the release of  $F^-$  from the topically treated HAP discs, the formation of a protective barrier composed of  $Ag_3PO_4$ ,  $CaF_2$  and FHA, and, the abrasion effects of topical treatments.

## 9.4 Difference Between the Effects of Topical Treatments with Riva-SC and 3.16 M $\text{Ag}[\text{NH}_3]_2\text{F}$ on Demineralisation of HAP Discs

The effects of topical treatment with Riva-SC (3.16 M  $\text{Ag}[\text{NH}_3]_2\text{F}$ , Silver Capsule of Riva Star SDI Ltd, Australia) on demineralisation of HAP discs were similar to those of laboratory-prepared (3.16 M)  $\text{Ag}[\text{NH}_3]_2\text{F}$  (**Fig. 8.7 ~ Fig. 8.24**). This suggests that they have the same inhibitory effects on the demineralisation of HAP discs, and therefore, the same mechanisms (**Fig. 9.5 ~ Fig. 9.7**).

However, the rates of  $\text{F}^-$  release from the HAP discs topically treated with Riva-SC, and the mean atomic percentages of Ag detected on the HAP disc surfaces topically treated with Riva-SC were not significantly different from other treatment groups like the laboratory-prepared (3.16 M)  $\text{Ag}[\text{NH}_3]_2\text{F}$  due to the high standard errors (**Fig. 8.14** and **Fig. 8.18**). This may be due to that the composition of each Silver Capsule of Riva Star used in the study was not consistent. Therefore, a higher sample size is required to show the statistical differences. According to the SDS of the silver capsules of the Riva Star (SDI, 2016b), they contain 35 ~ 40 wt% AgF and 15 ~ 20 wt% ammonia.



## 9.5 Conclusions

In conclusion, the demineralisation inhibitory mechanism of topical treatment with  $\text{AgNO}_3$  on HAP discs is associated with the formation of a protective barrier composed of  $\text{Ag}_3\text{PO}_4$ , and the abrasion effects of the topical treatment (see **Fig. 9.4**). Whereas, the demineralisation inhibitory mechanism of topical treatment with  $\text{AgF}$  or  $\text{Ag}[\text{NH}_3]_2\text{F}$  on HAP discs is associated with  $\text{F}^-$  released from the topically treated HAP discs, the formation of a protective barrier composed of  $\text{Ag}_3\text{PO}_4$ ,  $\text{CaF}_2$  and FHA, and the abrasion effects of topical treatments.

The effects of topical treatment with Silver Capsule of Riva Star (3.16 M SDF, SDI Ltd, Australia) on demineralisation of HAP discs are similar to those of laboratory-prepared 3.16 M  $\text{Ag}[\text{NH}_3]_2\text{F}$ .

# Chapter 10 DOSE-RESPONSE EFFECTS OF TOPICAL TREATMENTS WITH DIFFERENT CONCENTRATIONS OF SILVER COMPOUNDS ON DEMINERALISATION OF HUMAN ENAMEL

## 10.1 Introduction

Even though numerous clinical trials have demonstrated the cariostatic efficacy of treatments with these silver compounds (Craig *et al.*, 1987; Green, 1989; Miller, 1905; Milgrom *et al.*, 2018) (Chapter 3), the inhibitory mechanisms of topical treatments with AgNO<sub>3</sub>, AgF and Ag[NH<sub>3</sub>]<sub>2</sub>F on demineralisation of human enamel still remain obscure.

Today, Ag[NH<sub>3</sub>]<sub>2</sub>F is one of the most popular topically applied silver compounds used in clinical practice and has been reported to prevent and arrest dental caries in many clinical trials (Horst *et al.*, 2016). Commercial Ag[NH<sub>3</sub>]<sub>2</sub>F products containing different concentrations are available on the market (Fung *et al.*, 2013), with 38 wt% (2.36 M) the most commonly used and 50.9 wt% (3.16 M) the highest (Horst *et al.*, 2016; SDI, 2016b). Several studies have shown that treatment with 38 wt% (2.36 M) Ag[NH<sub>3</sub>]<sub>2</sub>F is more effective than 12 wt% (0.75 M) Ag[NH<sub>3</sub>]<sub>2</sub>F in arresting dental caries (Fung *et al.*, 2016; Fung *et al.*, 2018; Yee *et al.*, 2009). However, detailed dose-response effects of a range of topical treatments with silver compounds, including AgNO<sub>3</sub>, AgF and Ag[NH<sub>3</sub>]<sub>2</sub>F, on the demineralisation of human enamel have not been carried out.

## 10.2 Aims

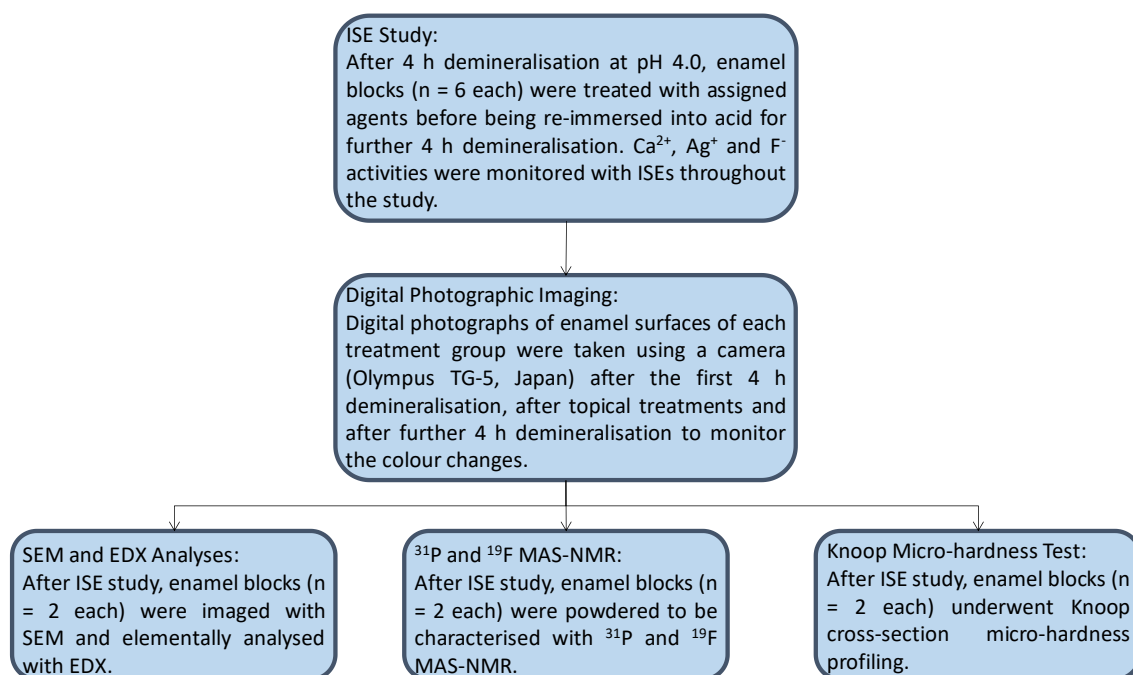
The inhibitory mechanisms of  $\text{AgNO}_3$ ,  $\text{AgF}$  and  $\text{Ag}[\text{NH}_3]_2\text{F}$ , on demineralisation of HAP discs have been discussed in Chapter 9. However, HAP discs and human enamel are different in composition and structure (Section 1.3). Therefore, the first aim of this chapter was to understand the inhibitory mechanisms of  $\text{AgNO}_3$ ,  $\text{AgF}$  and  $\text{Ag}[\text{NH}_3]_2\text{F}$  topical treatments on demineralisation of human enamel. This was achieved by investigating the effects of topical treatments with  $\text{AgNO}_3$ ,  $\text{AgF}$  and  $\text{Ag}[\text{NH}_3]_2\text{F}$  on demineralisation of human enamel, using;  $\text{Ca}^{2+}$ ,  $\text{Ag}^+$  and  $\text{F}^-$  ion selective electrodes (ISEs), digital camera, scanning electron microscopy (SEM), energy dispersive X-ray analysis (EDX),  $^{31}\text{P}$  and  $^{19}\text{F}$  MAS-NMR, and Knoop micro-hardness tester.

The second aim was to investigate the dose-response effects of topical treatments with silver compounds on the demineralisation of human enamel. This was achieved by investigating the effects of topical treatments with 0.75 M, 2.36 M and 3.16 M of  $\text{AgNO}_3$ ,  $\text{AgF}$  and  $\text{Ag}[\text{NH}_3]_2\text{F}$  on demineralisation of human enamel, also using the techniques mentioned above.

The third aim was to compare the inhibitory efficacy and the effects of topical treatment with a commercial  $\text{Ag}[\text{NH}_3]_2\text{F}$  product with laboratory-prepared  $\text{Ag}[\text{NH}_3]_2\text{F}$  on the demineralisation of human enamel. This was achieved by investigating the effects of topical treatment with the Silver Capsule of Riva Star on demineralisation of human enamel using the techniques mentioned above.

### 10.3 Materials and Methods

The protocol used in this study is shown as a flowchart in **Fig. 10.1**. Firstly, the effects of silver compounds on the demineralisation of human enamel (n = 6 each) were investigated using ISEs as described in Chapter 8. Next, enamel blocks from each treatment group underwent digital photographic imaging, SEM and EDX, MAS-NMR, and Knoop micro-hardness analyses.



**Figure 10.1** – Flowchart of the protocol of the study.

### 10.3.1 ISE Study



**Figure 10.2** – Nail-varnished human enamel blocks.

Sixty-six enamel blocks were sectioned from caries-free permanent molars (QMREC 2011/99) using a cutting machine (Struers Accutom-5, USA). Blocks were polished (300 LVAC, Kemet, UK) with carbide papers with roughness up to P4000 under copious water cooling to flatten and remove approximately 100  $\mu$  m (thickness measured with calliper) of the enamel surface. The polishing procedure was required to avoid interference from high fluoride concentration in the outermost layer of enamel, which varies between individuals (Section 1.2.1), during demineralisation. Subsequently, blocks were varnished with red nail lacquer (KIKO, Italy) to leave only a 3 mm X 4 mm window on each block exposed (**Fig 10.2**). The window sizes were standardised to control the area exposed to acid challenge. Afterwards, blocks were allocated into eleven treatment groups ( $n = 6$  each) (shown in **Table 10.1**). The demineralisation solution was made using 0.1 M  $\text{CH}_3\text{COOH}$  buffered to pH 4.0, using KOH, as described in Section 6.3.2.

Calibrations of  $\text{Ca}^{2+}$ ,  $\text{F}^-$  and  $\text{Ag}^+$  ISEs were conducted before each experiment, as described in Section 6.3.3, but at  $37 \pm 0.3$  °C (LLOD of  $\text{Ca}^{2+}$ : 0.023 mM, LLOD of  $\text{F}^-$ : 0.001 mM, LLOD of  $\text{Ag}^+$ : 0.001 mM). Further, the activity coefficient of each ion was calculated with an ionic speciation program (Chemist, MicroMath, USA) (activity coefficient of  $\text{Ca}^{2+} \approx 0.6$ ,  $\text{F}^- \approx 1$ ,  $\text{Ag}^+ \approx 1$ ).

**Table 10.1** – Compositions of treatment groups.

Group names	Compositions	*Preparation
DW Tx	De-ionised water	From Triplered Ltd (UK)
0.75 M AgNO <sub>3</sub> Tx	0.75 M AgNO <sub>3</sub>	0.26 g AgNO <sub>3</sub> + 2 mL DW
2.36 M AgNO <sub>3</sub> Tx	2.36 M AgNO <sub>3</sub>	0.80 g AgNO <sub>3</sub> + 2 mL DW
3.16 M AgNO <sub>3</sub> Tx	3.16 M AgNO <sub>3</sub>	1.07 g AgNO <sub>3</sub> + 2 mL DW
0.75 M AgF Tx	0.75 M AgF	0.20 g AgF + 2 mL DW
2.36 M AgF Tx	2.36 M AgF	0.60 g AgF + 2 mL DW
3.16 M AgF Tx	3.16 M AgF	0.80 g AgF + 2 mL DW
0.75 M Ag[NH <sub>3</sub> ] <sub>2</sub> F Tx	0.75 M SDF	0.20 g AgF + 1 mL DW + 1 mL 30 wt% NH <sub>4</sub> OH
2.36 M Ag[NH <sub>3</sub> ] <sub>2</sub> F Tx	2.36 M SDF	0.60 g AgF + 1 mL DW + 1 mL 30 wt% NH <sub>4</sub> OH
3.16 M Ag[NH <sub>3</sub> ] <sub>2</sub> F Tx	3.16 M SDF	0.80 g AgF + 1 mL DW + 1 mL 30 wt% NH <sub>4</sub> OH
Riva-SC Tx	Silver Capsule (3.16 M)	From Riva Star of SDI Ltd (Australia)

\* = all chemicals shown in preparation are from Sigma-Aldrich, UK

The setup and the protocol of the ISE study was the same as described in Section 8.3.1. Firstly, each varnished enamel block was immersed in 50 mL of demineralisation solution at  $37 \pm 0.3$  °C for 4 h using a temperature stabilised stirrer (Stuart UC152D/KIT, UK), and Ca<sup>2+</sup>, Ag<sup>+</sup> and F<sup>-</sup> ISEs were used to simultaneously monitor the activities of Ca<sup>2+</sup>, Ag<sup>+</sup> and F<sup>-</sup> at intervals of 1 min as demineralisation progressed. Thereafter, each demineralised enamel block was taken out, rinsed, air-dried and topically treated for 1 min with assigned application agent using a micro-brush (Centrix, USA), followed by air-drying (Crystal and Niederman, 2016). Each enamel block was then demineralised again for a further 4 h, and all the ion activities were further monitored at 1 min intervals as before.

Finally, the activity of Ca<sup>2+</sup> (mM) was plotted as a function of time (h) for each group, and the percentage reduction in the rate of calcium loss from enamel (PRCL<sub>enamel</sub>) for each application was calculated, as described in Section 6.3.4. The activities of F<sup>-</sup> and Ag<sup>+</sup> were similarly plotted as a function of time.

### 10.3.2 Digital Photographs

Digital photographs of enamel surfaces in each treatment group were taken using a digital camera (Olympus TG-5, Japan) after the first 4 h demineralisation, after topical treatments and after further 4 h demineralisation, in order to monitor the colour changes at each step.

### 10.3.3 SEM and EDX Analyses

After the ISE study, experimented enamel blocks from each treatment group of ISE study (n = 2 each) were carbon-coated to be imaged with SEM and elementally analysed with EDX. SEM (FEI Inspect-F, USA) was operated at a high voltage of 5.00 kV and 5000 X magnification. Both SEM imaging and EDX analysis were conducted in the middle areas of the exposed windows to avoid the interference from the varnish.

### 10.3.4 $^{31}\text{P}$ and $^{19}\text{F}$ MAS-NMR Analyses

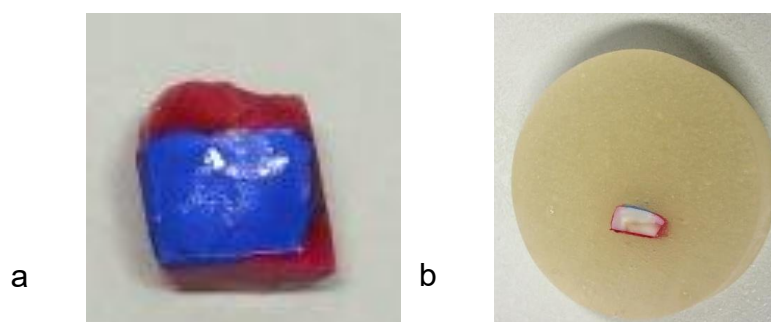
The varnished areas of the experimented enamel blocks were removed using a micro-motor handpiece (SAESHIN, USA), in order to avoid any interference from varnish chemicals during the MAS-NMR analysis. After removal of the nail varnished areas, experimented enamel blocks from each treatment group of ISE study (n = 2 each) were ground with a grinding machine (Glen Creston Ltd, UK) for 30 s with a frequency of 30/s into powders (weight = 0.1 g).

The enamel powders were then analysed with  $^{31}\text{P}$  MAS-NMR and  $^{19}\text{F}$  MAS-NMR (600 MHz Bruker, Coventry, UK). Solid-state  $^{31}\text{P}$  MAS-NMR analysis was carried out using a 14.1 Tesla spectrometer at a Larmor frequency of 242.94 Mega-hertz (MHz) for a 4 h scan with a recycle delay of 1 min. Solid-state  $^{19}\text{F}$  MAS-NMR analysis was carried out using a 14.1 Tesla spectrometer at a Larmor

frequency of 564.66 MHz for a 20 h scan with a recycle delay of 30 s. All spectra were obtained under magic angle spinning conditions of 20 kHz.

### 10.3.5 Knoop Micro-Hardness Analysis

Experimented enamel blocks from each treatment group of ISE study (n = 2 each) were varnished with blue nail lacquer (KIKO, Italy) to highlight and protect the window areas (**Fig. 10.3a**) during embedding of the block into acrylic resin (Kemdent, UK). Next, half of each enamel blocks were removed by polishing with carbide papers with roughness up to P4000 under copious water cooling in order to expose the middle area of each enamel cross-sections (**Fig. 10.3b**).



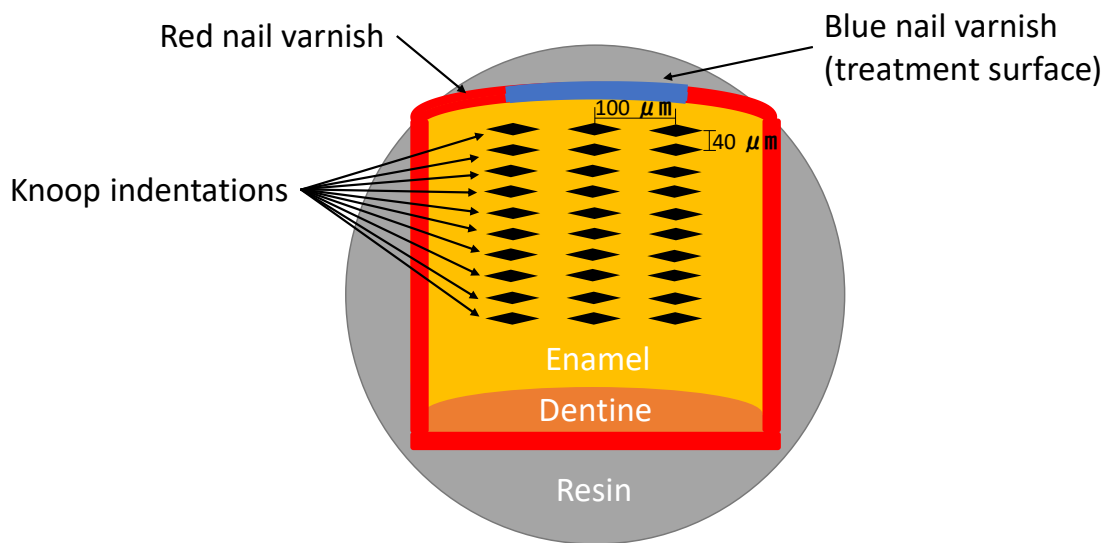
**Figure 10.3** – (a) Demineralised lesion of enamel block varnished with blue nail lacquer. (b) Resin-embedded block for micro-hardness test.

Before carrying out Knoop hardness indentation, microscopic photographs (40 X) were taken by attaching a digital camera (Olympus TG-5, Japan) to the eyepiece of the Knoop hardness tester to compare the appearances of enamel lesion treated with different topical application agents.

Next, the embedded enamel blocks then underwent Knoop cross-sectional micro-hardness profiling (CSMH) using a Knoop micro-hardness tester (MicroMet 4, UK). Each indentation was conducted with a load of 50 gf for 15 s, as suggested by Craig and Peyton (1958). The micro-hardness of the enamel was determined at 10 adjacent sites at increments of 40  $\mu\text{m}$  from the centre of the



blue nail varnished lesion surface toward dentine (**Fig. 10.4**). Three sets of indentations were carried out on each block at the same depth 100  $\mu\text{m}$  apart (as shown in **Fig. 10.4**). The median values of the three sets of indentations conducted at the same depth level on each block were then recorded, as described by Chu and Lo (2008). Finally, the averaged values from the two enamel blocks in each treatment group were collected.

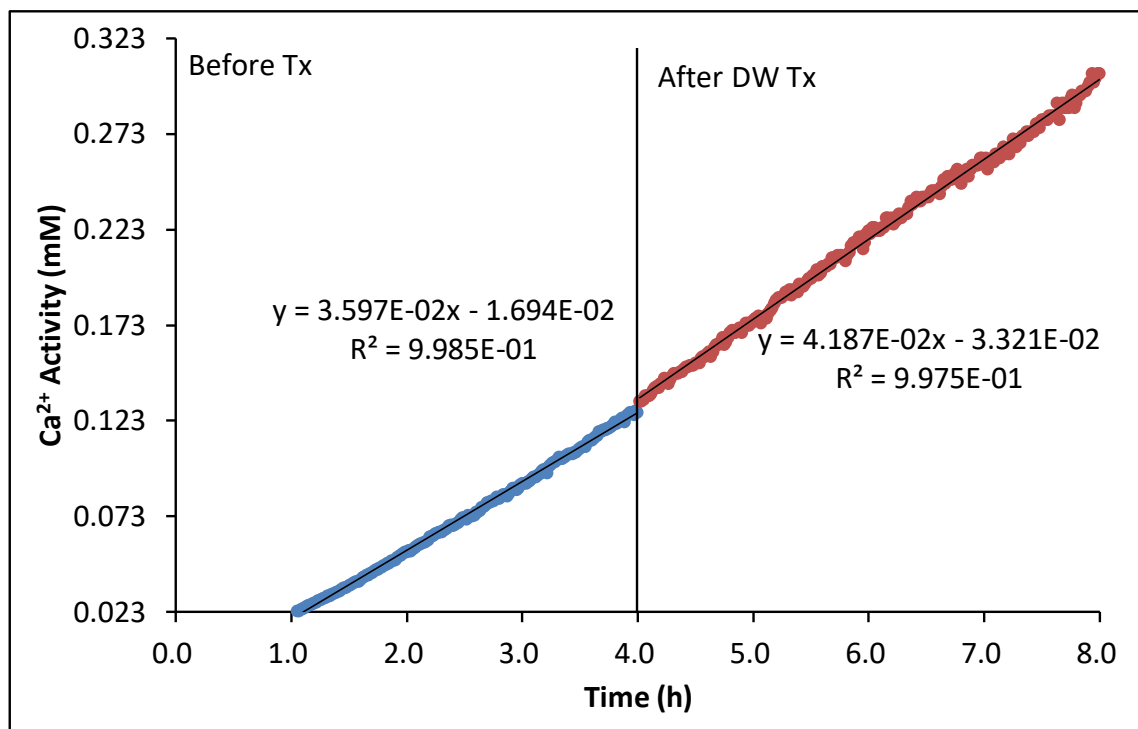


**Figure 10.4** – Schematic representation of Knoop CSMH.

## 10.4 Results

### 10.4.1 Ca<sup>2+</sup> ISE Study

**Fig. 10.5** shows a typical plot of Ca<sup>2+</sup> release from an enamel block of the DW treatment group. The Ca<sup>2+</sup> release was linear with time both before and after treatment. The rate of Ca<sup>2+</sup> release was increased following the DW treatment (**Table 10.2**). All six enamel blocks of the DW treatment group showed a similar linear Ca<sup>2+</sup> release, both before and after treatments, and a similar increase in the rate of Ca<sup>2+</sup> release following treatments. Errors of gradients were calculated using SigmaPlot 10.0 (Systat Software, California, USA).



**Figure 10.5** - Typical Ca<sup>2+</sup> release of DW treatment group.

**Table 10.2** – The  $RCL_{enamel}$  before and after DW topical treatment of the **Fig. 10.5**.

Treatment	$R_b \pm SE$ (X 10 <sup>-3</sup> mM/h)	$R_a \pm SE$ (X 10 <sup>-3</sup> mM/h)	p value
DW Tx	35.97 ± 0.10	41.87 ± 0.10	< 0.01

**Fig. 10.6** shows a typical plot of  $\text{Ca}^{2+}$  release from an enamel block of the 0.75 M  $\text{AgNO}_3$  treatment group. The  $\text{Ca}^{2+}$  release was linear with time both before and after treatment. The rate of  $\text{Ca}^{2+}$  release was decreased following the 0.75 M  $\text{AgNO}_3$  treatment (**Table 10.3**). All six enamel blocks of the 0.75 M  $\text{AgNO}_3$  treatment group showed a similar linear  $\text{Ca}^{2+}$  release, both before and after treatments, and a similar reduction in the rate of  $\text{Ca}^{2+}$  release following treatments.

**Fig. 10.7** and **Fig. 10.8** show typical plots of  $\text{Ca}^{2+}$  release from the enamel blocks of the 2.36 M and 3.16 M  $\text{AgNO}_3$  treatment groups. The  $\text{Ca}^{2+}$  release was also linear with time both before and after treatments. However, the reduction in the rates of  $\text{Ca}^{2+}$  release decreased with increasing concentration of  $\text{AgNO}_3$  (**Table 10.3**).

**Table 10.3** - The  $RCL_{\text{enamel}}$  before and after  $\text{AgNO}_3$  topical treatments of the **Fig. 10.6 ~ 10.8**.

Treatment	$R_b \pm \text{SE}$ ( $\times 10^{-3}$ mM/h)	$R_a \pm \text{SE}$ ( $\times 10^{-3}$ mM/h)	p value
0.75 M $\text{AgNO}_3$ Tx	$21.64 \pm 0.10$	$16.97 \pm 0.09$	< 0.01
2.36 M $\text{AgNO}_3$ Tx	$34.33 \pm 0.10$	$34.57 \pm 0.30$	< 0.01
3.16 M $\text{AgNO}_3$ Tx	$33.24 \pm 0.10$	$33.54 \pm 0.20$	< 0.01

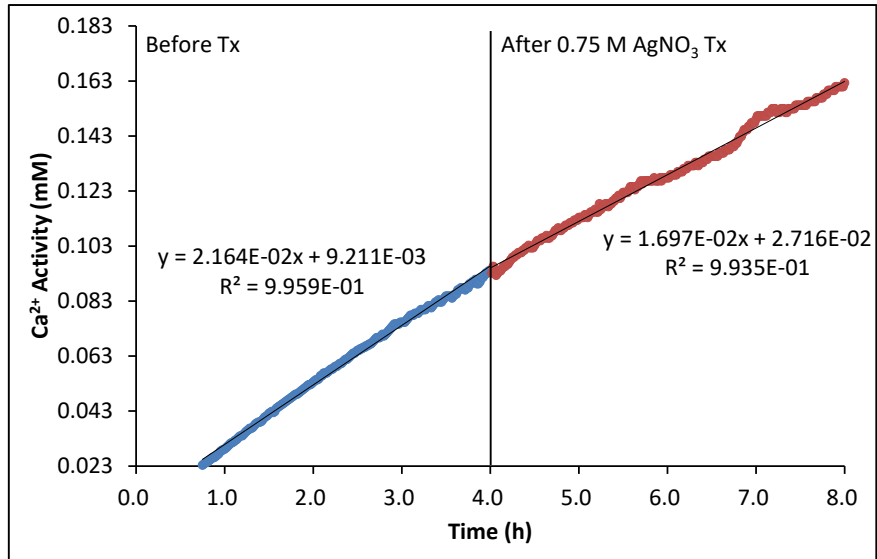


Figure 10.6 - Typical  $\text{Ca}^{2+}$  release of 0.75 M  $\text{AgNO}_3$  treatment group.

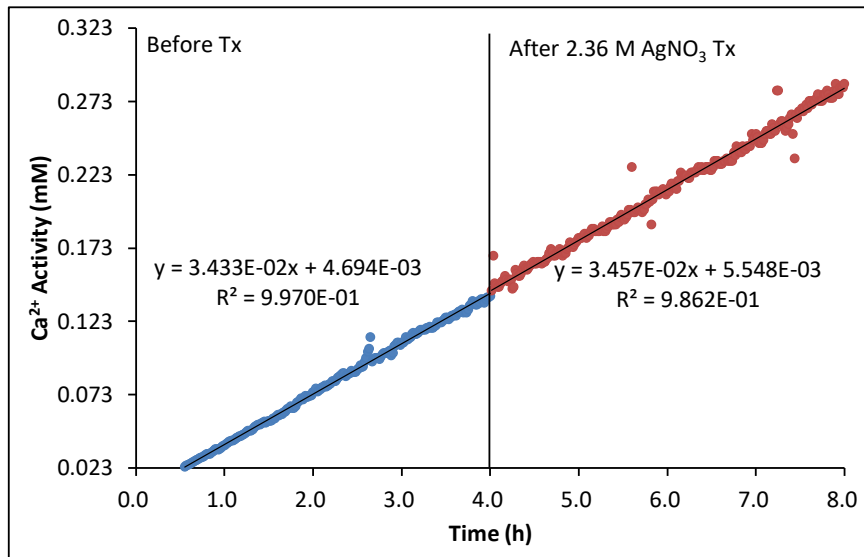


Figure 10.7 - Typical  $\text{Ca}^{2+}$  release of 2.36 M  $\text{AgNO}_3$  treatment group.

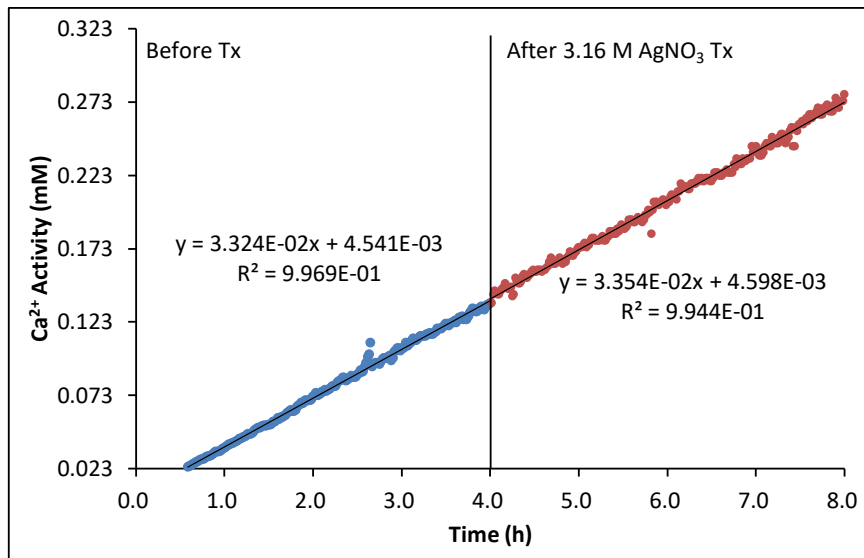


Figure 10.8 - Typical  $\text{Ca}^{2+}$  release of 3.16 M  $\text{AgNO}_3$  treatment group.

**Fig. 10.9** shows a typical plot of  $\text{Ca}^{2+}$  release from an enamel block of the 0.75 M AgF treatment group. The  $\text{Ca}^{2+}$  release was linear with time both before and after treatment. The rate of  $\text{Ca}^{2+}$  release was decreased following the 0.75 M AgF treatment (**Table 10.4**). All six enamel blocks of the 0.75 M AgF treatment group showed a similar linear  $\text{Ca}^{2+}$  release, both before and after treatments, and a similar reduction in the rate of  $\text{Ca}^{2+}$  release following treatments.

**Fig. 10.10** and **Fig. 10.11** show typical plots of  $\text{Ca}^{2+}$  release from the enamel blocks of the 2.36 M and 3.16 M AgF treatment groups, The  $\text{Ca}^{2+}$  release was also linear with time both before and after treatments. Further, the reduction in the rates of  $\text{Ca}^{2+}$  increased with increasing concentration of AgF (**Table 10.4**).

**Table 10.4** - The  $RCL_{\text{enamel}}$  before and after AgF topical treatments of the **Fig. 10.9 ~ 10.11**.

Treatment	$R_b \pm \text{SE}$ ( $\times 10^{-3}$ mM/h)	$R_a \pm \text{SE}$ ( $\times 10^{-3}$ mM/h)	p value
0.75 M AgF Tx	$29.69 \pm 0.08$	$13.34 \pm 0.05$	< 0.01
2.36 M AgF Tx	$33.89 \pm 0.10$	$12.01 \pm 0.10$	< 0.01
3.16 M AgF Tx	$24.97 \pm 0.07$	$5.34 \pm 0.04$	< 0.01

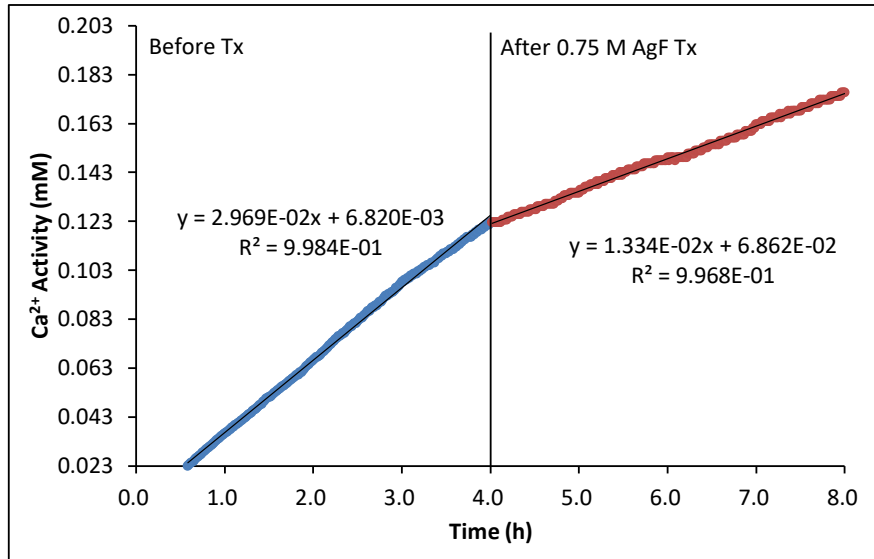


Figure 10.9 - Typical Ca<sup>2+</sup> release of 0.75 M AgF treatment group.

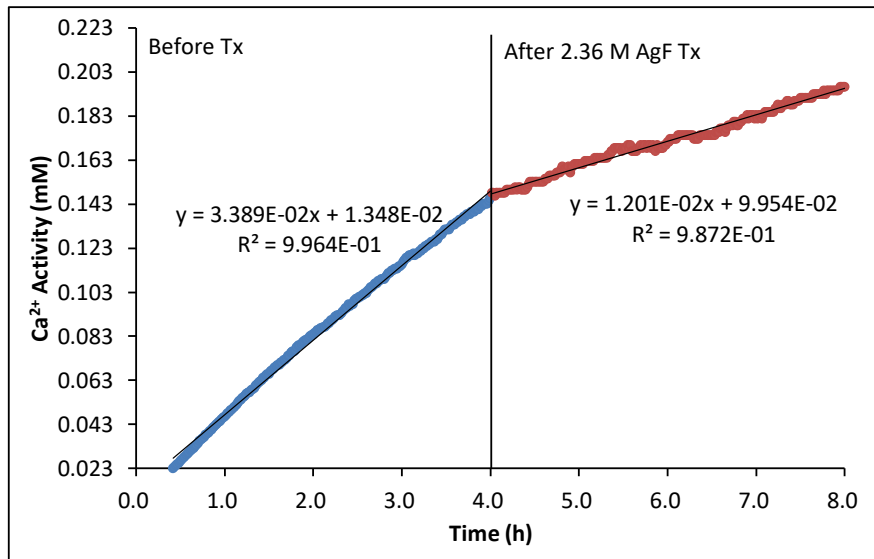


Figure 10.10 - Typical Ca<sup>2+</sup> release of 2.36 M AgF treatment group.

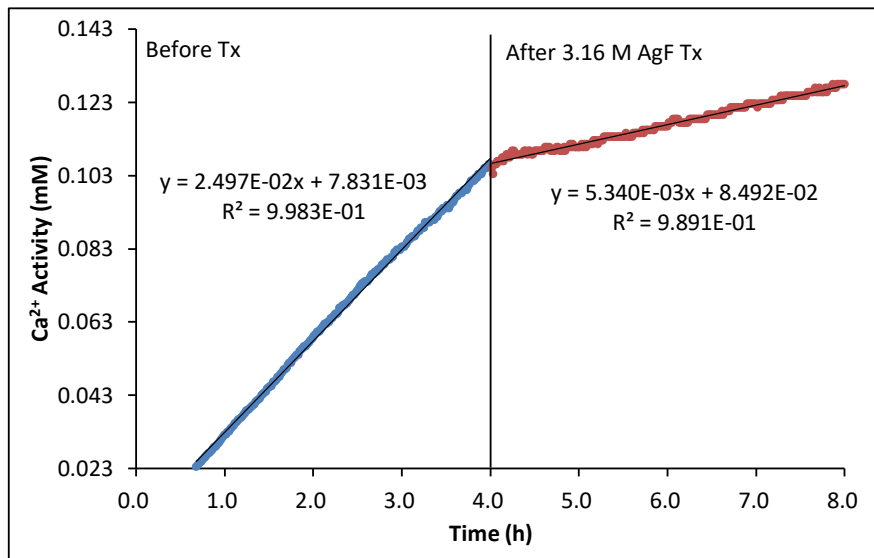


Figure 10.11 - Typical Ca<sup>2+</sup> release of 3.16 M AgF treatment group.

**Fig. 10.12** shows a typical plot of  $\text{Ca}^{2+}$  release from an enamel block of the 0.75 M  $\text{Ag}[\text{NH}_3]_2\text{F}$  treatment group. The  $\text{Ca}^{2+}$  release was linear with time both before and after treatment. The rate of  $\text{Ca}^{2+}$  release was decreased following the 0.75 M  $\text{Ag}[\text{NH}_3]_2\text{F}$  treatment (**Table 10.5**). All six enamel blocks of the 0.75 M  $\text{Ag}[\text{NH}_3]_2\text{F}$  treatment group showed a similar linear  $\text{Ca}^{2+}$  release, both before and after treatments, and a similar reduction in the rate of  $\text{Ca}^{2+}$  release following treatments.

**Fig. 10.13** and **Fig. 10.14** show typical plots of  $\text{Ca}^{2+}$  release from the enamel blocks of the 2.36 M and 3.16 M  $\text{Ag}[\text{NH}_3]_2\text{F}$  treatment groups. The  $\text{Ca}^{2+}$  release was also linear with time both before and after treatments. Further, the reduction in the rates of  $\text{Ca}^{2+}$  increased with increasing concentration of  $\text{Ag}[\text{NH}_3]_2\text{F}$  (**Table 10.5**).

**Table 10.5** - The  $RCL_{\text{enamel}}$  before and after  $\text{Ag}[\text{NH}_3]_2\text{F}$  topical treatments of the **Fig. 10.12 ~ 10.14**.

Treatment	$R_b \pm \text{SE}$ ( $\times 10^{-3}$ mM/h)	$R_a \pm \text{SE}$ ( $\times 10^{-3}$ mM/h)	$p$ value
0.75 M $\text{Ag}[\text{NH}_3]_2\text{F}$ Tx	$36.02 \pm 0.10$	$23.94 \pm 0.10$	< 0.01
2.36 M $\text{Ag}[\text{NH}_3]_2\text{F}$ Tx	$31.29 \pm 0.10$	$15.48 \pm 0.10$	< 0.01
3.16 M $\text{Ag}[\text{NH}_3]_2\text{F}$ Tx	$46.44 \pm 0.10$	$18.01 \pm 0.20$	< 0.01

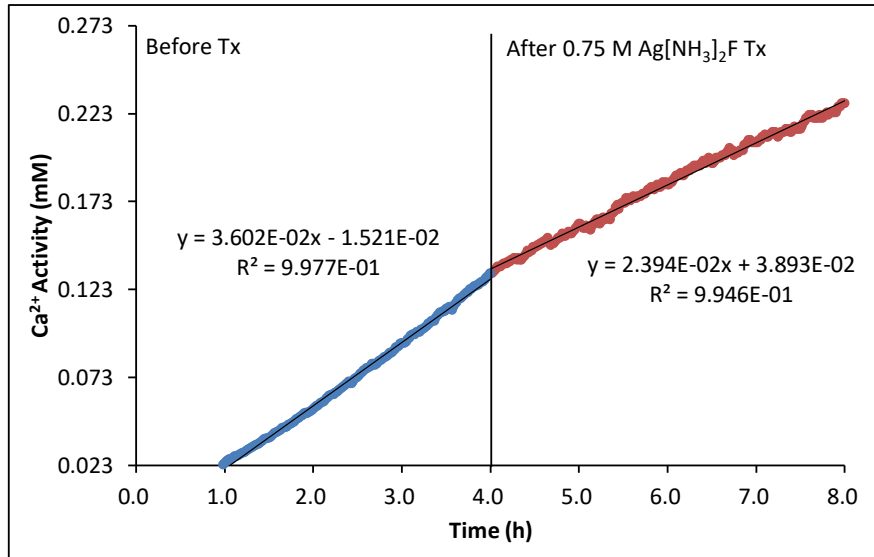


Figure 10.12 - Typical  $\text{Ca}^{2+}$  release of 0.75 M  $\text{Ag}[\text{NH}_3]_2\text{F}$  treatment group.

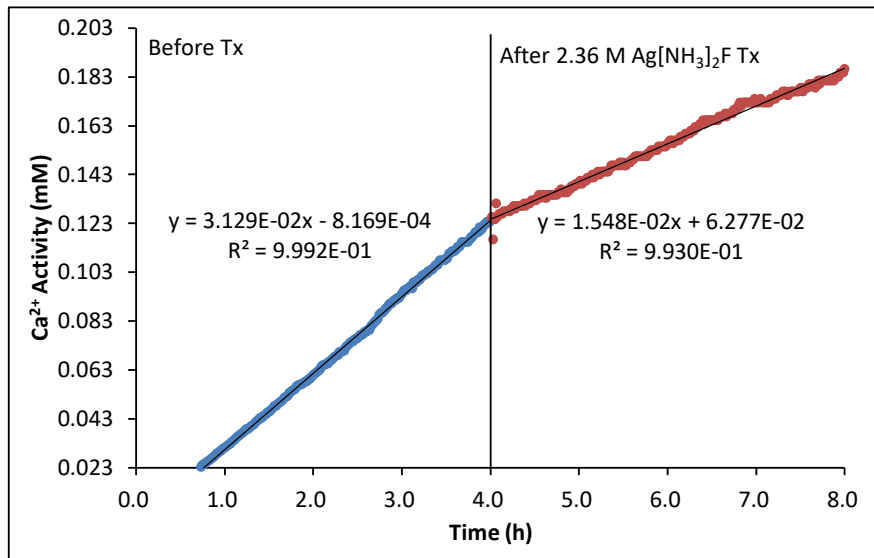


Figure 10.13 - Typical  $\text{Ca}^{2+}$  release of 2.36 M  $\text{Ag}[\text{NH}_3]_2\text{F}$  treatment group.

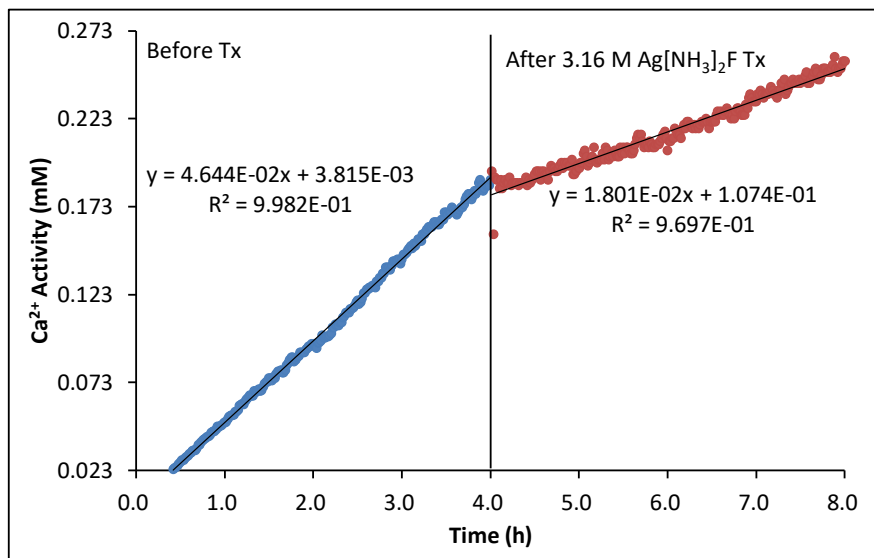
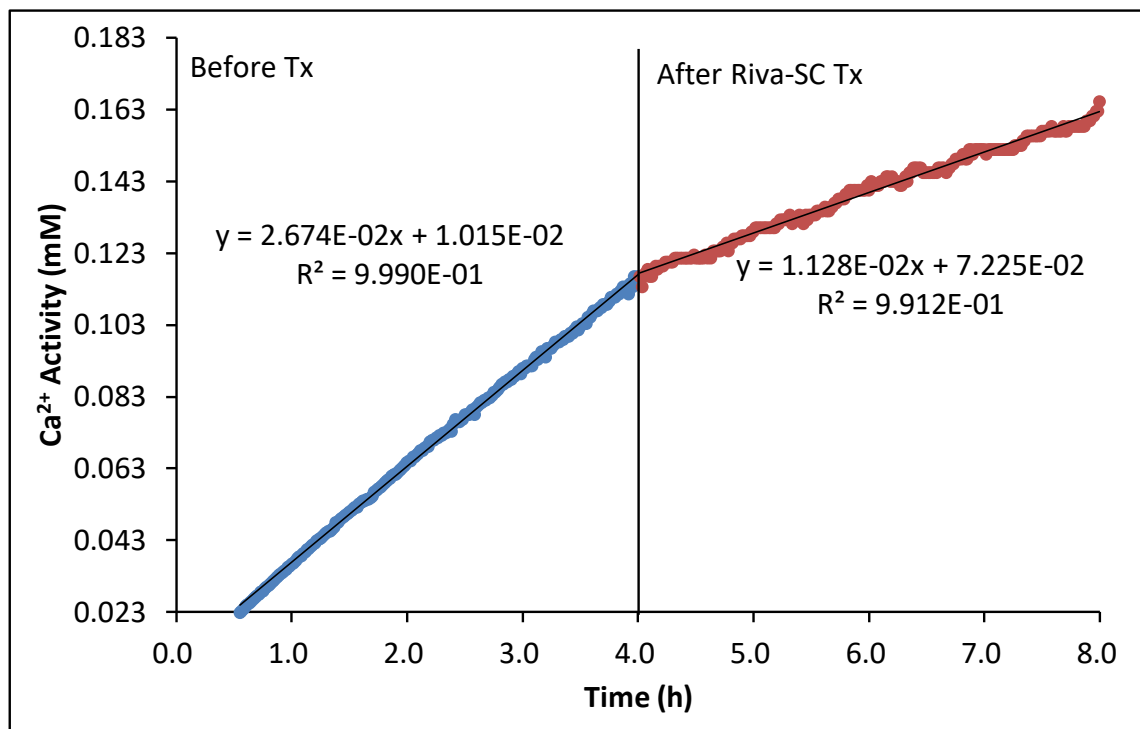


Figure 10.14 - Typical  $\text{Ca}^{2+}$  release of 3.16 M  $\text{Ag}[\text{NH}_3]_2\text{F}$  treatment group.



**Fig. 10.15** shows a typical plot of  $\text{Ca}^{2+}$  release from the enamel block of the Riva-SC treatment group. The  $\text{Ca}^{2+}$  release was linear with time both before and after treatment. The rate of  $\text{Ca}^{2+}$  release was decreased following the Riva-SC treatment (**Table 10.6**). All six enamel blocks of the Riva-SC treatment group showed a similar linear  $\text{Ca}^{2+}$  release, both before and after treatments, and a similar reduction in the rate of  $\text{Ca}^{2+}$  release following treatments.



**Figure 10.15** – Typical  $\text{Ca}^{2+}$  release of Riva-SC treatment group.

**Table 10.6** - The  $\text{RCL}_{\text{enamel}}$  before and after Riva-SC topical treatment of the **Fig. 10.15**.

Treatment	$R_b \pm \text{SE}$ ( $\times 10^{-3}$ mM/h)	$R_a \pm \text{SE}$ ( $\times 10^{-3}$ mM/h)	p value
Riva-SC Tx	$26.74 \pm 0.10$	$11.28 \pm 0.10$	$< 0.01$

#### 10.4.1.1 Summary of the Ca<sup>2+</sup> Release from the Enamel Blocks of Each Treatment Group

**Table 10.7** shows the rates of calcium loss of enamel ( $R_{CL_{enamel}}$ ) before and after treatments, and the percentages reduction in the rates of calcium loss of enamel ( $PR_{CL_{enamel}}$ ) of every enamel in all treatment groups. Every  $R_a$  ( $R_{CL_{enamel}}$ ) measured was significantly different ( $p < 0.05$ ) from the  $R_b$  ( $R_{CL_{enamel}}$ ) of the same enamel block.

The mean  $R_{CL_{enamel}}$  before treatments of all treatment groups were similar ( $\approx 0.030$  mM/h), whereas, the mean  $R_{CL_{enamel}}$  following treatments were different. The mean  $R_{CL_{enamel}}$  following topical treatments with fluoride-containing silver compounds like AgF, Ag[NH<sub>3</sub>]<sub>2</sub>F and Riva-SC, were much lower than those following topical treatments with AgNO<sub>3</sub> and DW. Further, the  $PR_{CL_{enamel}}$  of AgF and Ag[NH<sub>3</sub>]<sub>2</sub>F treatment groups increased with increasing concentrations, whereas, the  $PR_{CL_{enamel}}$  of AgNO<sub>3</sub> treatment group decreased with increasing concentration.

Only in the DW treatment group, the mean  $R_{CL_{enamel}}$  following treatments ( $R_a$ ) was faster than the mean  $R_{CL_{enamel}}$  before treatments ( $R_b$ ).

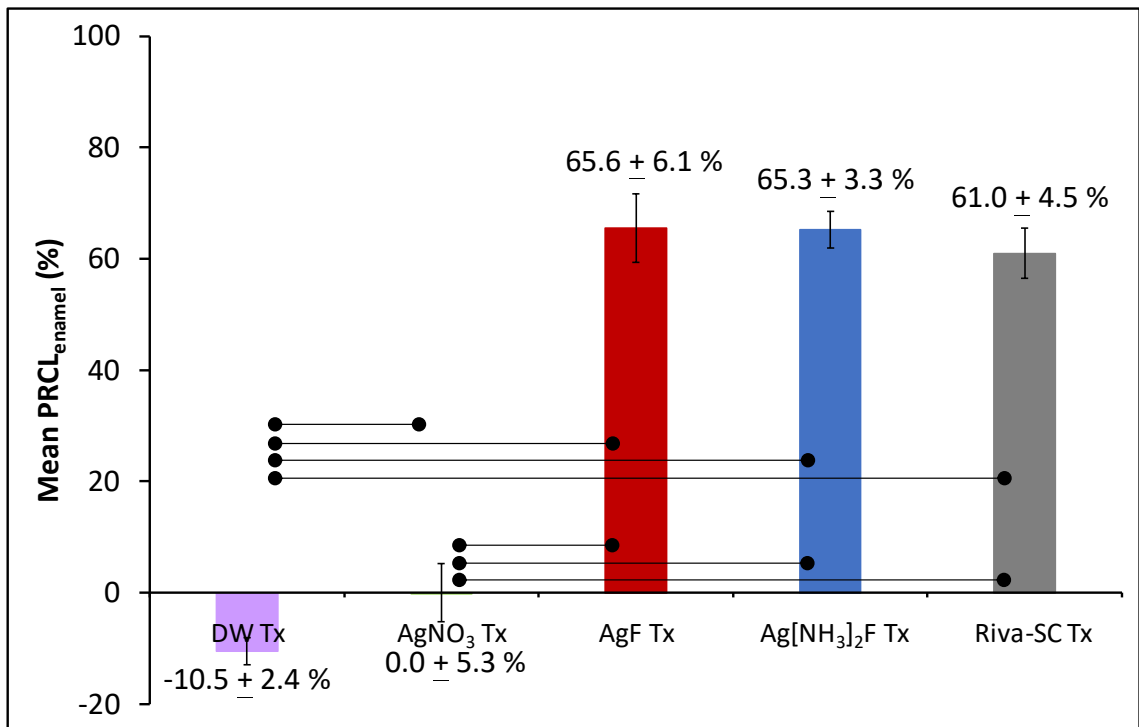
**Table 10.7 - The  $RCL_{enamel}$  and  $PRCL_{enamel}$  of every Enamel in each treatment group.**

Tx Group	Enamel	$R_b \pm SE$ ( $\times 10^{-3}$ mM/h)	$R_a \pm SE$ ( $\times 10^{-3}$ mM/h)	$PRCL_{enamel}$ (%)
DW Tx	1	21.65 $\pm$ 0.20	22.16 $\pm$ 0.10	-2.4
	2	35.97 $\pm$ 0.10	41.87 $\pm$ 0.10	-16.4
	3	34.43 $\pm$ 0.20	38.80 $\pm$ 0.20	-12.7
	4	46.69 $\pm$ 0.20	51.09 $\pm$ 0.10	-9.4
	5	29.10 $\pm$ 0.20	30.69 $\pm$ 0.10	-5.5
	6	20.13 $\pm$ 0.10	23.49 $\pm$ 0.10	-16.7
	Average	31.33 $\pm$ 4.05	34.68 $\pm$ 4.60	-10.5 $\pm$ 2.4
0.75 M AgNO <sub>3</sub> Tx	1	33.18 $\pm$ 0.20	22.32 $\pm$ 0.10	32.7
	2	33.91 $\pm$ 0.02	27.78 $\pm$ 0.20	18.1
	3	21.64 $\pm$ 0.10	16.97 $\pm$ 0.09	21.6
	4	46.20 $\pm$ 0.20	41.95 $\pm$ 0.10	9.2
	5	11.92 $\pm$ 0.20	8.92 $\pm$ 0.10	25.2
	6	14.12 $\pm$ 0.10	10.60 $\pm$ 0.10	24.9
	Average	26.83 $\pm$ 5.41	21.42 $\pm$ 5.02	21.9 $\pm$ 3.2
2.36 M AgNO <sub>3</sub> Tx	1	40.99 $\pm$ 0.40	31.20 $\pm$ 0.50	23.9
	2	21.51 $\pm$ 0.20	22.79 $\pm$ 0.20	-6.0
	3	19.13 $\pm$ 0.10	14.93 $\pm$ 0.10	22.0
	4	34.33 $\pm$ 0.10	34.57 $\pm$ 0.30	-0.7
	5	28.00 $\pm$ 0.10	30.43 $\pm$ 0.10	-8.7
	6	31.58 $\pm$ 0.10	32.56 $\pm$ 0.30	-3.1
	Average	29.26 $\pm$ 3.33	27.74 $\pm$ 3.04	4.6 $\pm$ 5.9
3.16 M AgNO <sub>3</sub> Tx	1	25.92 $\pm$ 0.10	28.83 $\pm$ 0.30	-11.2
	2	28.39 $\pm$ 0.10	31.12 $\pm$ 0.30	-9.6
	3	43.16 $\pm$ 0.20	32.64 $\pm$ 0.20	24.4
	4	39.34 $\pm$ 0.20	40.99 $\pm$ 0.30	-4.2
	5	38.20 $\pm$ 0.10	37.62 $\pm$ 0.20	1.5
	6	33.24 $\pm$ 0.10	33.54 $\pm$ 0.20	-0.9
	Average	34.71 $\pm$ 2.74	34.12 $\pm$ 1.82	0.0 $\pm$ 5.3
0.75 M AgF Tx	1	29.69 $\pm$ 0.08	13.34 $\pm$ 0.05	55.1
	2	50.55 $\pm$ 0.10	39.52 $\pm$ 0.10	21.8
	3	21.34 $\pm$ 0.01	8.43 $\pm$ 0.10	60.5
	4	19.57 $\pm$ 0.01	9.41 $\pm$ 0.10	51.9
	5	42.16 $\pm$ 0.10	21.95 $\pm$ 0.10	47.9
	6	20.33 $\pm$ 0.10	11.71 $\pm$ 0.20	42.4
	Average	30.61 $\pm$ 5.31	17.39 $\pm$ 4.84	46.6 $\pm$ 5.6
2.36 M AgF Tx	1	33.89 $\pm$ 0.10	12.01 $\pm$ 0.10	64.6
	2	34.10 $\pm$ 0.10	19.23 $\pm$ 0.10	43.7
	3	24.19 $\pm$ 0.10	8.60 $\pm$ 0.10	64.4
	4	25.20 $\pm$ 0.20	4.72 $\pm$ 0.10	81.3
	5	15.01 $\pm$ 0.10	7.53 $\pm$ 0.10	49.8
	6	35.77 $\pm$ 0.10	13.04 $\pm$ 0.10	63.5
	Average	28.03 $\pm$ 3.28	10.86 $\pm$ 2.08	61.2 $\pm$ 5.4
3.16 M AgF Tx	1	44.57 $\pm$ 0.20	11.04 $\pm$ 0.20	75.2
	2	25.14 $\pm$ 0.10	5.82 $\pm$ 0.21	76.8
	3	52.56 $\pm$ 0.11	24.84 $\pm$ 0.10	52.7
	4	24.97 $\pm$ 0.07	5.34 $\pm$ 0.04	78.6
	5	33.86 $\pm$ 0.10	10.82 $\pm$ 0.12	68.0
	6	41.03 $\pm$ 0.10	23.87 $\pm$ 0.20	41.8
	Average	37.02 $\pm$ 4.51	13.62 $\pm$ 3.54	65.6 $\pm$ 6.1

Table 10.7 continued.

Tx Group	Enamel	$R_b \pm SE$ ( $\times 10^{-3}$ mM/h)	$R_a \pm SE$ ( $\times 10^{-3}$ mM/h)	PRCL <sub>enamel</sub> (%)
0.75 M Ag[NH <sub>3</sub> ] <sub>2</sub> F Tx	1	36.02 $\pm$ 0.10	23.94 $\pm$ 0.10	33.5
	2	55.34 $\pm$ 0.21	32.87 $\pm$ 0.30	40.6
	3	38.17 $\pm$ 0.30	23.85 $\pm$ 0.60	37.5
	4	21.52 $\pm$ 0.20	11.25 $\pm$ 0.10	47.7
	5	23.24 $\pm$ 0.30	13.29 $\pm$ 0.30	42.8
	6	29.00 $\pm$ 0.30	12.28 $\pm$ 0.20	57.7
	Average	33.88 $\pm$ 5.07	19.58 $\pm$ 3.54	43.3 $\pm$ 3.5
2.36 M Ag[NH <sub>3</sub> ] <sub>2</sub> F Tx	1	47.68 $\pm$ 0.10	25.53 $\pm$ 0.30	46.5
	2	29.82 $\pm$ 0.10	8.73 $\pm$ 0.20	70.7
	3	20.93 $\pm$ 0.10	5.29 $\pm$ 0.10	74.7
	4	18.64 $\pm$ 0.10	7.53 $\pm$ 0.10	59.6
	5	31.29 $\pm$ 0.10	15.48 $\pm$ 0.10	50.5
	6	32.78 $\pm$ 0.10	12.04 $\pm$ 0.40	63.3
	Average	30.19 $\pm$ 4.22	12.43 $\pm$ 3.00	60.9 $\pm$ 4.5
3.16 M Ag[NH <sub>3</sub> ] <sub>2</sub> F Tx	1	20.82 $\pm$ 0.10	9.31 $\pm$ 0.20	55.3
	2	42.52 $\pm$ 0.20	15.20 $\pm$ 0.20	64.3
	3	17.54 $\pm$ 0.10	4.10 $\pm$ 0.20	76.6
	4	26.80 $\pm$ 0.20	7.29 $\pm$ 0.10	72.8
	5	46.44 $\pm$ 0.10	18.01 $\pm$ 0.20	61.2
	6	32.82 $\pm$ 0.10	12.69 $\pm$ 0.10	61.3
	Average	31.16 $\pm$ 4.75	11.10 $\pm$ 2.11	65.3 $\pm$ 3.3
Riva-SC Tx	1	17.08 $\pm$ 0.10	5.40 $\pm$ 0.10	68.4
	2	45.50 $\pm$ 0.20	18.25 $\pm$ 0.20	59.9
	3	35.26 $\pm$ 0.20	20.74 $\pm$ 0.20	41.2
	4	26.74 $\pm$ 0.10	11.28 $\pm$ 0.10	57.8
	5	23.81 $\pm$ 0.10	7.03 $\pm$ 0.20	70.5
	6	41.89 $\pm$ 0.20	13.31 $\pm$ 0.10	68.2
	Average	31.71 $\pm$ 4.50	12.67 $\pm$ 2.47	61.0 $\pm$ 4.5

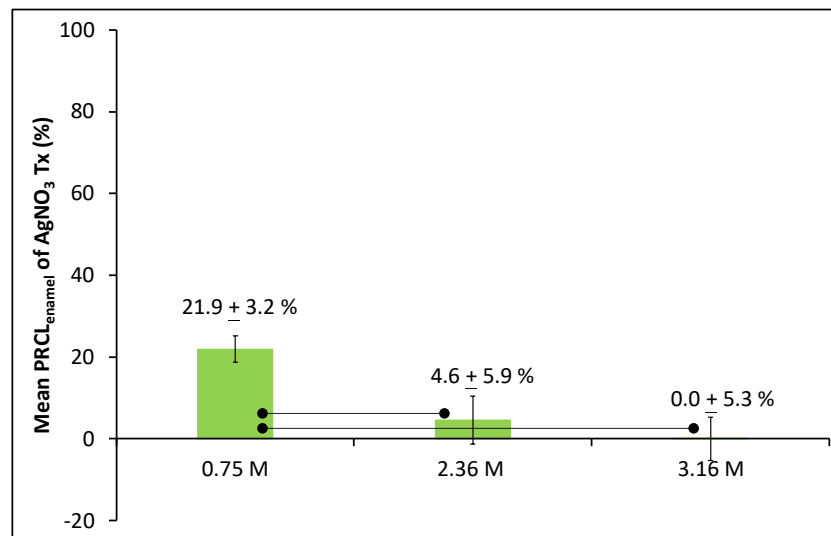
**Fig. 10.16** shows the mean  $PRCL_{enamel}$  of 3.16 M  $AgNO_3$ , 3.16 M  $AgF$ , 3.16 M  $Ag[NH_3]_2F$ , Riva-SC and DW treatment groups. The mean  $PRCL_{enamel}$  of 3.16 M  $AgF$ , 3.16 M  $Ag[NH_3]_2F$  and Riva-SC treatment groups were much higher than those of 3.16 M  $AgNO_3$  treatment group, while the mean  $PRCL_{enamel}$  of DW treatment group was negative. There were no significant differences between the mean  $PRCL_{enamel}$  of  $AgF$ ,  $Ag[NH_3]_2F$  and Riva-SC treatment groups.



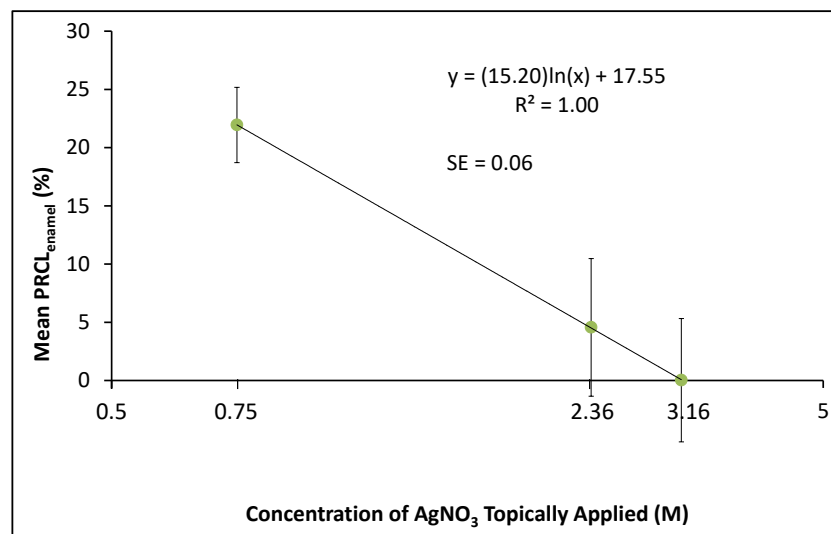
**Figure 10.16** - The mean  $PRCL_{enamel}$  of 3.16 M  $AgNO_3$ , 3.16 M  $AgF$ , 3.16 M  $Ag[NH_3]_2F$ , Riva-SC and DW treatment groups. Error bars show the standard errors. Linking lines between treatment groups indicate significant differences at  $p < 0.05$  between them.

**Fig. 10.17** shows the mean PRCL<sub>enamel</sub> of 0.75 M, 2.36 M and 3.16 M AgNO<sub>3</sub> treatment groups. The mean PRCL<sub>enamel</sub> of AgNO<sub>3</sub> treatment groups decreased with increasing concentration of AgNO<sub>3</sub>. However, there was no significant difference between the mean PRCL<sub>enamel</sub> of 2.36 M and 3.16 M AgNO<sub>3</sub> treatment groups.

**Fig. 10.18** shows that there was a log-linear dose-response relationship between the mean PRCL<sub>enamel</sub> of topical treatment with AgNO<sub>3</sub> and the concentration of topically applied AgNO<sub>3</sub>.



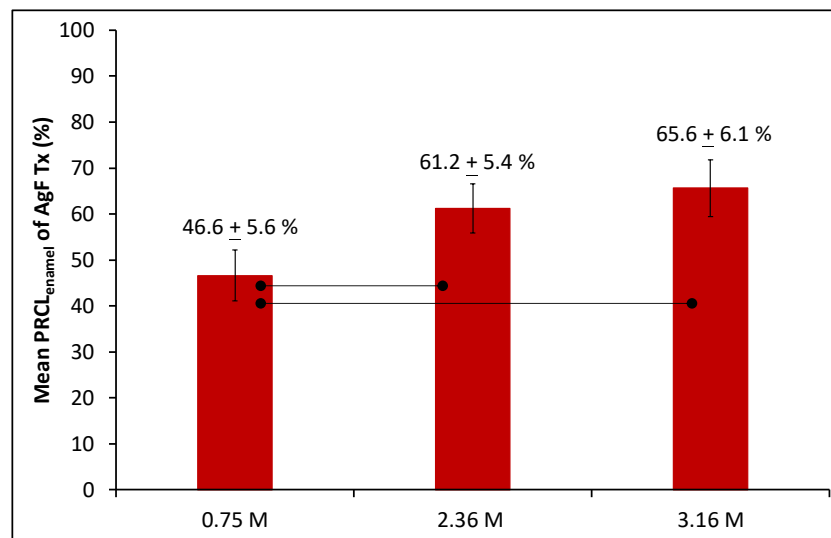
**Figure 10.17** – The mean PRCL<sub>enamel</sub> of 0.75 M, 2.36 M and 3.16 M AgNO<sub>3</sub> treatment groups.



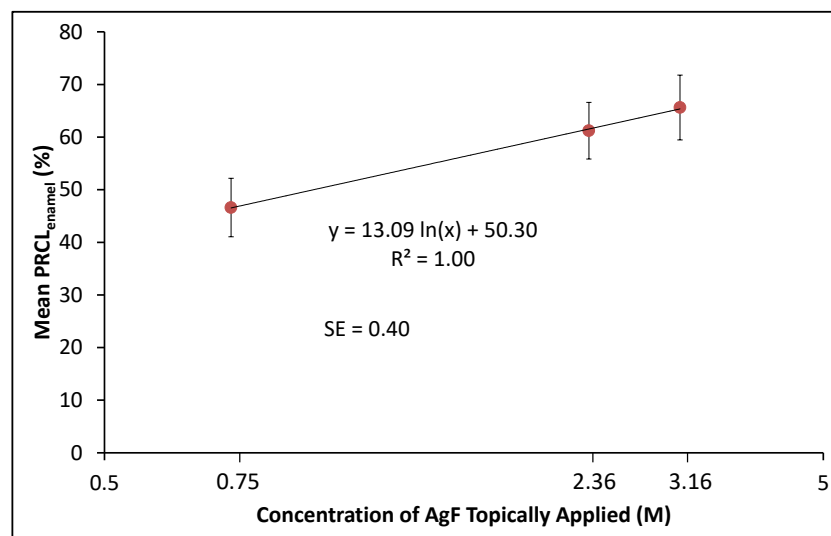
**Figure 10.18** - A log-linear dose-response relationship between the mean PRCL<sub>enamel</sub> of AgNO<sub>3</sub> and [AgNO<sub>3</sub>].

**Fig. 10.19** shows the mean PRCL<sub>enamel</sub> of 0.75 M, 2.36 M and 3.16 M AgF treatment groups. The mean PRCL<sub>enamel</sub> of AgF treatment groups increased with increasing concentration of AgF. However, there was no significant difference between the mean PRCL<sub>enamel</sub> of 2.36 M and 3.16 M AgF treatment groups.

**Fig. 10.20** shows that there was a log-linear dose-response relationship between the mean PRCL<sub>enamel</sub> of topical treatment with AgF and the concentration of topically applied AgF.



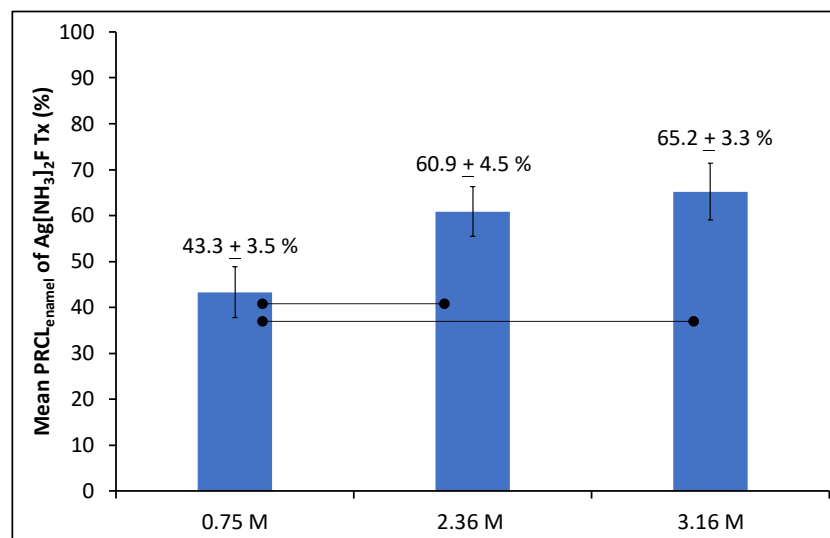
**Figure 10.19** - The mean PRCL<sub>enamel</sub> of 0.75 M, 2.36 M and 3.16 M AgF treatment groups.



**Figure 10.20** - A log-linear dose-response relationship between the mean PRCL<sub>enamel</sub> of AgF and [AgF].

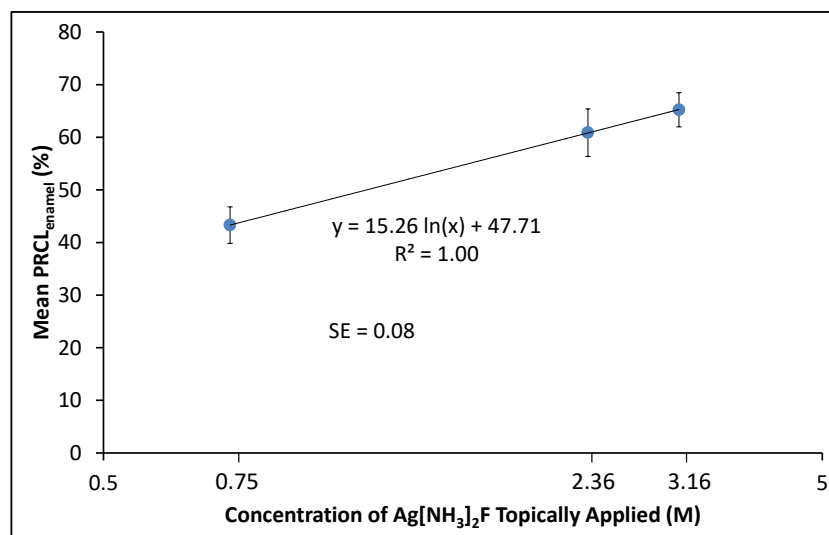
**Fig. 10.21** shows the mean  $PRCL_{\text{enamel}}$  of 0.75 M, 2.36 M and 3.16 M  $Ag[NH_3]_2F$  treatment groups. The mean  $PRCL_{\text{enamel}}$  of  $Ag[NH_3]_2F$  treatment groups increased with increasing concentration of  $Ag[NH_3]_2F$ . However, there was no significant difference between the mean  $PRCL_{\text{enamel}}$  of 2.36 M and 3.16 M  $Ag[NH_3]_2F$  treatment groups.

**Fig. 10.22** shows that there was a log-linear dose-response relationship between the mean  $PRCL_{\text{enamel}}$  of topical treatment with  $Ag[NH_3]_2F$  and the concentration of topically applied  $Ag[NH_3]_2F$ .



**Figure 10.21** - The mean  $PRCL_{\text{enamel}}$  of 0.75 M, 2.36 M and 3.16 M  $Ag[NH_3]_2F$  treatment groups.





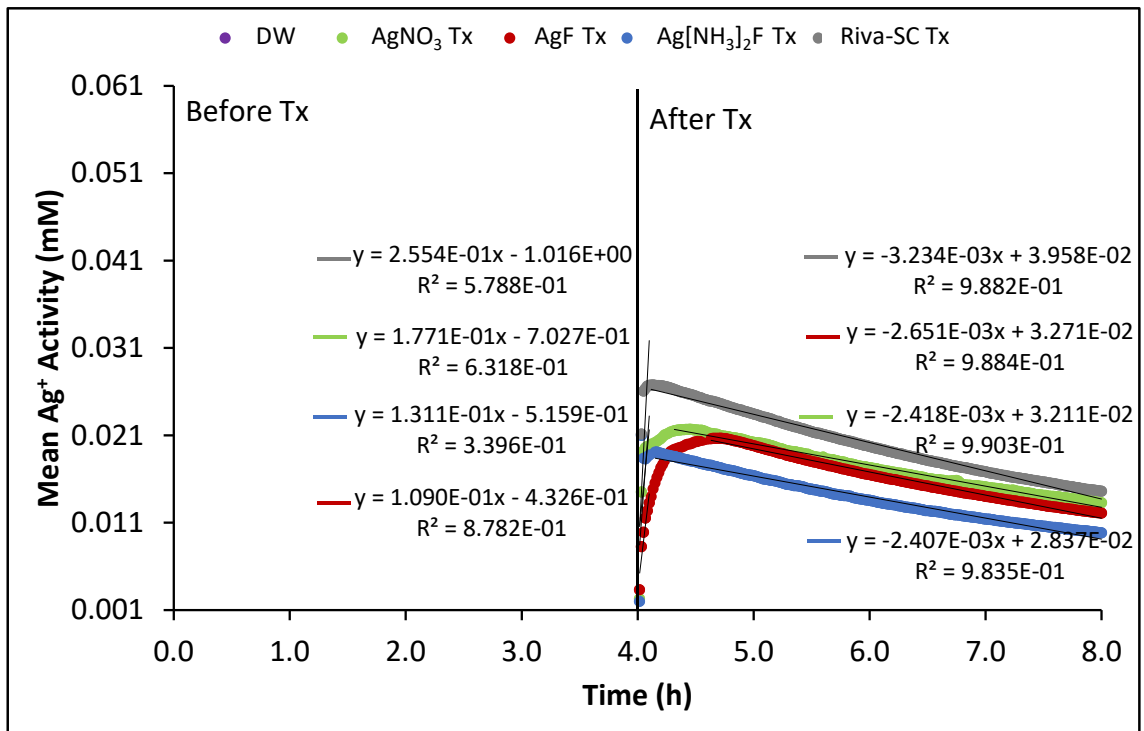
**Figure 10.22** - A log-linear dose-response relationship between the mean PRCL<sub>enamel</sub> of Ag[NH<sub>3</sub>]<sub>2</sub>F and [Ag[NH<sub>3</sub>]<sub>2</sub>F].

#### 10.4.2 Ag<sup>+</sup> ISE Study

**Fig. 10.23** shows the Ag<sup>+</sup> release profiles of 3.16 M AgNO<sub>3</sub>, 3.16 M AgF, 3.16 M Ag[NH<sub>3</sub>]<sub>2</sub>F, Riva-SC and DW treatment groups, which were based on the mean activities of Ag<sup>+</sup> released from the six enamel blocks of each treatment group. After re-immersion of enamel blocks topically treated with silver compounds into acids, all the mean activities of Ag<sup>+</sup> in the solution increased rapidly from zero, and then subsequently decreased continually.

Even though the Ag<sup>+</sup> release profiles are not linear, the approximate rates of the changes in the mean Ag<sup>+</sup> activities can be extrapolated by the slopes of trendlines of initial increase and later decrease in Ag<sup>+</sup> activities. The standard error of each trendline was shown later in **Table 10.8**.

No Ag<sup>+</sup> release was detected in DW treatment group.



**Figure 10.23** - The mean  $\text{Ag}^+$  release from enamel under pH 4.0 demineralisation before and after topical treatments with DW, and 3.16 M silver compounds.

**Fig. 10.24 ~ Fig. 10.26** show the  $\text{Ag}^+$  release profiles of 0.75 M, 2.36 M and 3.16 M  $\text{AgNO}_3$ ,  $\text{AgF}$  and  $\text{Ag}[\text{NH}_3]_2\text{F}$  treatment groups, which were based on the mean activities of  $\text{Ag}^+$  released from the six enamel blocks of each treatment group.

After re-immersion of enamel blocks topically treated with  $\text{AgNO}_3$ ,  $\text{AgF}$  and  $\text{Ag}[\text{NH}_3]_2\text{F}$  into acids, all the mean activities of  $\text{Ag}^+$  in the solution increased rapidly from zero, and then subsequently decreased continually.

Even though the  $\text{Ag}^+$  release profiles are not linear, the approximate rates of the changes in the mean  $\text{Ag}^+$  activities can be extrapolated by the slopes of trendlines of initial increase and later decrease in  $\text{Ag}^+$  activities. The standard error of each trendline was shown later in **Table 10.8**.

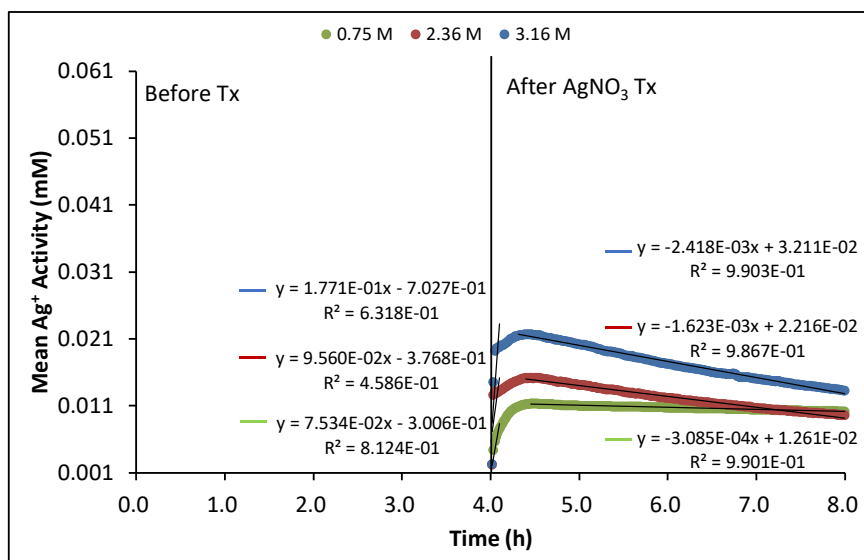


Figure 10.24 - The  $\text{Ag}^+$  release profiles of 0.75 M, 2.36 M and 3.16 M  $\text{AgNO}_3$  treatment groups.

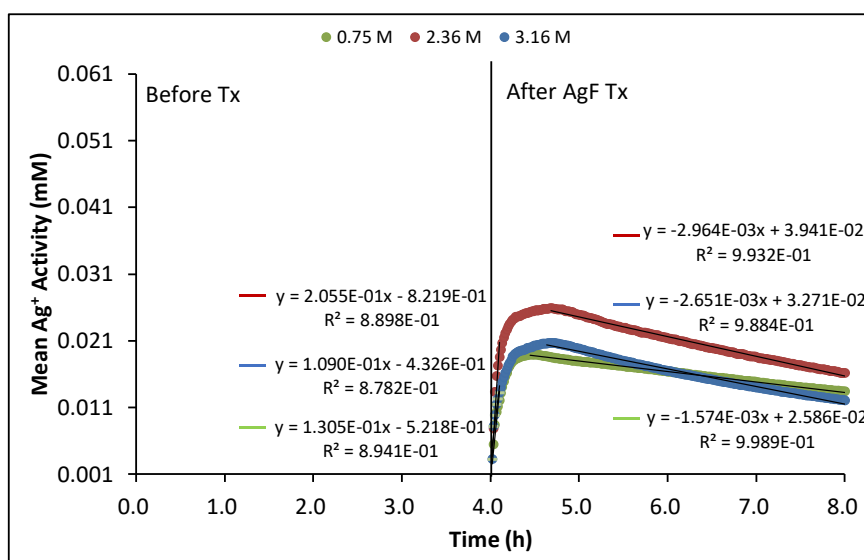


Figure 10.25 - The  $\text{Ag}^+$  release profiles of 0.75 M, 2.36 M and 3.16 M  $\text{AgF}$  treatment groups.

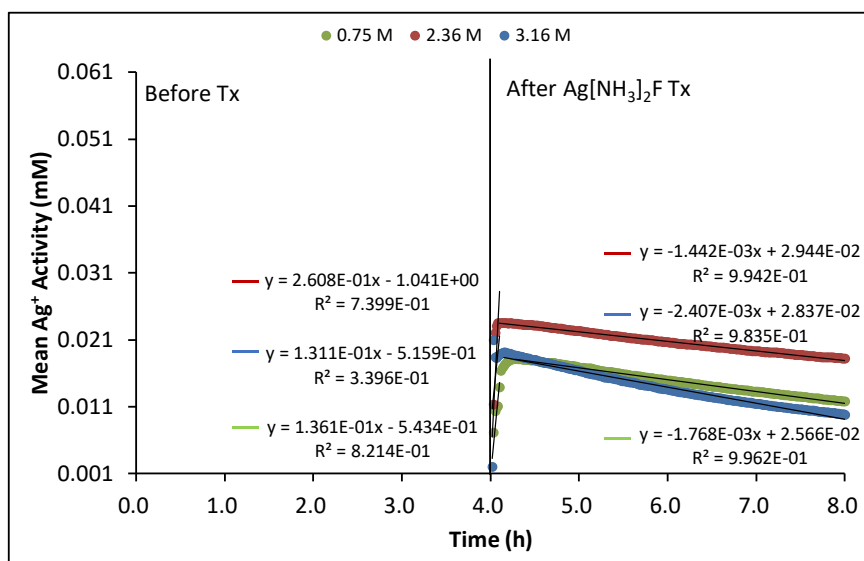


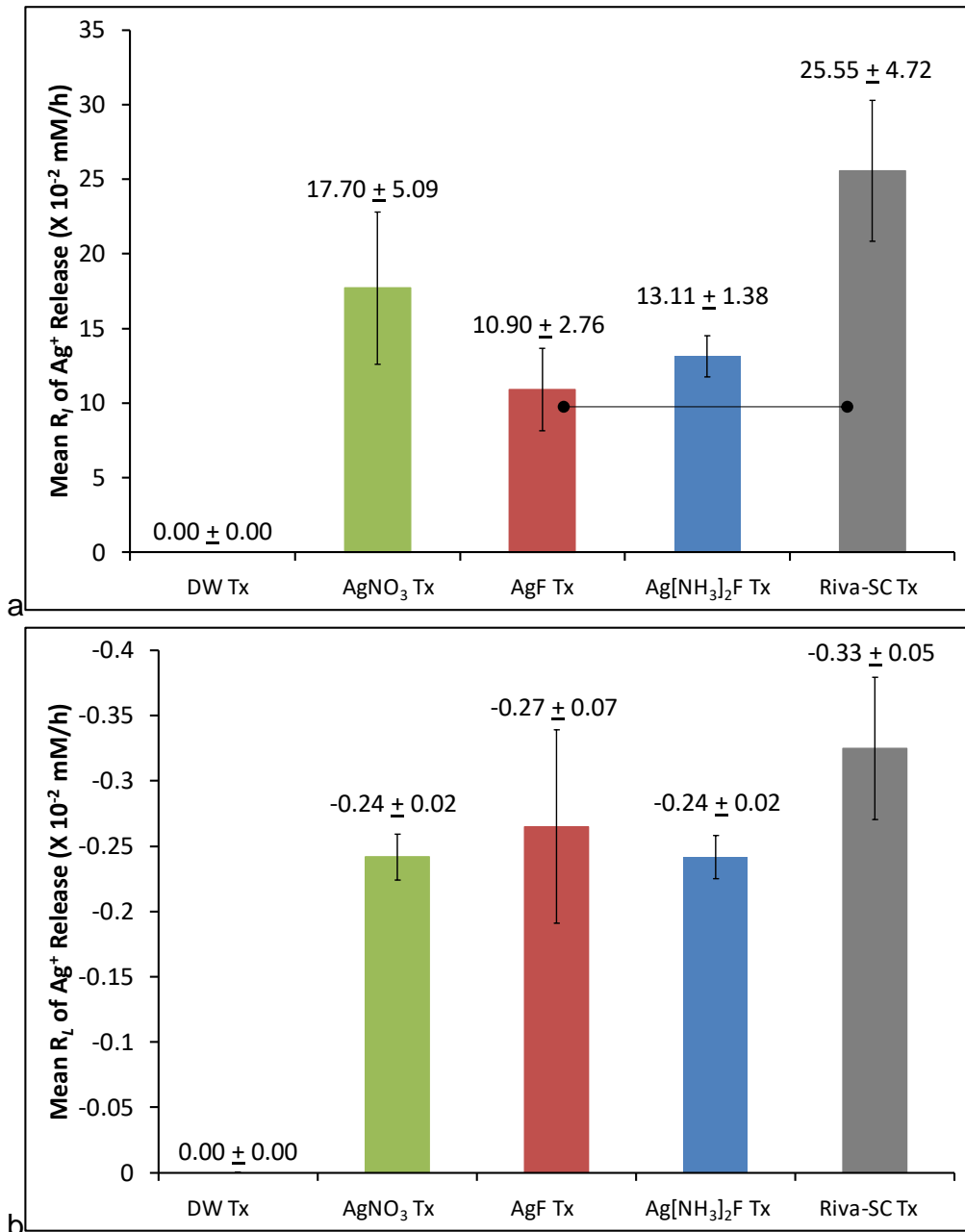
Figure 10.26 - The  $\text{Ag}^+$  release profiles of 0.75 M, 2.36 M and 3.16 M  $\text{Ag}[\text{NH}_3]_2\text{F}$  treatment groups.

**Table 10.8** shows the mean initial rates ( $R_I$ ) of increase in the  $\text{Ag}^+$  activities and the mean later rates ( $R_L$ ) of decrease in the  $\text{Ag}^+$  activities of all treatment groups.

*Table 10.8 – Mean  $R_I$  and mean  $R_L$  of the  $\text{Ag}^+$  release following each treatment.*

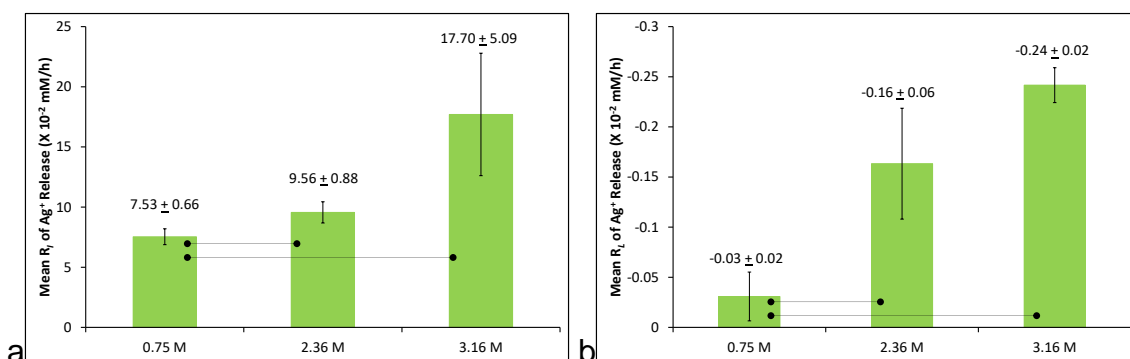
Tx Group	Mean $R_I$ +/-SE (X $10^{-2}$ mM/h)	Mean $R_L$ +/-SE (X $10^{-2}$ mM/h)
DW Tx	0.00 $\pm$ 0.00	0.00 $\pm$ 0.00
0.75 M $\text{AgNO}_3$ Tx	7.53 $\pm$ 0.66	-0.03 $\pm$ 0.02
2.36 M $\text{AgNO}_3$ Tx	9.56 $\pm$ 0.88	-0.16 $\pm$ 0.06
3.16 M $\text{AgNO}_3$ Tx	17.71 $\pm$ 5.09	-0.24 $\pm$ 0.02
0.75 M $\text{AgF}$ Tx	13.05 $\pm$ 4.37	-0.16 $\pm$ 0.04
2.36 M $\text{AgF}$ Tx	20.55 $\pm$ 5.09	-0.30 $\pm$ 0.06
3.16 M $\text{AgF}$ Tx	10.90 $\pm$ 2.76	-0.27 $\pm$ 0.07
0.75 M $\text{Ag}[\text{NH}_3]_2\text{F}$ Tx	13.61 $\pm$ 3.36	-0.18 $\pm$ 0.05
2.36 M $\text{Ag}[\text{NH}_3]_2\text{F}$ Tx	26.08 $\pm$ 7.02	-0.14 $\pm$ 0.03
3.16 M $\text{Ag}[\text{NH}_3]_2\text{F}$ Tx	13.11 $\pm$ 1.38	-0.24 $\pm$ 0.02
Riva-SC Tx	25.54 $\pm$ 4.72	-0.32 $\pm$ 0.05

**Fig. 10.27a** and **b** shows the mean  $R_i$  and the mean  $R_L$  of  $Ag^+$  release of 3.16 M  $AgNO_3$ , 3.16 M  $AgF$ , 3.16 M  $Ag[NH_3]_2F$ , Riva-SC and DW treatment groups. There was a significant difference between the  $R_i$  of 3.16 M  $AgF$  and Riva-SC treatment groups. However, there were no significant differences between the  $R_L$  of each treatment group.

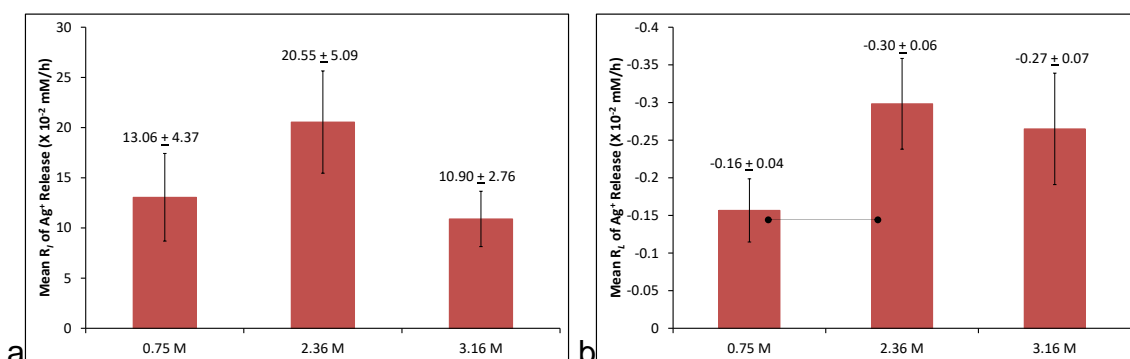


**Figure 10.27** - (a) Mean  $R_i$  and (b) mean  $R_L$  of the  $Ag^+$  release of DW and 3.16 M treatment groups.

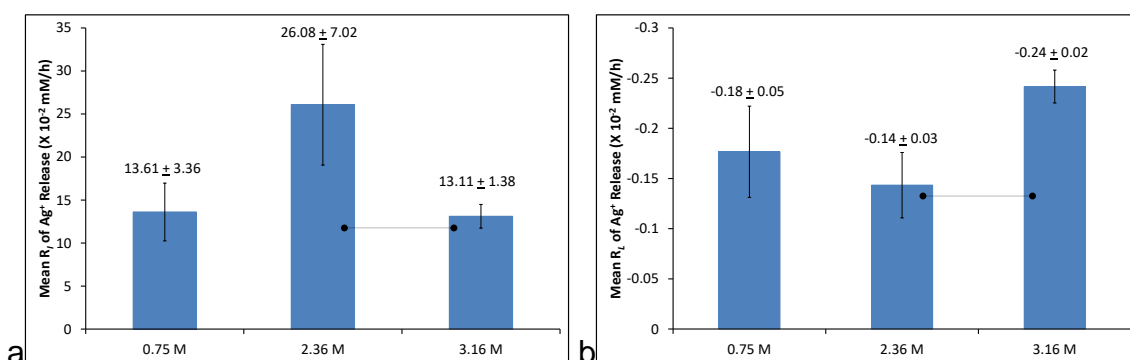
**Fig. 10.28 ~ Fig. 10.30** show the mean  $R_I$  and the mean  $R_L$  of  $Ag^+$  release of 0.75 M, 2.36 M and 3.16 M  $AgNO_3$ ,  $AgF$  and  $Ag[NH_3]_2F$  treatment groups. In  $AgNO_3$  treatment groups, both the mean  $R_I$  and the mean  $R_L$  of  $Ag^+$  release increased with concentration. However, in  $AgF$  and  $Ag[NH_3]_2F$  treatment groups, no relationships between either the mean  $R_I$  or the mean  $R_L$  of the  $Ag^+$  release, and the concentrations were found.



**Figure 10.28 - (a) Mean  $R_I$  and (b) mean  $R_L$  of the  $Ag^+$  release of  $AgNO_3$  treatment groups.**



**Figure 10.29 - (a) Mean  $R_I$  and (b) mean  $R_L$  of the  $Ag^+$  release of  $AgF$  treatment groups.**



**Figure 10.30 - (a) Mean  $R_I$  and (b) mean  $R_L$  of the  $Ag^+$  release of  $Ag[NH_3]_2F$  treatment groups.**

#### 10.4.2.1 Mean [Ag<sup>+</sup>] during the post-treatment 4 h periods of Each Treatment Group

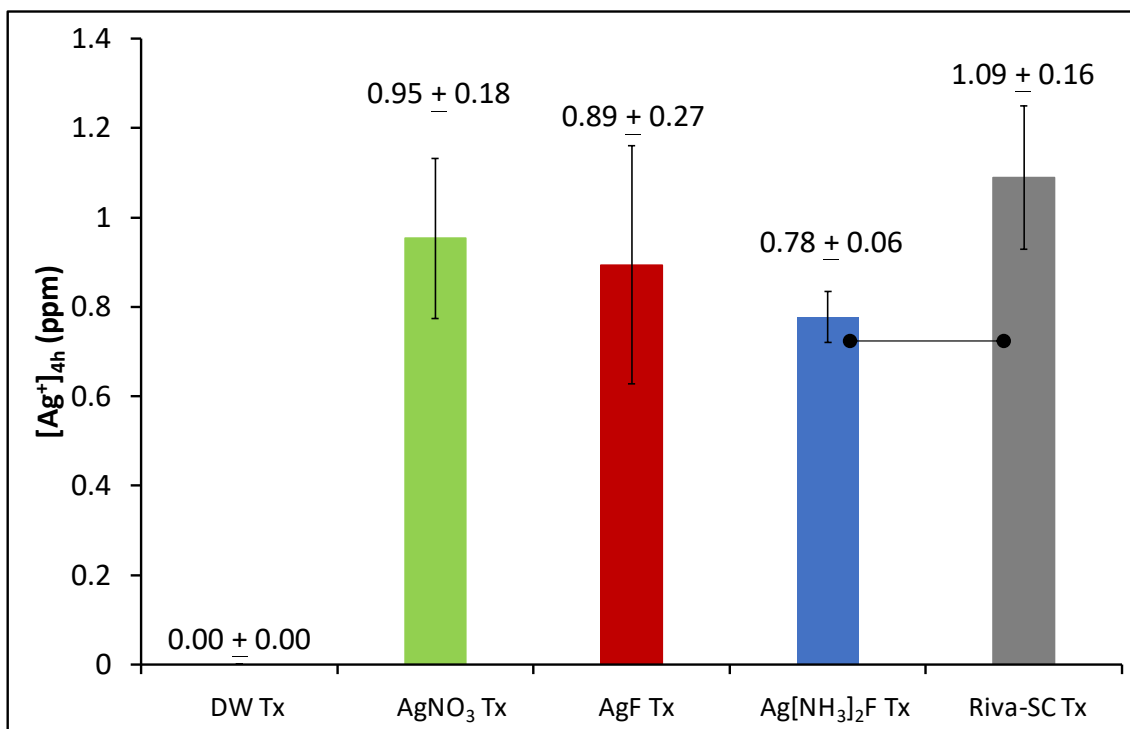
The mean [Ag<sup>+</sup>] during the 4 h demineralisation period after re-immersion of the topically treated enamel blocks into acid ([Ag<sup>+</sup>]<sub>4h</sub>) (**Table 10.9**) of each treatment group was calculated, in order to compare the effects of Ag<sup>+</sup> in the acid on the demineralisation of the enamel.

**Table 10.9** – The mean [Ag<sup>+</sup>] during the 4 h demineralisation period after re-immersion of the topically treated enamel blocks into acids ([Ag<sup>+</sup>]<sub>4h</sub>) of each treatment group.

Tx groups	[Ag <sup>+</sup> ] <sub>4h</sub>	
DW	0.0 ± 0.0 X 10 <sup>-3</sup> mM	0.00 ± 0.00 ppm
0.75 M AgNO <sub>3</sub>	5.4 ± 0.2 X 10 <sup>-3</sup> mM	0.58 ± 0.02 ppm
2.36 M AgNO <sub>3</sub>	6.3 ± 0.4 X 10 <sup>-3</sup> mM	0.68 ± 0.04 ppm
3.16 M AgNO <sub>3</sub>	8.8 ± 1.7 X 10 <sup>-3</sup> mM	0.95 ± 0.18 ppm
0.75 M AgF	8.3 ± 2.1 X 10 <sup>-3</sup> mM	0.89 ± 0.22 ppm
2.36 M AgF	10.7 ± 2.3 X 10 <sup>-3</sup> mM	1.16 ± 0.25 ppm
3.16 M AgF	8.3 ± 2.5 X 10 <sup>-3</sup> mM	0.89 ± 0.27 ppm
0.75 M Ag[NH <sub>3</sub> ] <sub>2</sub> F	7.5 ± 1.0 X 10 <sup>-3</sup> mM	0.81 ± 0.11 ppm
2.36 M Ag[NH <sub>3</sub> ] <sub>2</sub> F	10.5 ± 2.6 X 10 <sup>-3</sup> mM	1.14 ± 0.28 ppm
3.16 M Ag[NH <sub>3</sub> ] <sub>2</sub> F	7.2 ± 0.3 X 10 <sup>-3</sup> mM	0.78 ± 0.06 ppm
Riva-SC	10.1 ± 1.5 X 10 <sup>-3</sup> mM	1.09 ± 0.16 ppm



**Fig. 10.31** shows the  $[Ag^+]_{4h}$  (ppm) of 3.16 M  $AgNO_3$ , 3.16 M  $AgF$ , 3.16 M  $Ag[NH_3]_2F$ , Riva-SC and DW treatment groups. The  $[Ag^+]_{4h}$  of the Riva-SC treatment group was the highest. However, the only significant difference was between the  $[Ag^+]_{4h}$  of  $Ag[NH_3]_2F$  and Riva-SC treatment groups.



**Figure 10.31** – The  $[Ag^+]_{4h}$  (ppm) of 3.16 M  $AgNO_3$ , 3.16 M  $AgF$ , 3.16 M  $Ag[NH_3]_2F$ , Riva-SC and DW treatment groups. Error bars show the standard errors. Linking lines between bars indicate significant differences at  $p < 0.05$  between treatment groups.

**Fig. 10.32** shows the  $[Ag^+]_{4h}$  (ppm) of 0.75 M, 2.36 M and 3.16 M  $AgNO_3$  treatment groups. The  $[Ag^+]_{4h}$  of the  $AgNO_3$  treatment groups increased with increasing concentration of  $AgNO_3$ . However, there was no significant difference between the  $[Ag^+]_{4h}$  of the 2.36 M and 3.16 M treatment groups.

**Fig. 10.33** shows the  $[Ag^+]_{4h}$  (ppm) of 0.75 M, 2.36 M and 3.16 M  $AgF$  treatment groups. There were no significant differences between the  $[Ag^+]_{4h}$  of 0.75 M, 2.36 M and 3.16 M  $AgF$  treatment groups.

**Fig. 10.34** shows the  $[Ag^+]_{4h}$  (ppm) of 0.75 M, 2.36 M and 3.16 M  $Ag[NH_3]_2F$  treatment groups. There were no significant differences between the  $[Ag^+]_{4h}$  of 0.75 M, 2.36 M and 3.16 M  $Ag[NH_3]_2F$  treatment groups.

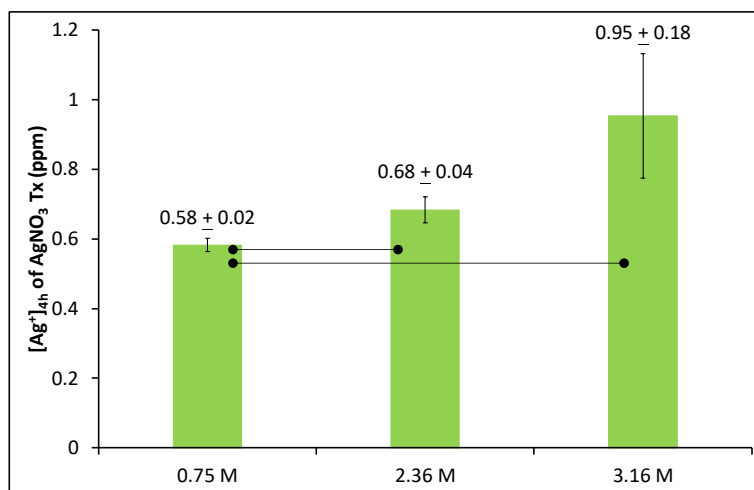


Figure 10.32 - The  $[Ag^+]_{4h}$  (ppm) of 0.75 M, 2.36 M and 3.16 M  $AgNO_3$  treatment groups.

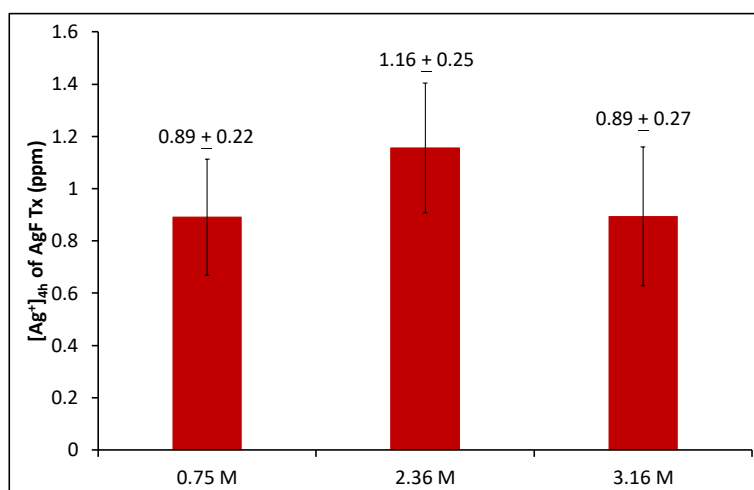


Figure 10.33 - The  $[Ag^+]_{4h}$  (ppm) of 0.75 M, 2.36 M and 3.16 M  $AgF$  treatment groups.

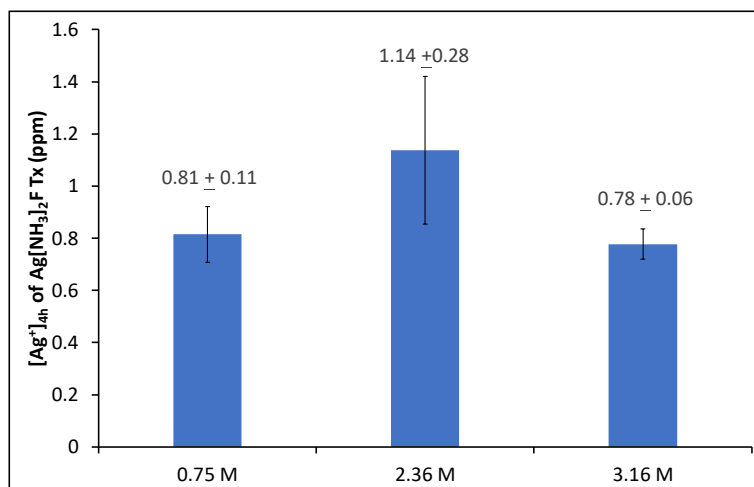


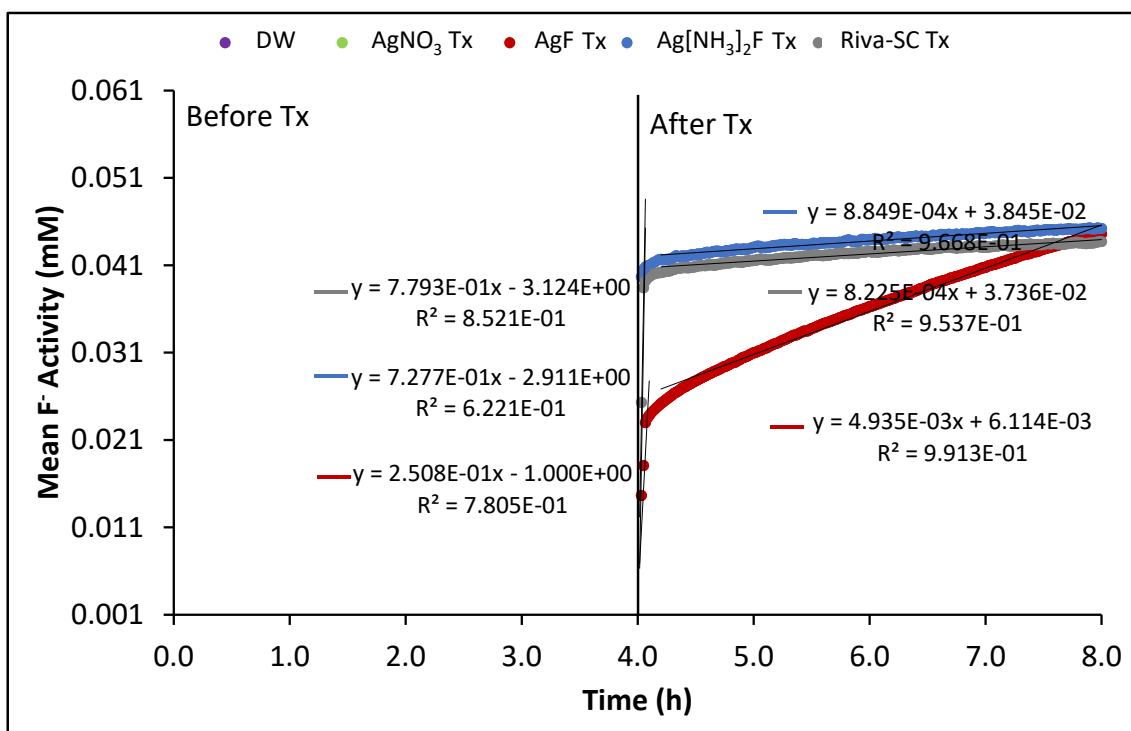
Figure 10.34 - The  $[Ag^+]_{4h}$  (ppm) of 0.75 M, 2.36 M and 3.16 M  $Ag[NH_3]_2F$  treatment groups.

### 10.4.3 F<sup>-</sup> ISE Study

**Fig. 10.35** shows the F<sup>-</sup> release profiles of 3.16 M AgNO<sub>3</sub>, 3.16 M AgF, 3.16 M Ag[NH<sub>3</sub>]<sub>2</sub>F, Riva-SC and DW treatment groups, which were based on the mean activities of F<sup>-</sup> released from the six enamel blocks each treatment group. After re-immersion of enamel blocks topically treated with fluoride-containing silver compounds back into acids, there was a rapid increase in all the mean activities of F<sup>-</sup> from zero, which slowed with time.

Even though the F<sup>-</sup> release profiles are not linear, the approximate rates of the changes in the mean F<sup>-</sup> activities can be extrapolated by the slopes of trendlines of initial and later increase in F<sup>-</sup> activities. The standard error of each trendline was shown later in **Table 10.10**.

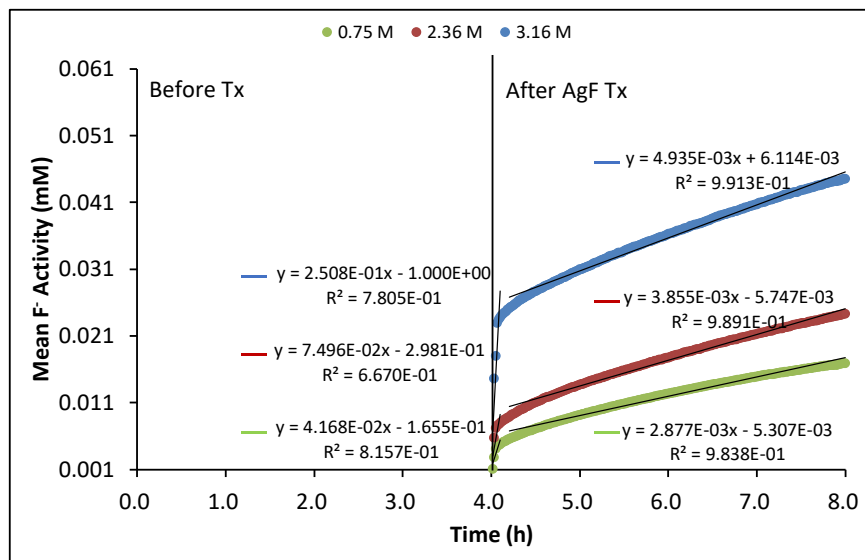
No F<sup>-</sup> release was detected in DW and AgNO<sub>3</sub> treatment groups.



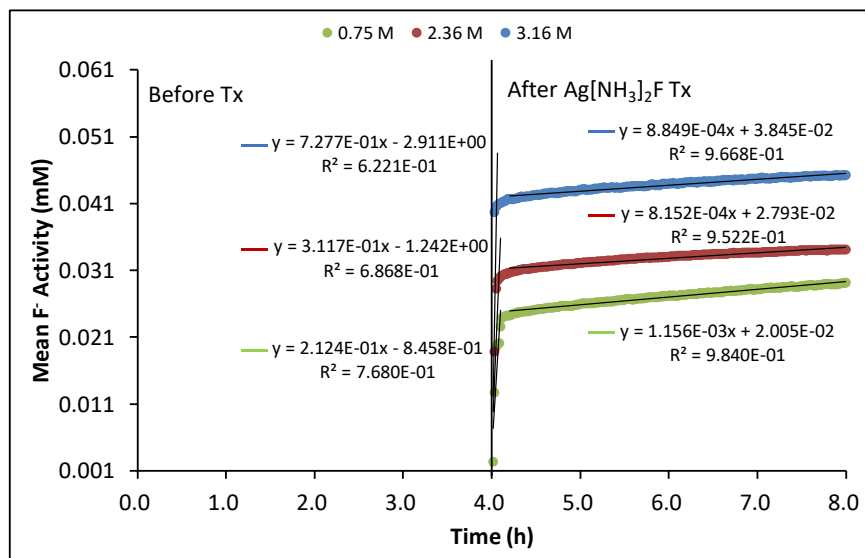
**Figure 10.35** - The mean F<sup>-</sup> release from enamel under pH 4.0 demineralisation before and after topical treatment with DW, and 3.16 M silver compounds.

**Fig. 10.36** and **Fig. 10.37** show the  $F^-$  release profiles of 0.75 M, 2.36 M and 3.16 M AgF and  $Ag[NH_3]_2F$  treatment groups, which were based on the mean activities of  $F^-$  released from the six enamel blocks of each treatment group. After re-immersion of enamel blocks topically treated with AgF and  $Ag[NH_3]_2F$  back into acids, there was a rapid increase in all the mean activities of  $F^-$  from zero, which slowed with time.

Even though the  $F^-$  release profiles are not linear, the approximate rates of the changes in the mean  $F^-$  activities can be extrapolated by the slopes of trendlines of initial and later increase in  $F^-$  activities. The standard error of each trendline is shown later in **Table 10.10**.



**Figure 10.36** - The  $F^-$  release profiles of 0.75 M, 2.36 M and 3.16 M AgF treatment groups.



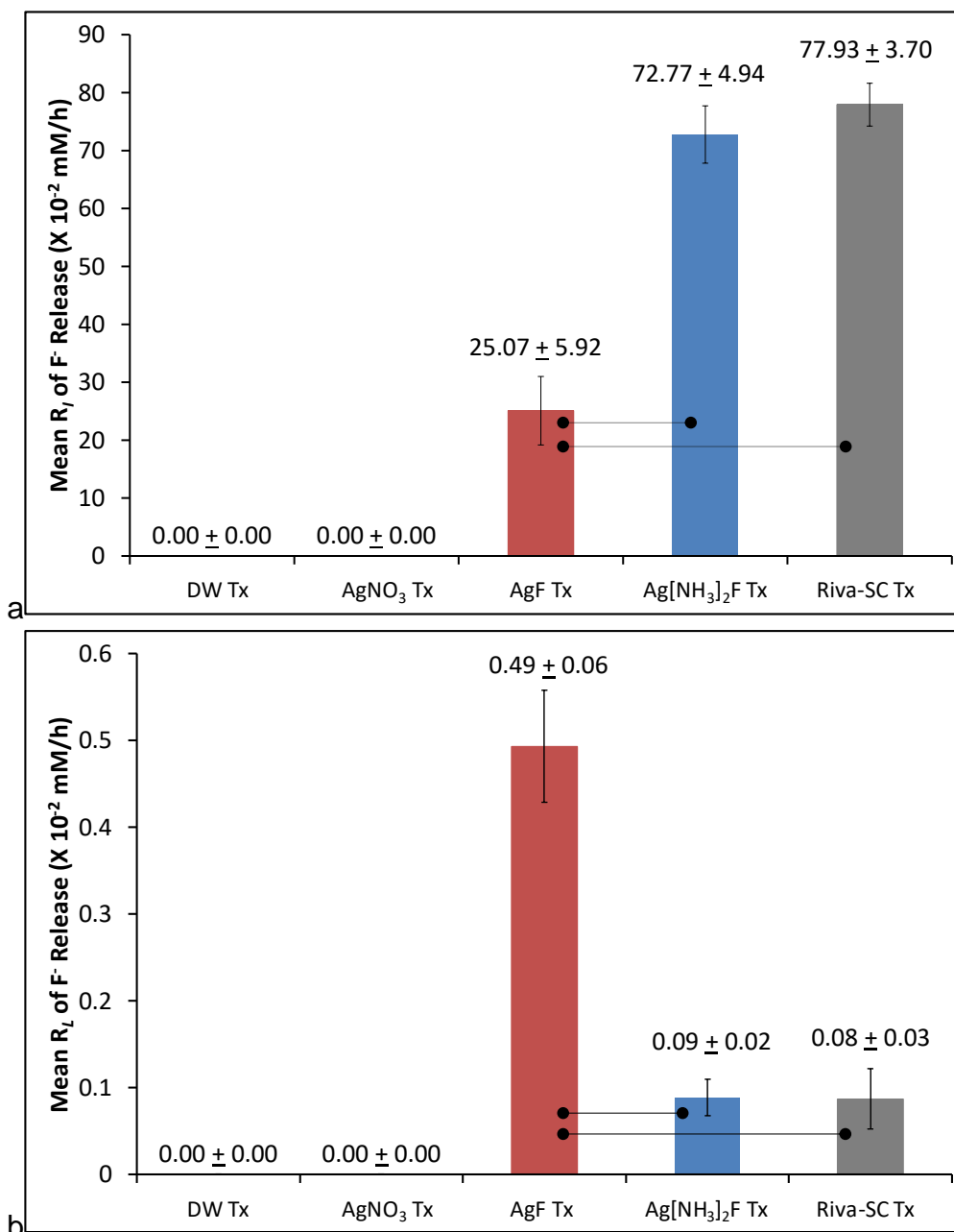
**Figure 10.37** - The  $F^-$  release profiles of 0.75 M, 2.36 M and 3.16 M  $Ag[NH_3]_2F$  treatment groups.

**Table 10.10** shows the mean initial rates ( $R_i$ ) of increase in the  $F^-$  activities and the mean later rates ( $R_L$ ) of increase in the  $F^-$  activities of all treatment groups.

*Table 10.10 – Mean  $R_i$  and mean  $R_L$  of the  $F^-$  release following each treatment.*

Tx Group	Mean $R_i$ +/- SE (X $10^{-2}$ mM/h)	Mean $R_L$ +/- SE (X $10^{-2}$ mM/h)
DW Tx	0.00 ± 0.00	0.00 ± 0.00
0.75 M AgNO <sub>3</sub> Tx	0.00 ± 0.00	0.00 ± 0.00
2.36 M AgNO <sub>3</sub> Tx	0.00 ± 0.00	0.00 ± 0.00
3.16 M AgNO <sub>3</sub> Tx	0.00 ± 0.00	0.00 ± 0.00
0.75 M AgF Tx	4.17 ± 2.29	0.29 ± 0.04
2.36 M AgF Tx	7.50 ± 1.31	0.39 ± 0.05
3.16 M AgF Tx	25.08 ± 5.92	0.49 ± 0.06
0.75 M Ag[NH <sub>3</sub> ] <sub>2</sub> F Tx	21.24 ± 5.49	0.12 ± 0.04
2.36 M Ag[NH <sub>3</sub> ] <sub>2</sub> F Tx	31.17 ± 3.37	0.08 ± 0.01
3.16 M Ag[NH <sub>3</sub> ] <sub>2</sub> F Tx	72.77 ± 4.94	0.09 ± 0.02
Riva-SC Tx	77.93 ± 3.70	0.08 ± 0.03

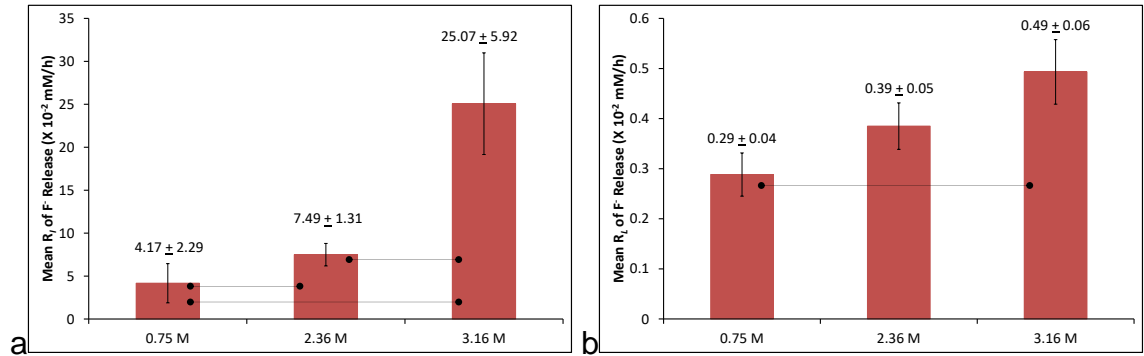
**Fig. 10.38a** and **b** shows the mean  $R_I$  and the mean  $R_L$  of  $F^-$  release of 3.16 M  $AgNO_3$ , 3.16 M  $AgF$ , 3.16 M  $Ag[NH_3]_2F$ , Riva-SC and DW treatment groups. The mean  $R_I$  of 3.16 M  $Ag[NH_3]_2F$  and Riva-SC treatment groups were significantly higher than that of 3.16 M  $AgF$  treatment group. However, the mean  $R_L$  of 3.16 M  $Ag[NH_3]_2F$  and Riva-SC treatment groups were significantly lower than that of 3.16 M  $AgF$  treatment group.



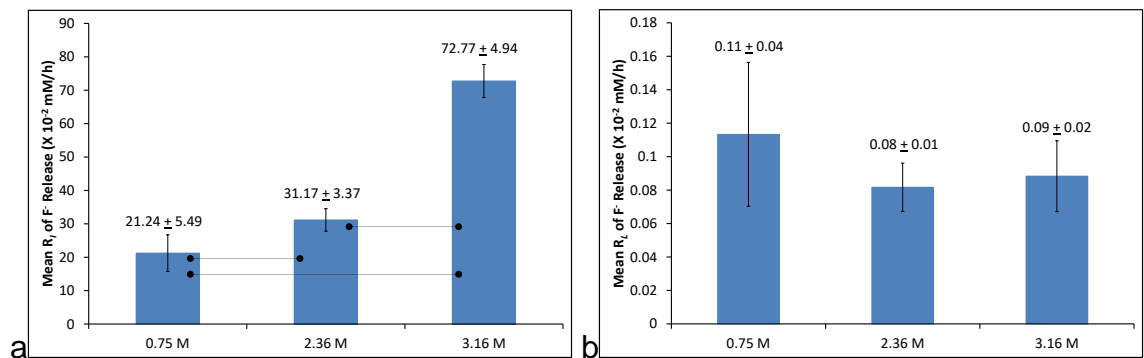
**Figure 10.38** - (a) Mean  $R_I$  and (b) mean  $R_L$  of the  $F^-$  release of DW and 3.16 M treatment groups.

**Fig. 10.39** and **Fig. 10.40** show the mean  $R_I$  and the mean  $R_L$  of  $F^-$  release of 0.75 M, 2.36 M and 3.16 M  $AgF$  and  $Ag[NH_3]_2F$  treatment groups. In  $AgF$

treatment groups, both the mean  $R_I$  and the mean  $R_L$  of  $F^-$  release increased with concentration. In  $Ag[NH_3]_2F$  treatment groups, the mean  $R_I$  of  $F^-$  release increased with concentration. However, there was no relationship between the mean  $R_L$  of  $F^-$  release and the concentration of topically applied  $Ag[NH_3]_2F$  was found.



**Figure 10.39** - (a) Mean  $R_I$  and (b) mean  $R_L$  of the  $F^-$  release of 0.75 M, 2.36 M and 3.16 M  $AgF$  treatment groups.



**Figure 10.40** - (a) Mean  $R_I$  and (b) mean  $R_L$  of the  $F^-$  release of 0.75 M, 2.36 M and 3.16 M  $Ag[NH_3]_2F$  treatment groups.

#### 10.4.3.1 Mean [F<sup>-</sup>] during the post-treatment 4 h periods of Each Treatment Group

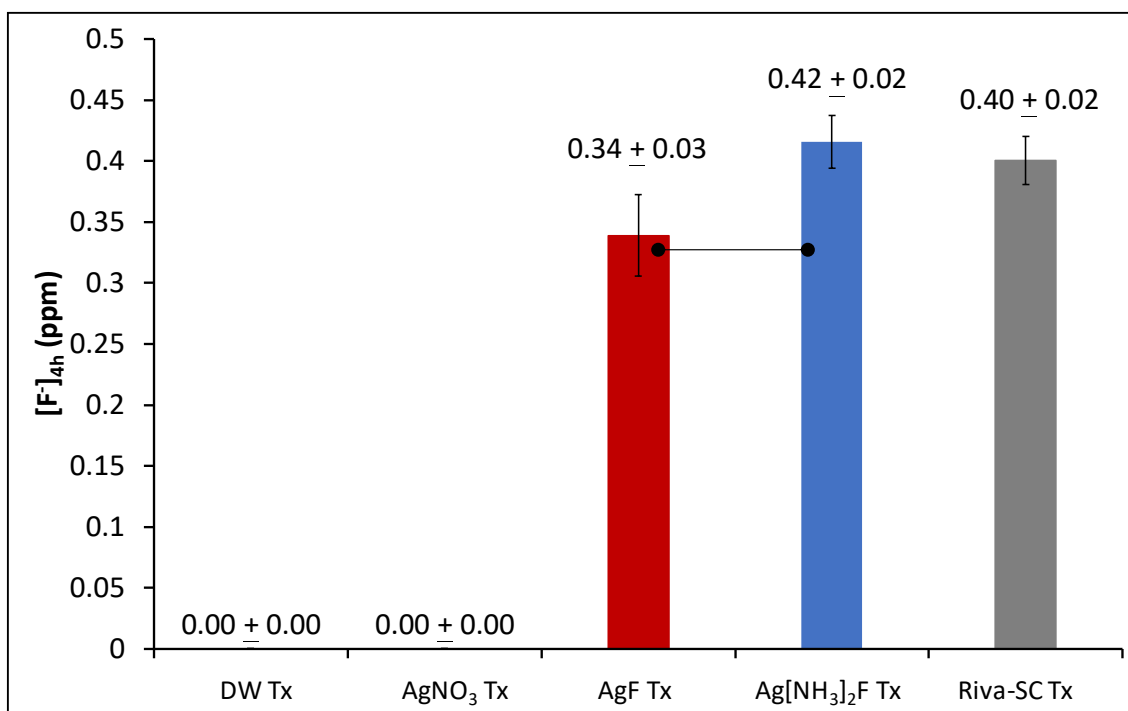
The mean [F<sup>-</sup>] during the 4 h demineralisation period after re-immersion of the topically treated enamel blocks into acid ([F<sup>-</sup>]<sub>4h</sub>) (**Table 10.11**) of each treatment group was calculated, in order to compare the effects of F<sup>-</sup> in the acid on the demineralisation of the enamel.

**Table 10.11** – The mean [F<sup>-</sup>] during the 4 h demineralisation period after re-immersion of the topically treated enamel blocks into acids ([F<sup>-</sup>]<sub>4h</sub>) of each treatment group.

Tx groups	[F <sup>-</sup> ] <sub>4h</sub>	
DW	0.0 ± 0.0 X 10 <sup>-3</sup> mM	0.00 ± 0.00 ppm
0.75 M AgNO <sub>3</sub>	0.0 ± 0.0 X 10 <sup>-3</sup> mM	0.00 ± 0.00 ppm
2.36 M AgNO <sub>3</sub>	0.0 ± 0.0 X 10 <sup>-3</sup> mM	0.00 ± 0.00 ppm
3.16 M AgNO <sub>3</sub>	0.0 ± 0.0 X 10 <sup>-3</sup> mM	0.00 ± 0.00 ppm
0.75 M AgF	6.2 ± 0.6 X 10 <sup>-3</sup> mM	0.12 ± 0.01 ppm
2.36 M AgF	8.8 ± 0.8 X 10 <sup>-3</sup> mM	0.17 ± 0.01 ppm
3.16 M AgF	17.8 ± 1.8 X 10 <sup>-3</sup> mM	0.34 ± 0.03 ppm
0.75 M Ag[NH <sub>3</sub> ] <sub>2</sub> F	13.5 ± 1.7 X 10 <sup>-3</sup> mM	0.26 ± 0.03 ppm
2.36 M Ag[NH <sub>3</sub> ] <sub>2</sub> F	16.5 ± 2.5 X 10 <sup>-3</sup> mM	0.31 ± 0.05 ppm
3.16 M Ag[NH <sub>3</sub> ] <sub>2</sub> F	21.9 ± 1.2 X 10 <sup>-3</sup> mM	0.42 ± 0.02 ppm
Riva-SC	21.1 ± 1.0 X 10 <sup>-3</sup> mM	0.40 ± 0.02 ppm



**Fig. 10.41** shows the  $[F^-]_{4h}$  (ppm) of 3.16 M  $AgNO_3$ , 3.16 M  $AgF$ , 3.16 M  $Ag[NH_3]_2F$ , Riva-SC and DW treatment groups. The  $[F^-]_{4h}$  of the 3.16 M  $Ag[NH_3]_2F$  and Riva-SC treatment groups were higher than that of the 3.16 M  $AgF$  treatment group. However, there was no significant difference between the  $[F^-]_{4h}$  of  $Ag[NH_3]_2F$  and Riva-SC treatment groups, and there was no significant difference between the  $[F^-]_{4h}$  of  $AgF$  and Riva-SC treatment groups



**Figure 10.41** - The  $[F^-]_{4h}$  (ppm) of 3.16 M  $AgNO_3$ , 3.16 M  $AgF$ , 3.16 M  $Ag[NH_3]_2F$ , Riva-SC and DW treatment groups. Error bars show the standard errors. Linking lines between bars indicate significant differences at  $p < 0.05$  between treatment groups.

**Fig. 10.42** shows the  $[F^-]_{4h}$  (ppm) of 0.75 M, 2.36 M and 3.16 M  $AgF$  treatment groups. The  $[F^-]_{4h}$  in the solution increased with increasing concentration of  $AgF$ .

**Fig. 10.43** shows the  $[F^-]_{4h}$  (ppm) of 0.75 M, 2.36 M and 3.16 M  $Ag[NH_3]_2F$  treatment groups. The  $[F^-]_{4h}$  in the solution increased with increasing concentration of  $Ag[NH_3]_2F$ .

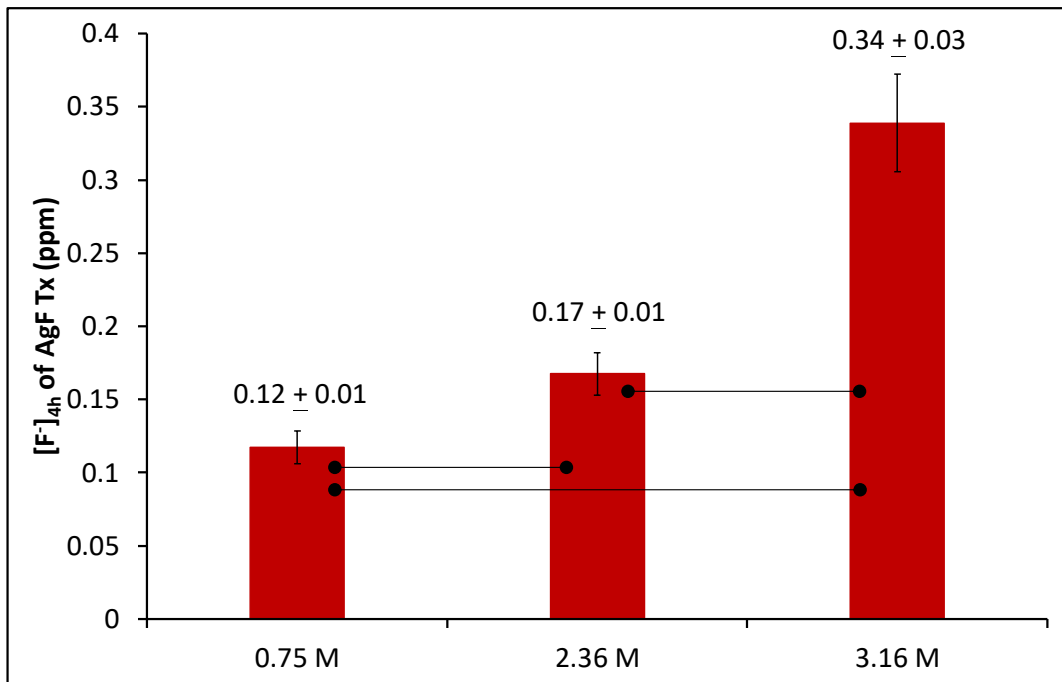


Figure 10.42 - The  $[F]_{4h}$  (ppm) of 0.75 M, 2.36 M and 3.16 M AgF treatment groups.

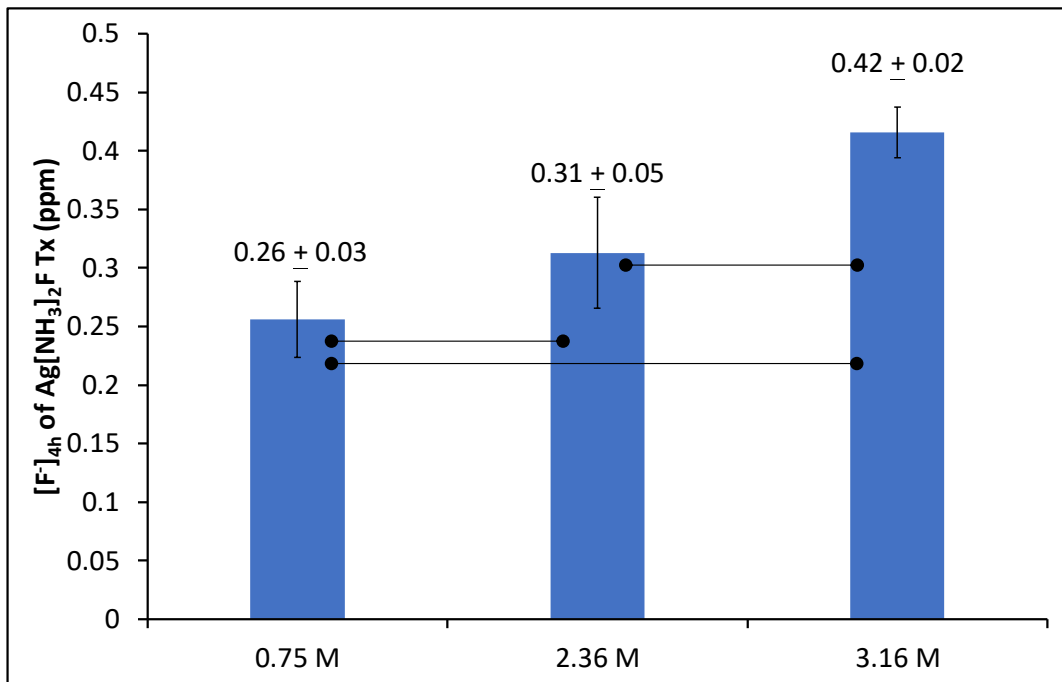








Figure 10.43 - The  $[F]_{4h}$  (ppm) of 0.75 M, 2.36 M and 3.16 M  $Ag[NH_3]_2F$  treatment groups.









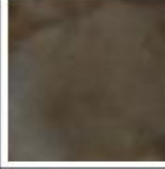








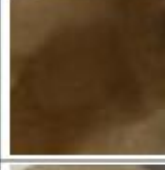
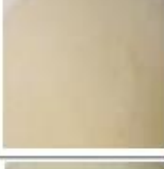








#### 10.4.4 Digital Photographs

**Fig. 10.44** and **Fig. 10.45** show that following topical treatments with  $\text{AgNO}_3$ ,  $\text{AgF}$ , and  $\text{Ag}[\text{NH}_3]_2\text{F}$ , yellow staining was observed, which then turned to black after further 4 h demineralisation. Further, the yellow and black staining increased with increasing concentrations of  $\text{AgNO}_3$ ,  $\text{AgF}$ , and  $\text{Ag}[\text{NH}_3]_2\text{F}$ .

No staining was observed on the enamel surfaces topically treated with DW.

	After the first 4 h demin.	After topical treatment	After further 4 h demin.
DW Tx			
Riva-SC Tx			

**Figure 10.44** - The colours of enamel treated with DW and Riva-SC following different treatments of the ISE study.

	After the first 4 h demin.	After topical treatment	After further 4 h demin.
0.75 M AgNO <sub>3</sub> Tx			
2.36 M AgNO <sub>3</sub> Tx			
3.16 M AgNO <sub>3</sub> Tx			
0.75 M AgF Tx			
2.36 M AgF Tx			
3.16 M AgF Tx			
0.75 M Ag[NH <sub>3</sub> ] <sub>2</sub> F Tx			
2.36 M Ag[NH <sub>3</sub> ] <sub>2</sub> F Tx			
3.16 M Ag[NH <sub>3</sub> ] <sub>2</sub> F Tx			

*Figure 10.45 - The colours of enamel treated with different concentrations of AgNO<sub>3</sub>, AgF and Ag[NH<sub>3</sub>]<sub>2</sub>F following different treatments of the ISE study.*

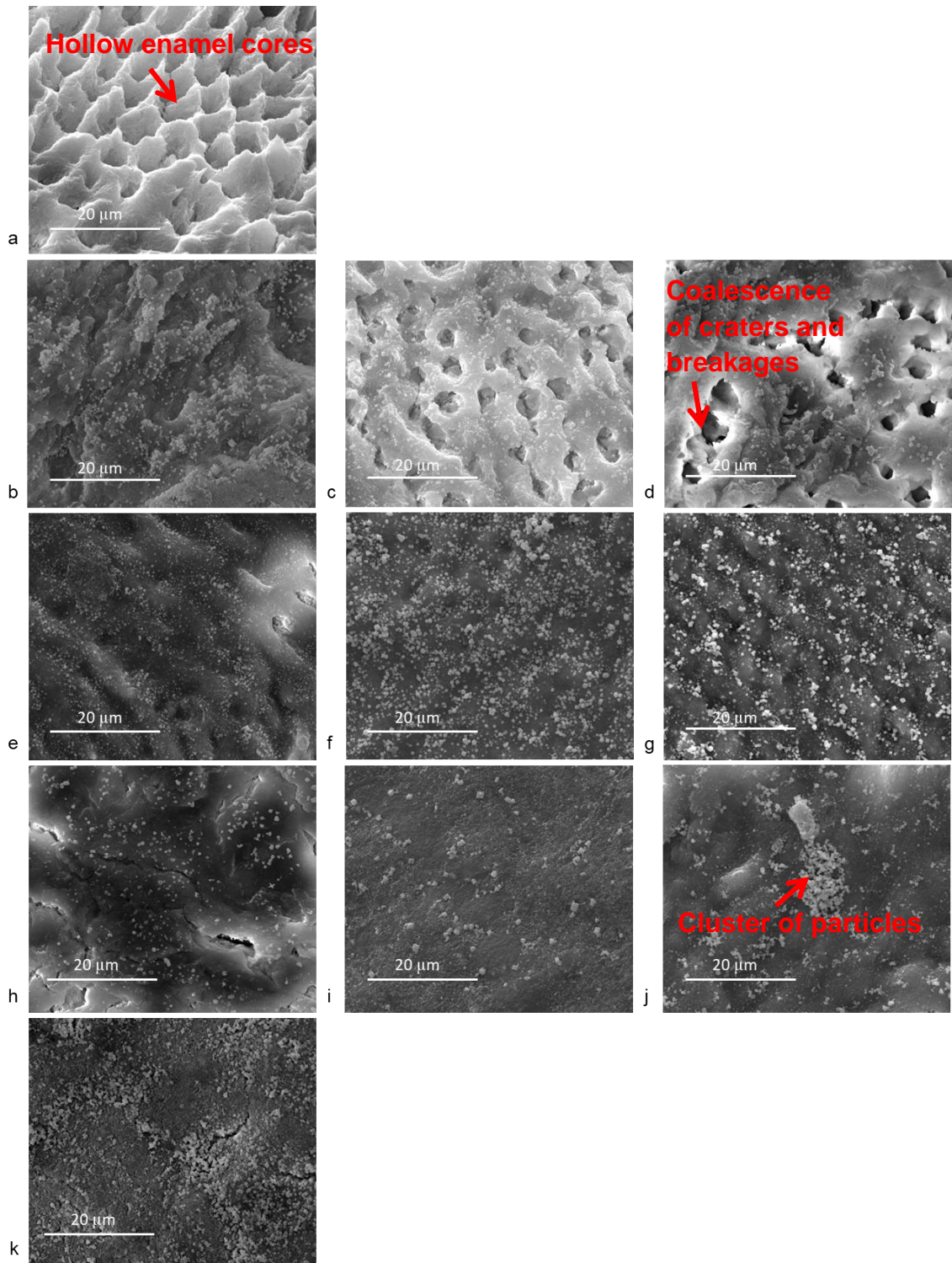
### 10.4.5 SEM Images Analysis

**Fig. 10.46a** is a typical SEM image of enamel topically treated with DW after demineralisation, showing hollow enamel cores, breakages and irregular craters on the enamel surfaces.

**Fig. 10.46b ~ Fig. 10.46d** are typical SEM images of enamel topically treated with  $\text{AgNO}_3$  after demineralisation, showing craters and breakages on the enamel surfaces. Demineralised pores were observed on the enamel surfaces topically treated with 3.16 M and 2.36 M  $\text{AgNO}_3$ . However, only uneven demineralised surfaces were observed on the surfaces topically treated with 0.75 M  $\text{AgNO}_3$ , (**Fig. 10.46b**). Further, the demineralised pores observed on the 3.16 M  $\text{AgNO}_3$  treated enamel surfaces were deeper than those observed on the 2.36 M  $\text{AgNO}_3$  treated enamel surfaces. Numerous cubic particles ( $\sim 1.5 \mu\text{m}$ ) (**Fig. 10.46b ~ Fig. 10.46d**) were deposited on all enamel surfaces treated with  $\text{AgNO}_3$ . Further, the number of particles increased with increasing concentration of  $\text{AgNO}_3$ .

**Fig. 10.46e ~ Fig. 10.46j** are typical SEM images of enamel topically treated with AgF and  $\text{Ag}[\text{NH}_3]_2\text{F}$  after demineralisation, showing that mainly ripple-like features observed on all enamel surfaces. On enamel surfaces treated with 0.75 M AgF and 0.75 M  $\text{Ag}[\text{NH}_3]_2\text{F}$ , focal pores (Worawongvasu, 2015) and narrow breakages were also found (**Fig. 10.46e** and **Fig. 10.46h**). Numerous cubic particles ( $\sim 1.5 \mu\text{m}$ ) and granular particles ( $\sim 1 \mu\text{m}$ ) were observed on enamel surfaces treated with AgF and  $\text{Ag}[\text{NH}_3]_2\text{F}$  (**Fig. 10.46e ~ Fig. 10.46j**). Further, the number of these particles increased with increasing concentrations of AgF and  $\text{Ag}[\text{NH}_3]_2\text{F}$ .

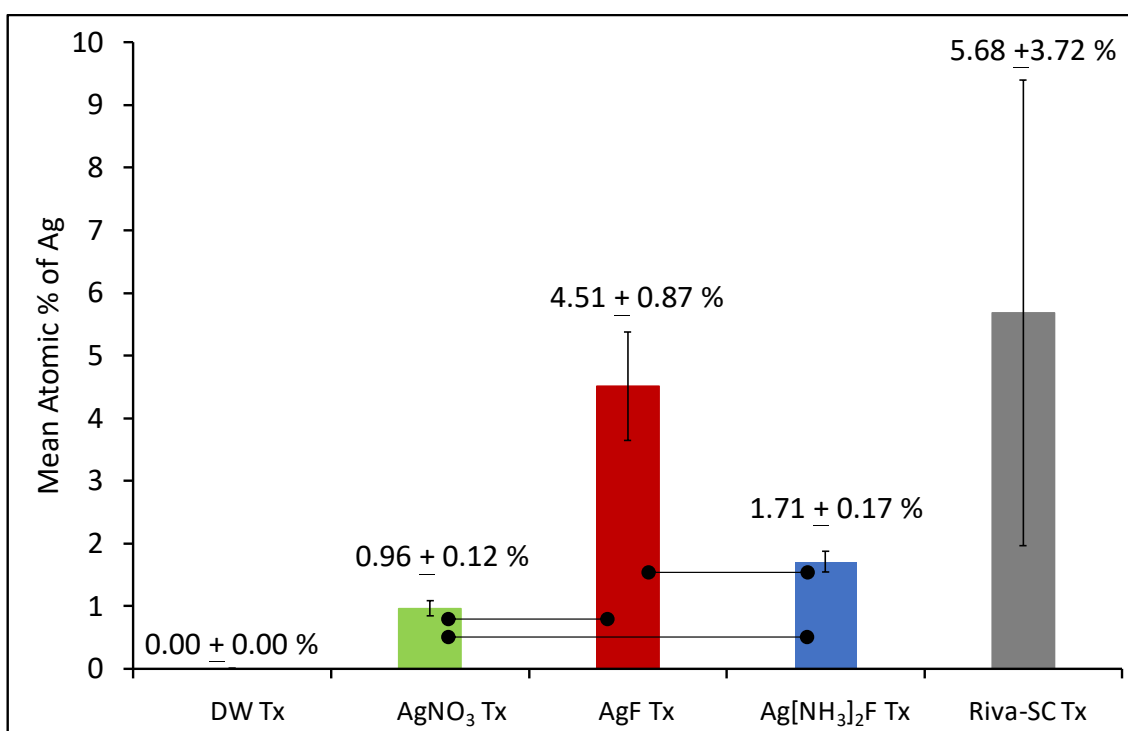
**Fig. 10.46k** is a typical SEM image of enamel topically treated with Riva-SC after demineralisation, showing similar demineralised surfaces to those topically treated with AgF and  $\text{Ag}[\text{NH}_3]_2\text{F}$ . Further, numerous cubic particles ( $\sim 1.5 \mu\text{m}$ ) and granular particles ( $\sim 1 \mu\text{m}$ ) were also observed on the surfaces topically treated Riva-SC. Narrow breakages were occasionally observed.



**Figure 10.46** - Typical SEM images of enamel blocks of (a) DW Tx, (b) 0.75 M AgNO<sub>3</sub> Tx, (c) 2.36 M AgNO<sub>3</sub> Tx and (d) 3.16 M AgNO<sub>3</sub> Tx, (e) 0.75 M AgF Tx, (f) 2.36 M AgF Tx and (g) 3.16 M AgF Tx, (h) 0.75 M Ag[NH<sub>3</sub>]<sub>2</sub>F Tx, (i) 2.36 M Ag[NH<sub>3</sub>]<sub>2</sub>F Tx and (j) 3.16 M Ag[NH<sub>3</sub>]<sub>2</sub>F Tx, and (k) Riva-SC Tx.

## 10.4.6 EDX Analysis

**Fig. 10.47** shows the mean atomic percentages of Ag detected on the enamel surfaces topically treated with 3.16 M AgNO<sub>3</sub>, 3.16 M AgF, 3.16 M Ag[NH<sub>3</sub>]<sub>2</sub>F, Riva-SC and DW after demineralisation. Elemental Ag was present on the enamel surfaces topically treated with 3.16 M AgNO<sub>3</sub>, 3.16 M AgF, 3.16 M Ag[NH<sub>3</sub>]<sub>2</sub>F and Riva-SC. The mean atomic percentage of Ag detected in 3.16 M AgF treatment group was higher than that in 3.16 M Ag[NH<sub>3</sub>]<sub>2</sub>F treatment group, both of which were higher than 3.16 M AgNO<sub>3</sub> treatment group. There were no significant differences between the mean atomic Ag % of Riva-SC and other treatment groups.



**Figure 10.47** – The mean atomic percentages of Ag of 3.16 M AgNO<sub>3</sub>, 3.16 M AgF, 3.16 M Ag[NH<sub>3</sub>]<sub>2</sub>F, Riva-SC and DW treatment groups. Linking lines between bars indicate significant differences at  $p < 0.05$  between treatment groups.

**Fig. 10.48** shows the mean atomic percentages of Ag detected on the enamel surfaces topically treated with 0.75 M, 2.36 M and 3.16 M  $\text{AgNO}_3$ . All the mean Ag atomic percentages were low, and there were no significant differences between the mean atomic percentages of Ag of each treatment group.

**Fig. 10.49** shows the mean atomic percentages of Ag detected on the enamel surfaces topically treated with 0.75 M, 2.36 M and 3.16 M AgF. The mean Ag atomic percentage increased with increasing concentration of AgF. However, there was no significant difference between the mean Ag atomic percentages of 2.36 M AgF and 3.16 M AgF treatment groups.

**Fig. 10.50** shows the mean atomic percentages of Ag detected on the enamel surfaces topically treated with 0.75 M, 2.36 M and 3.16 M  $\text{Ag}[\text{NH}_3]_2\text{F}$ . The mean Ag atomic percentage increased with increasing concentration of  $\text{Ag}[\text{NH}_3]_2\text{F}$ .



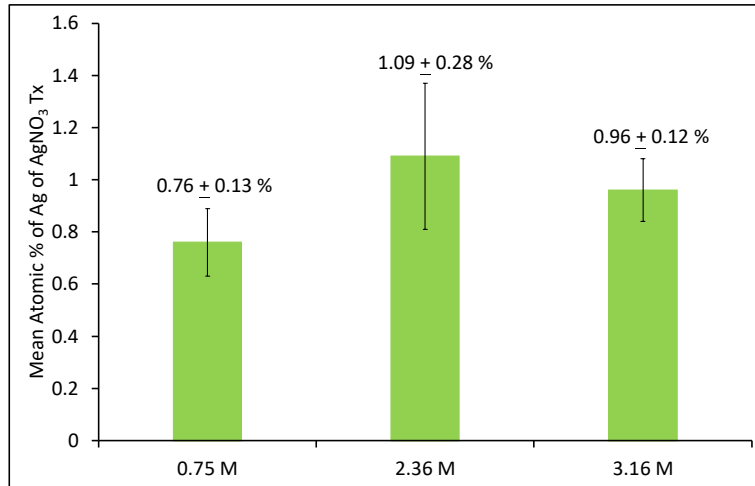


Figure 10.48 - The mean atomic percentages of Ag of  $\text{AgNO}_3$  treatment groups.

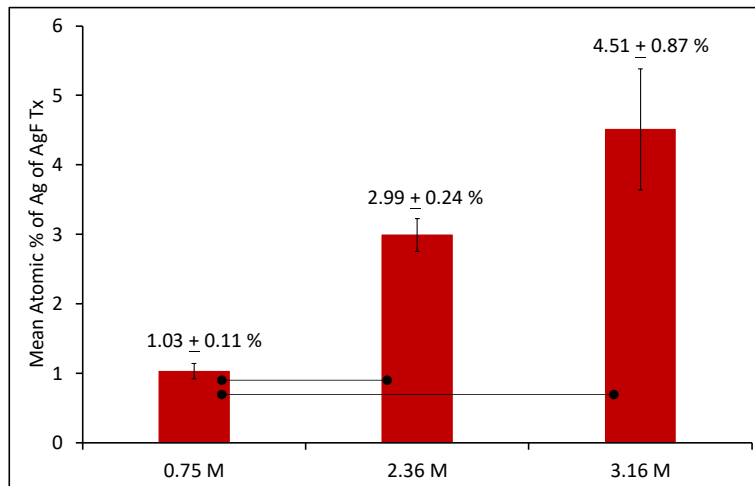


Figure 10.49 - The mean atomic percentages of Ag of  $\text{AgF}$  treatment groups.

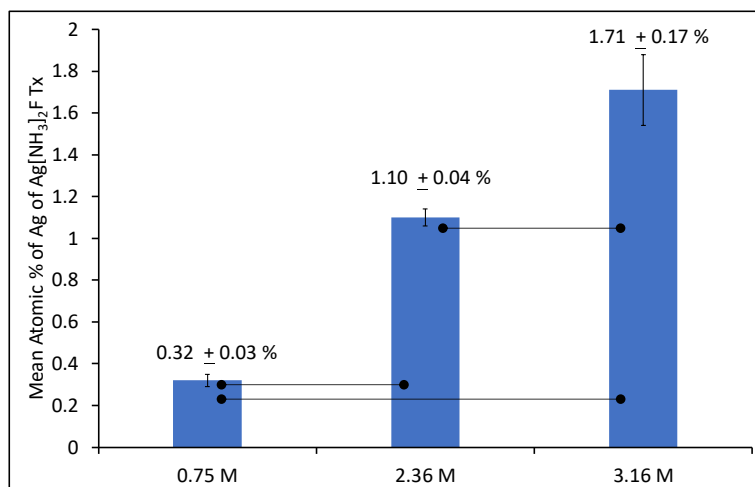
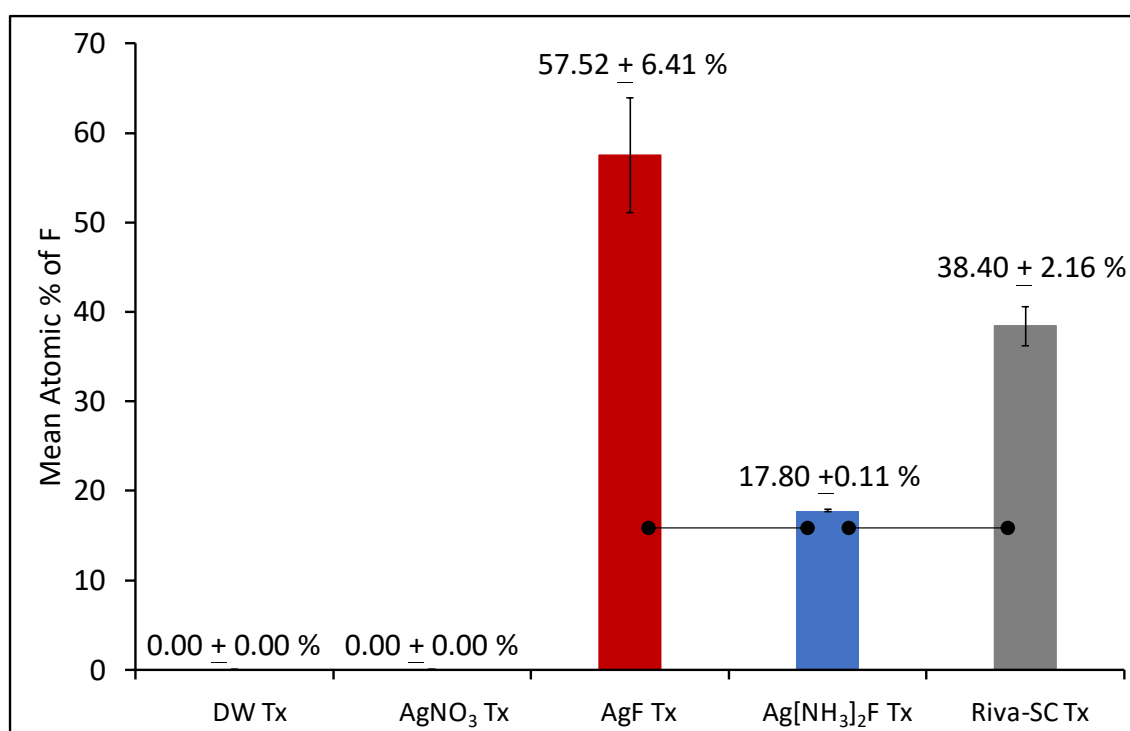


Figure 10.50 - The mean atomic percentages of Ag of  $\text{Ag}[\text{NH}_3]_2\text{F}$  treatment groups.

**Fig. 10.51** shows the mean atomic percentages of F detected on the enamel surfaces topically treated with 3.16 M AgNO<sub>3</sub>, 3.16 M AgF, 3.16 M Ag[NH<sub>3</sub>]<sub>2</sub>F, Riva-SC and DW after demineralisation. Elemental F was present on the enamel surfaces topically treated with 3.16 M AgF, 3.16 M Ag[NH<sub>3</sub>]<sub>2</sub>F and Riva-SC. The mean atomic percentages of F detected in 3.16 M AgF and Riva-SC treatment groups were higher than that in 3.16 M Ag[NH<sub>3</sub>]<sub>2</sub>F treatment group. There was no significant difference between the mean atomic F % of Riva-SC and 3.16 M AgF treatment groups.

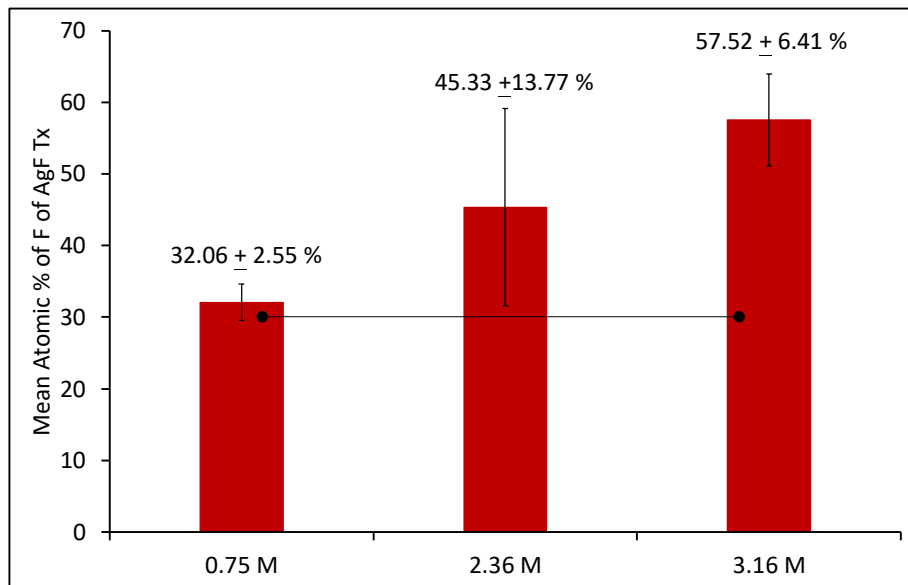


**Figure 10.51** - The mean atomic percentages of F of 3.16 M AgNO<sub>3</sub>, 3.16 M AgF, 3.16 M Ag[NH<sub>3</sub>]<sub>2</sub>F, Riva-SC and DW treatment groups. Error bars show the standard errors. Linking lines between bars indicate significant differences at  $p < 0.05$  between treatment groups.

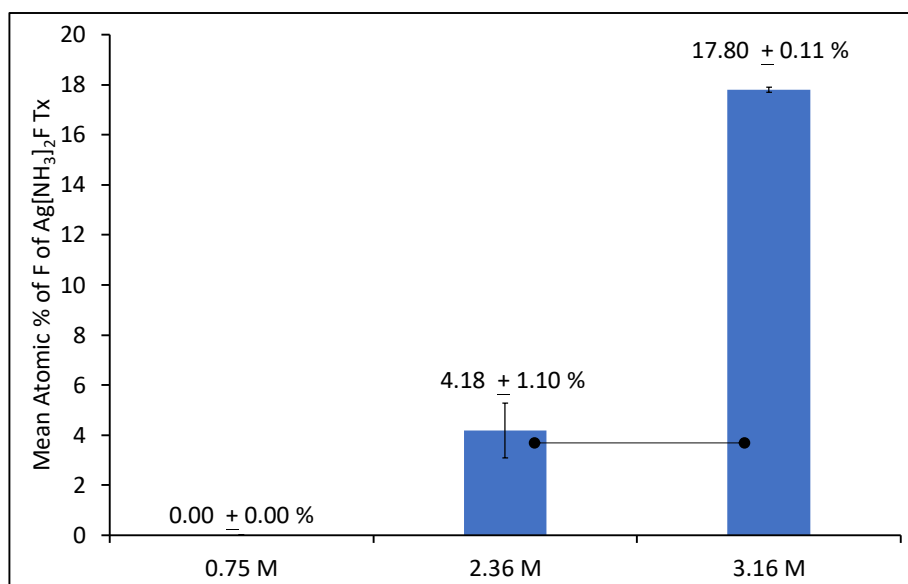
**Fig. 10.52** shows the mean atomic percentages of F detected on the enamel surfaces topically treated with 0.75 M, 2.36 M and 3.16 M AgF. The mean F atomic percentage increased with increasing concentration of AgF. There was no significant difference between the mean F atomic percentages of 2.36 M AgF and 3.16 M AgF treatment groups. Further, there was no significant difference

between the mean F atomic percentages of 2.36 M AgF and 0.75 M AgF treatment groups.

**Fig. 10.53** shows the mean atomic percentages of F detected on the enamel surfaces topically treated with 0.75 M, 2.36 M and 3.16 M Ag[NH<sub>3</sub>]<sub>2</sub>F. The mean F atomic percentage increased with increasing concentration of Ag[NH<sub>3</sub>]<sub>2</sub>F. No F was detected on the enamel surfaces topically treated with 0.75 M Ag[NH<sub>3</sub>]<sub>2</sub>F.



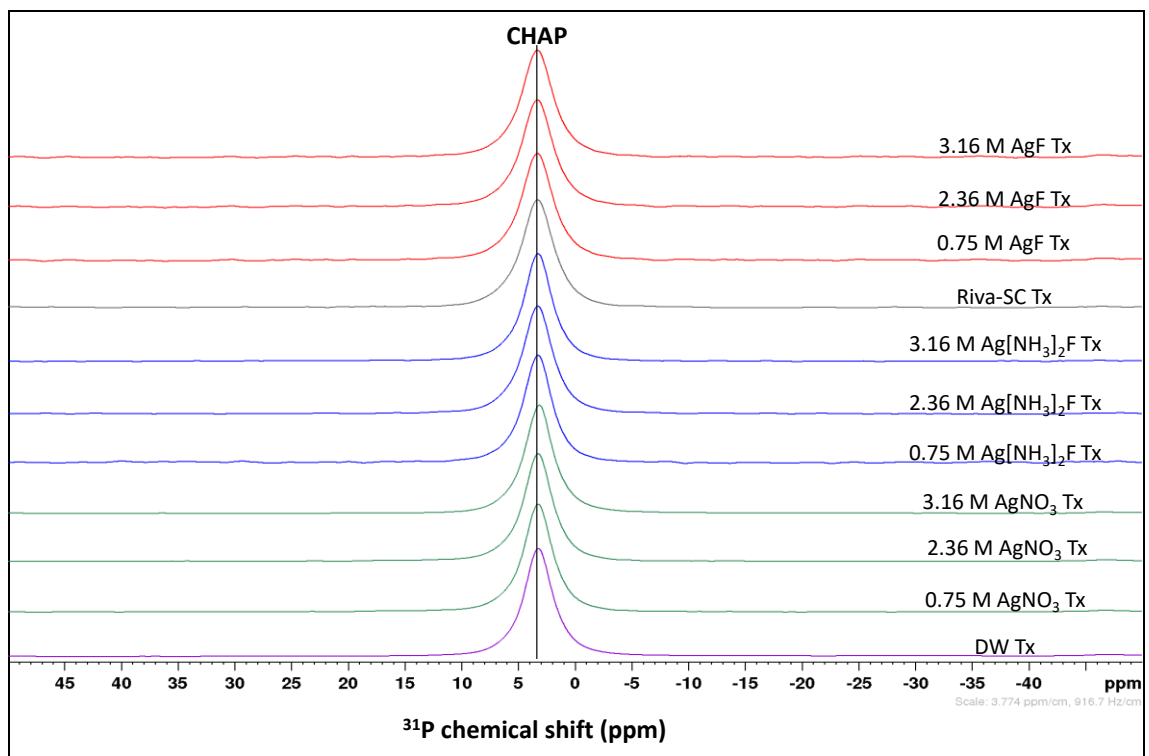
*Figure 10.52 - The mean atomic percentages of F of AgF treatment groups.*



*Figure 10.53 - The mean atomic percentages of F of Ag[NH<sub>3</sub>]<sub>2</sub>F treatment groups.*

### 10.4.7 $^{31}\text{P}$ MAS-NMR Analysis

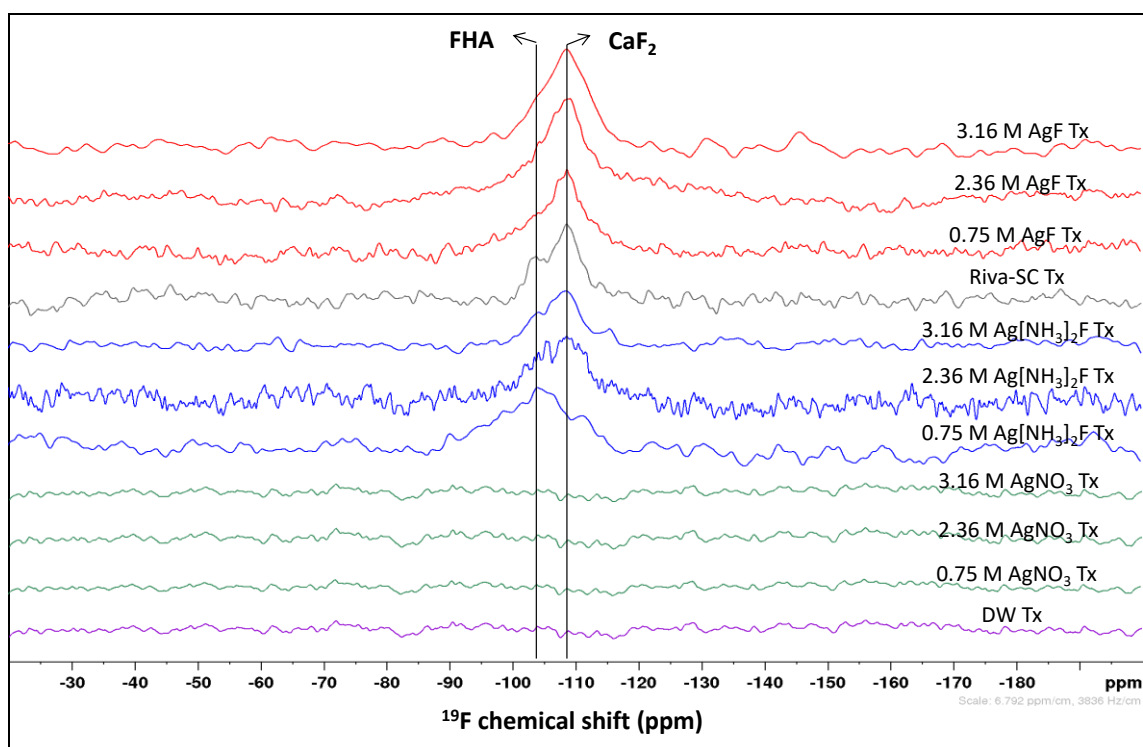
The  $^{31}\text{P}$  MAS-NMR spectra (**Fig. 10.54**) showed that only the chemical shift peaks of carbonate hydroxyapatite (CHAP) (3.3 ppm) were detected in powdered enamel treated with topical application agents. CHAP is the major components of enamel mineral (Section 1.2)



**Figure 10.54** –  $^{31}\text{P}$  MAS-NMR spectra of each treatment group before and after pH 4.0 acid challenge.

## 10.4.8 $^{19}\text{F}$ MAS-NMR Analysis

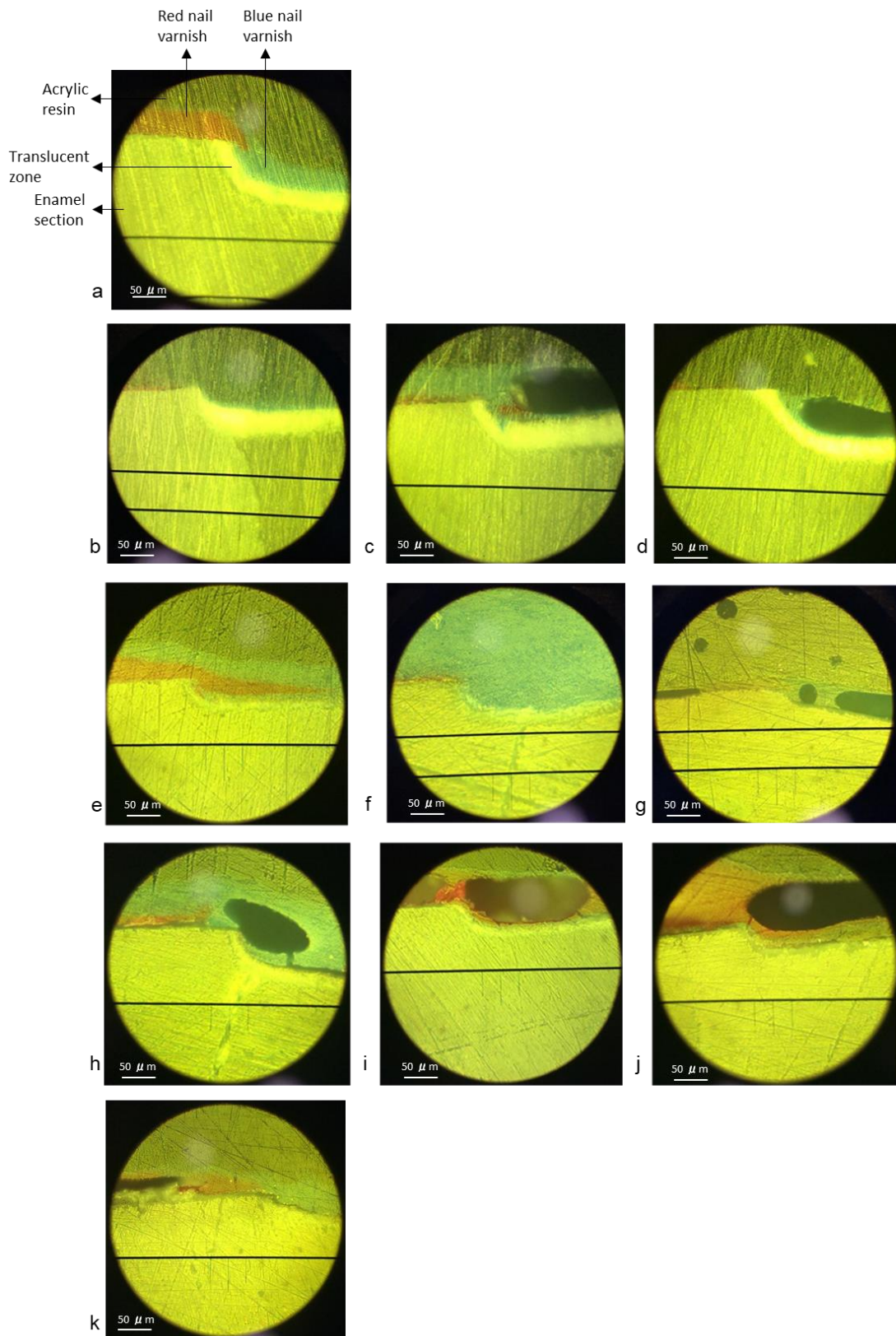
The  $^{19}\text{F}$  MAS-NMR spectra (**Fig. 10.55**) showed that no fluoride compounds were detected in powdered enamel treated with DW or different concentrations of  $\text{AgNO}_3$ . However, both  $\text{CaF}_2$  (-109.1 ppm) and fluorohydroxyapatite (FHA) (-104.1 ppm) were detected in powdered enamel treated with different concentrations of AgF and  $\text{Ag}[\text{NH}_3]_2\text{F}$ , and Riva-SC. The proportions of  $\text{CaF}_2$  detected in AgF treatment groups were higher than those detected in  $\text{Ag}[\text{NH}_3]_2\text{F}$  treatment groups. Further, the proportions of  $\text{CaF}_2$  increased with increasing concentrations of AgF and  $\text{Ag}[\text{NH}_3]_2\text{F}$  topically applied. However, even after long MAS-NMR scans (20 h), only very small amounts of  $\text{CaF}_2$  and FHA were detected, which could not be deconvoluted (Section 5.6).



**Figure 10.55** –  $^{19}\text{F}$  MAS-NMR spectra of each treatment group before and after pH 4.0 acid challenge.

#### 10.4.9 Microscopic photographs of Human Enamel Sections

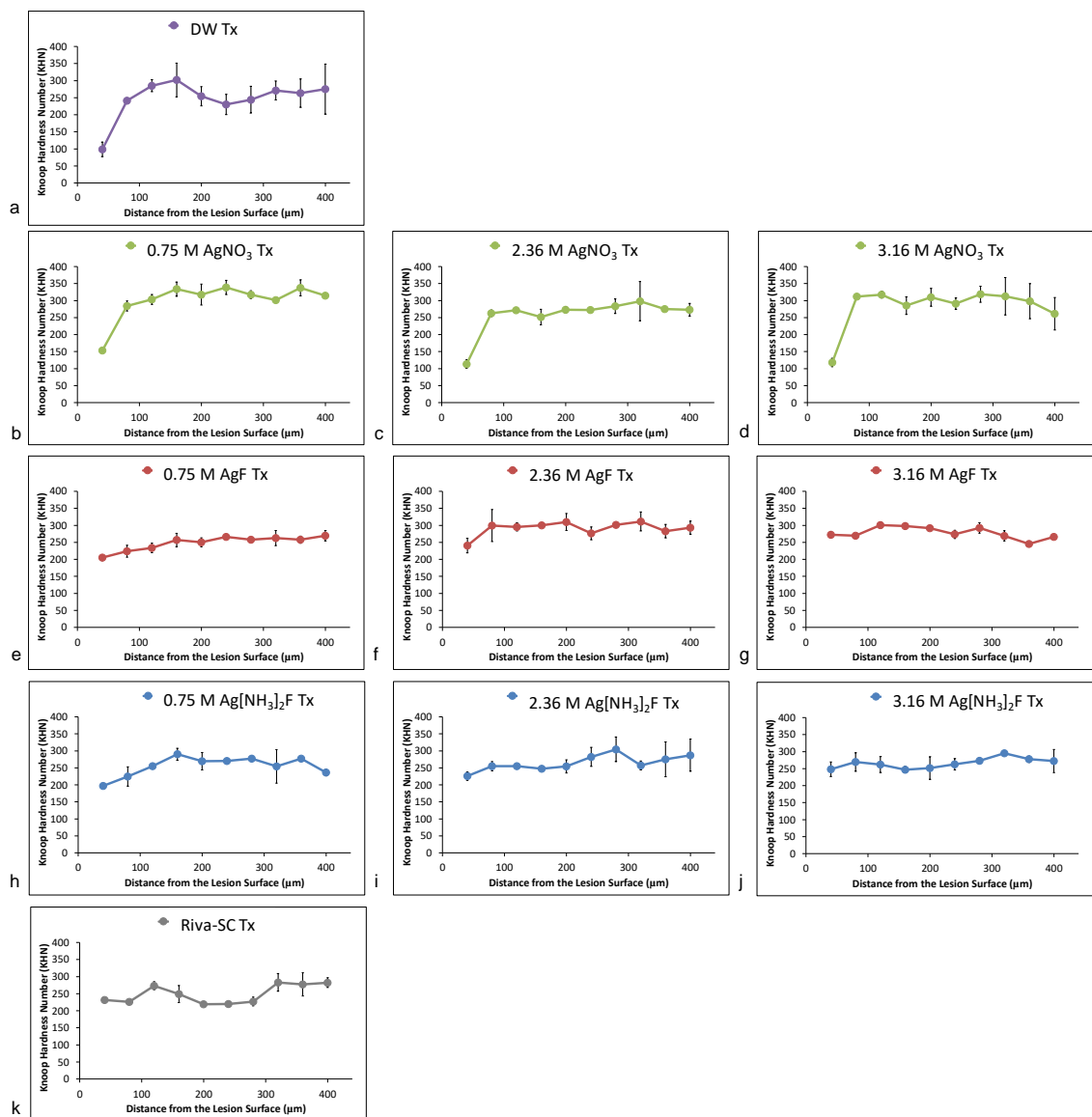
Typical microscopic photographs, taken using a digital camera attached to the eyepiece of the Knoop hardness tester suggested two types of lesions. The first type was a deep erosive-like lesion overlaying a more translucent zone of a carious lesion, observed in the enamel blocks topically treated with DW or AgNO<sub>3</sub> (**Fig. 10.56a ~ Fig. 10.56d**), as described by Larsen (1990). The second type was a shallow erosive-like lesion with or without the presence of a more translucent zone of carious lesion underneath, observed in the enamel blocks topically treated with AgF, Ag[NH<sub>3</sub>]<sub>2</sub>F or Riva-SC (**Fig. 10.56e ~ Fig. 10.56k**).



**Figure 10.56** - Typical images (40X) of lesions sections of (a) DW Tx, (b) 0.75 M AgNO<sub>3</sub> Tx, (c) 2.36 M AgNO<sub>3</sub> Tx and (d) 3.16 M AgNO<sub>3</sub> Tx, (e) 0.75 M AgF Tx, (f) 2.36 M AgF Tx and (g) 3.16 M AgF Tx, (h) 0.75 M Ag[NH<sub>3</sub>]<sub>2</sub>F Tx, (i) 2.36 M Ag[NH<sub>3</sub>]<sub>2</sub>F Tx and (j) 3.16 M Ag[NH<sub>3</sub>]<sub>2</sub>F Tx, and (k) Riva-SC Tx.

## 10.4.10 Knoop CSMH profiles of Human Enamel Sections

The Knoop CSMH profiles (**Fig. 10.57a ~ Fig. 10.57d**) showed that the KHN values recorded at the depth level of 40  $\mu\text{m}$  were low only in DW and  $\text{AgNO}_3$  treatment groups. Whereas, the KHN values recorded at all depth levels along the thickness of enamel sections in AgF,  $\text{Ag}[\text{NH}_3]_2\text{F}$  and Riva-SC treatment groups were high and similar to each other (**Fig. 10.57e ~ Fig. 10.57k**).



**Figure 10.57**– Knoop CSMH of (a) DW Tx, (b ~ d)  $\text{AgNO}_3$  Tx, (e ~ g) AgF Tx and (h ~ j)  $\text{Ag}[\text{NH}_3]_2\text{F}$  Tx in different concentrations, and (k) Riva-SC Tx.



## Chapter 11 DISCUSSION OF THE EFFECTS OF TOPICAL TREATMENTS WITH SILVER COMPOUNDS ON DEMINERALISATION OF HUMAN ENAMEL AND PROPOSED MODELS FOR MECHANISMS

This discussion chapter will be focused on the effects of topical treatments with DW and 3.16 M silver compounds on the demineralisation of human enamel. The dose-response effects of topical treatments with silver compounds on the demineralisation of human enamel will be discussed later in Chapter 12.

The release of  $\text{Ca}^{2+}$  from the demineralising enamel blocks was approximately linear with time (**Fig. 10.5 ~ Fig. 10.15**). This is similar to previous ISE studies on HAP discs (Huang *et al.*, 2018), and SMR results previously reported of enamel mineral loss from enamel during demineralisation (Anderson *et al.*, 1998; Hassanali *et al.*, 2017; Wang *et al.*, 2005).

After demineralisation, the uneven enamel surfaces were observed (**Fig. 10.46a ~ Fig. 10.46k**), which demonstrated the aggressive destruction from the acid attack. Hollow enamel cores, breakages and focal pores were found on the demineralised surfaces, which are typical demineralised enamel lesions reported in previous studies (Wang *et al.*, 2006; Worawongvasu, 2015).

## 11.1 Effects of Topical Treatment with De-ionised Water on Demineralisation of Human Enamel

In the ISE study, following the topical treatment with de-ionised water (DW) on human enamel, the demineralisation of human enamel increased ( $PRCL_{\text{enamel}} = -10.5 \pm 2.4 \%$ ) (**Fig. 10.16**). The increase in demineralisation rate of enamel may be due to the removal of softened human enamel surfaces during the topical application using a micro-brush, which exposed more soluble enamel layers underneath. Deeper layers of enamel are more soluble due to a higher content of destabilising agents such as  $CO_3^{2-}$  and  $Mg^{2+}$  (Robinson *et al.*, 2000) (Section 1.2.1). Therefore, demineralisation of human enamel is accelerated by the abrasion effects from using a micro-brush during the topical treatments.

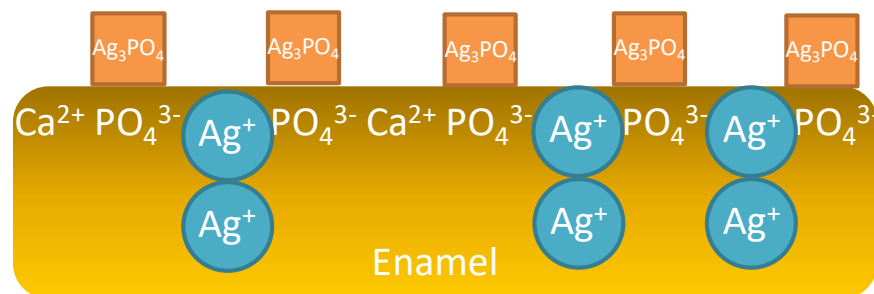
After the ISE study, uneven enamel surfaces with hollow enamel cores were observed with SEM (**Fig. 10.46a**), which demonstrated a typical “honeycomb” erosion lesion, as described by Wang *et al.* (2006) (Section 2.3.2). Deep erosion lesions covering a more translucent zone of carious lesions were observed in the human enamel samples topically treated with DW (**Fig. 10.56a**). Larsen has proposed that when demineralised enamel lesions are produced artificially in aqueous solutions undersaturated with respect to both HAP and fluorapatite (FAP), the outer enamel surface is initially removed by erosion, followed by a uniform development of a carious lesion beneath the erosive lesion, so-called “double lesion” (Larsen, 1990).

As KHN numbers are associated with the mineral content in the tested enamels (Davidson *et al.*, 1974), a double lesion resulting from demineralisation might be the reason for the low Knoop hardness values recorded at the depth levels of 40  $\mu\text{m}$  (around 100 KHN) in enamel sections topically treated with DW (**Fig. 10.57a**), compared to those recorded at deeper levels (around 260 KHN).

## 11.2 Effects of Topical Treatment with AgNO<sub>3</sub> on Demineralisation of Human Enamel and Proposed Mechanistic Models

### 11.2.1 Following Topical Treatment with AgNO<sub>3</sub>

In the ISE study, immediately following topical treatment with 3.16 M AgNO<sub>3</sub> on human enamel, yellow staining was observed on the human enamel surfaces (**Fig. 10.45**), which indicated the formation of yellow Ag<sub>3</sub>PO<sub>4</sub> (Lewis, 1920). This was consistent with the formation of a Ag<sub>3</sub>PO<sub>4</sub> protective barrier on HAP discs topically treated with AgNO<sub>3</sub> reported in Chapter 9. In Chapter 7, Ag<sup>+</sup> was proposed to substitute for the Ca<sup>2+</sup> in human enamel. Therefore, some Ag<sup>+</sup> substituted enamel mineral could also be formed following the topical treatment with 3.16 M AgNO<sub>3</sub>. This is shown schematically in **Fig. 11.1**.



**Figure 11.1** – Schematic representation of an enamel block topically treated with 3.16 M AgNO<sub>3</sub>. Ag<sub>3</sub>PO<sub>4</sub> is formed on the enamel surface and some Ca<sup>2+</sup> in the enamel mineral is substituted by Ag<sup>+</sup>.

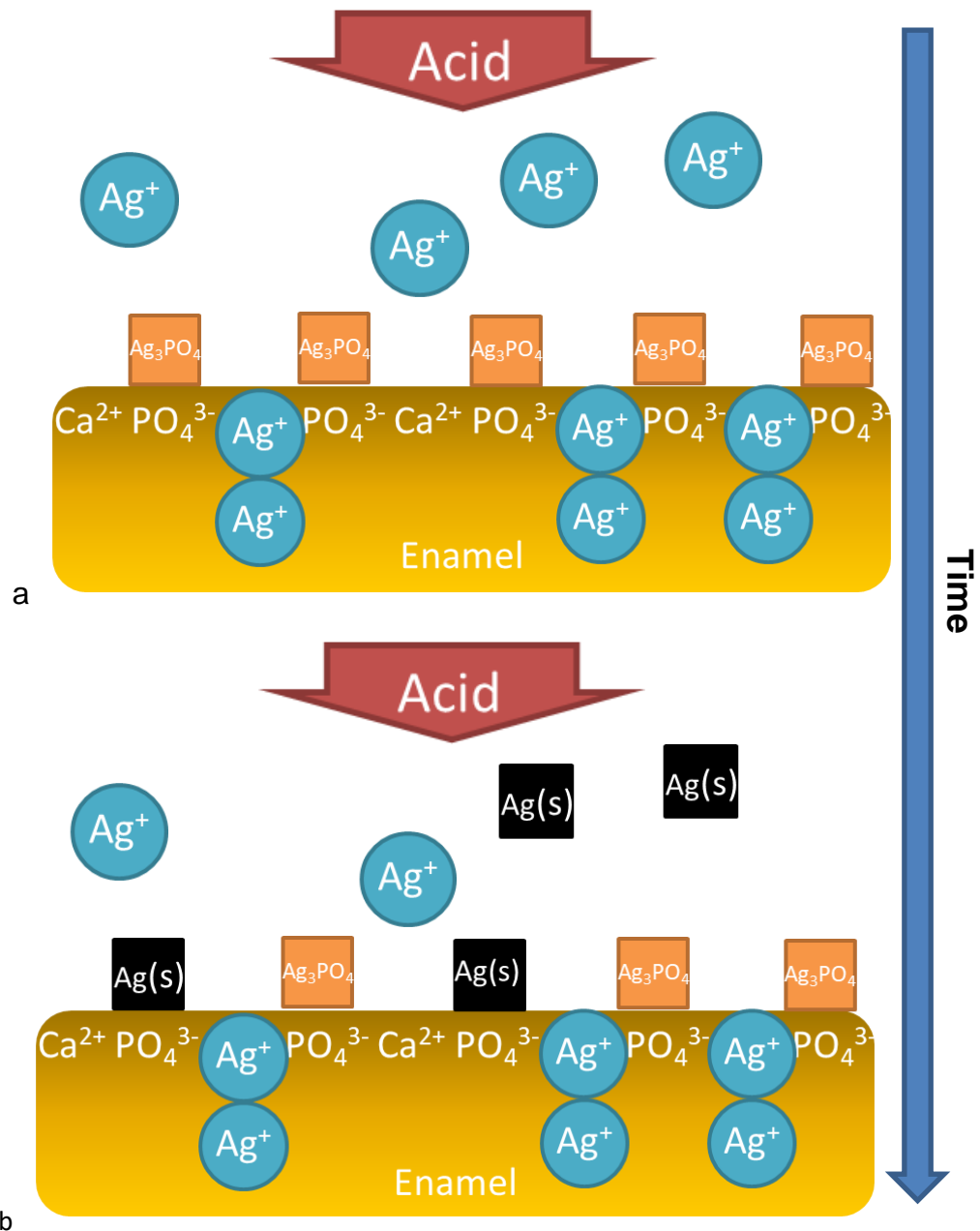
### 11.2.2 After Re-immersion of Human Enamel Topically Treated with AgNO<sub>3</sub> into Acid

After re-immersing the human enamel topically treated with 3.16 M AgNO<sub>3</sub> back into acid, the ISE data showed that there was little change in the rate of Ca<sup>2+</sup> release (PRCL<sub>enamel</sub> = 0.0±5.3 %) (**Fig. 10.16**). This indicated that if 3.16 M AgNO<sub>3</sub> is used in the clinical practice, no inhibitory efficacy of the treatment can

be expected and the cariostatic efficacy of the treatment will only rely on its antibacterial properties (Lansdown, 2002). Even though a  $\text{Ag}_3\text{PO}_4$  protective barrier was formed on the enamel surfaces following  $\text{AgNO}_3$  treatment (Yamaga *et al.*, 1972) (Section 3.2), the inhibitory efficacy against demineralisation was low. The low inhibitory efficacy of the 3.16 M  $\text{AgNO}_3$  topical treatment should be due to the accelerating effects from the micro-brush abrasion during the topical treatment ( $\text{PRCL}_{\text{enamel}} = -10.5 \pm 2.4 \%$ ) (Section 11.1). Further, the formation of  $\text{Ag}^+$  substituted enamel also compromised the inhibitory efficacy (Chapter 7). Gradually, the yellow  $\text{Ag}_3\text{PO}_4$  particles on the treated enamel surfaces were reduced to black metallic silver due to the photosensitivity of  $\text{Ag}^+$ , as described by Liu *et al.* (2012c).

The  $\text{Ag}^+$  released from the enamel sample topically treated with 3.16 M  $\text{AgNO}_3$  was detected with Ag ISEs after the re-immersion of the enamel block back into acid (**Fig. 10.23**). The initial increase in the mean  $\text{Ag}^+$  activity could result from the release of  $\text{Ag}^+$  loosely attached to the enamel surfaces, whereas, the later decrease in the mean  $\text{Ag}^+$  activity could result from chemical reduction of  $\text{Ag}^+$ . The small metallic silver particles reduced from  $\text{Ag}^+$  in the solution will be dispersed due to the agitation of the magnetic stirrer.

**Fig. 11.2a** shows that, after re-immersing the human enamel topically treated with 3.16 M  $\text{AgNO}_3$  back into acid,  $\text{Ag}^+$  loosely attached to the enamel surfaces is released into solution. Further, the  $\text{Ag}_3\text{PO}_4$  protective barrier protects the enamel from demineralisation. **Fig. 11.2b** shows that some  $\text{Ag}^+$  in the solution and some  $\text{Ag}_3\text{PO}_4$  on the enamel surface are gradually reduced to black metallic silver. Further, the metallic silver reduced from the  $\text{Ag}^+$  in the solution will be dispersed in the solution.



**Figure 11.2** – Schematic representation of an enamel block topically treated with 3.16 M  $\text{AgNO}_3$  following re-immersion back into acid. After immersion of a)  $\text{Ag}^+$  loosely attached to enamel surfaces is released into solution. b) Gradually, some  $\text{Ag}_3\text{PO}_4$  on the enamel surface and some  $\text{Ag}^+$  in the solution are reduced to black metallic silver.

### 11.2.3 After Removal of Human Enamel Topically Treated with $\text{AgNO}_3$ from Acid

After removing the enamel block topically treated with 3.16 M  $\text{AgNO}_3$  from acid, SEM images showed that the enamel surfaces were less uneven than the

surfaces topically treated with DW (**Fig. 10.46a** and **Fig. 10.46d**), which demonstrated the inhibitory efficacy of topical treatment with 3.16 M AgNO<sub>3</sub>. Deeper lesions observed on the enamel surfaces may be due to the loss of Ag<sup>+</sup> substituted enamel, which has higher susceptibility than enamel.

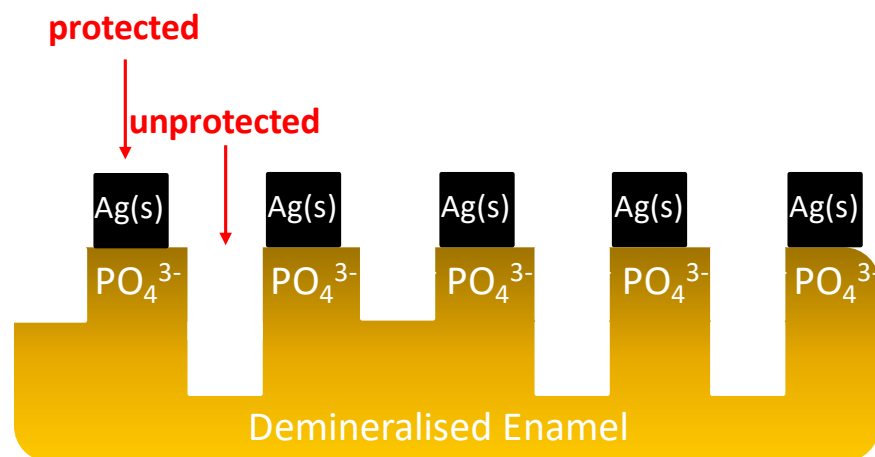
Cubic particles were observed on the enamel surfaces topically treated with 3.16 M AgNO<sub>3</sub> (**Fig. 10.46d**). Lou *et al.* (2011) previously found that cubic Ag<sub>3</sub>PO<sub>4</sub> in the HAP powders mixed with AgNO<sub>3</sub> was gradually reduced to cubic metallic silver. Therefore, in the present study, these cubic particles deposited on the enamel surfaces may be Ag<sub>3</sub>PO<sub>4</sub> or metallic silver. However, as only black staining was observed on the enamel surfaces topically treated with 3.16 M AgNO<sub>3</sub> (**Fig. 10.45**), and no Ag<sub>3</sub>PO<sub>4</sub> was detected with <sup>31</sup>P MAS-NMR in the powdered enamel treated with 3.16 M AgNO<sub>3</sub> (**Fig. 10.54**), most of the Ag<sub>3</sub>PO<sub>4</sub> should be reduced to metallic silver over the post-treatment 4 h demineralisation period.

**Fig. 10.8** shows that, during the post-treatment 4 h demineralisation period, the Ca<sup>2+</sup> release from demineralising human enamel following the 3.16 M AgNO<sub>3</sub> topical treatment was linear with time, even though Ag<sub>3</sub>PO<sub>4</sub> in the protective barrier was gradually reduced to metallic silver. This indicates that the efficacy of topical treatment with 3.16 M AgNO<sub>3</sub> was not subsequently affected by the chemical reduction of Ag<sub>3</sub>PO<sub>4</sub> in the protective barrier to metallic silver. Therefore, the black metallic silver particles reduced from Ag<sub>3</sub>PO<sub>4</sub> particles continued to play the same role as Ag<sub>3</sub>PO<sub>4</sub> particles in the protective barrier during demineralisation. It has been proposed that topical AgNO<sub>3</sub> can lead to formation of a black protective barrier on the treated tooth surface to inhibit demineralisation (Miller, 1905). Further, it has been reported that the black staining of teeth restored with amalgam can lead to the inhibition of dental caries progression (Stebbins, 1891).

The microscopic photographs taken through the eyepiece of the Knoop micro-hardness tester showed “double lesions” in enamel sections topically treated with 3.16 M of AgNO<sub>3</sub> (**Fig. 10.56d**), which were similar to those reported enamel sections topically treated with DW (**Fig. 10.56a**). Further, lower Knoop hardness values were recorded at the depth levels of 40 μm (around 120 KHN) in enamel

sections typically treated with 3.16 M  $\text{AgNO}_3$ , compared to those recorded at deeper levels (around 280 KHN) (**Fig. 10.57d**), which was also similar to the results of DW topical treatment group (**Fig. 10.57a**). This indicates that the inhibitory efficacy of the  $\text{AgNO}_3$  treatment was low. A previous study has also reported that there was no difference between the lesion depths of enamels treated with  $\text{AgNO}_3$  and DW after demineralisation (Liu *et al.*, 2012b).

**Fig. 11.3** shows that, after removing the enamel block topically treated with 3.16 M  $\text{AgNO}_3$  from acid, deeper lesions are developed in the  $\text{Ag}^+$  substituted enamel, therefore uneven demineralised enamel surface is observed. Further, all the  $\text{Ag}_3\text{PO}_4$  on the enamel surface is reduced to metallic silver causing black staining. These metallic silver particles continue to protect the enamel as  $\text{Ag}_3\text{PO}_4$  during the demineralisation.



**Figure 11.3** – Schematic representation of an enamel block topically treated with  $\text{AgNO}_3$  after 4 h demineralisation. Deeper lesions are developed in the substituted enamel, therefore uneven demineralised enamel surface is observed. Further, all the  $\text{Ag}_3\text{PO}_4$  is reduced to black metallic silver causing black staining.

#### 11.2.4 Analysis of the Inhibitory Efficacy of the Topical Treatment with $\text{AgNO}_3$ on Demineralisation of Human Enamel

As discussed in Section 9.2.4, inhibitory efficacy of topical treatment can be influenced by the abrasion effects from using a micro-brush during the topical treatment and the effects of topically applied agent (**Fig. 9.4**). Therefore, as the abrasion effects from using a micro-brush during the topical treatments ( $PRCL_{\text{enamel}} = -10.5 \pm 2.4 \%$ ) accelerated the demineralisation of human enamel, the inhibitory efficacy ( $PRCL_{\text{enamel}} = 0.0 \pm 5.3 \%$ ) observed following the topical treatment with 3.16 M  $AgNO_3$  should totally rely on the effects of topically applied  $AgNO_3$ .

The effects of topically applied  $AgNO_3$  include the effects of the reaction products deposited on the enamel surfaces and the effects of the ions released from the topically treated enamel blocks (**Fig. 9.4**).  $Ag_3PO_4$  particles were formed as a protective barrier on the enamel topically treated with 3.16 M  $AgNO_3$  (Section 11.2.2), which contributed to the inhibitory efficacy. However, as the  $Ag^+$  in the solution released from the treated enamel accelerated the demineralisation of enamel (see Chapter 7), the inhibitory efficacy was compromised. The  $[Ag^+]_{4h}$  in the solution following 3.16 M topical treatment was  $0.95 \pm 0.18$  ppm (**Table 10.9**). According to the log-linear dose-response of  $Ag^+$  on demineralisation of enamel reported previously (**Fig. 7.4**), the effect of the  $Ag^+$  at 0.95 ppm will accelerate the enamel demineralisation by 1.1 % ( $PRML_{\text{enamel}}$ ).

### 11.2.5 Conclusions

In conclusion, Sections 11.2.1, 11.2.2 11.2.3 and 11.2.4 show that the inhibitory efficacy of topical treatment with  $AgNO_3$  on demineralisation of enamel is associated with the formation of a protective barrier composed of  $Ag_3PO_4$ . This is similar to the inhibitory mechanism of topical treatment with  $AgNO_3$  on demineralisation of HAP discs (Chapter 9).

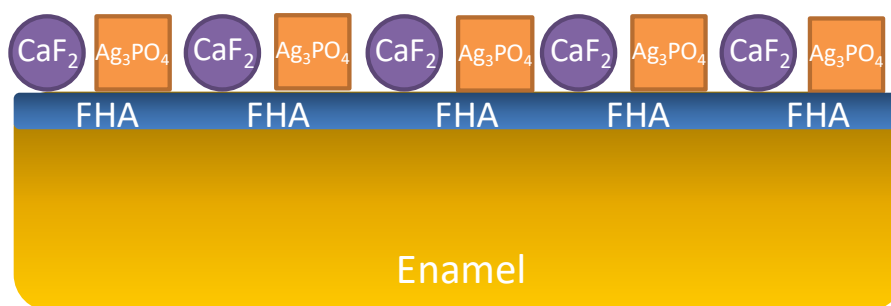
## 11.3 Effects of Topical Treatments with $AgF$ and $Ag[NH_3]_2F$ on Demineralisation of Human Enamel and Proposed Mechanistic Models



### 11.3.1 Following Topical Treatments with AgF and Ag[NH<sub>3</sub>]<sub>2</sub>F

In the ISE study, immediately following topical treatment with 3.16 M AgF and 3.16 M Ag[NH<sub>3</sub>]<sub>2</sub>F on human enamel, yellow staining was observed on the human enamel surfaces (**Fig.10.45**), which indicated the formation of yellow Ag<sub>3</sub>PO<sub>4</sub>. Further, CaF<sub>2</sub> and fluorohydroxyapatite (FHA) in the powdered enamel treated with 3.16 M AgF and 3.16 M Ag[NH<sub>3</sub>]<sub>2</sub>F were also detected with <sup>19</sup>F MAS-NMR (**Fig. 10.55**). These powdered enamel samples were collected after the ISE study. As the [F<sup>-</sup>]<sub>4h</sub> of 3.16 M AgF and 3.16 M Ag[NH<sub>3</sub>]<sub>2</sub>F treatment groups during the post-treatment 4 h demineralisation periods of the ISE study were too low (< 1 ppm) (**Table 10.11**) to facilitate the formation of CaF<sub>2</sub> (Rosin-Grget *et al.*, 2013) (Section 2.4), these CaF<sub>2</sub> and FHA should be formed during topical treatments. It has been reported that, under pH 4.0 acid challenge, CaF<sub>2</sub> (with minor FHA) could be predominantly formed on human enamel *only* when the concentration of F<sup>-</sup> in the solution was above 135 ppm (Mohammed *et al.*, 2013). Previous study has found Ag<sub>3</sub>PO<sub>4</sub> and CaF<sub>2</sub> in enamel powder mixed with Ag[NH<sub>3</sub>]<sub>2</sub>F (Suzuki *et al.*, 1974). However, no FHA was found due to the limitation of characterisation ability of X-ray diffraction analysis (XRD).

Therefore, the CaF<sub>2</sub> and FHA participate in the formation of the protective barrier following 3.16 M AgF and 3.16 M Ag[NH<sub>3</sub>]<sub>2</sub>F topical treatments. As Ca<sup>2+</sup> lost from enamel due to the formation of Ag<sup>+</sup> substituted enamel can be preserved as CaF<sub>2</sub>, and unstable Ag<sup>+</sup> substituted enamel can be replaced by more stable FHA (Robinson, 2009), enamel blocks topically treated with 3.16 M AgF, and 3.16 M Ag[NH<sub>3</sub>]<sub>2</sub>F should be better protected against demineralisation than those topically treated with 3.16 M AgNO<sub>3</sub>. This is shown schematically in **Fig. 11.4**.



**Figure 11.4** – Schematic representation of an enamel block topically treated with AgF or Ag[NH<sub>3</sub>]<sub>2</sub>F. Ag<sub>3</sub>PO<sub>4</sub>, CaF<sub>2</sub> and FHA are formed on the enamel surface.

### 11.3.2 After Re-immersion of Human Enamel Topically Treated with AgF and Ag[NH<sub>3</sub>]<sub>2</sub>F into Acid

After re-immersing the human enamel topically treated with 3.16 M AgF and 3.16 M Ag[NH<sub>3</sub>]<sub>2</sub>F back into acid, the ISE data showed that there was an immediate reduction in the rate of Ca<sup>2+</sup> release (**Fig. 10.11** and **Fig 10.14**). The mean PRCL<sub>enamel</sub> of the 3.16 M AgF and 3.16 M Ag[NH<sub>3</sub>]<sub>2</sub>F (65.6±6.1 % and 65.3±3.3 %) were much higher than that of the 3.16 M AgNO<sub>3</sub> treatment group (0.0±5.3 %) (**Fig. 10.16**), showing that the inhibitory efficacy of F<sup>-</sup> was greater than that of Ag<sup>+</sup>. Previous studies also found that Ag[NH<sub>3</sub>]<sub>2</sub>F treated demineralised enamel block released less Ca<sup>2+</sup> into demineralisation solution leading to less mineral loss (Wu and Yang, 2002, Rosas et al., 2014). The pronounced inhibitory efficacy of topical treatments with these fluoride-containing silver compounds should be associated with the additional deposition of CaF<sub>2</sub> and the formation of acid-resistant FHA (Arends and Christoffersen, 1990; ten Cate, 1997) (Section 2.4). Therefore, the inhibitory efficacy of topical treatment with 3.16 M AgF and 3.16 M Ag[NH<sub>3</sub>]<sub>2</sub>F are associated with the formation of a protective barrier composed of Ag<sub>3</sub>PO<sub>4</sub>, CaF<sub>2</sub> and FHA. Gradually, yellow Ag<sub>3</sub>PO<sub>4</sub> on the treated enamel surfaces was reduced to black metallic silver due to the photosensitivity of Ag<sup>+</sup>, as described by Liu *et al.* (2012c).

The Ag<sup>+</sup> released from the human enamel topically treated with 3.16 M AgF, and 3.16 M Ag[NH<sub>3</sub>]<sub>2</sub>F were detected with Ag<sup>+</sup> ISEs after the re-immersion of the enamel back into acid (**Fig. 10.23**). As mentioned in 3.16 M AgNO<sub>3</sub> treatment group (Section 11.2.2), the initial increase in the mean Ag<sup>+</sup> activity could result

from the release of  $\text{Ag}^+$  loosely attached to the enamel surfaces, whereas, the later decrease in the mean  $\text{Ag}^+$  activity could result from chemical reduction of  $\text{Ag}^+$ . These metallic silver particles will be dispersed in the solution due to the agitation of the magnetic stirrer.

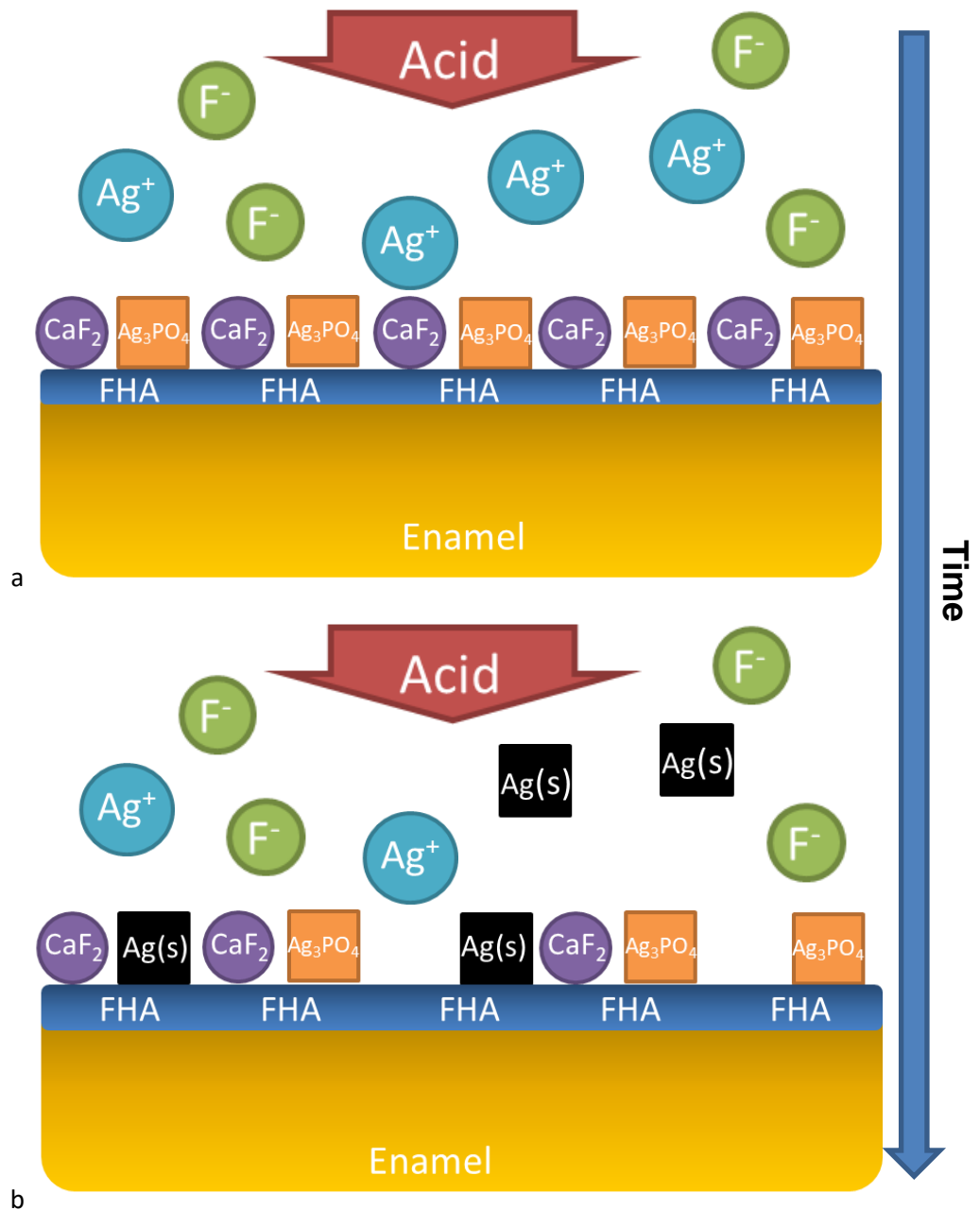
**Fig. 10.27a** and **b** shows that the increase rate of  $\text{Ag}^+$  activities and the later decrease rate of  $\text{Ag}^+$  activities following 3.16 M  $\text{AgF}$  and 3.16 M  $\text{Ag}[\text{NH}_3]_2\text{F}$  topical treatments were similar. This indicates that the ability of ammonia in hindering the chemical reduction of  $\text{Ag}^+$  was not obvious following the  $\text{Ag}[\text{NH}_3]_2\text{F}$  topical treatment (Liu *et al.*, 2012b) (Section 3.4). Similar  $\text{Ag}^+$  release profiles explain why there were no significant differences between the  $[\text{Ag}^+]_{4\text{h}}$  of 3.16 M  $\text{AgF}$  and 3.16 M  $\text{Ag}[\text{NH}_3]_2\text{F}$  treatment groups (**Fig. 10.31**). Therefore, the effects of  $\text{Ag}^+$  in the solution on both 3.16 M  $\text{AgF}$  and 3.16 M  $\text{Ag}[\text{NH}_3]_2\text{F}$  topically treated enamel blocks should be similar.

The  $\text{F}^-$  released from the human enamel topically treated with 3.16 M  $\text{AgF}$ , and 3.16 M  $\text{Ag}[\text{NH}_3]_2\text{F}$  were detected with  $\text{F}^-$  ISEs after the re-immersion of the enamel back into acid (**Fig. 10.35**). The initial increase in the mean  $\text{F}^-$  activity could result from the release of  $\text{F}^-$  loosely attached to the enamel surfaces (Arends and Christoffersen, 1990; Dijkman *et al.*, 1982), whereas, the later increase in the mean  $\text{F}^-$  activity could result from the slow dissolution of  $\text{CaF}_2$ -like globules ( $\text{CaF}_2$  with the adsorption of  $\text{HPO}_4^{2-}$ ), favouring the formation of FHA (ten Cate, 2013; Vogel, 2011) (Section 2.4). The rates of initial  $\text{F}^-$  release from human enamel (**Fig. 10.35**) are faster than the rates of initial  $\text{F}^-$  release from HAP discs observed in chapter 8 (**Fig. 8.13**). This may be due to the porosity of human enamel (about 1 ~ 2 %) being lower than that of HAP discs (about 20 %), so the diffusion of  $\text{F}^-$  from the human enamel is faster due to reduced adsorption ability of  $\text{F}^-$  to the human enamel.

**Fig. 10.38a** and **b** shows that the initial increase rate of  $\text{F}^-$  activity following 3.16 M  $\text{Ag}[\text{NH}_3]_2\text{F}$  topical treatment was faster than that following 3.16 M  $\text{AgF}$  topical treatment. However, the later increase rate of  $\text{F}^-$  activity following 3.16 M  $\text{Ag}[\text{NH}_3]_2\text{F}$  topical treatment was slower than that following 3.16 M  $\text{AgF}$  topical treatment. This may be due to that the proportion of  $\text{CaF}_2$  without the adsorption of  $\text{HPO}_4^{2-}$ , which has higher solubility, formed following 3.16 M  $\text{Ag}[\text{NH}_3]_2\text{F}$  topical

treatment was higher than that following 3.16 M AgF topical treatment, leading to faster initial  $F^-$  release. Further, the proportion of  $CaF_2$  with the adsorption of  $HPO_4^{2-}$  ( $CaF_2$ -like globule) formed following 3.16 M  $Ag[NH_3]_2F$  topical treatment was lower than that following 3.16 M AgF topical treatment, leading slower later  $F^-$  release. The much faster initial  $F^-$  release following 3.16 M  $Ag[NH_3]_2F$  topical treatment resulted in significant higher  $[F^-]_{4h}$  than that detected following 3.16 M AgF topical treatment (**Fig. 10.41**). Therefore, the effects of  $F^-$  in the solution on 3.16 M  $Ag[NH_3]_2F$  topically treated enamel blocks should be higher than those on 3.16 M AgF topically treated enamel blocks. Less  $CaF_2$ -like globules formed following 3.16 M  $Ag[NH_3]_2F$  topical treatment may be due to the interference of the adsorption of  $HPO_4^{2-}$  around  $CaF_2$  surfaces. The most likely interference factor could be the ammonium ( $NH_4^+$ ) dissolved from the  $Ag[NH_3]_2F$ . However, further studies are required to confirm the postulation.

**Fig. 11.5a** shows that, after re-immersing the human enamel topically treated with 3.16 M AgF or 3.16 M  $Ag[NH_3]_2F$  back into acid, both  $Ag^+$  and  $F^-$  loosely attached to enamel surface are released into solution. Further, the protective barrier composed of  $Ag_3PO_4$ ,  $CaF_2$  and FHA protects the enamel from demineralisation. **Fig. 11.5b** shows that some  $Ag^+$  in the solution and some  $Ag_3PO_4$  on the enamel surface are gradually reduced to metallic silver. Further, some  $CaF_2$  on the enamel surface is gradually dissolved, providing  $F^-$  for further formation of FHA.



**Figure 11.5** – Schematic representation of an enamel block topically treated with  $\text{AgF}$  or  $\text{Ag}[\text{NH}_3]_2\text{F}$  following re-immersion back into acid. a) Both  $\text{Ag}^+$  and  $\text{F}^-$  loosely attached to enamel surface are released into solution. b) Gradually, some  $\text{Ag}_3\text{PO}_4$  on the enamel surface and some  $\text{Ag}^+$  in the solution are reduced to metallic silver, and some  $\text{CaF}_2$  on the enamel surface is dissolved, providing  $\text{F}^-$  for further formation of FHA.

### 11.3.3 After Removal of Human Enamel Topically Treated with AgF and Ag[NH<sub>3</sub>]<sub>2</sub>F from Acid

After removing the human enamel topically treated with 3.16 M AgF and 3.16 M Ag[NH<sub>3</sub>]<sub>2</sub>F from acid, SEM images showed that the enamel surfaces were less uneven than those topically treated with 3.16 M AgNO<sub>3</sub> (**Fig. 10.46d**, **Fig. 10.46g** and **Fig. 10.46j**), which demonstrated that the inhibitory efficacy of F<sup>-</sup> was greater than that of Ag<sup>+</sup>.

Cubic and granular particles were observed on the enamel surfaces (**Fig. 10.46g** and **Fig. 10.46j**). These cubic particles should mostly be black cubic metallic silver rather than yellow cubic Ag<sub>3</sub>PO<sub>4</sub> (Lou *et al.*, 2011), as only black staining was observed on the enamel surfaces (**Fig. 10.45**), and no Ag<sub>3</sub>PO<sub>4</sub> was detected with <sup>31</sup>P MAS-NMR in the powdered enamel treated with 3.16 M AgF and 3.16 M Ag[NH<sub>3</sub>]<sub>2</sub>F (**Fig. 10.54**). This indicates that most of the Ag<sub>3</sub>PO<sub>4</sub> was chemically reduced to metallic silver during the post-treatment 4 h demineralisation period. Black staining of the AgF or Ag[NH<sub>3</sub>]<sub>2</sub>F treated dental lesions has been reported by multiple clinical and *in vitro* studies (Peng *et al.*, 2012, Chu *et al.*, 2014, Zhao *et al.*, 2017). On the other hand, the granular particles should be CaF<sub>2</sub>-like globules (Buzalaf *et al.*, 2011; Rolla and Saxegaard, 1990) (Section 2.4). These CaF<sub>2</sub>-like globules sometimes clustered as an agglomeration on the treated enamel surfaces (Navarro *et al.*, 2001), as could be seen on the enamel surfaces treated with 3.16 M Ag[NH<sub>3</sub>]<sub>2</sub>F (**Fig. 10.46j**).

The mean atomic percentage of Ag detected on the enamel surfaces topically treated with 3.16 M AgF was significantly higher than that of 3.16 M AgNO<sub>3</sub> (**Fig. 10.47**). This indicates that following 3.16 M AgF topical treatment, which facilitated the CaF<sub>2</sub> formation (**Fig. 10.55**), more Ag<sub>3</sub>PO<sub>4</sub> was formed due to the further PO<sub>4</sub><sup>3-</sup> release from the dissociation of enamel (Mohammed *et al.*, 2013). These Ag<sub>3</sub>PO<sub>4</sub> particles were then reduced to metallic silver to be detected with EDX. The mean atomic percentage of Ag detected on the enamel surfaces topically treated with 3.16 M Ag[NH<sub>3</sub>]<sub>2</sub>F was significantly lower than that of 3.16 M AgF (**Fig. 10.47**). It may be due to that Ag<sub>3</sub>PO<sub>4</sub> can be dissolved in ammonium

(Firsching, 1961) (Section 3.4.2). Therefore less metallic silver could be reduced from  $\text{Ag}_3\text{PO}_4$  following 3.16 M  $\text{Ag}[\text{NH}_3]_2\text{F}$  treatment.

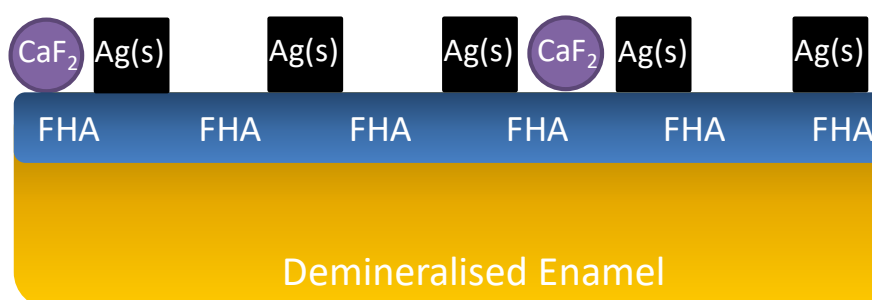
The mean atomic percentage of F detected on the enamel surfaces topically treated with 3.16 M AgF was significantly higher than that of 3.16 M  $\text{Ag}[\text{NH}_3]_2\text{F}$  treatment group (**Fig. 10.51**), which was consistent with higher proportions of  $\text{CaF}_2$  detected in powdered enamel treated with 3.16 M AgF than those treated with 3.16 M  $\text{Ag}[\text{NH}_3]_2\text{F}$  (**Fig. 10.55**). The lower mean atomic percentage of F detected on the 3.16 M  $\text{Ag}[\text{NH}_3]_2\text{F}$  topically treated enamel surfaces should be due to the faster initial  $\text{F}^-$  release (**Fig. 10.38a**), as discussed in Section 11.3.2.

**Fig. 10.11** and **Fig. 10.14** show that, during the post-treatment 4 h demineralisation period, the inhibited  $\text{Ca}^{2+}$  release from demineralising human enamel following the topical treatments with 3.16 M AgF and 3.16 M  $\text{Ag}[\text{NH}_3]_2\text{F}$  was linear with time, even though  $\text{Ag}_3\text{PO}_4$  in the protective barrier was chemically reduced and  $\text{CaF}_2$  in the protective barrier was dissolved. This indicates that the inhibitory efficacy of topical treatments with these fluoride-containing silver compounds was not subsequently affected by the chemical reduction of  $\text{Ag}_3\text{PO}_4$  to metallic silver and the dissolution of  $\text{CaF}_2$ . As mentioned in Section 11.2.3, the metallic silver particles reduced from  $\text{Ag}_3\text{PO}_4$  particles continue to play the same role as the  $\text{Ag}_3\text{PO}_4$  particles in the protective barrier. Therefore, further FHA formation due to the supply of  $\text{F}^-$  from  $\text{CaF}_2$  dissolution should compensate for the protective effect lost from the dissolution of  $\text{CaF}_2$  particles in the protective barrier.

Using the microscopy of the Knoop micro-hardness tester, the lesions observed in enamel sections topically treated with 3.16 M AgF, 3.16 M  $\text{Ag}[\text{NH}_3]_2\text{F}$  were all shallower (**Fig. 10.56g** and **j**) than those observed in 3.16 M  $\text{AgNO}_3$  treatment group (**Fig. 10.56d**). This should be due to the participation of  $\text{F}^-$ . Larsen has proposed that in a solution with a higher concentration of  $\text{F}^-$ , the artificial demineralised erosive lesion is shallower (Larsen, 1990). It has been reported that  $\text{F}^-$  of  $\text{Ag}[\text{NH}_3]_2\text{F}$  can penetrate intact human enamel up to a depth of 20  $\mu\text{m}$  (Suzuki et al., 1974). In the present study, the penetration depth of  $\text{F}^-$  should be higher as  $\text{Ag}[\text{NH}_3]_2\text{F}$  was applied on *demineralised* enamel surfaces. The Knoop CSMH profiles of enamel sections topically treated with 3.16 M AgF, and 3.16 M

Ag[NH<sub>3</sub>]<sub>2</sub>F (**Fig. 10.57g** and **j**) all had similar KHN values (around 280 KHN) along the entire depth from lesion surfaces, which is due to the pronounced protective effect of these fluoride-containing silver compound topical treatments. A previous study also found that Ag[NH<sub>3</sub>]<sub>2</sub>F treated enamel block immersed in lactic acid for two days had less lesion depth and increased micro-hardness compared to the negative control group (Li et al., 1984). Further, it has been proposed that carious enamel treated with Ag[NH<sub>3</sub>]<sub>2</sub>F had increased micro-hardness up to a depth of about 150  $\mu$  m, compared to lesions treated with de-ionised water (Zhao et al., 2017).

**Fig. 11.6** shows that, after removing the human enamel topically treated with 3.16 AgF or 3.16 M Ag[NH<sub>3</sub>]<sub>2</sub>F from acid, all the Ag<sub>3</sub>PO<sub>4</sub> on the enamel is reduced to metallic silver causing black staining. Further, most of the CaF<sub>2</sub> is dissolved, which favours further formation of FHA. The enamel surface covered by the metallic silver, CaF<sub>2</sub> and FHA is protected during the demineralisation.



**Figure 11.6** – Schematic representation of an enamel block topically treated with AgF or Ag[NH<sub>3</sub>]<sub>2</sub>F after 4 h demineralisation. All the Ag<sub>3</sub>PO<sub>4</sub> is reduced to metallic silver causing black staining and most of the CaF<sub>2</sub> is dissolved which favours further formation of FHA.

### 11.3.4 Analysis of the Inhibitory Efficacy of the Topical Treatments with AgF, Ag[NH<sub>3</sub>]<sub>2</sub>F and Riva-SC on Demineralisation of Human Enamel

As discussed in Section 9.2.4, the inhibitory efficacy of the topical treatment on demineralisation can be influenced by the abrasion effects from using a micro-brush during the topical treatment and the effects of topical application agent (**Fig.**



**9.4).** However, as the abrasion effect of topical treatment accelerates the demineralisation of human enamel by  $10.5 \pm 2.4$  %, the inhibitory efficacy of topical treatments with 3.16 M AgF ( $PRCL_{\text{enamel}} = 65.6 \pm 6.1$  %) and 3.16 M Ag[NH<sub>3</sub>]<sub>2</sub>F ( $PRCL_{\text{enamel}} = 65.3 \pm 3.3$  %) should all be attributed to the effects of topical application agents.

The effects of topical application agents include the effects of the reaction products deposited on the enamel surfaces and the effects of the ions released from the topically treated enamel (**Fig. 9.4**). Ag<sub>3</sub>PO<sub>4</sub>, CaF<sub>2</sub> and FHA were formed as a protective barrier on the enamel topically treated with 3.16 M AgF and 3.16 M Ag[NH<sub>3</sub>]<sub>2</sub>F (Section 11.3.1), which contributed to the inhibitory efficacy.

After re-immersing the enamel topically treated with these fluoride-containing silver compounds back into acids, both Ag<sup>+</sup> and F<sup>-</sup> were released. The [Ag<sup>+</sup>]<sub>4h</sub> of 3.16 M AgF and 3.16 M Ag[NH<sub>3</sub>]<sub>2</sub>F treatment groups were  $\approx 0.89 \pm 0.27$  ppm and  $\approx 0.78 \pm 0.06$  ppm (**Table 10.9**). Therefore, according to the log-linear dose-response of Ag<sup>+</sup> on demineralisation of enamel (**Fig. 7.4**), the effects of the Ag<sup>+</sup> at 0.89 ppm and 0.78 ppm will accelerate the enamel demineralisation by 0.90 % and 0.59 % ( $PRML_{\text{enamel}}$ ), respectively. On the other hand, the [F<sup>-</sup>]<sub>4h</sub> of 3.16 M AgF and 3.16 M Ag[NH<sub>3</sub>]<sub>2</sub>F treatment groups were  $\approx 0.34 \pm 0.03$  ppm and  $\approx 0.42 \pm 0.02$  ppm (**Table 10.11**). Therefore, according to the log-linear dose-response of F<sup>-</sup> on demineralisation of enamel (**Fig. 6.7b**), the effects of the F<sup>-</sup> at 0.34 ppm and 0.42 ppm will inhibit the demineralisation by 29.91 % and 32.18 % ( $PRML_{\text{enamel}}$ ), respectively.

Even though the inhibitory efficacy ( $PRML_{\text{enamel}}$ ) resulting from the F<sup>-</sup> in solution following 3.16 M AgF topical treatment is lower than that following 3.16 M Ag[NH<sub>3</sub>]<sub>2</sub>F topical treatment, the  $PRCL_{\text{enamel}}$  of topical treatments with 3.16 M AgF and 3.16 M Ag[NH<sub>3</sub>]<sub>2</sub>F were similar (**Fig. 10.16**). Therefore, the inhibitory efficacy from the protective barrier formed on the human enamel surfaces topically treated with 3.16 M AgF was higher than that formed on the human enamel surfaces topically treated with 3.16 M Ag[NH<sub>3</sub>]<sub>2</sub>F, This is consistent with higher amounts of silver and fluoride compounds detected on the 3.16 M AgF topically treated enamel surfaces (**Fig. 10.47** and **Fig. 10.51**),

### 11.3.5 Conclusions

In conclusion, Sections 11.3.1, 11.3.2 11.3.3 and 11.3.4 show that the inhibitory efficacy of topical treatments with 3.16 M AgF and 3.16 M Ag[NH<sub>3</sub>]<sub>2</sub>F on demineralisation of human enamel is associated with the release of F<sup>-</sup> from the topically treated enamel surfaces and the formation of a protective barrier composed of Ag<sub>3</sub>PO<sub>4</sub>, CaF<sub>2</sub> and FHA. This is similar to the inhibitory mechanisms of topical treatment with AgF and Ag[NH<sub>3</sub>]<sub>2</sub>F on demineralisation of HAP discs (Chapter 9).

## 11.4 Difference Between the Effects of Topical Treatments with Riva-SC and 3.16 M Ag[NH<sub>3</sub>]<sub>2</sub>F on Demineralisation of Human enamel

The effects of topical treatment with Riva-SC (3.16 M Ag[NH<sub>3</sub>]<sub>2</sub>F, Silver Capsule of Riva Star SDI Ltd, Australia) on demineralisation of human enamel were similar to those of laboratory-prepared 3.16 M Ag[NH<sub>3</sub>]<sub>2</sub>F (**Fig. 10.14 ~ Fig. 10.57**). This suggests that they have the same inhibitory mechanism on the demineralisation of human enamel (**Fig. 11.4 ~ Fig. 11.6**). However, the mean atomic percentage of Ag detected on the enamel surfaces topically treated with Riva-SC was not significantly different from other treatment groups (**Fig. 10.47**). This may be due to that the composition of each Silver Capsules of Riva Star used in the study was not consistent. Therefore, a higher sample size is required to show the statistical differences. Further, the mean atomic percentage of F of Riva-SC treatment group was higher than that of 3.16 M Ag[NH<sub>3</sub>]<sub>2</sub>F treatment group (**Fig. 10.51**). This may be due to that the ammonia contents in some Silver Capsules of Riva Star were lower than that in the laboratory-prepared 3.16 M Ag[NH<sub>3</sub>]<sub>2</sub>F (as discussed in Section 11.3.2).

## 11.5 Conclusions

In conclusion, the inhibitory mechanism of topical treatment with  $\text{AgNO}_3$  on human enamel is associated with the formation of a  $\text{Ag}_3\text{PO}_4$  protective barrier. Whereas, the inhibitory mechanism of topical treatment with  $\text{AgF}$  or  $\text{Ag}[\text{NH}_3]_2\text{F}$  is associated with the  $\text{F}^-$  released from the topically treated enamel and the formation of a protective barrier, composed of  $\text{Ag}_3\text{PO}_4$ ,  $\text{CaF}_2$  and FHA. The inhibitory mechanisms of topical treatments with silver compounds on demineralisation of human enamel are similar to those of HAP discs.

The effects of topical treatment with Silver Capsule of Riva Star (3.16 M SDF, SDI Ltd, Australia) on demineralisation of human enamel are similar to those of topical treatment with laboratory-prepared 3.16 M  $\text{Ag}[\text{NH}_3]_2\text{F}$ .

## **Chapter 12 DISCUSSION OF DOSE-RESPONSE EFFECTS OF TOPICAL TREATMENTS WITH SILVER COMPOUNDS ON DEMINERALISATION OF HUMAN ENAMEL AND PROPOSED MODELS FOR MECHANISMS**

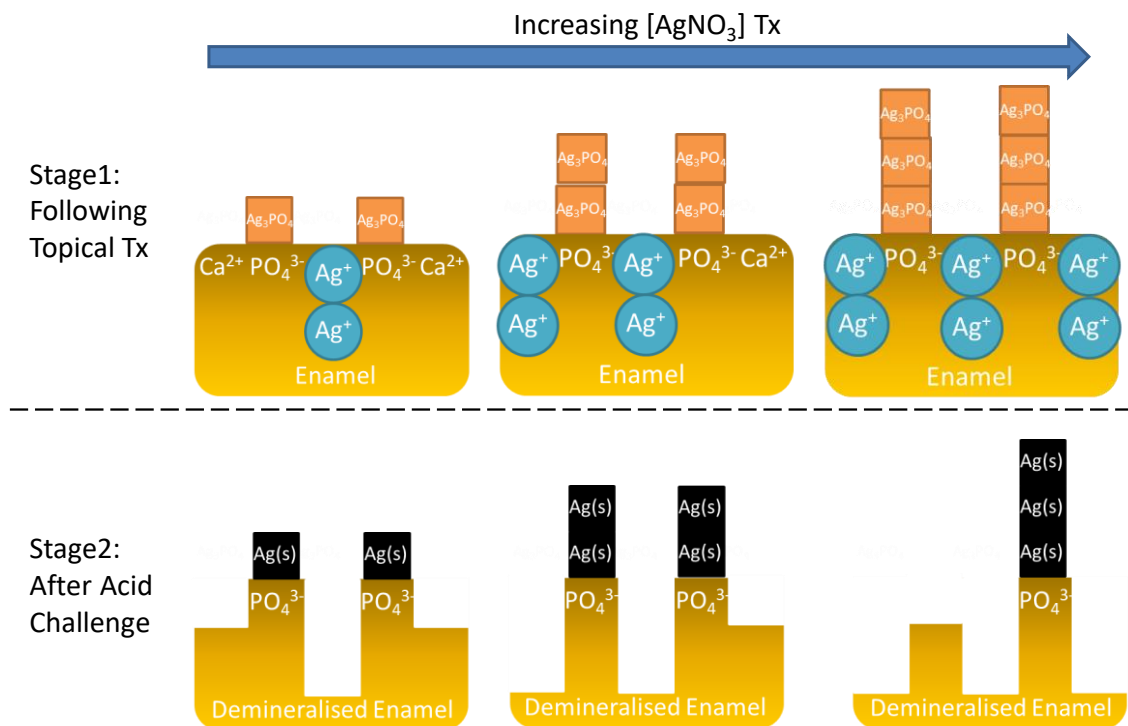
The effects of topical treatments with 2.36 M, 0.75 M and 3.16 M of these silver compounds on enamel demineralisation were investigated (Chapter 10), in order to understand the dose-response mechanisms of topical treatments with  $\text{AgNO}_3$ ,  $\text{AgF}$  and  $\text{Ag}[\text{NH}_3]_2\text{F}$  on demineralisation of human enamel. These concentrations are the same as those used in the commercial silver compounds such as Caristop 12% (0.75 M  $\text{Ag}[\text{NH}_3]_2\text{F}$ , Biodinamica Química E Farmacéutica Ltda), Saforide (2.36 M  $\text{Ag}[\text{NH}_3]_2\text{F}$ , Toyo Seiyaku Kasei Co. Ltd) and Riva Star (3.16 M  $\text{Ag}[\text{NH}_3]_2\text{F}$ , SDI Ltd, Australia) (Fung et al., 2013, SDI, 2016a). Therefore, the dose-response results reported in this study were clinically relevant to the topical treatment outcomes using these concentrations of silver compounds.

## 12.1 Dose-response Effects of Topical Treatment with AgNO<sub>3</sub> on Demineralisation of Human Enamel and Proposed Mechanistic Models

The Ca<sup>2+</sup> ISE data (**Fig. 10.17**) showed that the mean PRCL<sub>enamel</sub> of topical treatment with AgNO<sub>3</sub> *decreased* with increasing concentration. The SEM images also demonstrated similar dose-response (**Fig. 10.46b ~ d**). Craters and breakages observed on the surfaces topically treated with 3.16 M AgNO<sub>3</sub> (**Fig. 10.46d**) were larger and deeper than those observed on the enamel surfaces topically treated with 2.36 M AgNO<sub>3</sub> (**Fig. 10.46c**). Further, on the enamel surfaces topically treated with 0.75 M AgNO<sub>3</sub>, only uneven surfaces were observed (**Fig. 10.46b**). No dose-response was observed in the enamel sections and the Knoop CSMH profiles (**Fig. 10.56b ~ d** and **Fig. 10.57b ~ d**), as the change in the inhibitory efficacy was too small. A previous study reported that 5 min immersion of human enamel blocks in 2.36 M AgNO<sub>3</sub> led to negligible inhibition efficacy in demineralisation at pH 4.4 (Liu *et al.*, 2012b), which is different from the PRCL<sub>enamel</sub> (= 4.6±5.9 %) of the 2.36 M AgNO<sub>3</sub> topical treatment observed in the present study. This may be due to the inhibitory efficacy of the agent in their study being based on the reduction in the lesion depth measured with Micro-CT, whereas, the inhibitory efficacy in the present study was based on the subtle change in the rates of Ca<sup>2+</sup> release. This may explain the lower inhibitory efficacy of the topical 2.36 M AgNO<sub>3</sub> treatment observed in the present study.

Cubic metallic silver particles (reduced from Ag<sub>3</sub>PO<sub>4</sub>) found on the enamel surfaces topically treated with higher concentrations of AgNO<sub>3</sub> were larger and more packed together (**Fig. 10.46b ~ d**), leading to the darker black staining observed on the enamel surfaces (**Fig. 10.45**), which indicates that the components in the protective barrier accumulated with increasing concentration of topically applied AgNO<sub>3</sub>. The increased protective barrier would lead to increased inhibitory efficacy, which contradicts the dose-response of (PRCL<sub>enamel</sub>) observed in the Ca<sup>2+</sup> ISE data (**Fig. 10.17**).

The conflict can be explained by the loss of the protective barrier formed on the lost enamel structures due to the formation of craters and breakages. As more enamel structures were lost following the topical treatment with higher concentrations of topically applied  $\text{AgNO}_3$  (**Fig. 10.46b ~ d**), leading to the loss of protective barrier, the inhibitory efficacy of the treatment decreased (**Fig. 10.17**). This is consistent with the decreased mean percentage of Ag detected on enamel surfaces topically treated with 3.16 M  $\text{AgNO}_3$  ( $0.96 \pm 0.12$  %), compared to that detected on those topically treated with 2.36 M  $\text{AgNO}_3$  ( $1.09 \pm 0.28$  %) (**Fig. 10.47**). The structure loss should be due to the formation of  $\text{Ag}^+$  substituted enamel, whose susceptibility increased with increasing incorporation of  $\text{Ag}^+$  (Chapter 7). The proposed dose-response mechanism of  $\text{AgNO}_3$  topical treatment on human enamel is shown schematically in **Fig. 12.1**.



**Figure 12.1** – Schematic representation of proposed dose-response inhibitory mechanism of topical treatment with  $\text{AgNO}_3$  on human enamel demineralisation. Following topical treatment with  $\text{AgNO}_3$ , both formation of  $\text{Ag}_3\text{PO}_4$  and  $\text{Ag}^+$  substituted enamel increases with increasing concentration. After acid challenge,  $\text{Ag}_3\text{PO}_4$  is reduced to metallic silver. The enamel surface with more  $\text{Ag}^+$  substituted enamel is more destroyed. Further, some metallic silver is lost due to the loss of enamel structure.

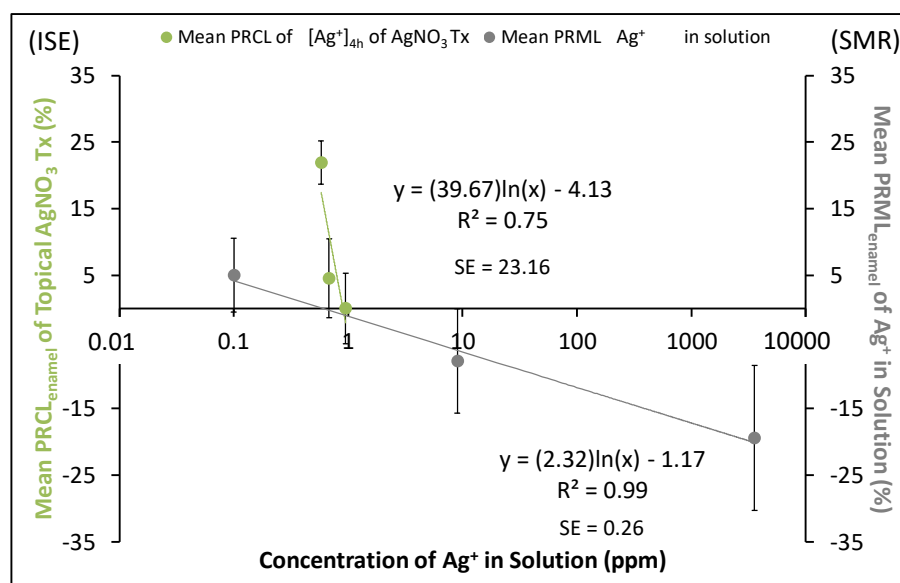
### 12.1.1 The Dose-response Effects of Ag<sup>+</sup> on the Dose-response Inhibitory Efficacy of the Topical Treatment with AgNO<sub>3</sub> on Enamel Demineralisation

In the ISE study, the accelerating enamel demineralisation effects of Ag<sup>+</sup> due to the formation of Ag<sup>+</sup> substituted enamel (Chapter 7) can be expected during AgNO<sub>3</sub> topical treatment on enamel, and, after re-immersion back into acid.

There was a log-linear relationship ( $R^2 = 1.00$ ) between the mean PRCL<sub>enamel</sub> and the concentration of AgNO<sub>3</sub> (**Fig. 10.18**), which is similar to the dose-response PRML<sub>enamel</sub> of Ag<sup>+</sup> in solution reported in the SMR study (**Fig. 7.4**). This indicates that the dose-response effects of the topical treatment with AgNO<sub>3</sub> are associated with the accelerating enamel demineralisation effect of Ag<sup>+</sup> in the topically applied AgNO<sub>3</sub>.

After re-immersing the enamel topically treated with AgNO<sub>3</sub> back into acid, the [Ag<sup>+</sup>]<sub>4h</sub> increased with increasing concentration of AgNO<sub>3</sub> (**Fig. 10.32**). Further, **Fig. 12.2** shows that a log-linear relationship was found between the mean PRCL<sub>enamel</sub> of AgNO<sub>3</sub> topical treatment and the [Ag<sup>+</sup>]<sub>4h</sub> ( $R^2 = 0.74$ ) (Green line), which is similar to the dose-response PRML<sub>enamel</sub> of Ag<sup>+</sup> in solution reported in the SMR study (Grey line). This indicates that the dose-response inhibitory of the AgNO<sub>3</sub> topical treatment is also associated with the accelerating enamel demineralisation effect of Ag<sup>+</sup> in the demineralisation solution.

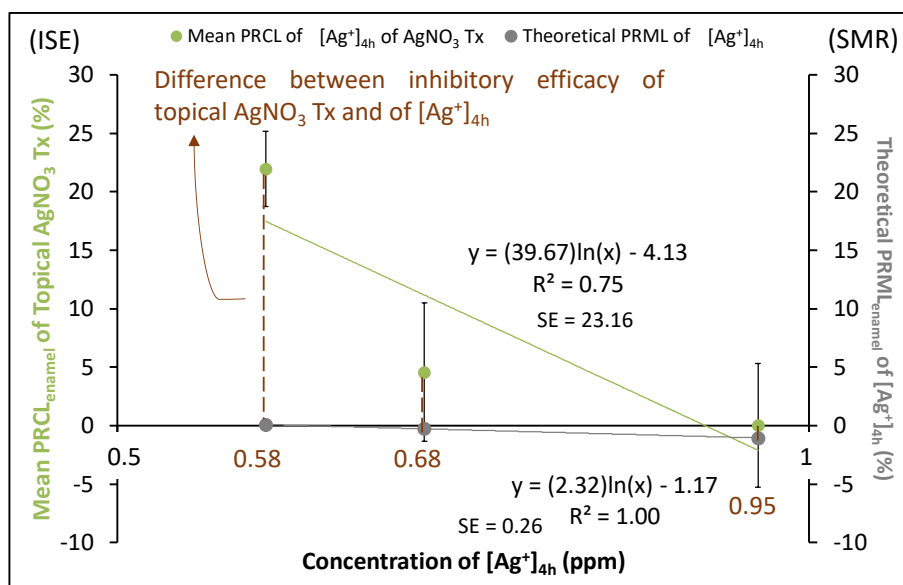




**Figure 12.2** - Comparison of the log-linear relationship between the mean PRCL<sub>enamel</sub> of AgNO<sub>3</sub> topical treatment and the [Ag<sup>+</sup>]<sub>4h</sub> (Green line), and the log-linear relationship between the mean PRML<sub>enamel</sub> of Ag<sup>+</sup> and the [Ag<sup>+</sup>] in solution (Grey line). Error bars show the standard errors.

However, the  $R^2$  value of the dose-response PRCL<sub>enamel</sub> of [Ag<sup>+</sup>]<sub>4h</sub> ( $R^2 = 0.75$ ) is lower than the  $R^2$  value of the dose-response PRCL<sub>enamel</sub> of topically applied [AgNO<sub>3</sub>] ( $R^2 = 1.00$ ). Further, the slope value ( $= -39.67$  %/ppm) of the dose-response PRCL<sub>enamel</sub> of [Ag<sup>+</sup>]<sub>4h</sub> reported in the present ISE study (Green line) was much steeper than the slope value ( $= -2.32$  %/ppm) of the dose-response PRML<sub>enamel</sub> of Ag<sup>+</sup> in solution reported in the SMR study (Grey line), (**Fig. 12.2**). Therefore, the dose-response inhibitory efficacy of topical treatment with AgNO<sub>3</sub> was mainly due to the high [Ag<sup>+</sup>] in the topical application agent (all [AgNO<sub>3</sub>] > 80000 ppm Ag<sup>+</sup>) rather than the low [Ag<sup>+</sup>] in the demineralisation solution (all [Ag<sup>+</sup>]<sub>4h</sub> < 1 ppm Ag<sup>+</sup>).

There are differences between the inhibitory efficacy (PRCL<sub>enamel</sub>) of AgNO<sub>3</sub> topical treatments observed in the present ISE study (Green line), and the theoretical inhibitory efficacy (PRML<sub>enamel</sub>) of [Ag<sup>+</sup>]<sub>4h</sub> obtained from the dose-response PRML<sub>enamel</sub> of Ag<sup>+</sup> in solution reported in the SMR study (Grey line) (**Fig. 12.3**). The difference is due to the topical applied AgNO<sub>3</sub>, which facilitates the formation of a protective barrier on the topically treated enamel. Further, the difference decreased with increasing concentration, which is due to the loss of enamel structure, leading to the loss of the protective barrier.



**Figure 12.3**– The difference between the inhibitory efficacy ( $PRCL_{enamel}$ ) of  $AgNO_3$  (Green dots) observed in ISE study and the theoretical inhibitory efficacy ( $PRML_{enamel}$ ) of  $[Ag^+]_{4h}$  (Grey dots) obtained from dose-response  $PRML_{enamel}$  of  $Ag^+$  reported in the SMR study.

## 12.2 Dose-response Effects of Topical Treatments with AgF and Ag[NH<sub>3</sub>]<sub>2</sub>F on Demineralisation of Human Enamel and Proposed Mechanistic Models

The Ca<sup>2+</sup> ISE data (**Fig. 10.19** and **Fig. 10.21**) showed that the mean PRCL<sub>enamel</sub> of AgF and Ag[NH<sub>3</sub>]<sub>2</sub>F topical treatments *increased* with increasing concentrations. The SEM images also demonstrated similar dose-response (**Fig. 10.46e ~ j**). Only ripple-like demineralised lesions were observed on the enamel surfaces topically treated with 2.36 M and 3.16 M of AgF and Ag[NH<sub>3</sub>]<sub>2</sub>F (**Fig. 10.46f, g, i and j**), whereas, demineralised holes were observed on the surfaces topically treated with 0.75 M AgF and 0.75 M Ag[NH<sub>3</sub>]<sub>2</sub>F (**Fig. 10.46e and h**). No dose-response was observed in the enamel sections and the Knoop CSMH profiles (**Fig. 10.56e ~ j** and **Fig. 10.57e ~ j**), as the change in the inhibitory efficacy was too small.

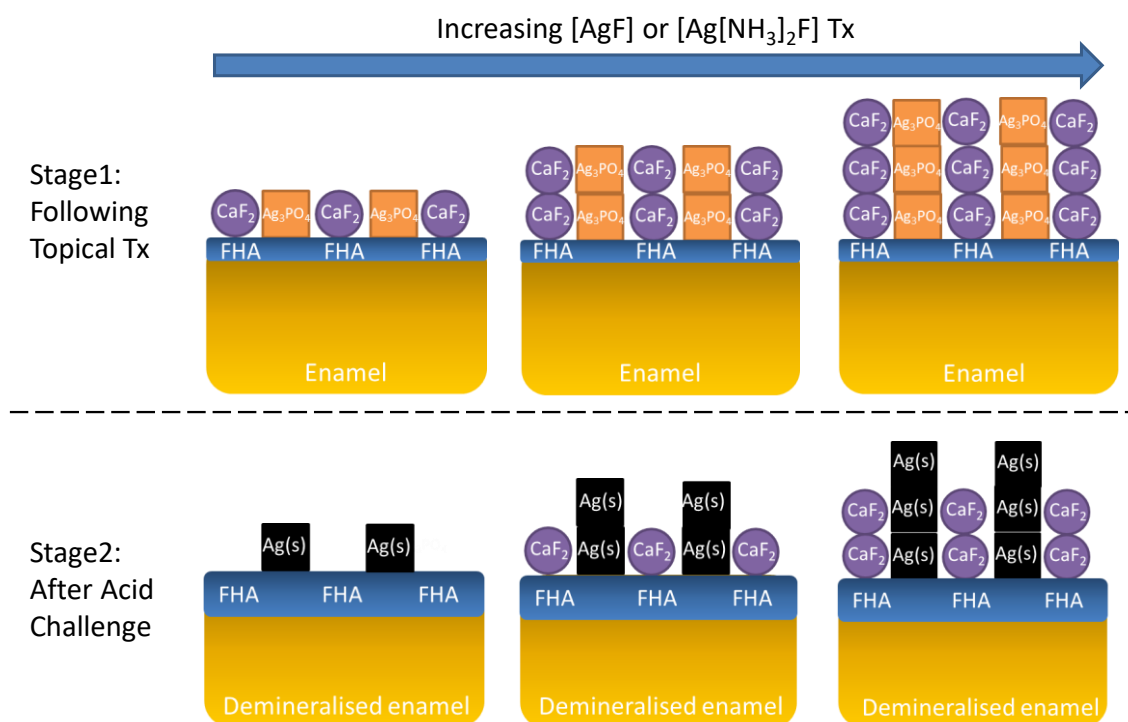
The amount of cubic metallic silver particles (reduced from Ag<sub>3</sub>PO<sub>4</sub>) found on the enamel surfaces topically treated with AgF and Ag[NH<sub>3</sub>]<sub>2</sub>F increased with increasing concentrations of AgF and Ag[NH<sub>3</sub>]<sub>2</sub>F (**Fig. 10.46e ~ j**), leading to increased black staining observed on the enamel surfaces topically treated with higher concentrations of AgF and Ag[NH<sub>3</sub>]<sub>2</sub>F (**Fig. 10.45**). Further, the mean atomic percentages of Ag detected on the enamel surfaces also increased with increasing concentrations of AgF and Ag[NH<sub>3</sub>]<sub>2</sub>F (**Fig. 10.49** and **Fig. 10.50**). All these findings indicate that the amount of metallic silver accumulated in the protective barrier with increasing concentration of topically applied AgF and Ag[NH<sub>3</sub>]<sub>2</sub>F.

It is also noted that the amount of granular CaF<sub>2</sub> particles found on the enamel surfaces topically treated with AgF and Ag[NH<sub>3</sub>]<sub>2</sub>F increased with increasing concentrations of AgF and Ag[NH<sub>3</sub>]<sub>2</sub>F (**Fig. 10.46e ~ j**). Further, the mean atomic percentages of F detected on the enamel surfaces increased with increasing concentrations of AgF and Ag[NH<sub>3</sub>]<sub>2</sub>F (**Fig. 10.52** and **Fig. 10.53**). Also, the proportion of CaF<sub>2</sub> detected with <sup>19</sup>F MAS-NMR in the powdered enamel samples topically treated with AgF and Ag[NH<sub>3</sub>]<sub>2</sub>F increased with increasing concentrations (**Fig. 10.55**). All these findings indicate that the amount of CaF<sub>2</sub>

also accumulated in the protective barrier with increasing concentration of topically applied AgF and Ag[NH<sub>3</sub>]<sub>2</sub>F.

As CaF<sub>2</sub> can act as a reservoir of F<sup>-</sup> for the formation of FHA (ten Cate, 1997) (Section 2.4), the amount of FHA should also accumulate in the protective barrier with increasing concentration of topically applied AgF and Ag[NH<sub>3</sub>]<sub>2</sub>F. Even though, from the current <sup>19</sup>F MAS-NMR spectra (**Fig. 10.55**), it was difficult to tell whether the proportion of FHA in the powdered enamel samples increased with increasing concentrations of AgF and Ag[NH<sub>3</sub>]<sub>2</sub>F due to the small amounts of FHA formed following the topical treatments, previous <sup>19</sup>F MAS-NMR study has shown that the incorporation of fluoride into enamel mineral, forming FHA, increased with increasing [F<sup>-</sup>] in the solution (Mohammed *et al.*, 2013). In the present study, FHA was detected with <sup>19</sup>F MAS-NMR in the powdered enamel treated with 0.75 M Ag[NH<sub>3</sub>]<sub>2</sub>F (**Fig. 10.55**), but no F was detected with EDX on the enamel surfaces topically with 0.75 M Ag[NH<sub>3</sub>]<sub>2</sub>F (**Fig. 10.53**). This might be due to the detected limit of EDX, which has been proposed to be around 0.1 wt% (Goldstein *et al.*, 2003).

The inhibitory efficacy of topical treatments with AgF and Ag[NH<sub>3</sub>]<sub>2</sub>F, and, the amounts of metallic silver (reduced from Ag<sub>3</sub>PO<sub>4</sub>), CaF<sub>2</sub> and FHA increased with increasing concentration. Therefore, the increased inhibitory efficacy of topical treatments with AgF and Ag[NH<sub>3</sub>]<sub>2</sub>F is associated with the accumulation of the components in the protective barrier. The proposed dose-response mechanism of AgF or Ag[NH<sub>3</sub>]<sub>2</sub>F topical treatment on human enamel is shown schematically in **Fig. 12.4**.



**Figure 12.4** – Schematic representation of proposed dose-response inhibitory mechanism of topical treatment with AgF or Ag[NH<sub>3</sub>]<sub>2</sub>F on human enamel demineralisation. Following topical treatment with AgF or Ag[NH<sub>3</sub>]<sub>2</sub>F, the formation of Ag<sub>3</sub>PO<sub>4</sub>, CaF<sub>2</sub> and FHA increases with increasing concentration. After acid challenge, Ag<sub>3</sub>PO<sub>4</sub> is reduced to metallic silver and CaF<sub>2</sub> is dissolved for further formation of FHA.

### 12.2.1 The Dose-response Effects of Ag<sup>+</sup> on the Dose-response Inhibitory Efficacy of the Topical Treatment with AgF and Ag[NH<sub>3</sub>]<sub>2</sub>F on Enamel Demineralisation

In the ISE study, the accelerating enamel demineralisation effects of Ag<sup>+</sup> due to the formation of Ag<sup>+</sup> substituted enamel (Chapter 7) can be expected during AgF and Ag[NH<sub>3</sub>]<sub>2</sub>F topical treatments on enamel, and, after re-immersion back into acid.

However, the direction of the log-linear relationships between the mean PRCL<sub>enamel</sub> and the concentrations of AgF and Ag[NH<sub>3</sub>]<sub>2</sub>F (**Fig. 10.20** and **Fig. 10.22**) is different from the dose-response PRML<sub>enamel</sub> of Ag<sup>+</sup> in solution reported in the SMR study (**Fig. 7.4**). Further, after re-immersing the enamel topically treated with AgF and Ag[NH<sub>3</sub>]<sub>2</sub>F back into acid, there were no significant differences between the [Ag<sup>+</sup>]<sub>4h</sub> following different concentrations AgF and

Ag[NH<sub>3</sub>]<sub>2</sub>F topical treatments (Fig. 10.33 and Fig. 10.34). Fig. 12.5 and Fig. 12.6 show that there were no log-linear relationships between the mean PRCL<sub>enamel</sub> of either AgF or Ag[NH<sub>3</sub>]<sub>2</sub>F topical treatment, and their [Ag<sup>+</sup>]<sub>4h</sub> (R<sup>2</sup> = 0.09 and 0.06) (Red and Blue lines), which is different from the log-linear dose-response relationship between the mean PRML<sub>enamel</sub> of Ag<sup>+</sup> and the [Ag<sup>+</sup>] reported in SMR study (Grey line). Therefore, the dose-response effects of Ag<sup>+</sup> did not have much influence on the dose-response inhibitory efficacy (PRCL<sub>enamel</sub>) of the AgF and Ag[NH<sub>3</sub>]<sub>2</sub>F topical treatments.

The difference between the dose-response PRCL<sub>enamel</sub> of AgF and Ag[NH<sub>3</sub>]<sub>2</sub>F topical treatments and that of AgNO<sub>3</sub> topical treatment may be due to the involvement of F<sup>-</sup>. As discussed in Sections 11.3.1, following topical treatments with AgF and Ag[NH<sub>3</sub>]<sub>2</sub>F, Ca<sup>2+</sup> lost from enamel due to the formation of Ag<sup>+</sup> substituted enamel can be preserved as CaF<sub>2</sub>, and unstable Ag<sup>+</sup> substituted enamel will be replaced by more stable FHA (Robinson, 2009).

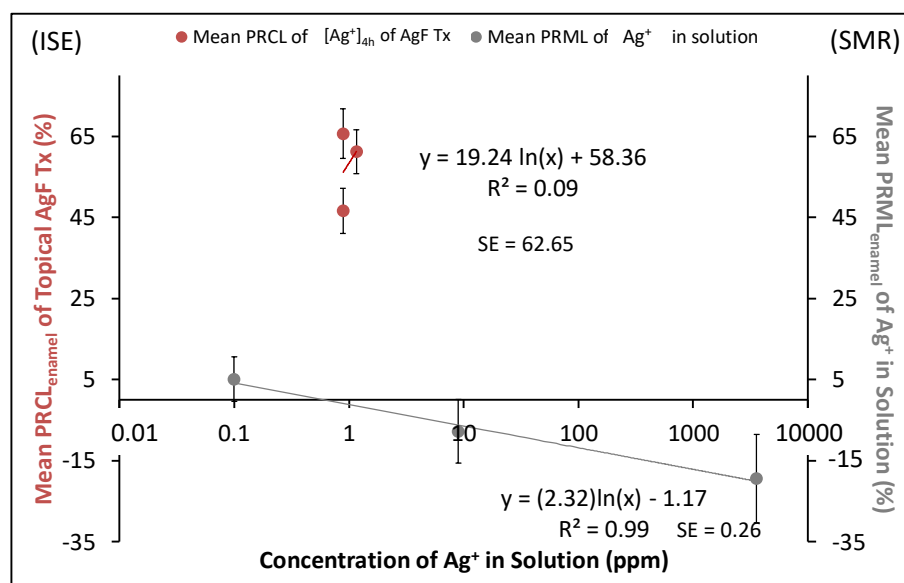
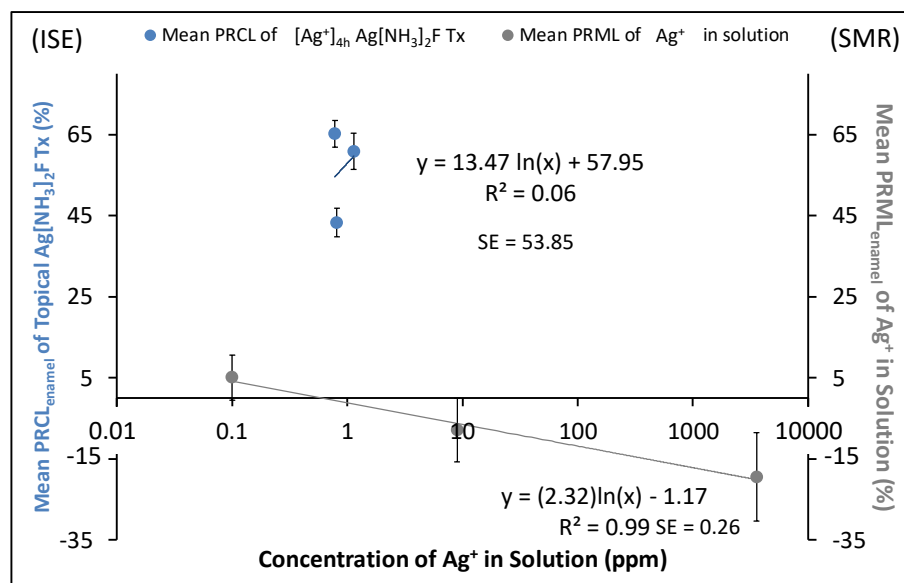


Figure 12.5 - Comparison of the log-linear relationship between the mean PRCL<sub>enamel</sub> of AgF topical treatment and the [Ag<sup>+</sup>]<sub>4h</sub> (Red line) and the log-linear relationship between the mean PRML<sub>enamel</sub> of Ag<sup>+</sup> and the [Ag<sup>+</sup>] in solution (Grey line). Error bars show the standard errors.



**Figure 12.6** - Comparison of the log-linear relationship between the mean PRCL<sub>enameL</sub> of Ag[NH<sub>3</sub>]<sub>2</sub>F topical treatment and the [Ag<sup>+</sup>]<sub>4h</sub> (Blue line) and the log-linear relationship between the mean PRML<sub>enameL</sub> of Ag<sup>+</sup> and the [Ag<sup>+</sup>] in solution (Grey line). Error bars show the standard errors.

### 12.2.2 The Dose-response Effects of F<sup>-</sup> on the Dose-response Inhibitory Efficacy of the Topical Treatments with AgF and Ag[NH<sub>3</sub>]<sub>2</sub>F on Enamel Demineralisation

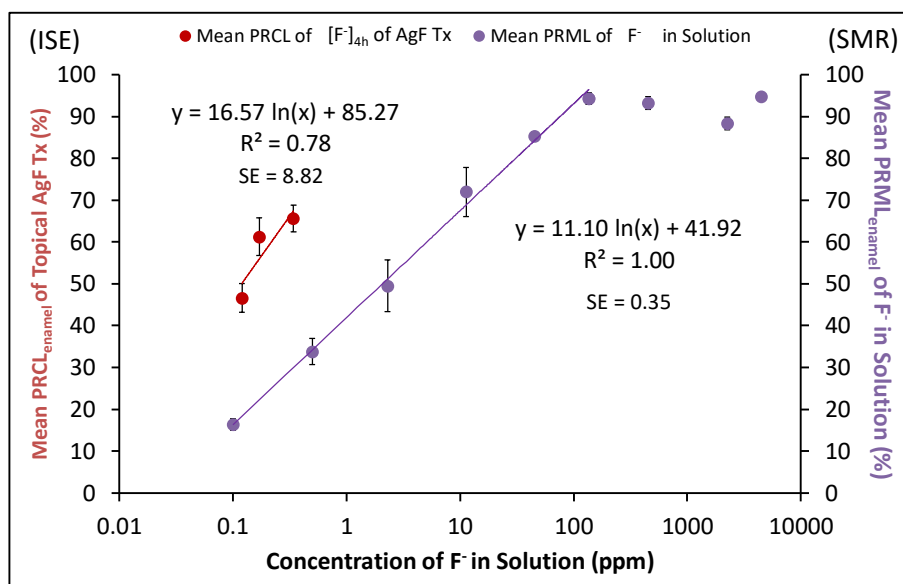
In the ISE study, the inhibiting enamel demineralisation effect of F<sup>-</sup> due to the formation of FHA and CaF<sub>2</sub> (Mohammed *et al.*, 2014a) can be expected during topical treatments with AgF and Ag[NH<sub>3</sub>]<sub>2</sub>F on enamel, and, after re-immersion into acid.

The log-linear relationships between the mean PRCL<sub>enameL</sub> and the concentrations of AgF and Ag[NH<sub>3</sub>]<sub>2</sub>F (**Fig. 10.20** and **Fig. 10.22**) are similar to the dose-response PRML<sub>enameL</sub> of F<sup>-</sup> in solution reported in the SMR study (**Fig. 6.7b**). This indicates that the dose-response effects of the topical treatment with AgF and Ag[NH<sub>3</sub>]<sub>2</sub>F are associated with the inhibiting enamel demineralisation effect of F<sup>-</sup> in the topically applied AgF and Ag[NH<sub>3</sub>]<sub>2</sub>F.

After re-immersing the enamel topically treated with AgF and Ag[NH<sub>3</sub>]<sub>2</sub>F back into acid, the [F<sup>-</sup>]<sub>4h</sub> increased with concentrations of AgF and Ag[NH<sub>3</sub>]<sub>2</sub>F (**Fig. 10.42** and **Fig. 10.43**). Further, **Fig. 12.7** and **Fig. 12.8** show that a log-linear relationship was found between the mean PRCL<sub>enameL</sub> of topical treatments with

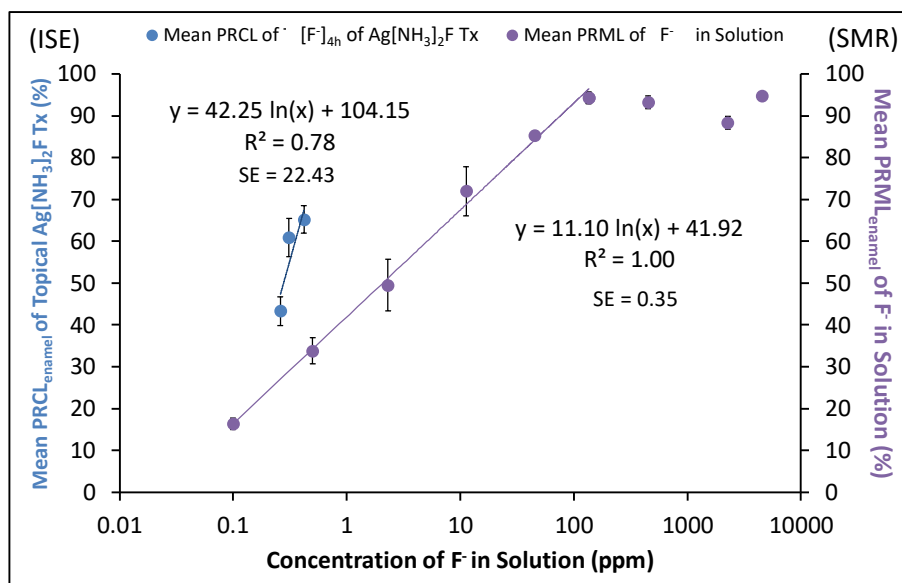
AgF and Ag[NH<sub>3</sub>]<sub>2</sub>F, and their [F<sup>-</sup>]<sub>4h</sub> (Red and Blue lines), which is similar to the dose-response PRML<sub>enamel</sub> of F<sup>-</sup> in solution reported in the SMR study (Purple line). This indicates that the dose-response effects of the topical treatments with AgF and Ag[NH<sub>3</sub>]<sub>2</sub>F are also associated with the inhibiting enamel demineralisation effect of F<sup>-</sup> in the demineralisation solutions.

However, the R<sup>2</sup> values of the dose-response PRCL<sub>enamel</sub> of [F<sup>-</sup>]<sub>4h</sub> (R<sup>2</sup> = 0.78 and 0.78) are lower than the R<sup>2</sup> values of the dose-response PRCL<sub>enamel</sub> of topically applied [AgF] and [Ag[NH<sub>3</sub>]<sub>2</sub>F] (R<sup>2</sup> = 1.00). Further, the slope values (= 16.57 %/ppm and 42.25 %/ppm) of the dose-response PRCL<sub>enamel</sub> of [F<sup>-</sup>]<sub>4h</sub> reported in the present ISE study (Red and Blue lines) were steeper than the slope value (= 11.10 %/ppm) of the dose-response PRML<sub>enamel</sub> of F<sup>-</sup> in solution reported in the SMR study (Purple line) (**Fig. 12.7** and **Fig. 12.8**). Therefore, the dose-response inhibitory efficacy of topical treatments with AgF and Ag[NH<sub>3</sub>]<sub>2</sub>F was mainly due to the high [F<sup>-</sup>] in the topical application agents (all [AgF] and [Ag[NH<sub>3</sub>]<sub>2</sub>F] > 14250 ppm F<sup>-</sup>) rather than the low [F<sup>-</sup>] in the demineralisation solutions (all [F<sup>-</sup>]<sub>4h</sub> < 1 ppm F<sup>-</sup>).



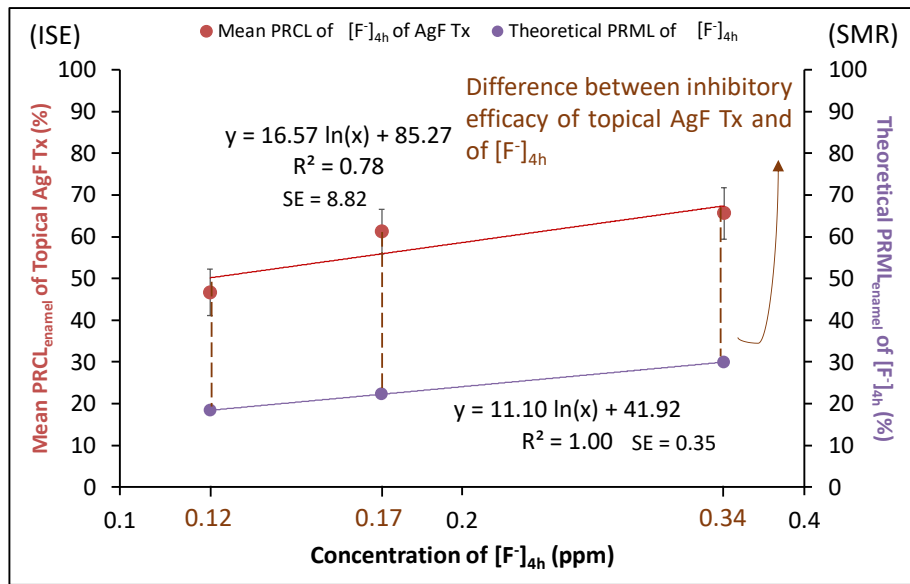
**Figure 12.7** - Comparison of the log-linear relationship between the mean PRCL<sub>enamel</sub> of AgF topical treatment and the [F<sup>-</sup>]<sub>4h</sub> (Red line) and the log-linear relationship between the mean PRML<sub>enamel</sub> of F<sup>-</sup> and the [F<sup>-</sup>] in solution (Purple line). Error bars show the standard errors.



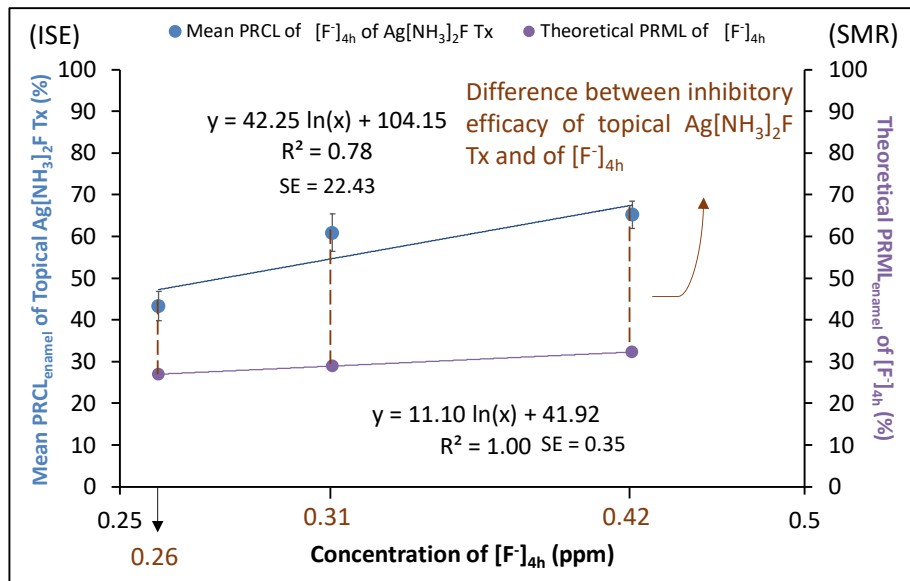


**Figure 12.8** - Comparison of the log-linear relationship between the mean PRCL<sub>enameL</sub> of Ag[NH<sub>3</sub>]<sub>2</sub>F topical treatment and the [F<sup>-</sup>]<sub>4h</sub> (Blue line) and the log-linear relationship between the mean PRML<sub>enameL</sub> of F<sup>-</sup> and the [F<sup>-</sup>] in solution (Purple line). Error bars show the standard errors.

There are differences between the inhibitory efficacy (PRCL<sub>enameL</sub>) of AgF and Ag[NH<sub>3</sub>]<sub>2</sub>F topical treatments observed in the present ISE study (Red and Blue lines), and the theoretical inhibitory efficacy (PRML<sub>enameL</sub>) of [F<sup>-</sup>]<sub>4h</sub> obtained from the dose-response PRML<sub>enameL</sub> of F<sup>-</sup> in solution reported in the SMR study (Purple line) (**Fig. 12.9** and **Fig. 12.10**). The differences are due to the topical applied AgF and Ag[NH<sub>3</sub>]<sub>2</sub>F, which facilitate the formation of a protective barrier on the topically treated enamel. Further, the differences increased with increasing concentrations, which is due to the accumulation of components in the protective barrier.



**Figure 12.9** - The difference between the inhibitory efficacy (PRCL<sub>enameL</sub>) of AgF (Red dots) observed in ISE study and the theoretical inhibitory efficacy (PRML<sub>enameL</sub>) of  $[F]_{4h}$  (Purple dots) obtained from dose-response PRML<sub>enameL</sub> of F reported in the SMR study.



**Figure 12.10** - The difference between the inhibitory efficacy (PRCL<sub>enameL</sub>) of Ag $[NH_3]_2F$  (Blue dots) observed in ISE study and the theoretical inhibitory efficacy (PRML<sub>enameL</sub>) of  $[F]_{4h}$  (Purple dots) obtained from dose-response PRML<sub>enameL</sub> of F reported in the SMR study.

## 12.3 Conclusions

In conclusion, the dose-response inhibitory mechanism of topical treatment with  $\text{AgNO}_3$  on human enamel demineralisation is associated with the substitution of  $\text{Ca}^{2+}$  in enamel mineral by  $\text{Ag}^+$ . Whereas, the dose-response inhibitory mechanisms of topical treatments with  $\text{AgF}$  and  $\text{Ag}[\text{NH}_3]_2\text{F}$  on human enamel demineralisation are associated with the increased release of  $\text{F}^-$  from the topically treated enamel surfaces, and the accumulation of the components in the protective barrier.

For  $\text{AgNO}_3$ , the dose-response effects of  $\text{Ag}^+$  influence the dose-response inhibitory efficacy. Whereas, for  $\text{AgF}$  and  $\text{Ag}[\text{NH}_3]_2\text{F}$ , only dose-response effects of  $\text{F}^-$  play a major role in the dose-response inhibitory efficacy.

**PART V: DISCUSSION,  
CONCLUSIONS, FUTURE  
WORK AND CLINICAL  
RELEVANCE**

## Chapter 13 DISCUSSION

### 13.1 Comparison of Effects of Topical Treatments with Silver Compounds on Demineralisation of HAP Discs and Human Enamel

This study demonstrated the effects of topical treatments with silver nitrate ( $\text{AgNO}_3$ ), silver fluoride ( $\text{AgF}$ ), silver diammine fluoride (SDF;  $\text{Ag}[\text{NH}_3]_2\text{F}$ ) and Silver Capsule of Riva Star (3.16 M SDF, SDI Ltd, Australia) (Riva-SC) on the inhibition of demineralisation of hydroxyapatite (HAP) discs (Chapter 8) and human enamel (Chapter 10). Even though HAP discs have been accepted as a good model for human enamel in many demineralisation studies (Anderson *et al.*, 2004a; do Amaral *et al.*, 2016; Jones *et al.*, 2013; Kosoric *et al.*, 2010), it is compositionally and structurally different from human enamel (Section 1.3).

This section aims to compare the effects of topical treatments with silver compounds (3.16 M) on the demineralisation of HAP discs and human enamel.

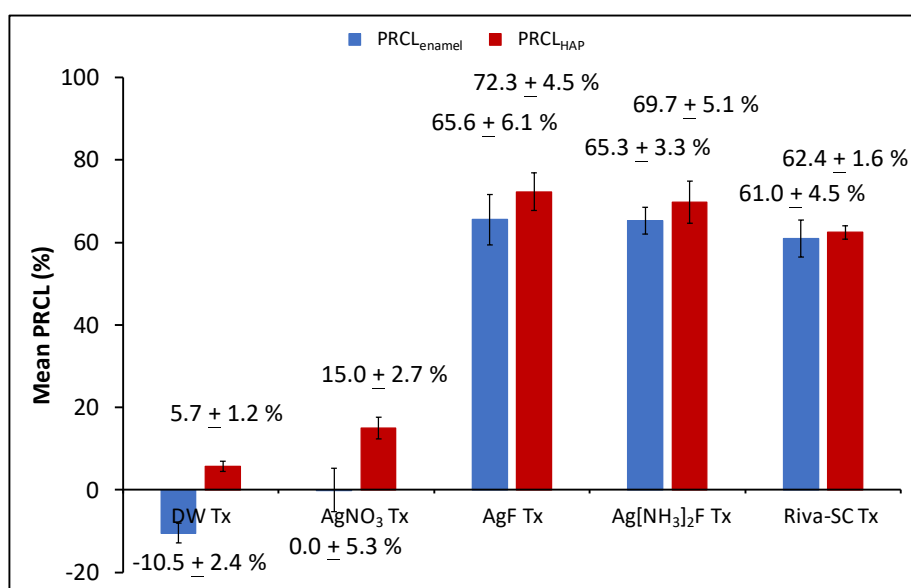
#### 13.1.1 Before Topical Treatments with Silver Compounds

In the ISE study (Chapter 8 and 10), before topical treatment with each silver compound, the release of  $\text{Ca}^{2+}$  from both HAP discs and human enamel in the demineralisation solution was linear with time (**Fig. 8.4 ~ Fig. 8.8** and **Fig. 10.5 ~ Fig. 10.15**). However, the rates of  $\text{Ca}^{2+}$  release from demineralising human enamel ( $\approx 0.030$  mM/h) (**Table 10.7**) were faster than those from demineralising HAP discs ( $\approx 0.010$  mM/h) (**Table 8.7**). This should be due to the presence of carbonate in human enamel, acting as a destabilising agent (Mukundan *et al.*, 1999) (Section 1.3).

### 13.1.2 Following Topical Treatments with Silver Compounds

Immediately following topical treatments with all silver compounds ( $\text{AgNO}_3$ ,  $\text{AgF}$ ,  $\text{Ag}[\text{NH}_3]_2\text{F}$  and Riva-SC) on both HAP discs and human enamel, yellow staining was observed (**Fig. 8.16**, **Fig. 10.44** and **Fig. 10.45**), suggesting the formation of yellow  $\text{Ag}_3\text{PO}_4$  (Lewis, 1920). Further, in the treatment groups of fluoride-containing silver compounds ( $\text{AgF}$ ,  $\text{Ag}[\text{NH}_3]_2\text{F}$  and Riva-SC),  $\text{CaF}_2$  and FHA were detected in the powder samples of both HAP and human enamel (**Fig. 8.21** and **Fig. 10.55**). This suggests that the reaction products formed following topical treatments with silver compounds on both HAP discs and human enamel are the same.

### 13.1.3 After Re-immersion of Topically Treated HAP Discs and Human Enamel into Acids

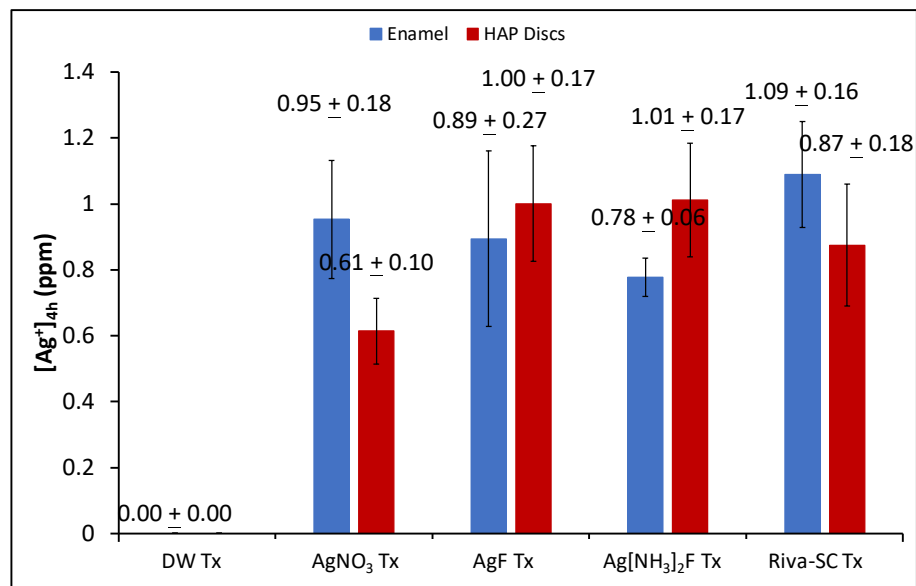


**Figure 13.1** – Mean  $\text{PRCL}_{\text{enamel}}$  and mean  $\text{PRCL}_{\text{HAP}}$  of all treatment groups.

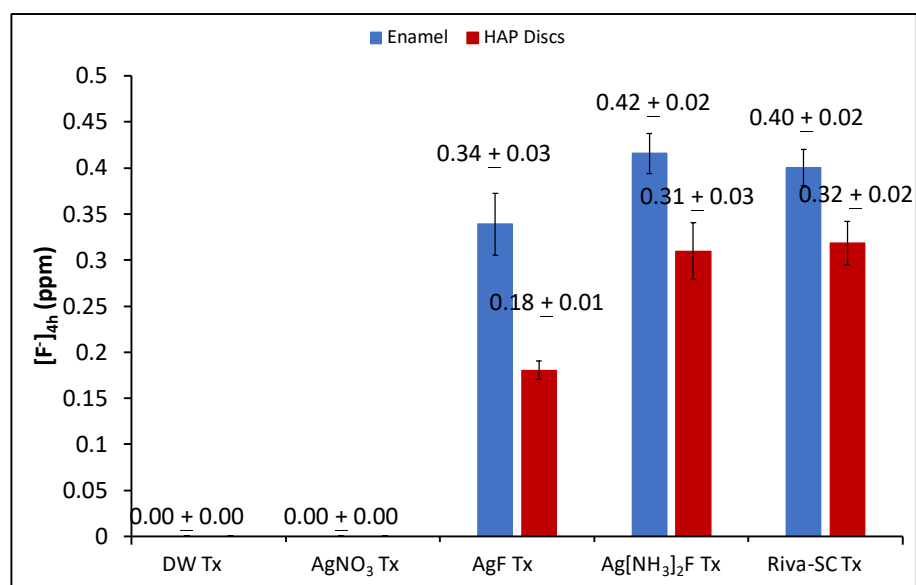
After re-immersing the HAP discs and human enamel topically treated with DW, the rate of  $\text{Ca}^{2+}$  release from demineralising HAP discs was decreased (**Fig. 8.4**) due to the removal of softened HAP surfaces and the exposure of intact deeper

HAP layers (Section 9.1), whereas, the rate of  $\text{Ca}^{2+}$  release from demineralising human enamel was increased (**Fig. 10.5**) due to the removal of softened enamel surfaces and the exposure of more soluble deeper enamel layers (Section 11.1). Therefore, the abrasion effects of using a micro-brush during topical treatments on HAP discs and human enamel are different. This should be the reason why  $\text{PRCL}_{\text{enamel}}$  of silver compound treatment group were all slightly lower than the  $\text{PRCL}_{\text{HAP}}$  (**Fig. 13.1**).

The  $[\text{Ag}^+]_{4\text{h}}$  of both HAP disc and human enamel treatment groups were similar (**Fig. 13.2**). However, the  $[\text{F}^-]_{4\text{h}}$  of human enamel treatment groups were all slightly higher than those of HAP disc treatment groups (**Fig. 13.3**). This should result from the minor additional amounts of fluoride in the human enamel, which is an unavoidable interference even though the superficial layers of enamel abundant in fluoride were removed before the study.



**Figure 13.2** –  $[\text{Ag}^+]_{4\text{h}}$  of enamel and HAP disc treatment groups.



**Figure 13.3** -  $[F]_{4h}$  of enamel and HAP disc treatment groups.

### 13.1.4 After Removal of HAP Discs and Human Enamel Topically Treated with Silver Compounds from Acids

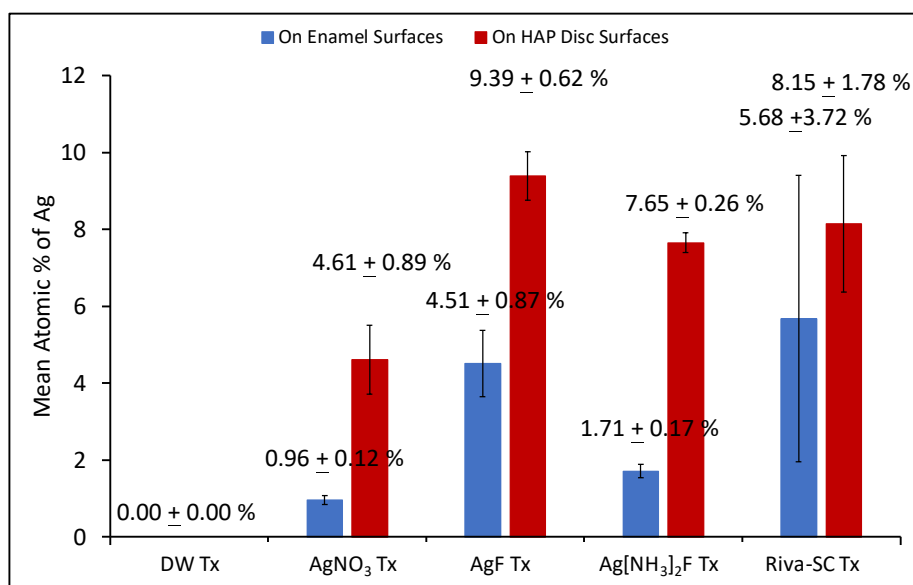
After removing the HAP discs and human enamel topically treated with DW, the SEM images showed pores on the demineralised HAP disc surfaces (**Fig. 8.17a**), whereas, hollow enamel cores were found on the demineralised enamel surfaces (**Fig. 10.46a**). This results from the difference in the structures of these two sample types (Section 1.2.2 and Section 1.3). Demineralised surfaces of human enamel are more irregular than those of HAP discs due to the compositional variation in the human enamel (Section 1.2.1).

On both HAP discs and human enamel, cubic metallic silver particles were found on the surfaces topically treated with silver compounds (AgNO<sub>3</sub>, AgF, Ag[NH<sub>3</sub>]<sub>2</sub>F and Riva-SC). Further, additional granular CaF<sub>2</sub> particles were found on the surfaces topically treated with fluoride-containing silver compounds (AgF, Ag[NH<sub>3</sub>]<sub>2</sub>F and Riva-SC) (**Fig. 8.17b ~ e** and **Fig. 10.46d, g, j, k**).

Elemental Ag was detected on both HAP disc and human enamel surfaces topically treated with silver compounds (AgNO<sub>3</sub>, AgF, Ag[NH<sub>3</sub>]<sub>2</sub>F and Riva-SC) (**Fig. 8.18** and **Fig. 10.47**). The ratios of the mean atomic percentages of Ag detected on both HAP disc and enamel surfaces topically treated with these silver



compounds were the same; AgF Tx > Riva-SC Tx > Ag[NH<sub>3</sub>]<sub>2</sub>F Tx > AgNO<sub>3</sub> Tx. However, the mean atomic percentages of Ag detected on the HAP disc surfaces were all higher than those detected on the similarly treated enamel (**Fig. 13.4**). This could be due to that the metallic silver particles deposited on the HAP discs (~ 3 μm) were larger than those (~ 1.5 μm) on the enamel, and can be more easily detected by EDX (Section 8.4.5 and Section 10.4.5). The larger size of metallic silver particles on the HAP discs may be due to that the evenly demineralised HAP disc surfaces made the exposure of Ag<sub>3</sub>PO<sub>4</sub> deposits to light and heat easier than the irregular demineralised enamel surfaces.

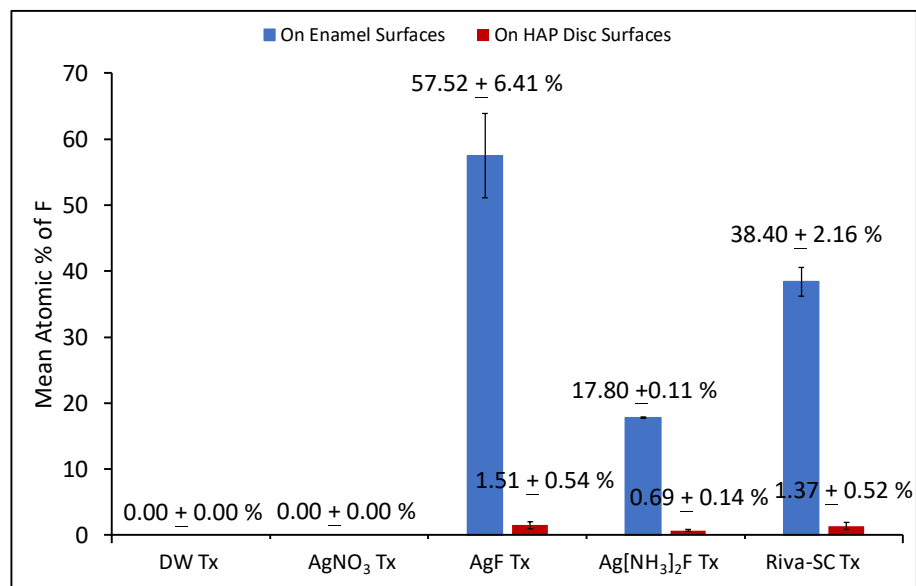


**Figure 13.4** - Mean percentages of Ag detected on HAP disc and human enamel surfaces.

Elemental F was detected on both HAP disc and human enamel surfaces topically treated with fluoride-containing silver compounds (AgF, Ag[NH<sub>3</sub>]<sub>2</sub>F and Riva-SC) (**Fig. 8.19** and **Fig. 10.51**). The ratios of the mean atomic percentages of F detected on both HAP disc and enamel surfaces topically treated with these fluoride-containing silver compounds were the same; AgF Tx > Riva-SC Tx > Ag[NH<sub>3</sub>]<sub>2</sub>F Tx. However, the mean atomic percentages of F detected on the enamel surfaces topically treated with 3.16 M AgF, 3.16 M Ag[NH<sub>3</sub>]<sub>2</sub>F and Riva-SC (> 15 %) were all much higher than those detected on the similarly treated HAP discs (< 2 %) (**Fig. 13.5**). This could be due to the exposure of more soluble

deeper layers of human enamel by the abrasion effects of topical treatments. As the formation of  $\text{CaF}_2$  requires slight dissolution of the enamel surfaces in order to provide the necessary  $\text{Ca}^{2+}$  (Buzalaf *et al.*, 2011) (Section 2.4), more soluble enamel mineral favours more  $\text{CaF}_2$  formation.

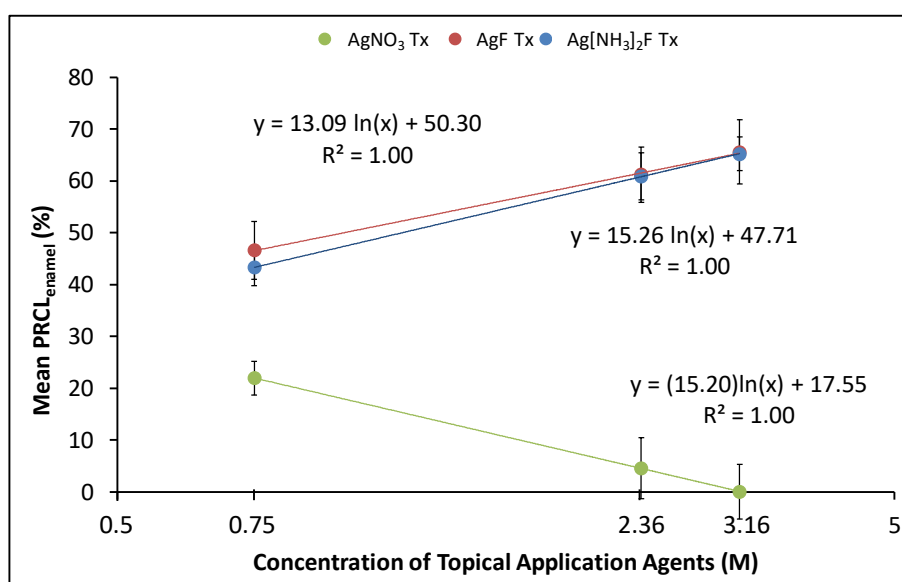
Therefore, as there was much more  $\text{CaF}_2$  in the protective barriers formed on the enamel surfaces topically treated with fluoride-containing silver compounds (AgF,  $\text{Ag}[\text{NH}_3]_2\text{F}$  and Riva-SC) than those formed on the HAP discs, the inhibitory efficacy from the enamel protective barriers should be much higher than those from the HAP disc protective barrier. This explains why even though the abrasion effects accelerated the  $\text{Ca}^{2+}$  release from enamel by  $10.61 \pm 2.39\%$ , the  $\text{PRCL}_{\text{enamel}}$  of these fluoride-containing silver compound treatment groups were still similar to the  $\text{PRCL}_{\text{HAP}}$  (**Fig. 13.1**).



**Figure 13.5** – Mean percentages of F detected on HAP disc and human enamel surfaces.

## 13.2 Clinical Implications of the Dose-response Effects of Topical Treatments with Silver Compounds on Demineralisation of Human Enamel

In the present study, the protocol of topical treatments on human enamel followed the one mostly recommended to be used in the clinical practice (Crystal *et al.*, 2017). Further, the concentrations of the silver compounds, including 0.75 M, 2.36 M and 3.16 M, were the concentrations used in the commercial products (Fung *et al.*, 2013; SDI, 2016a) (Section 3.4.2).



**Figure 13.6** – Dose-response effects of topical treatments with AgNO<sub>3</sub> (Green line), AgF (Red line) and Ag[NH<sub>3</sub>]<sub>2</sub>F (Blue line) on demineralisation of human enamel.

### 13.2.1 Topical Treatments with Different Concentrations of AgNO<sub>3</sub> on Demineralisation of Human Enamel

As the PRCL<sub>enamel</sub> of topical treatment with 3.16 M AgNO<sub>3</sub> on enamel demineralisation was 0.0±5.3 % (**Fig. 10.17**), 3.16 M was a “threshold”, at which concentration the topical treatment cannot exert any further inhibitory efficacy on demineralisation. Therefore, the only cariostatic effect of the 3.16 M AgNO<sub>3</sub> topical treatment on enamel caries will be the antibacterial properties of AgNO<sub>3</sub>

(Lansdown, 2006; Thibodeau *et al.*, 1978). On the other hand, as the inhibitory efficacy of topical treatments with 0.75 M and 2.36 M AgNO<sub>3</sub> was 21.9±3.2 % and 4.6±5.9 % observed (**Fig. 10.17**), both inhibitory efficacy and antibacterial properties can contribute to the cariostatic effect following topical treatments with these concentrations of AgNO<sub>3</sub>. However, the PRCL<sub>enamel</sub> of 2.36 M AgNO<sub>3</sub> topical treatment was not significantly higher than that of 3.16 M AgNO<sub>3</sub>. Therefore, the inhibitory efficacy of 2.36 M AgNO<sub>3</sub> topical treatments may also be negligible. An *in vitro* study found that 5 min immersion of human enamel in 2.36 M AgNO<sub>3</sub> did not inhibit the demineralisation of enamel at pH 4.4 (Liu *et al.*, 2012b).

The inhibitory efficacy of AgNO<sub>3</sub> topical treatment increases with decreasing concentration (**Fig. 13.6**). Further, as most of the cariogenic bacteria can be inhibited by 20 ppm Ag<sup>+</sup>, the application of 0.75 M AgNO<sub>3</sub> (81000 ppm Ag<sup>+</sup>) is unnecessary. Therefore, AgNO<sub>3</sub> with concentrations lower than 0.75 M can be applied in the topical treatment on enamel caries to exert antibacterial properties and optimal inhibitory efficacy at the same time.

### 13.2.2 Topical Treatments with Different Concentrations of AgF or Ag[NH<sub>3</sub>]<sub>2</sub>F on Demineralisation of Human Enamel

The PRCL<sub>enamel</sub> of topical treatments with fluoride-containing silver compounds (AgF and Ag[NH<sub>3</sub>]<sub>2</sub>F) were much higher than that of AgNO<sub>3</sub> (**Fig. 10.16**). Therefore, fluoride-containing silver compounds used in the clinical practice can exert both pronounced inhibitory efficacy of enamel demineralisation and antibacterial properties.

Ag[NH<sub>3</sub>]<sub>2</sub>F is one of the most popular fluoride-containing silver compounds used in the clinical practice (Horst *et al.*, 2016), which has a wide concentration range of commercial products available (Fung *et al.*, 2013; SDI, 2016a). The Ag[NH<sub>3</sub>]<sub>2</sub>F product with the lowest concentration (Saforide 3.8%, Tokyo Seiyaku Kasei Co. Ltd, 4484 ppm F<sup>-</sup>) contains fluoride concentration similar to that of fluoride dentifrice (100 ~ 1500 ppm F<sup>-</sup>) (Mohammed *et al.*, 2014a), whereas, the

Ag[NH<sub>3</sub>]<sub>2</sub>F product with the highest concentration (Riva Star, SDI Ltd, 60000 ppm F<sup>-</sup>) contains fluoride concentration much higher than that of fluoride varnish (~22000 ppm F<sup>-</sup>) (Hazelrigg *et al.*, 2003). As the inhibitory efficacy of the topical treatment with Ag[NH<sub>3</sub>]<sub>2</sub>F increases with increasing concentration (**Fig. 13.6**), concentrations of Ag[NH<sub>3</sub>]<sub>2</sub>F higher than 3.16 M (60000 ppm F<sup>-</sup>) can be used to optimise the inhibitory efficacy of the topical treatment.

However, the safety concerns about the extremely high F<sup>-</sup> concentration in the silver compounds have been expressed (Gotjamanos, 1997; Gotjamanos and Afonso, 1997; Gotjamanos and Orton, 1998). Even though a previous study has proposed that the concentrations of Ag[NH<sub>3</sub>]<sub>2</sub>F products used in clinical practice is hundreds times less than the lethal dose of Ag[NH<sub>3</sub>]<sub>2</sub>F by oral administration (520 mg/kg) (Horst *et al.*, 2016), some patients have reported tooth pain, gum pain, gum swelling and gum bleaching after being treated with Ag[NH<sub>3</sub>]<sub>2</sub>F (Duangthip *et al.*, 2018). Therefore, high concentration fluoride-containing silver compounds should be used with caution.

## Chapter 14 CONCLUSIONS, FUTURE WORK AND CLINICAL RELEVANCE

### 14.1 Conclusions

The conclusions from this study are as follows:

1. Real-time  $\text{Ca}^{2+}$  ISEs can be used in *in vitro* study for quantifying the demineralisation inhibitory efficacy of inhibitors by real-time monitoring demineralisation kinetics before and after the treatment.
2. There is a dose-response effect of  $\text{Ag}^+$  on the demineralisation of human enamel. The accelerating effect of  $\text{Ag}^+$  on demineralisation increased with increasing concentration. Further, a log-linear relationship was found between the inhibitory efficacy and the concentration of  $\text{Ag}^+$  in the solution.
3. Topical treatments with silver compounds, including  $\text{AgNO}_3$ ,  $\text{AgF}$  and  $\text{Ag}[\text{NH}_3]_2\text{F}$ , inhibited the demineralisation of hydroxyapatite (HAP) discs and human enamel. The inhibitory mechanism of topical treatment with  $\text{AgNO}_3$  is associated with; 1) the formation of a protective barrier composed of  $\text{Ag}_3\text{PO}_4$ . Whereas, the inhibitory mechanism of topical treatment with  $\text{AgF}$  or  $\text{Ag}[\text{NH}_3]_2\text{F}$  is associated with; 1) the release of  $\text{F}^-$  from the topically treated dental mineral surfaces, 2) the formation of a protective barrier composed of  $\text{Ag}_3\text{PO}_4$ ,  $\text{CaF}_2$  and FHA. Further, the abrasion effects of the topical treatments inhibited the demineralisation of HAP discs but accelerated the demineralisation of human enamel.
4. The inhibitory efficacy of topical treatment with  $\text{AgNO}_3$  on human enamel demineralisation decreased with increasing concentration due to; 1) substitution of  $\text{Ca}^{2+}$  in enamel mineral by  $\text{Ag}^+$ , which destabilises the treated enamel surfaces. Whereas, the inhibitory efficacy of topical treatment with  $\text{AgF}$  or  $\text{Ag}[\text{NH}_3]_2\text{F}$  increased with increasing concentration due to; 1) the increased release of  $\text{F}^-$

from the topically treated enamel surfaces, 2) the accumulation of the components in the protective barrier on the treated enamel surfaces. Further, a log-linear relationship between the dose-response inhibitory efficacy of topical treatment with  $\text{AgNO}_3$ ,  $\text{AgF}$  or  $\text{Ag}[\text{NH}_3]_2\text{F}$  on demineralisation of human enamel and the topically applied concentration of  $\text{AgNO}_3$ ,  $\text{AgF}$  or  $\text{Ag}[\text{NH}_3]_2\text{F}$  was found.

5. The effects of topical treatments with Silver Capsule of Riva Star (SDI Ltd, Australia) on the demineralisation of HAP discs and human enamel are similar to those of topical treatments with laboratory-prepared 3.16 M  $\text{Ag}[\text{NH}_3]_2\text{F}$ .

## 14.2 Future Work

The current *in vitro* study was carried out under conditions without any effects of the physiological factors in the oral environment. This allowed the strict chemical control of individual variables of multi-factorial diseases like dental caries and dental erosion. However, physiological factors in the *in vivo* situation, including dietary habits, personal oral hygiene conditions, the functions of salivary glands, and a pellicle coating, also influence caries and erosion progression (Hunter, 1988; Kidd, 2005). Therefore, in order to fully understand the effects of topical treatments with silver compounds, further studies are required to investigate the additional effects of these physiological factors. Furthermore, the effects of a dynamic pH cycling process need to be considered in order to simulate *in situ* conditions.

Hydroxyapatite (HAP) discs were used as enamel analogues in this study in order to avoid inhomogeneities from human enamel. Bovine enamel could be another choice to be used in the future study (Laurance-Young *et al.*, 2011), which has more uniform composition than human enamel but more physiological features than HAP discs (Mellberg, 1992). Further, only one protocol of topical treatment with silver compound was used in the present study. Even though the protocol has been proposed to be the optimum for cariostatic effectiveness (Crystal *et al.*, 2017), other delivery protocols should be investigated. For example, University of California San Francisco (UCSF) proposed that the application time of  $\text{Ag}[\text{NH}_3]_2\text{F}$  should be more than 1 min, followed by rinsing of the treated lesion (Horst *et al.*, 2016). Even though concerns have been expressed about losing effectiveness by the rinsing procedure (Horst, 2018), the discrepancy between the inhibitory efficacies exerted by these two protocols could be compared using the real-time ISE methodology. Further, by modifying the protocol used in the study, a novel protocol, which exerts higher inhibitory efficacy might be found.

An inhibitory efficacy up to 65 % of topical treatment with AgF or  $\text{Ag}[\text{NH}_3]_2\text{F}$  was found with increasing concentrations (up to 3.16 M) in the present study, but higher concentrations could be used in the future dose-response study to



measure optimal inhibitory efficacy. Further, the inhibitory efficacy obtained was based on 4 h demineralisation only, and so longer periods could be used to investigate the inhibitory efficacy over longer time periods. For example, as the secretion of saliva is lowest during 8 h sleep, which increases caries risk (Dawes, 2008), an 8 h demineralisation period can be used.

### 14.3 Clinical Relevance

In clinical practice, topical treatment with  $\text{Ag}[\text{NH}_3]_2\text{F}$  is a better choice over  $\text{AgNO}_3$  and  $\text{AgF}$  used for the management of dental caries.  $\text{Ag}[\text{NH}_3]_2\text{F}$  topical treatment has higher inhibitory efficacy on enamel demineralisation than  $\text{AgNO}_3$  and is able to stabilise the  $\text{Ag}^+$ . Biannual application of 38 wt% (2.36 M)  $\text{Ag}[\text{NH}_3]_2\text{F}$  is the most effective protocol for treating dental caries (Duangthip *et al.*, 2017; Fung *et al.*, 2016; Fung *et al.*, 2018) (Section 3.4.2). However, as this study has reported, the inhibitory efficacy of  $\text{Ag}[\text{NH}_3]_2\text{F}$  increases with increasing concentration, so there is a potential that annual applications of  $\text{Ag}[\text{NH}_3]_2\text{F}$  with concentrations higher than 2.36 M will be sufficient to exert similar cariostatic effects on human enamel.

However, the black staining remains an aesthetic problem. SSKI has been introduced, which can be applied to remove the black staining of the lesions topically treated with  $\text{Ag}[\text{NH}_3]_2\text{F}$  (Ngo *et al.*, 2002) (Section 3.4). Future clinical trials are required to investigate whether the black staining of the treated lesions can be effectively and permanently removed by using SSKI without compromising the inhibitory efficacy of the  $\text{Ag}[\text{NH}_3]_2\text{F}$  topical treatment.

# **PART VI: REFERENCES**

- ABOU NEEL, E. A., ALJABO, A., STRANGE, A., IBRAHIM, S., COATHUP, M., YOUNG, A. M., BOZEC, L. & MUDERA, V. 2016. Demineralization-remineralization dynamics in teeth and bone. *Int J Nanomedicine*, 11, 4743-4763.
- ACMAL. 2014. *Basic Science - Energy Dispersive Spectrometer* [Online]. [http://mcff.mtu.edu/acmal/electronmicroscopy/MA\\_EDS\\_Basic\\_Science.htm](http://mcff.mtu.edu/acmal/electronmicroscopy/MA_EDS_Basic_Science.htm). [Accessed 8.4 2017].
- ADEJUMO, O., GEORGE-TAYLOR, O., KOLAPO, A., OLUBAMIWA, A., FAYOKUN, R. & ALAWODE, O. 2009. Determination of Fluoride Concentration in Various Brands of Toothpaste Marketed in Nigeria Using Ion Selective Electrode Method. *Advances in Medical and Dental Sciences*, 3, 46-50.
- ALIA, A., GANAPATHY, S. & DE GROOT, H. J. 2009. Magic Angle Spinning (MAS) NMR: a new tool to study the spatial and electronic structure of photosynthetic complexes. *Photosynth Res*, 102, 415-25.
- ALL-ABOUT-PH.COM. 2017. *The glass pH measuring electrode* [Online]. <http://www.all-about-ph.com/measuring-electrode.html>. [Accessed 8.4 2017].
- AMAECHE, B. T. & HIGHAM, S. M. 2005. Dental erosion: possible approaches to prevention and control. *J Dent*, 33, 243-52.
- ANDERSON, M. 2002. Risk assessment and epidemiology of dental caries: review of the literature. *Pediatr Dent*, 24, 377-85.
- ANDERSON, P., BOLLET-QUIVOGNE, F. R., DOWKER, S. E. & ELLIOTT, J. C. 2004a. Demineralization in enamel and hydroxyapatite aggregates at increasing ionic strengths. *Arch Oral Biol*, 49, 199-207.
- ANDERSON, P., BOLLET-QUIVOGNE, F. R. G., DOWKER, S. E. P. & ELLIOTT, J. C. 2004b. Demineralization in enamel and hydroxyapatite aggregates at increasing ionic strengths. *Archives of Oral Biology*, 49, 199-207.
- ANDERSON, P. & ELLIOTT, J. 1993. Scanning Microradiography. *Microbeam Analysis Journal*, 30-31.
- ANDERSON, P., HECTOR, M. P. & RAMPERSAD, M. A. 2001. Critical pH in resting and stimulated whole saliva in groups of children and adults. *Int J Paediatr Dent*, 11, 266-73.
- ANDERSON, P., LEVINKIND, M. & ELLIOTT, J. C. 1998. Scanning microradiographic studies of rates of in vitro demineralization in human and bovine dental enamel. *Archives of Oral Biology*, 43, 649-656.
- ARENDS, J. & CHRISTOFFERSEN, J. 1990. Nature and role of loosely bound fluoride in dental caries. *J Dent Res*, 69 Spec No, 601-5; discussion 634-6.
- ARENDS, J., JONGEBLOED, W., OGAARD, B. & ROLLA, G. 1987. SEM and microradiographic investigation of initial enamel caries. *Scand J Dent Res*, 95, 193-201.
- ARENDS, J. & TEN CATE, J. M. 1981. Tooth enamel remineralization. *Journal of Crystal Growth*, 53, 135-147.
- ASTM, E.-E. 2012. Standard Test Method for Knoop and Vickers Hardness of Materials.
- BAGRAMIAN, R. A., GARCIA-GODOY, F. & VOLPE, A. R. 2009. The global increase in dental caries. A pending public health crisis. *Am J Dent*, 22, 3-8.
- BARBIER, O., ARREOLA-MENDOZA, L. & DEL RAZO, L. M. 2010. Molecular mechanisms of fluoride toxicity. *Chemico-biological interactions*, 188, 319-333.
- BAYSAN, A. & ANDERSON, P. 2009. Non-Contact Optical Profilometry for Detection of Surface Changes of Hydroxyapatite Discs during Acid Attack. *ORCA*.
- BERKOVITZ, B. K. B. 2011. Master dentistry Vol. 3, Oral biology. 3rd ed. Edinburgh: Churchill Livingstone.
- BJORVATN, K. & MORCH, T. 1979. The calcium selective electrode--a possible tool in dental research. *Acta Odontol Scand*, 37, 259-65.

- BOLLET-QUIVOGNE, F. R., ANDERSON, P., DOWKER, S. E. & ELLIOTT, J. C. 2005. Scanning microradiographic study on the influence of diffusion in the external liquid on the rate of demineralization in hydroxyapatite aggregates. *Eur J Oral Sci*. Denmark.
- BOWEN, W. H. 2013. The Stephan Curve revisited. *Odontology*, 101, 2-8.
- BOYDE, A. 1964. *The structure and development of mammalian enamel*. PhD.
- BOYDE, A. 1979. Carbonate Concentration, Crystal Centers, Core Dissolution, Caries, Cross Striations, Circadian Rhythms, and Compositional Contrast in the SEM. *Journal of Dental Research*, 58, 981–983.
- BRAGA, M. M., MENDES, F. M., DE BENEDETTO, M. S. & IMPARATO, J. C. 2009. Effect of silver diamine fluoride on incipient caries lesions in erupting permanent first molars: a pilot study. *J Dent Child (Chic)*, 76, 28-33.
- BRATOVČIĆ, A. & ODOBASIĆ, A. 2011. *Determination of Fluoride and Chloride Contents in Drinking Water by Ion Selective Electrode, Environmental Monitoring, Dr Ema Ekundayo (Ed.)*, <http://www.intechopen.com/books/environmental-monitoring/determination-of-fluoride-and-chloride-contents-in-drinking-water-by-ion-selective-electrode>, InTech.
- BRATTHALL, D., HANSEL-PETERSSON, G. & SUNDBERG, H. 1996. Reasons for the caries decline: what do the experts believe? *Eur J Oral Sci*, 104, 416-22; discussion 423-5, 430-2.
- BUHLMANN, P. & CHEN, L. D. 2012. Ion-Selective Electrodes With Ionophore-Doped Sensing Membranes. *Supramolecular devices*, 2539-2579.
- BUSCH, S., SCHWARZ, U. & KNIEP, R. 2001. Morphogenesis and Structure of Human Teeth in Relation to Biomimetically Grown Fluorapatite–Gelatin Composites. *Chemistry of Materials*, 13, 3260-3271.
- BUZALAF, M. A., PESSAN, J. P., HONORIO, H. M. & TEN CATE, J. M. 2011. Mechanisms of action of fluoride for caries control. *Monogr Oral Sci*, 22, 97-114.
- CAIRNS, A. M., WATSON, M., CREANOR, S. L. & FOYE, R. H. 2002. The pH and titratable acidity of a range of diluting drinks and their potential effect on dental erosion. *J Dent*, 30, 313-7.
- CAREY, C. M. & VOGEL, G. L. 2000. Measurement of Calcium Activity in Oral Fluids by Ion Selective Electrode: Method Evaluation and Simplified Calculation of Ion Activity Products *Journal of Research of the National Institute of Standards and Technology*, 105, 267-273.
- CHEN, L. D., MANDAL, D., POZZI, G., GLADYSZ, J. A. & BUHLMANN, P. 2011. Potentiometric sensors based on fluoros membranes doped with highly selective ionophores for carbonate. *J Am Chem Soc*, 133, 20869-77.
- CHRISTIAN, G. D. 2004. *Analytical chemistry*, Hoboken, NJ, Wiley.
- CHU, C. H., LEE, A. H., ZHENG, L., MEI, M. L. & CHAN, G. C. 2014. Arresting rampant dental caries with silver diamine fluoride in a young teenager suffering from chronic oral graft versus host disease post-bone marrow transplantation: a case report. *BMC Res Notes*, 7, 3.
- CHU, C. H. & LO, E. C. 2008a. Microhardness of dentine in primary teeth after topical fluoride applications. *J Dent*, 36, 387-91.
- CHU, C. H. & LO, E. C. 2008b. Promoting caries arrest in children with silver diamine fluoride: a review. *Oral Health Prev Dent*, 6, 315-21.
- CHU, C. H., LO, E. C. & LIN, H. C. 2002. Effectiveness of silver diamine fluoride and sodium fluoride varnish in arresting dentin caries in Chinese pre-school children. *J Dent Res*, 81, 767-70.
- CHU, C. H., MEI, L., SENEVIRATNE, C. J. & LO, E. C. 2012. Effects of silver diamine fluoride on dentine carious lesions induced by *Streptococcus mutans* and *Actinomyces naeslundii* biofilms. *Int J Paediatr Dent*, 22, 2-10.

- CHUMBIMUNI-TORRES, K. Y., BAKKER, E. & WANG, J. 2009. REAL-TIME PROBING OF THE GROWTH DYNAMICS OF NANOPARTICLES USING POTENTIOMETRIC ION-SELECTIVE ELECTRODES. *Electrochem commun*, 11, 1964-1967.
- COCHRANE, N. J., ANDERSON, P., DAVIS, G. R., ADAMS, G. G., STACEY, M. A. & REYNOLDS, E. C. 2012. An X-ray microtomographic study of natural white-spot enamel lesions. *J Dent Res*, 91, 185-91.
- CONTRERAS, V., TORO, M. J., ELIAS-BONETA, A. R. & ENCARNACION-BURGOS, A. 2017. Effectiveness of silver diamine fluoride in caries prevention and arrest: a systematic literature review. *Gen Dent*, 65, 22-29.
- COVINGTON & KENNETH, A. 1979. *Ion-selective electrode methodology*, Boca Raton, Fla, CRC Press.
- CRAIG, G. G., POWELL, K. R. & COOPER, M. H. 1981. Caries progression in primary molars: 24-month results from a minimal treatment programme. *Community Dent Oral Epidemiol*, 9, 260-5.
- CRAIG, G. G., POWELL, K. R. & COOPER, M. H. 1987. Clinical appearance of permanent successors after nonextraction treatment of grossly carious primary molars in highly anxious children. *ASDC J Dent Child*, 54, 170-5.
- CRAIG, R. G. & PEYTON, F. A. 1958. The micro-hardness of enamel and dentin. *J Dent Res*, 37, 661-8.
- CRYSTAL, Y. O., MARGHALANI, A. A., URELES, S. D., WRIGHT, J. T., SULYANTO, R., DIVARIS, K., FONTANA, M. & GRAHAM, L. 2017. Use of Silver Diamine Fluoride for Dental Caries Management in Children and Adolescents, Including Those with Special Health Care Needs. *Pediatr Dent*, 39, 135-145.
- CRYSTAL, Y. O. & NIEDERMAN, R. 2016. Silver Diamine Fluoride Treatment Considerations in Children's Caries Management. *Pediatr Dent*, 38, 466-471.
- CUI, F. Z. & GE, J. 2007. New observations of the hierarchical structure of human enamel, from nanoscale to microscale. *J Tissue Eng Regen Med*, 1, 185-91.
- CURY, J. A. & TENUTA, L. M. 2009. Enamel remineralization: controlling the caries disease or treating early caries lesions? *Braz Oral Res*, 23 Suppl 1, 23-30.
- CURZON, M. & FEATHERSTONE, J. 1983. Chemical composition of enamel. In: EP, L. (ed.) *Handbook of Experimental Aspects of Oral Biochemistry*. Boca Raton: CRC Press.
- DAVIDSON, C. L., HOEKSTRA, I. S. & ARENDS, J. 1974. Microhardness of sound, decalcified and etched tooth enamel related to the calcium content. *Caries Res*, 8, 135-44.
- DAWES, C. 2003. What is the critical pH and why does a tooth dissolve in acid? *J Can Dent Assoc*, 69, 722-4.
- DAWES, C. 2008. Salivary flow patterns and the health of hard and soft oral tissues. *J Am Dent Assoc*. United States.
- DE ALMEIDA LDE, F., CAVALCANTI, Y. W. & VALENCA, A. M. 2011. In vitro antibacterial activity of silver diamine fluoride in different concentrations. *Acta Odontol Latinoam*, 24, 127-31.
- DIJKMAN, A. G., TAK, J. & ARENDS, J. 1982. Fluoride deposited topical applications in enamel. KOH-soluble and acquired fluoride. *Caries Res*, 16, 147-55.
- DISTLER, W. & KRONCKE, A. 1980. Acid formation by mixed cultures of cariogenic strains of *Streptococcus mutans* and *Veillonella alcalescens*. *Arch Oral Biol*, 25, 655-8.
- DO AMARAL, J. G., DELBEM, A. C., PESSAN, J. P., MANARELLI, M. M. & BARBOUR, M. E. 2016. Effects of polyphosphates and fluoride on hydroxyapatite dissolution: A pH-stat investigation. *Arch Oral Biol*, 63, 40-6.
- DONOVAN, T. 2011. COMMENTARY. Dental erosion: understanding this pervasive condition. *J Esthet Restor Dent*, 23, 217-8.

- DOS SANTOS, V. E., JR., DE VASCONCELOS, F. M., RIBEIRO, A. G. & ROSENBLATT, A. 2012. Paradigm shift in the effective treatment of caries in schoolchildren at risk. *Int Dent J*, 62, 47-51.
- DOUGLASS, A. B. 2003. Common Dental Emergencies. *Am Fam Physician*.
- DRIESENS, F. C. M. 1980. The mineral in bone, dentin and tooth enamel. *Bulletin des Soci*, 89, 663 - 689.
- DUANGTHIP, D., CHU, C. H. & LO, E. C. 2016. A randomized clinical trial on arresting dentine caries in preschool children by topical fluorides--18 month results. *J Dent*, 44, 57-63.
- DUANGTHIP, D., FUNG, M. H. T., WONG, M. C. M., CHU, C. H. & LO, E. C. M. 2018. Adverse Effects of Silver Diamine Fluoride Treatment among Preschool Children. *J Dent Res*, 97, 395-401.
- DUANGTHIP, D., WONG, M. C. M., CHU, C. H. & LO, E. C. M. 2017. Caries arrest by topical fluorides in preschool children: 30-month results. *J Dent*.
- EHRlich, H., KOUTSOUKOS, P. G., DEMADIS, K. D. & POKROVSKY, O. S. 2009. Principles of demineralization: modern strategies for the isolation of organic frameworks. Part II. Decalcification. *Micron*, 40, 169-93.
- ELLIOTT, J. C. 1994. *Structure and Chemistry of the Apatites and Other Calcium Orthophosphates*, Amsterdam, The Netherlands, Elsevier.
- ELLIOTT, J. C., ANDERSON, P., GAO, X. J., WONG, F. S. L., DAVIS, G. R. & DOWKER, S. E. P. 1994. Application of scanning microradiography and X-ray microtomography to studies of bones and teeth. *Journal of X-Ray Science and Technology*, 4, 102-117.
- ELSHARKAWY, S., AL-JAWAD, M., PANTANO, M. F., TEJEDA-MONTES, E., MEHTA, K., JAMAL, H., AGARWAL, S., SHUTURMINSKA, K., RICE, A., TARAKINA, N. V., WILSON, R. M., BUSHBY, A. J., ALONSO, M., RODRIGUEZ-CABELLO, J. C., BARBIERI, E., DEL RIO HERNANDEZ, A., STEVENS, M. M., PUGNO, N. M., ANDERSON, P. & MATA, A. 2018. Protein disorder-order interplay to guide the growth of hierarchical mineralized structures. *Nat Commun*, 9, 2145.
- ENGLAND, G. 2013. *Microhardness Test* [Online]. <https://www.gordonengland.co.uk/hardness/microhardness.htm> [Accessed 2018].
- FEATHERSTONE, J. D. 1977. Diffusion phenomena during artificial carious lesion formation. *J Dent Res*, 56 Special D, D48-52.
- FEATHERSTONE, J. D. 1999. Prevention and reversal of dental caries: role of low level fluoride. *Community Dent Oral Epidemiol*, 27, 31-40.
- FEATHERSTONE, J. D. 2004. The continuum of dental caries--evidence for a dynamic disease process. *J Dent Res*, 83 Spec No C, C39-42.
- FEATHERSTONE, J. D. 2008. Dental caries: a dynamic disease process. *Aust Dent J*, 53, 286-91.
- FEJERSKOV, O. 2004. Changing paradigms in concepts on dental caries: consequences for oral health care. *Caries Res*, 38, 182-91.
- FIRSCHING, F. H. 1961. Precipitation of Silver Phosphate from Homogenous Solution. *Analytical Chemistry*, 33, 873-874.
- FRANT, M. S. 1994. Historical perspective. History of the early commercialization of ion-selective electrodes. *Analyst*, 119, 2293-2301.
- FRANT, M. S. & ROSS, J. W., JR. 1968. Use of a total ionic strength adjustment buffer for electrode determination of fluoride in water supplies. *Anal Chem*, 40, 1169-71.
- FRENCKEN, J. E., PETERS, M. C., MANTON, D. J., LEAL, S. C., GORDAN, V. V. & EDEN, E. 2012. Minimal intervention dentistry for managing dental caries - a review: report of a FDI task group. *Int Dent J*, 62, 223-43.
- FUNG, M. H., WONG, M. C., LO, E. C. & CHU, C. 2013. Arresting early childhood caries with silver diamine fluoride -A literature review. *J Oral Hyg Health*, 1.

- FUNG, M. H. T., DUANGTHIP, D., WONG, M. C. M., LO, E. C. M. & CHU, C. H. 2016. Arresting Dentine Caries with Different Concentration and Periodicity of Silver Diamine Fluoride. *JDR Clin Trans Res*, 1, 143-152.
- FUNG, M. H. T., DUANGTHIP, D., WONG, M. C. M., LO, E. C. M. & CHU, C. H. 2018. Randomized Clinical Trial of 12% and 38% Silver Diamine Fluoride Treatment. *J Dent Res*, 97, 171-178.
- GAO, S. S., ZHAO, I. S., HIRAISHI, N., DUANGTHIP, D., MEI, M. L., LO, E. C. M. & CHU, C. H. 2016. Clinical Trials of Silver Diamine Fluoride in Arresting Caries among Children: A Systematic Review. *JDR Clinical & Translational Research*, 1, 201-210.
- GARCIA-GODOY, F. & HICKS, M. J. 2008. Maintaining the integrity of the enamel surface: the role of dental biofilm, saliva and preventive agents in enamel demineralization and remineralization. *J Am Dent Assoc*. United States.
- GERTH, H. U., DAMMASCHKE, T., SCHAFFER, E. & ZUCHNER, H. 2007. A three layer structure model of fluoridated enamel containing CaF<sub>2</sub>, Ca(OH)<sub>2</sub> and Fap. *Dent Mater*, 23, 1521-8.
- GOLDSTEIN, J. I., NEWBURY, D. E., PATRICK, ECHLIN, JOY, D. C., LYMAN, C. E., LIFSHIN, E., SAWYER, L. & MICHAEL, J. R. 2003. *Scanning Electron Microscopy and X-ray Microanalysis*, Boston, Springer.
- GOTJAMANOS, T. 1996. Pulp response in primary teeth with deep residual caries treated with silver fluoride and glass ionomer cement ('atraumatic' technique). *Aust Dent J*, 41, 328-34.
- GOTJAMANOS, T. 1997. Safety issues related to the use of silver fluoride in paediatric dentistry. *Aust Dent J*, 42, 166-8.
- GOTJAMANOS, T. & AFONSO, F. 1997. Unacceptably high levels of fluoride in commercial preparations of silver fluoride. *Aust Dent J*, 42, 52-3.
- GOTJAMANOS, T. & ORTON, V. 1998. Abnormally high fluoride levels in commercial preparations of 40 per cent silver fluoride solution: contraindications for use in children. *Aust Dent J*, 43, 422-7.
- GREEN, E. 1989. A clinical evaluation of two methods of caries prevention in newly-erupted first permanent molars. *Aust Dent J*, 34, 407-9.
- GUPTA, M., PANDIT, I., SRIVASTAVA, N. & GUGNANI, N. 2009. Dental Erosion in Children. *JOHCD*, 3, 59-61.
- HAMAMA, H. H., YIU, C. K. & BURROW, M. F. 2015. Effect of silver diamine fluoride and potassium iodide on residual bacteria in dentinal tubules. *Aust Dent J*, 60, 80-7.
- HARA, A. T. & ZERO, D. T. 2008. Analysis of the erosive potential of calcium-containing acidic beverages. *Eur J Oral Sci*, 116, 60-5.
- HARVEY, D. 2016. *Analytical Chemistry* [Online]. [http://chemwiki.ucdavis.edu/Core/Analytical\\_Chemistry/Analytical\\_Chemistry\\_2.0/11\\_Electrochemical\\_Methods/11.2%3A\\_Potentiometric\\_Methods](http://chemwiki.ucdavis.edu/Core/Analytical_Chemistry/Analytical_Chemistry_2.0/11_Electrochemical_Methods/11.2%3A_Potentiometric_Methods). [Accessed 8.4 2017].
- HASSANALI, L., WONG, F. S., LYNCH, R. J. M. & ANDERSON, P. 2017. A Novel Kinetic Method to Measure Apparent Solubility Product of Bulk Human Enamel.
- HAZELRIGG, C. O., DEAN, J. A. & FONTANA, M. 2003. Fluoride varnish concentration gradient and its effect on enamel demineralization. *Pediatr Dent*, 25, 119-26.
- HE, L. H. & SWAIN, M. V. 2007. Enamel - a "metallic-like" deformable biocomposite. *J Dent*. England.
- HE, L. H. & SWAIN, M. V. 2008. Understanding the mechanical behaviour of human enamel from its structural and compositional characteristics. *J Mech Behav Biomed Mater*. Netherlands.
- HELLWIG, E. & LENNON, A. M. 2004. Systemic versus topical fluoride. *Caries Res*, 38, 258-62.



- HICKS, J., GARCIA-GODOY, F. & FLAITZ, C. 2003. Biological factors in dental caries: role of saliva and dental plaque in the dynamic process of demineralization and remineralization (part 1). *J Clin Pediatr Dent*, 28, 47-52.
- HICKS, J., GARCIA-GODOY, F. & FLAITZ, C. 2004. Biological factors in dental caries enamel structure and the caries process in the dynamic process of demineralization and remineralization (part 2). *J Clin Pediatr Dent*, 28, 119-24.
- HIGHAM, S. 2014. Caries Process and prevention Strategies: Erosion.
- HORST, J. A. 2018. Silver Fluoride as a Treatment for Dental Caries. *Adv Dent Res*, 29, 135-140.
- HORST, J. A., ELLENIKIOTIS, H. & MILGROM, P. L. 2016. UCSF Protocol for Caries Arrest Using Silver Diamine Fluoride: Rationale, Indications and Consent. *J Calif Dent Assoc*, 44, 16-28.
- HUANG, W. T., SHAHID, S. & ANDERSON, P. 2018. Validation of a Real-Time ISE Methodology to Quantify the Influence of Inhibitors of Demineralization Kinetics in vitro Using a Hydroxyapatite Model System. *Caries Research*, 52, 598-603.
- HUNTER, P. B. 1988. Risk factors in dental caries. *Int Dent J*, 38, 211-7.
- IGGO, J. A. 2011. *NMR Spectroscopy in Inorganic Chemistry*, Oxford University Press.
- ITOTA, T., CARRICK, T. E., RUSBY, S., AL-NAIMI, O. T., YOSHIYAMA, M. & MCCABE, J. F. 2004. Determination of fluoride ions released from resin-based dental materials using ion-selective electrode and ion chromatograph. *J Dent*, 32, 117-22.
- JEFFCOAT, M. K. 1998. Osteoporosis: a possible modifying factor in oral bone loss. *Ann Periodontol*, 3, 312-21.
- JONES, S. B., REES, G. D., SHELLIS, R. P. & BARBOUR, M. E. 2013. The effect of monoalkyl phosphates and fluoride on dissolution of hydroxyapatite, and interactions with saliva. *Caries Res*, 47, 355-63.
- KIDD, E. A. M. 2005. *Essentials of dental caries*, Oxford ; New York, Oxford University Press.
- KILIÇEL, F. & DAĞ, B. 2014. Determination of Fluoride Ions in Resource and Mineral Waters of the Van Region by Using Ion-Selective Electrode Method. *Advances in Analytical Chemistry*, 4, 9-12.
- KIM, H.-J., HUMMEL, J. W., BIRRELL, S. J. & SUDDUTH, K. A. 2005. Evaluation of Phosphate Ion-Selective Membranes for Real-time Soil Nutrient Sensing. *ASAE Meeting Presentation*, Paper Number: 051033.
- KNIGHT, G. M., MCINTYRE, J. M., CRAIG, G. G., MULYANI, ZILM, P. S. & GULLY, N. J. 2005. An in vitro model to measure the effect of a silver fluoride and potassium iodide treatment on the permeability of demineralized dentine to *Streptococcus mutans*. *Aust Dent J*, 50, 242-5.
- KNIGHT, G. M., MCINTYRE, J. M., CRAIG, G. G., MULYANI, ZILM, P. S. & GULLY, N. J. 2007. Differences between normal and demineralized dentine pretreated with silver fluoride and potassium iodide after an in vitro challenge by *Streptococcus mutans*. *Aust Dent J*, 52, 16-21.
- KNIGHT, G. M., MCINTYRE, J. M., CRAIG, G. G., MULYANI, ZILM, P. S. & GULLY, N. J. 2009. Inability to form a biofilm of *Streptococcus mutans* on silver fluoride- and potassium iodide-treated demineralized dentin. *Quintessence Int*, 40, 155-61.
- KORYTA, J. & ŠTULÍK, K. 1983. *Ion-Selective Electrodes*, Cambridge, Cambridge University Press.
- KOSORIC, J., HECTOR, M. P. & ANDERSON, P. 2010. The influence of proteins on demineralization kinetics of hydroxyapatite aggregates. *J Biomed Mater Res A*, 94, 972-7.
- KUMAR, P., VINITHA, B. & FATHIMA, G. 2013. Bone grafts in dentistry. *J Pharm Bioallied Sci*, 5, S125-7.
- LAKSHMINARAYANAIHAH, N. 2012. *Membrane Electrodes*, Elsevier.
- LANSDOWN, A. B. 2002. Silver. I: Its antibacterial properties and mechanism of action. *J Wound Care*, 11, 125-30.

- LANSDOWN, A. B. 2006. Silver in health care: antimicrobial effects and safety in use. *Curr Probl Dermatol*, 33, 17-34.
- LARSEN, M. J. 1974. Demineralization of human enamel. *Scand J Dent Res*, 82, 491-5.
- LARSEN, M. J. 1990. Chemical events during tooth dissolution. *J Dent Res*, 69 Spec No, 575-80; discussion 634-6.
- LAURANCE-YOUNG, P., BOZEC, L., GRACIA, L., REES, G., LIPPERT, F., LYNCH, R. J. & KNOWLES, J. C. 2011. A review of the structure of human and bovine dental hard tissues and their physicochemical behaviour in relation to erosive challenge and remineralisation. *J Dent*, 39, 266-72.
- LEGEROS, R. Z. 1991. Calcium phosphates in oral biology and medicine. *Monogr Oral Sci*, 15, 1-201.
- LEWIS, E. I. 1920. *Inorganic chemistry*, Cambridge at the university press.
- LI, R., LO, E. C., LIU, B. Y., WONG, M. C. & CHU, C. H. 2016. Randomized clinical trial on arresting dental root caries through silver diammine fluoride applications in community-dwelling elders. *J Dent*, 51, 15-20.
- LI, X., WANG, J., JOINER, A. & CHANG, J. 2014. The remineralisation of enamel: a review of the literature. *J Dent*, 42 Suppl 1, S12-20.
- LIN, Z. Y., XIAO, J., YAN, J. H., LIU, P., LI, L. H. & YANG, G. W. 2015. Ag/AgCl plasmonic cubes with ultrahigh activity as advanced visible-light photocatalysts for photodegrading dyes. *Journal of Materials Chemistry A*, 3, 7649-7658.
- LING FENG, Q., NAM KIM, T., WU, J., SEO PARK, E., OCK KIM, J., YOUNG LIM, D. & ZHAI CUI, F. 1998. Antibacterial effects of Ag-HAp thin films on alumina substrates. *Thin Solid Films*, 335, 214-219.
- LINGAWI, H. S. 2012. *EFFECT OF DIVALENT METAL CATIONS ON HYDROXYAPATITE DISSOLUTION KINETICS RELEVANT TO DENTAL CARIES AND EROSION*. PhD, Queen Mary University of London.
- LINNETT, V. & SEOW, W. K. 2001. Dental erosion in children: a literature review. *Pediatr Dent*, 23, 37-43.
- LIU, B. Y., LO, E. C., CHU, C. H. & LIN, H. C. 2012a. Randomized trial on fluorides and sealants for fissure caries prevention. *J Dent Res*, 91, 753-8.
- LIU, B. Y., LO, E. C. & LI, C. M. 2012b. Effect of silver and fluoride ions on enamel demineralization: a quantitative study using micro-computed tomography. *Aust Dent J*, 57, 65-70.
- LIU, J.-K., LUO, C.-X., WANG, J.-D., YANG, X.-H. & ZHONG, X.-H. 2012c. Controlled synthesis of silver phosphate crystals with high photocatalytic activity and bacteriostatic activity. *CrystEngComm*, 14, 8714-8721.
- LI, Y., QIU, X. & LI, J. 1984. Effect of a silver ammonia fluoride solution on the prevention and inhibition of caries. *Zhonghua Kou Qiang Ke Za Zhi*, 19, 97-100
- LLODRA, J. C., RODRIGUEZ, A., FERRER, B., MENARDIA, V., RAMOS, T. & MORATO, M. 2005. Efficacy of silver diamine fluoride for caries reduction in primary teeth and first permanent molars of schoolchildren: 36-month clinical trial. *J Dent Res*, 84, 721-4.
- LO, E. C., CHU, C. H. & LIN, H. C. 2001. A community-based caries control program for pre-school children using topical fluorides: 18-month results. *J Dent Res*, 80, 2071-4.
- LOU, Y. L., BOTELHO, M. G. & DARVELL, B. W. 2011. Reaction of silver diamine [corrected] fluoride with hydroxyapatite and protein. *J Dent*, 39, 612-8.
- LU, X., ZHANG, H., GUO, Y., WANG, Y., GE, X., LENG, Y. & WATARI, F. 2011. Hexagonal hydroxyapatite formation on TiO<sub>2</sub> nanotubes under urea modulation. *CrystEngComm*, 13, 3741-3749.
- LUSSI, A. 2006a. *Dental Erosion From Diagnosis to Therapy*, Switzerland, S. Karger AG, P.O. Box, CH-4009 Basel.

- LUSSI, A. 2006b. *Dental Erosion From Diagnosis to Therapy*, S. Karger AG, P.O. Box, CH-4009 Basel (Switzerland).
- LUSSI, A., JAGGI, T. & SCHARER, S. 1993. The influence of different factors on in vitro enamel erosion. *Caries Res*, 27, 387-93.
- LYNCH, R. J. 2013. The primary and mixed dentition, post-eruptive enamel maturation and dental caries: a review. *Int Dent J*, 63 Suppl 2, 3-13.
- MAGALHAES, A. C., MORAES, S. M., RIOS, D. & BUZALAF, M. A. 2009a. Effect of ion supplementation of a commercial soft drink on tooth enamel erosion. *Food Addit Contam Part A Chem Anal Control Expo Risk Assess*, 26, 152-6.
- MAGALHAES, A. C., WIEGAND, A., RIOS, D., BUZALAF, M. A. & LUSSI, A. 2011. Fluoride in dental erosion. *Monogr Oral Sci*, 22, 158-70.
- MAGALHAES, A. C., WIEGAND, A., RIOS, D., HONORIO, H. M. & BUZALAF, M. A. 2009b. Insights into preventive measures for dental erosion. *J Appl Oral Sci*, 17, 75-86.
- MALDE, M. K., BJORVATN, K. & JULSHAMN, K. 2001. Determination of fluoride in food by the use of alkali fusion and fluoride ion-selective electrode *Food Chemistry*, 73, 373-379.
- MARSH, P. D. 2009. *Oral Microbiology*, London, Elsevier.
- MARSHALL, A. F. & LAWLESS, K. R. 1981. TEM study of the central dark line in enamel crystallites. *J Dent Res*, 60, 1773-82.
- MATINLINNA, J. P. 2015. *Handbook of Oral Biomaterials*, CRC Press Inc.
- MAYA, DOYCHINOVA, VESSELIN, KUSSOVSKI, TSVETAN, TONCHEV, SLAVCHO & DIMITROV 2015. PHOTODYNAMIC INACTIVATION OF HUMAN DENTAL BIOFILM ISOLATED STREPTOCOCCUS MUTANS WITH 2 PHOTSENSITIZERS – AN IN VITRO STUDY. *Scripta Scientifica Medica*, 47.
- MCCANN, H. G. 1968. The solubility of fluorapatite and its relationship to that of calcium fluoride. *Arch Oral Biol*, 13, 987-1001.
- MCCONNELL, D. & FOREMAN, D. W. 1966. The properties and Structure of Ca<sub>10</sub>(PO<sub>4</sub>)<sub>6</sub>(OH)<sub>2</sub>; its relation to tin (II) apatite. *The Canadian Mineralogist*, 8, 431-436.
- MCDONALD, S. P. & SHEIHAM, A. 1994. A clinical comparison of non-traumatic methods of treating dental caries. *Int Dent J*, 44, 465-70.
- MEI, M. L., CHU, C. H., LO, E. C. & SAMARANAYAKE, L. P. 2013a. Fluoride and silver concentrations of silver diamine fluoride solutions for dental use. *Int J Paediatr Dent*, 23, 279-85.
- MEI, M. L., CHU, C. H., LOW, K. H., CHE, C. M. & LO, E. C. 2013b. Caries arresting effect of silver diamine fluoride on dentine carious lesion with *S. mutans* and *L. acidophilus* dual-species cariogenic biofilm. *Med Oral Patol Oral Cir Bucal*, 18, e824-31.
- MEI, M. L., ITO, L., CAO, Y., LI, Q. L., CHU, C. H. & LO, E. C. 2014a. The inhibitory effects of silver diamine fluorides on cysteine cathepsins. *J Dent*, 42, 329-35.
- MEI, M. L., ITO, L., CAO, Y., LI, Q. L., LO, E. C. & CHU, C. H. 2013c. Inhibitory effect of silver diamine fluoride on dentine demineralisation and collagen degradation. *J Dent*, 41, 809-17.
- MEI, M. L., ITO, L., CAO, Y., LO, E. C., LI, Q. L. & CHU, C. H. 2014b. An ex vivo study of arrested primary teeth caries with silver diamine fluoride therapy. *J Dent*, 42, 395-402.
- MEI, M. L., LI, Q. L., CHU, C. H., LO, E. C. & SAMARANAYAKE, L. P. 2013d. Antibacterial effects of silver diamine fluoride on multi-species cariogenic biofilm on caries. *Ann Clin Microbiol Antimicrob*, 12, 4.
- MEI, M. L., LI, Q. L., CHU, C. H., YIU, C. K. & LO, E. C. 2012. The inhibitory effects of silver diamine fluoride at different concentrations on matrix metalloproteinases. *Dent Mater*, 28, 903-8.
- MEI, M. L., LO, E. C. & CHU, C. H. 2016. Clinical Use of Silver Diamine Fluoride in Dental Treatment. *Compend Contin Educ Dent*, 37, 93-8; quiz100.

- MEI, M. L., LO, E. C. M. & CHU, C. H. 2018. Arresting Dentine Caries with Silver Diamine Fluoride: What's Behind It? *J Dent Res*, 22034518774783.
- MEI, M. L., NUDELMAN, F., MARZEC, B., WALKER, J. M., LO, E. C. M., WALLS, A. W. & CHU, C. H. 2017. Formation of Fluorohydroxyapatite with Silver Diamine Fluoride. *J Dent Res*, 96, 1122-1128.
- MELLBERG, J. R. 1992. Hard-tissue substrates for evaluation of cariogenic and anti-cariogenic activity in situ. *J Dent Res*, 71 Spec No, 913-9.
- MEURMAN, J. H. & TEN CATE, J. M. 1996. Pathogenesis and modifying factors of dental erosion. *Eur J Oral Sci*, 104, 199-206.
- MIDDLETON, W. 1999. *ENERGY-DISPERSIVE X-RAY MICROANALYSIS - An Introduction*, Kevex Instruments, Inc.
- MILGROM, P., HORST, J. A., LUDWIG, S., ROTHEN, M., CHAFFEE, B. W., LYALINA, S., POLLARD, K. S., DERISI, J. L. & MANCL, L. 2018. Topical silver diamine fluoride for dental caries arrest in preschool children: A randomized controlled trial and microbiological analysis of caries associated microbes and resistance gene expression. *J Dent*, 68, 72-78.
- MILLER, W. D. 1905. Preventive Treatment of the Teeth with Special Reference to Silver Nitrate. *The Dental cosmos; a monthly record of dental science.*, 47, 913-922.
- MIURA, H., ARAKI, Y. & OHNO, H. 1993. A computer simulation of the reactions between hydroxyapatite and fluoride in aqueous acidic solutions. *Dent Mater J*, 12, 209-18.
- MOHAMMED, N. R., KENT, N. W., LYNCH, R. J., KARPUKHINA, N., HILL, R. & ANDERSON, P. 2013. Effects of fluoride on in vitro enamel demineralization analyzed by <sup>(1)</sup>(9)F MAS-NMR. *Caries Res*, 47, 421-8.
- MOHAMMED, N. R., LYNCH, R. J. & ANDERSON, P. 2014a. Effects of fluoride concentration on enamel demineralization kinetics in vitro. *J Dent*, 42, 613-8.
- MOHAMMED, N. R., LYNCH, R. J. & ANDERSON, P. 2015. Inhibitory Effects of Zinc Ions on Enamel Demineralisation Kinetics in vitro. *Caries Res*, 49, 600-5.
- MOHAMMED, N. R., MNEIMNE, M., HILL, R. G., AL-JAWAD, M., LYNCH, R. J. & ANDERSON, P. 2014b. Physical chemical effects of zinc on in vitro enamel demineralization. *J Dent*, 42, 1096-104.
- MOREIRA, R. D. S. 2012. *Epidemiology of Dental Caries in the World, Oral Health Care - Pediatric, Research, Epidemiology and Clinical Practices*, InTech.
- MORENO, E. C. & ZAHRADNIK, R. T. 1974. Chemistry of enamel subsurface demineralization in vitro. *J Dent Res*, 53, 226-35.
- MORENO, E. C. & ZAHRADNIK, R. T. 1979. Demineralization and remineralization of dental enamel. *J Dent Res*, 58, 896-903.
- MUKUNDAN, R., W., CRAWFORD, J., ELLIOTT, J., S.E., P. & DOWKER 1999. Rietveld refinement of the crystallographic structure of human dental enamel apatites. *American Mineralogist*, 84.
- MURDOCH-KINCH, C. A. & MCLEAN, M. E. 2003. Minimally invasive dentistry. *Journal of the American Dental Association*, 134, 87-95.
- NAVARRO, M., MONTE ALTO, L. A., CRUZ, R. A. & PRAZERES, J. 2001. Calcium fluoride uptake by human enamel after use of fluoridated mouthrinses. *Braz Dent J*, 12, 178-82.
- NEWBRUN, E. 1982. Sugar and dental caries: a review of human studies. *Science*, 217, 418-23.
- NGO, H., M.KNIGHT, G., GEORGE, G. & SEKIGUCHI, T. 2002. *United States Patent*. US 6,461,161 B1.
- NIH. 2014. *Dental Caries (Tooth Decay)* [Online]. <https://www.nidcr.nih.gov/DataStatistics/FindDataByTopic/DentalCaries/>. [Accessed Feb 20 2017].
- NIXON, W. C. 1969. Scanning electron microscopy. *Contemporary Physics*, 10, 71-96.
- OESCH, U., AMMANN, D. & SIMON, W. 1986. Ion-selective membrane electrodes for clinical use. *Clinical Chemistry*, 32, 1448-1459.

- PEARCE, E. I. F., COOTE, G. E. & LARSEN, M. J. 1995. The Distribution of Fluoride in Carious Human Enamel. *Journal of Dental Research*, 74, 1775-1782.
- PENG, J. J., BOTELHO, M. G. & MATINLINNA, J. P. 2012. Silver compounds used in dentistry for caries management: a review. *J Dent*, 40, 531-41.
- PETER, M. 2005. WDS VS EDS [Online].  
<http://www.mcswiggen.com/TechNotes/WDSvsEDS.htm>. [Accessed 9.4 2017].
- PUNYANIRUN, K., YOSPIBOONWONG, T., KUNAPINUN, T., THANYASRISUNG, P. & TRAIRATVORAKUL, C. 2018. Silver diamine fluoride remineralized artificial incipient caries in permanent teeth after bacterial pH-cycling in-vitro. *J Dent*, 69, 55-59.
- REN, Y.-F. 2011. Dental Erosion: Etiology, Diagnosis and Prevention.
- RICHARDS, D. 2016. Impact of diet on tooth erosion. *Evid Based Dent*, 17, 40.
- ROBERT, J. D. 1959. *Nuclear magnetic Resonance applications to organic chemistry*, McGRAW - HILL BOOK COMPANY, INC. NEW YORK, TORONTO, LONDON.
- ROBINSON, C. 2009. Fluoride and the caries lesion: interactions and mechanism of action. *Eur Arch Paediatr Dent*. England.
- ROBINSON, C., CONNELL, S., KIRKHAM, J., BROOKES, S. J., SHORE, R. C. & SMITH, A. M. 2004. The effect of fluoride on the developing tooth. *Caries Res*, 38, 268-76.
- ROBINSON, C., SHORE, R. C., BROOKES, S. J., STRAFFORD, S., WOOD, S. R. & KIRKHAM, J. 2000. The chemistry of enamel caries. *Critical Reviews in Oral Biology and Medicine*, 11, 481-495.
- ROBINSON, C. P. D., KIRKHAM, J. & SHORE, R. 1995. *Dental enamel: formation to destruction*, Boca Raton, CRC Press.
- ROLLA, G. 1988. On the role of calcium fluoride in the cariostatic mechanism of fluoride. *Acta Odontol Scand*, 46, 341-5.
- ROLLA, G. & SAXEGAARD, E. 1990. Critical evaluation of the composition and use of topical fluorides, with emphasis on the role of calcium fluoride in caries inhibition. *J Dent Res*, 69 Spec No, 780-5; discussion 820-3.
- ROSAS, S. G. P., TÉLLEZ, M. Á. A. & ESPINOZAI, E. V. 2014. In vitro efficiency of fluoride-containing compounds on remineralization of carious enamel lesions under cyclic pH conditions. *Revista Odontológica Mexicana*, 18, 96-104
- ROSENBLATT, A., STAMFORD, T. C. & NIEDERMAN, R. 2009. Silver diamine fluoride: a caries "silver-fluoride bullet". *J Dent Res*. United States.
- ROSIN-GRGET, K. & LINCIR, I. 2001. Current concept on the anticaries fluoride mechanism of the action. *Coll Antropol*, 25, 703-12.
- ROSIN-GRGET, K., PEROS, K., SUTEJ, I. & BASIC, K. 2013. The cariostatic mechanisms of fluoride. *Acta Med Acad*, 42, 179-88.
- RUIZ-PAYANA, A., ORTIZB, M. & DUARTE-GARDEAC, M. 2005. Determination of fluoride in drinking water and in urine of adolescents living in three counties in Northern Chihuahua Mexico using a fluoride ion selective electrode *Microchemical Journal*, 81, 19-22.
- RUNDLE, C. C. 2000. A beginners Guide to Ion-Selective electrode Measurements. Nico2000 Ltd, London, UK.
- RUSSELL, A. D. & HUGO, W. B. 1994. Antimicrobial activity and action of silver. *Prog Med Chem*, 31, 351-70.
- SAVAS, S., KUCUKYILMAZ, E., CELIK, E. U. & ATES, M. 2015. Effects of different antibacterial agents on enamel in a biofilm caries model. *J Oral Sci*, 57, 367-72.
- SCHAMSCHULA, R. G., SUGART, E., AGUS, H. M., UN, P. S. & TOTH, K. 1982. The fluoride content of human tooth enamel in relation to environmental exposure to fluoride. *Aust Dent J*, 27, 243-7.
- SCHWEITZER, J. 2014. *Scanning Electron Microscope* [Online].  
<https://www.purdue.edu/ehps/rem/rs/sem.htm>. [Accessed 8.4 2017].

- SDI. 2016a. *Riva Star SDS* [Online]. SDI Limited. [Accessed 4.4 2017].
- SDI 2016b. *Riva Star SDS*. Version No: 4.1.1.1 ed. Australia: SDI Limited.
- SELWITZ, R. H., ISMAIL, A. I. & PITTS, N. B. 2007. Dental caries. *Lancet*, 369, 51-9.
- SHAH, S., BHASKAR, V., VENKATARAGHAVAN, K., CHOUDHARY, P., GANESH, M. & TRIVEDI, K. 2013. Efficacy of silver diamine fluoride as an antibacterial as well as antiplaque agent compared to fluoride varnish and acidulated phosphate fluoride gel: an in vivo study. *Indian J Dent Res*, 24, 575-81.
- SHAH, S., BHASKAR, V., VENKATRAGHAVAN, K., CHOUDHARY, P., M., G. & TRIVEDI, K. 2014. Silver Diamine fluoride : A review and current applications. *Journal of advanced Oral Research*, 5.
- SHAH, S., KOSORIC, J., HECTOR, M. P. & ANDERSON, P. 2011. An in vitro scanning microradiography study of the reduction in hydroxyapatite demineralization rate by statherin-like peptides as a function of increasing N-terminal length. *Eur J Oral Sci*, 119 Suppl 1, 13-8.
- SHAW, L. & SMITH, A. J. 1999. Dental erosion--the problem and some practical solutions. *Br Dent J*, 186, 115-8.
- SHEIHAM, A. 2001. Dietary effects on dental diseases. *Public Health Nutr*, 4, 569-91.
- SHELLIS, R. P. & ADDY, M. 2014. The interactions between attrition, abrasion and erosion in tooth wear. *Monogr Oral Sci*, 25, 32-45.
- SHELLIS, R. P., BARBOUR, M. E., JONES, S. B. & ADDY, M. 2010. Effects of pH and acid concentration on erosive dissolution of enamel, dentine, and compressed hydroxyapatite. *Eur J Oral Sci*, 118, 475-82.
- SHELLIS, R. P., FEATHERSTONE, J. D. & LUSSI, A. 2014. Understanding the chemistry of dental erosion. *Monogr Oral Sci*, 25, 163-79.
- SHOOLERY, J. N. 1954. Nuclear magnetic resonance spectroscopy. *Analytical Chemistry*, 26, 1400-1403.
- SILVERSTONE, L. 1981. *Dental caries: aetiology, pathology and prevention*, Macmillan.
- SIMMER, J. P., PAPAGERAKIS, P., SMITH, C. E., FISHER, D. C., ROUNTREY, A. N., ZHENG, L. & HU, J. C. 2010. Regulation of dental enamel shape and hardness. *J Dent Res*, 89, 1024-38.
- SINGH, B., DUBEY, A. K., KUMAR, S., SAHA, N., BASU, B. & GUPTA, R. 2011. In vitro biocompatibility and antimicrobial activity of wet chemically prepared Ca<sub>10-x</sub>Ag<sub>x</sub>(PO<sub>4</sub>)<sub>6</sub>(OH)<sub>2</sub> (0.0≤x≤0.5) hydroxyapatites. *Materials Science and Engineering: C*, 31, 1320-1329.
- SINGH, S. & JINDAL, R. 2010. Evaluating the buffering capacity of various soft drinks, fruit juices and tea. *J Conserv Dent*, 13, 129-31.
- SKOOG, D. A., WEST, D. M. & HOLLER, F. J. 1996. *Fundamentals of analytical chemistry*, Fort Worth ; London, Saunders College.
- SOMASUNDARAM, P., VIMALA, N. & MANDKE, L. G. 2013. Protective potential of casein phosphopeptide amorphous calcium phosphate containing paste on enamel surfaces. *J Conserv Dent*, 16, 152-6.
- SRINIVASAN, K. & RECHNITZ, G. A. 1969. Selectivity studies on liquid membrane, ion-selective electrodes. 41(10), 1203-1208.
- STEBBINS, E. 1891. What value has argenti nitras as a therapeutic agent in dentistry ? *Int Dent J*, 12, 661-670.
- SUZUKI, T., NISHIDA, M., SOBUE, S. & MORIWAKI, Y. 1974. Effects of diammine silver fluoride on tooth enamel. *J Osaka Univ Dent Sch*, 14, 61-72.
- SWEPP, S. 2017. *Scanning Electron Microscopy (SEM)* [Online]. [http://serc.carleton.edu/research\\_education/geochemsheets/techniques/SEM.html](http://serc.carleton.edu/research_education/geochemsheets/techniques/SEM.html). [Accessed 8.4 2017].
- TAN, H. P., LO, E. C., DYSON, J. E., LUO, Y. & CORBET, E. F. 2010. A randomized trial on root caries prevention in elders. *J Dent Res*, 89, 1086-90.

- TARGINO, A. G., FLORES, M. A., DOS SANTOS JUNIOR, V. E., DE GODOY BENE BEZERRA, F., DE LUNA FREIRE, H., GALEMBECK, A. & ROSENBLATT, A. 2014. An innovative approach to treating dental decay in children. A new anti-caries agent. *J Mater Sci Mater Med*, 25, 2041-7.
- TEN CATE, J. M. 1997. Review on fluoride, with special emphasis on calcium fluoride mechanisms in caries prevention. *Eur J Oral Sci*, 105, 461-5.
- TEN CATE, J. M. 2013. Contemporary perspective on the use of fluoride products in caries prevention. *Br Dent J*, 214, 161-7.
- TEN CATE, J. M., BUIJS, M. J., MILLER, C. C. & EXTERKATE, R. A. 2008. Elevated fluoride products enhance remineralization of advanced enamel lesions. *J Dent Res*, 87, 943-7.
- TEN CATE, J. M. & FEATHERSTONE, J. D. 1991. Mechanistic aspects of the interactions between fluoride and dental enamel. *Crit Rev Oral Biol Med*, 2, 283-96.
- TEN CATE, J. M. & IMFELD, T. 1996. Dental erosion, summary. *Eur J Oral Sci*, 104, 241-4.
- TENUTA, L. M. & CURY, J. A. 2010. Fluoride: its role in dentistry. *Braz Oral Res*, 24 Suppl 1, 9-17.
- TEZEL, H., ATALAYIN, C., ERTURK, O. & KARASULU, E. 2011. Susceptibility of enamel treated with bleaching agents to mineral loss after cariogenic challenge. *Int J Dent*, 2011, 953835.
- THIBODEAU, E. A., HANDELMAN, S. L. & MARQUIS, R. E. 1978. Inhibition and killing of oral bacteria by silver ions generated with low intensity direct current. *J Dent Res*, 57, 922-6.
- TSAI, T. W. T. & CHAN, J. 2011. *Annual Reports on NMR Spectroscopy - Capter 1 Recent Progress in the Solid-State NMR Studies of Biomineralization*, Elsevier Ltd.
- TURP, J. C. & ALT, K. W. 1998. Anatomy and Morphology of Human Teeth. In: ALT, K. W., ROSING, F. W. & TESCHLER-NICOLA, M. (eds.) *Dental Anthropology*. Springer, Vienna.
- TWETMAN, S., AXELSSON, S., DAHLGREN, H., HOLM, A. K., KALLESTAL, C., LAGERLOF, F., LINGSTROM, P., MEJARE, I., NORDENRAM, G., NORLUND, A., PETERSSON, L. G. & SODER, B. 2003. Caries-preventive effect of fluoride toothpaste: a systematic review. *Acta Odontol Scand*, 61, 347-55.
- VERNON-PARRY, K. D. 2000. Scanning electron microscopy: an introduction. *III-Vs Review*, 13, 40-44.
- VILLA, A., ANABALON, M., ZOHOURI, V., MAGUIRE, A., FRANCO, A. M. & RUGG-GUNN, A. 2010. Relationships between fluoride intake, urinary fluoride excretion and fluoride retention in children and adults: An analysis of available data. *Caries research*, 44, 60-68.
- VOGEL, G. L. 2011. Oral fluoride reservoirs and the prevention of dental caries. *Monogr Oral Sci*, 22, 146-57.
- WANG, L., TANG, R., BONSTEIN, T., ORME, C. A., BUSH, P. J. & NANCOLLAS, G. H. 2005. A new model for nanoscale enamel dissolution. *J Phys Chem B*, 109, 999-1005.
- WANG, L. J., TANG, R., BONSTEIN, T., BUSH, P. & NANCOLLAS, G. H. 2006. Enamel demineralization in primary and permanent teeth. *J Dent Res*, 85, 359-63.
- WANG, P., LIN, H. C., CHEN, J. H. & LIANG, H. Y. 2010. The prevalence of dental erosion and associated risk factors in 12-13-year-old school children in Southern China. *BMC Public Health*, 10, 478.
- WEATHERELL, J. A. 1975. Composition of dental enamel. *British Medical Bulletin*, 31, 115 - 119.
- WEATHERELL, J. A., DEUTSCH, D., ROBINSON, C. & HALLSWORTH, A. S. 1977. Assimilation of fluoride by enamel throughout the life of the tooth. *Caries Res*, 11 Suppl 1, 85-115.
- WHITE, D. J., BOWMAN, W. D., FALLER, R. V., MOBLEY, M. J., WOLFGANG, R. A. & YESINOWSKI, J. P. 1988. <sup>19</sup>F MAS-NMR and solution chemical characterization of the reactions of fluoride with hydroxyapatite and powdered enamel. *Acta Odontol Scand*, 46, 375-89.



- WHITE, D. J. & NANCOLLAS, G. H. 1990. Physical and chemical considerations of the role of firmly and loosely bound fluoride in caries prevention. *J Dent Res*, 69 Spec No, 587-94; discussion 634-6.
- WHITE, D. J., NELSON, D. G. & FALLER, R. V. 1994. Mode of action of fluoride: application of new techniques and test methods to the examination of the mechanism of action of topical fluoride. *Adv Dent Res*, 8, 166-74.
- WHITE, I., MCINTYRE, J. & LOGAN, R. 2001. Studies on dental erosion: an in vitro model of root surface erosion. *Aust Dent J*, 46, 203-7.
- WILSON, K. & WALKER, J. M. 2000. *Principles and techniques of practical biochemistry*, New York, Cambridge University Press.
- WILSON, N. H. F. 2007. *Minimally invasive dentistry: the management of caries*, Chicago; London, Quintessence Pub.
- WORAWONGVASU, R. 2015. A Scanning Electron Microscopic Study of Enamel Surfaces of Incipient Caries. *Ultrastruct Pathol*, 39, 408-12.
- WROBLEWSKI, W. 2005. *Chemical Sensors Research Group* [Online]. <http://csrg.ch.pw.edu.pl/tutorials/ise/>. [Accessed 2016].
- WU, L. & YANG, F. 2002. Comparison of the effects of three fluoride-containing agents on the demineralization of deciduous teeth in vitro. 16, 216-218
- YAMAGA, R., NISHINO, M., YOSHIDA, S. & YOKOMIZO, I. 1972. Diammine silver fluoride and its clinical application. *J Osaka Univ Dent Sch*, 12, 1-20.
- YEE, R., HOLMGREN, C., MULDER, J., LAMA, D., WALKER, D. & VAN PALENSTEIN HELDERMAN, W. 2009. Efficacy of silver diamine fluoride for Arresting Caries Treatment. *J Dent Res*, 88, 644-7.
- YILMAZ, E. D., SCHNEIDER, G. A. & SWAIN, M. V. 2015. Influence of structural hierarchy on the fracture behaviour of tooth enamel. *Philos Trans A Math Phys Eng Sci*, 373.
- YIM, H. S., KIBBEY, C. E., MA, S. C., KLIZA, D. M., LIU, D., PARK, S. B., ESPADAS TORRE, C. & MEYERHOFF, M. E. 1993. Polymer membrane-based ion-, gas- and bio-selective potentiometric sensors. *Biosens Bioelectron*, 8, 1-38.
- ZEITCHEK & ANTHONY, M. 2013. *All solid-state-ion-selective electrodes for real-time measurement of relevant physiological phenomena*. M.S., Purdue University.
- ZHANG, W., MCGRATH, C., LO, E. C. & LI, J. Y. 2013. Silver diamine fluoride and education to prevent and arrest root caries among community-dwelling elders. *Caries Res*, 47, 284-90.
- ZHANG, Y. R., DU, W., ZHOU, X. D. & YU, H. Y. 2014. Review of research on the mechanical properties of the human tooth. *Int J Oral Sci*, 6, 61-9.
- ZHAO, I. S., GAO, S. S., HIRAISHI, N., BURROW, M. F., DUANGTHIP, D., MEI, M. L., LO, E. C. & CHU, C. H. 2017a. Mechanisms of silver diamine fluoride on arresting caries: a literature review. *Int Dent J*.
- ZHAO, I. S., MEI, M. L., LI, Q. L., LO, E. C. M. & CHU, C. H. 2017b. Arresting simulated dentine caries with adjunctive application of silver nitrate solution and sodium fluoride varnish: an in vitro study. *Int Dent J*, 67, 206-214.
- ZHI, Q. H., LO, E. C. & LIN, H. C. 2012. Randomized clinical trial on effectiveness of silver diamine fluoride and glass ionomer in arresting dentine caries in preschool children. *J Dent*, 40, 962-7.



# **PART VII: APPENDIXES**

## Appendix A: Tables of SDF studies

Clinical effects of SDF applications on coronal caries in primary and permanent teeth					
Studies (year/Sites)	Caries effect studied	Subjects/Dentitions	Durations	Groups compared (*application times)	Main findings
<b>McDonald and Sheiham (1994/UK)(McDonald and Sheiham, 1994)</b>	Arrest	52 children (2-9 years old)/primary	18 months	Gp 1: SnF <sub>2</sub> Gp 2: SDF/SnF <sub>2</sub> Gp 3: Minimal preparation + SDF/SnF <sub>2</sub> + composite resin Gp 4: Minimal preparation + composite resin Gp 5: no treatment	Caries in progress (%): Gp 1: 46.5 % Gp 2: 26.6 % Gp 3: 5.2 % Gp 4: 11.1 % Gp 5: 53.0 % Caries can be treated in a non-traumatic way.
<b>Gotjamanos T. (1996/Australia)(Gotjamanos, 1996)</b>	Arrest	55 carious primary teeth (from 6-13-year-olds)/primary	3-56 months	55 carious dentins treated with 50.9% SDF and GIC	SDF treatment for deep caries does not affect pulp vitality.
<b>Lo et al. (2001/China)(Lo et al., 2001)</b>	Arrest and prevention	375 children (3-5 years old)/primary	18 months	Gp 1: annual 38% SDF + carious tissue removal Gp 2: annual 38% SDF Gp 3: 3 monthly NaF (5%) + carious tissue removal Gp 4: 3-monthly NaF (5%) Gp 5: no treatment	Mean no. of new carious surfaces/arrest carious surfaces: Gp 1: 0.4/2.8 Gp 2: 0.4/3.0 Gp 3: 0.8/1.7 Gp 4: 0.6/1.5 Gp 5: 1.2/1.0 1. 38% SDF is more effective than 5% NaF in preventing and arresting caries. 2. Carious tissue removal is unnecessary for SDF treatment.
<b>Chu et al. (2002/China)(Chu et al., 2002)</b>	Arrest	375 children (3-5 years old)/primary	30 months	Gp 1: annual 38% SDF + carious tissue removal Gp 2: annual 38% SDF Gp 3: 3-monthly 5% NaF + carious tissue removal	Mean no. of arrest carious surfaces: Gp 1: 2.5 Gp 2: 2.8 Gp 3: 1.5 Gp 4: 1.5 Gp 5: 1.3 SDF is effective in caries arrest in primary teeth.

				Gp 4: 3-monthly NaF (5%) Gp 5: no treatment	
<b>Llodra et al. (2005/Cuba)(Llodra et al., 2005)</b>	Arrest and prevention	425 children( $\geq$ 6 years old)/primary and permanent 1 <sup>st</sup> molars	36 months	Gp 1: biannual 38% SDF Gp 2: no treatment (*3 min)	Mean no. of new carious surfaces (primary/permanent 1 <sup>st</sup> molars): Gp 1: 0.29/ 0.37 Gp 2: 1.43/1.06 SDF is effective for caries reduction in primary teeth and first permanent molars.
<b>Braga et al. (2009/Brazil)(Braga et al., 2009)</b>	Arrest	22 children/permanent 1 <sup>st</sup> molars	30 months	Gp 1: cross-tooth-brushing technique (CTT) Gp 2: 3 time weekly 10% SDF Gp 3: GIC sealant (*3 min)	All treatments are effective in control occlusal incipient caries.
<b>Yee et al. (2009/Nepal)(Yee et al., 2009)</b>	Arrest	976 children (3-9 years old)/primary	24 months	Gp 1: 38% SDF/tannic acid Gp 2: 38% SDF Gp 3: 12% SDF Gp 4: no treatment (*2 min)	Mean no. of arrest carious surfaces: Gp 1: 2.2 Gp 2: 2.1 Gp 3: 1.5 Gp 4: 1.0 38% SDF is more effective than 12% SDF in caries arrest.
<b>Zhi et al. (2012/China)(Zhi et al., 2012)</b>	Arrest	212 children(3-4 years old)/primary	24 months	Gp 1: annual 38% SDF Gp 2: biannual 38% SDF Gp 3: annual GIC	Caries arrest rates: Gp 1: 79% Gp 2: 91% Gp 3: 82% Increasing application frequency to biannual can enhance the caries arrest rate.
<b>Dos Santos et al. (2012/Brazil)(Dos Santos et al., 2012)</b>	Arrest	91 children/Primary	12 months	Gp 1: 30% SDF Gp 2: GIC (*3 min)	SDF was more effective than GIC (RR = 38.6%) for caries arrest.
<b>Liu et al. (2012/China)(Liu et al., 2012a)</b>	Prevention	501 children (mean age 9.1years)/permanent 1 <sup>st</sup> molars	24 months	Gp 1: Resin sealant Gp 2: biannual 5% NaF Gp 3: annual 38% SDF Gp 4: placebo control	Proportions of pit/fissure sites with dentin caries : Gp 1: 1.6% Gp 2: 2.4% Gp 3: 2.2% Gp 4: 4.6%

					All treatments are effective in preventing pit and fissure caries in permanent molars.
<b>Chu et al. (2014/ Hong Kong)(Chu et al., 2014)</b>	Arrest	A 14-year-old Chinese boy/permanent (rampant caries)		Patient with rampant caries was treated with 38% SDF, followed by provisional crown restoration.	Good prognosis with pain relief.
<b>Duangthip et al. (2016/Hong Kong)(Duangthip et al., 2016)</b>	Arrest	304 children (3-4 years old)/primary	18 months	Gp 1: annual 38% SDF Gp 2: 3 weekly 38% SDF Gp 3: 3 weekly 5% NaF (*10 sec)	Caries arrest rates Gp 1: 40% Gp 2: 35% Gp 3: 27% Annual or 3-weekly applications of 38% SDF is more effective in caries arrest than 3-weekly application of 5% NaF varnish.
<b>Fung et al. (2016/China)(Fung et al., 2016)</b>	Arrest	888 children (3-4 years old)/primary	18 months	Gp 1: annual 12% SDF Gp 2: biannual 12% SDF Gp 3: annual 38% SDF Gp 4: biannual 38% SDF	Caries arrest rates: Gp 1: 50% Gp 2: 55% Gp 3: 64% Gp 4: 74% SDF is more effective in caries arrest at 38% than 12% and when applied biannually rather than annually.
<b>Duangthip et al. (2017/Hong Kong)(Duangthip et al., 2017)</b>	Arrest	371 children (3-4 years old)/primary	30 months	Gp 1: annual 38% SDF Gp 2: 3 weekly 38% SDF Gp 3: 3 weekly 5% NaF (*10 sec)	Caries arrest rates Gp 1: 48% Gp 2: 33% Gp 3: 34% Annual application of 38% SDF is more effective than 3-weekly applications of SDF or NaF varnish.
<b>Fung et al. (2018/China)(Fung et al., 2018)</b>	Arrest	888 children (3-4 years old)/primary	30 months	Gp 1: annual 12% SDF Gp 2: biannual 12% SDF Gp 3: annual 38% SDF Gp 4: biannual 38% SDF	Caries arrest rates: Gp 1: 55.2%, Gp 2: 58.6%, Gp 3: 66.9%, Gp 4: 75.7% SDF is more effective in caries arrest at 38% than 12% and when applied biannually rather than annually. and
<b>Milgrom et al. (2018/USA)(Milgrom et al., 2018)</b>	Arrest	66 children (2~6years old)/primary	14 ~ 21 days	Gp 1: 38% SDF Gp 2: placebo	Averaged proportion of arrested caries lesions:

					Gp 1: 72% Gp 2: 5% *no harms were observed. Topical 38% silver diamine fluoride is effective and safe in arresting cavities in preschool children.
<b>Clinical effects of SDF applications on root caries</b>					
<b>Studies (year/Sites)</b>	<b>Caries effect studied</b>	<b>Subjects/Dentitions</b>	<b>Durations</b>	<b>Groups compared</b>	<b>Main findings</b>
<b>Tan et al. (2010/ Hong Kong)(Tan et al., 2010)</b>	Prevention	306 elders (mean age 78.8 ± 6.2 years)/permanent roots	3 years	Gp 1: oral hygiene instruction (OHI) Gp 2: OHI + 3-monthly chlorhexidine (CHX) Gp 3: OHI + 3-monthly NaF (5%) Gp 4: OHI + annual 38% SDF	New root caries surfaces: Gp 1: 2.5 Gp 2: 1.1 Gp 3: 0.9 Gp 4: 0.7 CHX, 5% NaF and 38% SDF were all more effective than OHI alone.
<b>Zhang et al. (2013/ Hong Kong)(Zhang et al., 2013)</b>	Arrest and prevention	277 elders (60-89 years old)/permanent roots	24 months	Gp 1: OHI Gp 2: OHI + annual 38% SDF Gp 3: OHI + annual 38% SDF + biannual oral health education (OHE)	New/arrested root caries surfaces: Gp 1: 1.33/0.04 Gp 2: 1.00/0.28 Gp 3: 0.70/0.33 Annual 38% SDF together with biannual OHE is effective in preventing and arrest caries.
<b>Li et al. (2016/ Hong Kong)(Li et al., 2016)</b>	Arrest	83 elders (mean age 72.2 ± 5.8 years) /permanent roots	30 months	Gp 1: no treatment Gp 2: 38% SDF Gp 3: 38% SDF/KI	Root caries arrest rates: Gp 1: 45% Gp 2: 90% Gp 3: 93% 1. 38% SDF application with or without KI application is effective in root caries arrest. 2. KI application does not reduce black staining of SDF in the long term.

<b>Cariostatic Effects of SDF on Dental Mineral.</b>		
<b>Studies (year)</b>	<b>Methodologies</b>	<b>Main findings</b>
<b>Chu et al. (2008)(Chu and Lo, 2008a)</b>	Carious primary teeth treated with either 38% SDF or 5% NaF were extracted to undergo Knoop hardness number (KHN) measurement.	The median KHN of arrested lesions (range, 20-46 or 196-451 MPa) were greater than those of soft lesions (range, 5-20, or 49-196 MPa) in the outer 25-200 µm.
<b>Lou et al. (2011)(Lou et al., 2011)</b>	Hydroxyapatite (HAP) powders mixed with 38% SDF, NaF or AgNO <sub>3</sub> were inspected with SEM, energy-dispersive X-ray analysis (EDX), and electron diffraction (ED).	Compounds formed on treated surfaces: SDF: CaF <sub>2</sub> and Ag(s) NaF: NaF globules AgNO <sub>3</sub> : Ag <sub>3</sub> PO <sub>4</sub> (turns black immediately)
<b>Liu et al. (2012)(Liu et al., 2012b)</b>	Sound premolars treated with AgF, KF, AgNO <sub>3</sub> or water, were subjected to demineralisation for 7 days before being inspected with micro-computed tomography (Micro-CT).	Topical applications of AgF and KF inhibited enamel demineralisation, while AgNO <sub>3</sub> application did not.
<b>Mei et al. (2013)(Mei et al., 2013d)</b>	Dentin caries generated by multi-species biofilms ( <i>Streptococcus mutans</i> , <i>Streptococcus sobrinus</i> , <i>Lactobacillus acidophilus</i> , <i>Lactobacillus rhamnosus</i> and <i>Actinomyces naeslundii</i> ) were treated with either 38% SDF or water, and were incubated in the artificial mouth for 21 days.	1. 38% SDF inhibits multi-species cariogenic biofilm formation on dentin carious lesions. 2. The hardness and percentages of calcium and phosphorus of SDF treated samples from the outermost 50µm were higher.
<b>Mei et al. (2014)(Mei et al., 2014b)</b>	Carious primary teeth treated with 38% SDF were inspected with Micro-CT, EDX, SEM, and transmission electron microscopy (TEM).	A highly remineralised zone rich in calcium and phosphate was found on the 38% SDF treated cavitated dentinal lesion.
<b>Punyanirun et al. (2018)(Punyanirun et al., 2018)</b>	Incipient caries on proximal surfaces of premolars were treated with 38% SDF before undergoing bacterial pH-cycling for 5 days. Micro-CT then was used for mineral density evaluation.	Compared to the use of 1000 ppm fluoride toothpaste alone, the adjunctive use of 38% SDF enhances the remineralization of initial carious lesions based on mineral density, depth, and remineralization percentage.
<b>Mei et al. (2017)(Mei et al., 2017)</b>	Calcium phosphate with different SDF concentrations (0.38, 1.52, 2.66, 3.80 mg/mL) were incubated at 37 °C for 24 h. The shape and organization of the crystals were examined by bright-field transmission electron microscopy and electron diffraction. Unit cell parameters of the obtained crystals were determined with powder X-ray diffraction. The vibrational and rotational modes of phosphate groups were analysed with Raman microscopy.	The results suggested that SDF reacted with calcium and phosphate ions and produced fluorohydroxyapatite (FAH).

Cariostatic effects of SDF on cariogenic bacteria		
Studies (year)	Methodologies	Main findings
<b>Knight et al. (2005)(Knight et al., 2005)</b>	Demineralized dentine discs treated with 50.9% SDF, 50.9% SDF/KI and KI were incubated in medium of <i>S. mutans</i> for 14 days. Afterwards, optical density of the medium chambers was measured to determine bacterial penetration and growth.	<i>S. mutans</i> migrated through all dentine discs. However, the samples treated with 50.9% SDF and SDF/KI had significantly lower optical densities.
<b>Knight et al. (2007)(Knight et al., 2007)</b>	Dentin discs with or without demineralisation, were treated with 50.9% SDF/KI. Next, were incubated with <i>S. mutans</i> for 14 days. Electron probe microanalysis (EPMA) and SEM were then used to inspect the samples. Bacterial growth was monitored by taking optical density readings.	SDF/KI can inhibit biofilm formation composed of <i>S. mutans</i> .
<b>Knight et al. (2009)(Knight et al., 2009)</b>	Demineralized dentin disks treated with either 50.9% SDF or 50.9% SDF/KI were incubated in <i>S. mutans</i> before being inspected by scanning microscopy (SEM) and electron probe microanalysis (EPMA).	The inhibition of <i>S. mutans</i> might be due to the presence of silver and fluoride in the outer layer (up to 450 µm) of SDF and SDF/KI treated samples, which make it more resistant to demineralisation.
<b>de Almeida et al. (2011)(de Almeida Lde et al., 2011)</b>	Antibacterial effects of different concentrations of SDF were studied using an agar diffusion method.	Both 12% and 30% can inhibit <i>S. mutans</i> .
<b>Chu et al. (2012)(Chu et al., 2012)</b>	Demineralized dentine blocks were incubated with either <i>S. mutans</i> or <i>A. naeslundii</i> to be treated with 38% SDF. Lesions were then assessed by microhardness testing (MHT), EDX and Fourier transform infrared spectroscopy (FTIR).	1. 38% SDF possesses anti-microbial activity against cariogenic biofilm of <i>S. mutans</i> or <i>A. naeslundii</i> , which inhibit the demineralisation. 2. The hardness and percentages of calcium and phosphorus of SDF treated samples.
<b>Mei et al. (2013)(Mei et al., 2013b)</b>	Carious lesions were created in dentine blocks by inoculating with dual-species biofilm ( <i>S. mutans</i> and <i>Lactobacillus acidophilus</i> ). They were then treated with either 38% SDF or water before being incubated at 37°C for 7 days. The biofilms were evaluated by colony forming units (CFU), SEM, and confocal microscopy (CLSM), while the carious lesion was inspected with XRD, Fourier transform infrared spectroscopy (FTIR) and immune-labeling.	38% SDF had antimicrobial activity against the cariogenic biofilms composed of <i>S. mutans</i> and <i>Lactobacillus acidophilus</i> .
<b>Shah et al. (2013)(Shah et al., 2013)</b>	<i>S. mutans</i> counts in the mouths of children treated with 38% SDF, fluoride varnish or APF gel. All subjects were evaluated at 72 h, 6 <sup>th</sup> , 12 <sup>th</sup> , and 18 <sup>th</sup> months of follow-up.	38% SDF is more effective in inhibiting <i>S. mutans</i> than fluoride varnish and APF gel <i>in vivo</i> .
<b>Targino et al. (2014)(Targino et al., 2014)</b>	Evaluate the antimicrobial and cytotoxic activity of 38% SDF. The minimum inhibition concentration (MIC) was evaluated by the spectrophotometric	The MIC and MBC for SDF were 33.33 ± 14.43 and 50.0 µg/mL, respectively.

	microdilution method and turbidity. The minimum bactericide concentration (MBC) was evaluated in brain heart infusion plates.	
<b>Hamama et al. (2015)(Hamama et al., 2015)</b>	Dentine discs infected with <i>S. mutans</i> were treated with 50.9% SDF/KI. The discs were then fractured into two halves, stained with fluorescent LIVE/DEAD stain and observed using confocal laser scanning microscopy.	The use of the SDF/KI is effective in reducing the numbers of <i>S. mutans</i> in dentinal tubules.
<b>Savas et al. (2015)(Savas et al., 2015)</b>	<i>S. mutans</i> biofilm demineralized enamels were treated with water, 38% SDF, acidulated phosphate fluoride (APF), ammonium hexafluorosilicate (AHF), ammonium hexafluorosilicate + cetylpyridinium chloride (AHF+CPC), or 0.2% chlorhexidine (CHX) before being incubated for two days. Numbers of viable microorganisms in the biofilms were counted.	38% SDF showed the highest antibacterial activity over other treatments.
<b>Cariostatic effects of SDF on dentinal organic content</b>		
<b>Studies (year)</b>	<b>Methodologies</b>	<b>Main findings</b>
<b>Mei et al. (2012)(Mei et al., 2012)</b>	The inhibitory effects of 12%, 30%, 38% SDF, NaF and AgNO <sub>3</sub> on matrix metalloproteinases (MMPs) were studied using MMP assay kits.	Inhibitory effect of SDF on MMPs increased with concentration. SDF had more inhibition on MMPs than solutions of NaF and AgNO <sub>3</sub> .
<b>Mei et al. (2013)(Mei et al., 2013c)</b>	Demineralized dentin blocks were treated with 38% SDF, 10% NaF, 42% AgNO <sub>3</sub> , and water. They were then subjected to pH cycling for 8 days before being inspected with SEM, X-ray diffraction (XRD), Micro-CT and spectrophotometry with a hydroxyproline assay.	1. Groups treated with 38% SDF and 42 % AgNO <sub>3</sub> had significantly less hydroxyproline liberated from the dentine matrix than groups F and W (p<0.01). 2. 38% SDF can inhibit demineralisation and preserved collagen from degradation.
<b>Mei et al. (2014)(Mei et al., 2014a)</b>	The inhibitory effects of 12%, 30%, 38% SDF, NaF and AgNO <sub>3</sub> on cathepsins were studied using cathepsin assay kits.	1. The solutions containing Ag <sup>+</sup> have significantly higher inhibitory effect than the solutions containing F <sup>-</sup> only (p<0.01). 2. SDF solution at all 3 tested concentrations significantly inhibited the activity of cathepsin.
<b>Zhao et al. (2017)(Zhao et al., 2017b)</b>	Dentine discs treated with 25% AgNO <sub>3</sub> followed by 5% NaF, 38% SDF or water were subjected to pH-cycling for 8 days before being inspected with SEM, X-ray diffraction (XRD), X-ray microtomography and spectrophotometry with a hydroxyproline assay.	25% AgNO <sub>3</sub> followed by 5% NaF or 38% SDF application can preserve dentinal collagen, and result in lower lesion depths.



## Appendix B: QMUL Skills Points Record

Type	A	B	C	D	Total
Conference Attendance (Five days)	15	10	0	0	25
Conference Attendance (Four days)	24	16	0	0	40
Conference Attendance (One day)	3	2	0	0	5
Conference Attendance (Three days)	18	12	0	0	30
Conference Attendance (Two days)	6	4	0	0	10
Conference attendance sub-total	18	12	0	0	30
Basic IT/Software course	1	0	0	0	1
Doctoral College event/course	0	2	3	2	7
E-Learning Course	0	0	0	2	2
Other CPD course	0	1	0	0	1
Other Teaching/demonstrating training	0	2.5	0	2.5	5
Other course/event attendance	4	0	0.5	0	4.5
Researcher Development Course	12	40.5	12	21.5	86
Course/event attendance sub-total	17	46	15.5	28	106.5
Conference Presentation (Oral)	9	9	0	12	30
Conference Presentation (Poster)	9	9	0	12	30
Internal Presentation (< or =30 mins)	2	2	0	4	8
Journal Club/Reading Group/lab meeting Presentation	3	0	0	3	6
Giving presentations sub-total	23	20	0	31	74
Journal Club/Reading Group/lab meeting/mentoring group - attendance	16.5	0	0	0	16.5
Meeting/club/reading group attendance sub-total	16.5	0	0	0	16.5
Seminar attendance (series)	2	0	0	0	2
Seminar attendance (single)	3	0	1	0	4
Seminar attendance sub-total	5	0	1	0	6
Mentoring/supervising of Project Student	8	4	0	8	20
Teaching/demonstrating/marking/preparation	0	15	0	15	30
Teaching sub-total	8	19	0	23	50
Refereed Publication (Journal Paper, Book chapter, not abstract) acceptance	2	0	0	8	10
Refereed Publication (Journal Paper, Book chapter, not abstract) submission	4	0	0	16	20
Written publications sub-total	6	0	0	24	30
<b>Total (with caps applied)</b>	<b>93.5</b>	<b>97</b>	<b>16.5</b>	<b>106</b>	<b>313</b>
<b>Target</b>	<b>60</b>	<b>20</b>	<b>15</b>	<b>30</b>	<b>210</b>

**Appendix C: Awards**

1. Third place of 2016 London Region Young Persons Lecture Competition



2. 2017 IADR Cariology Research Group Science Award



3. 2018 Armourers & Brasiers Travel Grant



4. 2018 BSODR Student Bursary



INTERNATIONAL ASSOCIATION FOR DENTAL RESEARCH



**Cariology Research Group Science Award**

PRESENTED TO THE GROUP OF

**Wei-Te Huang**

IADR 95<sup>th</sup>  
General Session

San Francisco, USA  
March 23, 2017

## Appendix D: Conference presentations

2016 IADR in Seoul, Korea (poster presentation #1053):

W. Huang\*, T. Duminis, D. G. Gillam, P. Anderson, S. Shahid "Cariostatic Influence of Commercial SDF on Hydroxyapatite Disc Demineralisation Kinetics"





**#1053**

### Cariostatic Influence of Commercial SDF on Hydroxyapatite Disc Demineralisation Kinetics

W. HUANG\*, T. Duminis, D. G. Gillam, P. Anderson, S. Shahid

### Objectives

To analyse and understand the cariostatic effect of silver diammine fluoride (SDF) and the synergistic role of Ag<sup>+</sup> and F<sup>-</sup> ions on the demineralisation kinetics of hydroxyapatite (HAP).

### Methods



Disc in pH4 acid (4hrs) > Treated with cariostatic agents > Return to same acid (4hrs)

Fig 1 – Procedures of the Exp.

No.	Contents of cariostatic agents
1	Riva Star(SDF + KI, 0.06g/mL F)
2	NaF(60000ppm F)
3	AgNO <sub>3</sub> (341280ppm Ag <sup>+</sup> )
4	AgNO <sub>3</sub> (341280ppm Ag <sup>+</sup> ) & KI(saturated)
5	KI(saturated)
6	AgNO <sub>3</sub> (341280ppm Ag <sup>+</sup> ) & NaF(60000ppm F)
7	AgNO <sub>3</sub> (341280ppm Ag <sup>+</sup> ) & NaF(60000ppm F) & KI

Table 1 – Contents of the application agents

HAP discs were put into pH4.0 acetic acid for 4hrs demineralisation and then removed to be treated by cariostatic agents (Table 1). The discs were subsequently immersed in the acid for further 4hrs demineralisation (Fig 1).

Throughout the 8hrs experiment, concentrations of Ca<sup>2+</sup> and Ag<sup>+</sup> were continuously monitored by ISE. The rate of Ca<sup>2+</sup> release with time was used as a proxy for the rate of demineralisation. Similarly treated HAP powder samples were analysed using <sup>31</sup>P and <sup>19</sup>F MAS-NMR.

### Results

Riva Star exerted 100% demineralisation inhibition (Fig 2) due to the formation of CaF<sub>2</sub> and Ag<sub>3</sub>PO<sub>4</sub> as detected by NMR (Fig 3&4). Furthermore no black staining was observed [1].

Discs treated with AgNO<sub>3</sub> showed an initial increase in Ca<sup>2+</sup> release followed by a reduction (Fig 5a) due to the formation of Ag<sub>3</sub>PO<sub>4</sub> as detected by <sup>31</sup>P NMR (Fig 3). This treatment produced black staining.

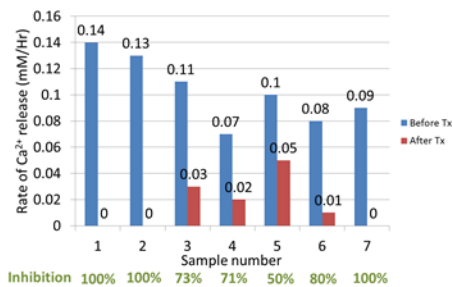


Fig 2 – Rates of [Ca<sup>2+</sup>] release before and after the cariostatic agents Tx (Table 1).

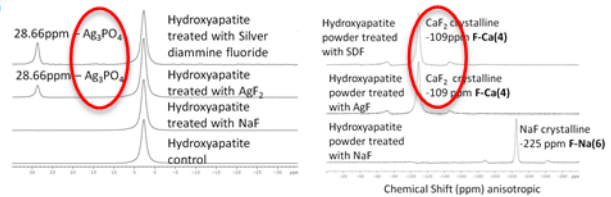


Fig 3 – <sup>31</sup>P MAS – NMR.

Fig 4 – <sup>19</sup>F MAS – NMR.

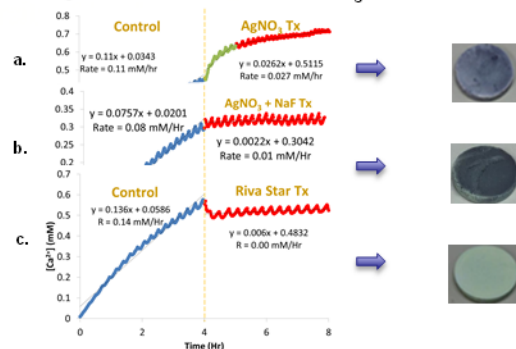


Fig 5 – ISE data of [Ca<sup>2+</sup>] variation. a. AgNO<sub>3</sub> group. b. AgNO<sub>3</sub>+NaF group. c. Riva Star group.

### Conclusions

The components of Riva Star work synergistically to inhibit the demineralisation process of the HAP discs. This may be due to the formation of insoluble Ag<sub>3</sub>PO<sub>4</sub> and CaF<sub>2</sub> as detected by NMR. The addition of KI as reducing agent also eliminates the black staining caused by the silver ion product application.

**Acknowledgement:** Thank SDI.Ltd for providing the samples and partially supporting my IADR.

### References

1. Yamaga, R., Nishino, M., Yoshida, S. & Yokomizo, I. 1972. Diammine silver fluoride and its clinical application. J Osaka Univ Dent Sch, 12, 1-20

wei-te.huang@qmul.ac.uk

2016 ORCA in Athens, Greece (poster and oral presentation #88):

W. Huang\*, T. Duminis, P. Anderson, S. Shahid "ISE Study of Effect of Silver Ions on Demineralisation of Hydroxyapatite Disc" (DOI: 10.1159/000445087)

### **Abstract**

Silver has traditionally been used in dentistry as a bactericide. However, recently it has been suggested that  $\text{Ag}^+$  influences enamel demineralisation directly. The aim was to understand the chemical interactions of  $\text{Ag}^+$  with enamel's mineral components during demineralisation using hydroxyapatite (HAP) discs as isotropic enamel analogues. Three HAP discs (PlasmaBiotol, UK; 20% porosity), 14 mm (D) X 2 mm (H) were demineralised for 4 h in 50 ml, 1.0 M buffered pH 4.0 acetic acid, 37 °C. The discs were then removed and treated with either 3.16 M  $\text{AgNO}_3$  solution; saturated KI solution; or 3.16 M  $\text{AgNO}_3$ + saturated KI solution. The discs were then further demineralised for 4 h. ISEs (Ion Selective Electrodes) were used to monitor the rate of demineralisation by measuring  $\text{Ca}^{2+}$  concentration increases in the solutions at 1 min intervals. The changes in  $\text{Ag}^+$  concentrations were also monitored contemporaneously. Similarly treated HAP powder samples were analysed using  $^{31}\text{P}$  MAS-NMR (Magic-angle spinning Nuclear Magnetic Resonance) to detect formation of phosphate salts. The rate of  $\text{Ca}^{2+}$  release before and after treatments were:

$\text{AgNO}_3$ : Initial increase in  $\text{Ca}^{2+}$  release rate from 0.11 mM/h to 0.17 mM/h for 1 h, reducing to 0.0266 mM/h thereafter. Overall decrease 24 %. Staining observed.

KI: Decrease in  $\text{Ca}^{2+}$  release rate from 0.095 mM/h to 0.045 mM/h. Overall decrease 47 %. No staining observed.

$\text{AgNO}_3$ +KI: Decreased in  $\text{Ca}^{2+}$  release rate from 0.072 mM/h to 0.0175 mM/h. Overall decrease 24 %. No staining observed.

$^{31}\text{P}$  MAS-NMR indicated formation of  $\text{Ag}_3\text{PO}_4$  for samples treated with  $\text{AgNO}_3$ , but not for KI treated nor  $\text{AgNO}_3$ +KI treated samples. Topical application of  $\text{AgNO}_3$  reduces demineralisation of HAP by forming a  $\text{Ag}_3\text{PO}_4$  protective barrier, but stains the surface. Addition of KI prevents formation of  $\text{Ag}_3\text{PO}_4$ , and also staining. However, KI does not detriment protection, possibly due to formation of an AgI protective barrier.



# ISE study of effect of silver ions on demineralisation of hydroxyapatite disc

W. Huang\*, T. Duminis, P. Anderson, S. Shahid

### Aim

- Silver has traditionally been used in dentistry as a bactericide.
- It has been suggested that Ag<sup>+</sup> also influences enamel demineralisation more directly.
- The aim was to understand the chemical interactions of Ag<sup>+</sup> with enamel's mineral components during demineralisation using compressed hydroxyapatite (HAP) discs as isotropic enamel analogues.

### Experimental approach

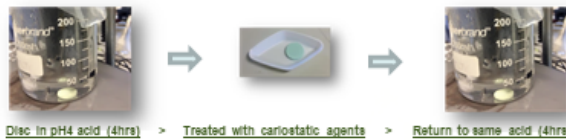


Fig 1 – Procedures of Exp.

Contents of cariostatic agents
AgNO <sub>3</sub> (341280 ppm Ag <sup>+</sup> )
KI (saturated)
AgNO <sub>3</sub> (341280 ppm Ag <sup>+</sup> ) & KI (saturated)

Table 1 – Contents of the application agents

- ISEs (Ion Selective Electrodes) were used to monitor demineralisation.
- Similarly treated HAP powder samples were analysed using <sup>31</sup>P MAS-NMR (Magic-angle spinning – Nuclear Magnetic Resonance) to detect formation of phosphate salts.

### Results

Fig.2 shows ISE profiles of Ca<sup>2+</sup> release before and after treatments:

**AgNO<sub>3</sub>:** Initial increase in Ca<sup>2+</sup> release for 1h after Tx, but reduced thereafter. Staining observed.

**KI:** Decrease in Ca<sup>2+</sup> release rate. No staining observed.

**AgNO<sub>3</sub>+KI:** Decrease in Ca<sup>2+</sup> release rate. No staining observed.

Fig.3 shows overall decrease in Ca<sup>2+</sup> release rate.

Fig.4 shows formation of Ag<sub>3</sub>PO<sub>4</sub> in AgNO<sub>3</sub> treated HAP powder.

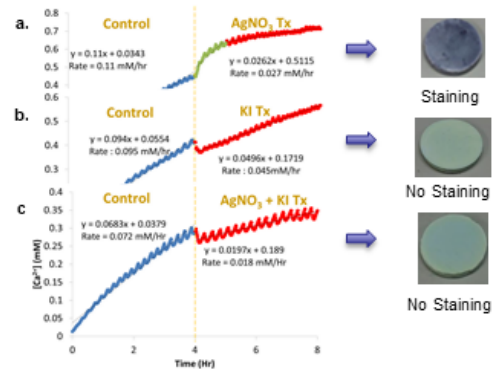


Fig 2 – ISE data of [Ca<sup>2+</sup>] variation.

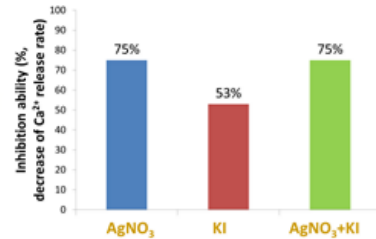


Fig 3 – Inhibition abilities of cariostatic agents by rates of Ca<sup>2+</sup> release.



Fig 4 – <sup>31</sup>P MAS – NMR. Showing Ag<sub>3</sub>PO<sub>4</sub> HAP in sample treated with AgNO<sub>3</sub> however, but not in AgNO<sub>3</sub> + KI sample.

### Conclusions

The topical application of AgNO<sub>3</sub> reduces demineralisation of HAP by the formation of a Ag<sub>3</sub>PO<sub>4</sub> protective barrier, but stains the surface following reduction to metallic silver. Addition of KI prevents formation of Ag<sub>3</sub>PO<sub>4</sub>, avoiding the staining, but does not detriment the protection, possibly due to the formation a AgI protective barrier, which is white and does not decompose.

### References

1. Yamaga, R., Nishino, M., Yoshida, S. & Yokomizo, I. 1972. Diammine silver fluoride and its clinical application. J Osaka Univ Dent Sch, 12, 1-20

wei-te.huang@qmul.ac.uk



2017 IADR in San Francisco, USA (oral presentation #0066):

W. Huang\*, T. Duminis, P. Anderson, S. Shahid "Cariostatic Effects of Commercial Silver Diammine Fluoride Components on Enamel"

### **Abstract**

**Objectives:** Silver Diammine Fluoride (SDF) has been used to manage dental caries for decades. Commercial SDF products contain silver and fluoride ions at high concentrations. However the mechanism behind its positive clinical outcome has not been clearly verified. The aim of this study was to investigate the cariostatic effects of the topical application of silver and fluoride ions individually, and in combination, on the demineralisation of human enamel.

**Methods:** Human permanent molars were sectioned to provide 8 caries-free smooth surfaces. These were polished and then 5mm X 5mm windows were created using nail varnish. The samples were demineralised for 4 h in 50 mL 0.1 M buffered acetic acid pH 4.0 at 37 °C. Ion selective electrodes (ISEs) were used to monitor Ca<sup>2+</sup> concentration changes in real-time throughout the experiment as a proxy for demineralisation. After 4h, the samples were removed and topically treated with the cariostatic agents shown in **Table 1** using a microbrush. The samples were then placed back into demineralisation solutions and Ca<sup>2+</sup> release was recorded for a further 4 h period. Furthermore, <sup>31</sup>P and <sup>19</sup>F MAS-NMR was used to assess the interaction of fluoride ions and silver ions with the apatite phase.

**Results:** The decrease in Ca<sup>2+</sup> release following topical application of cariostatic agents is shown in **Table 2**. The fluoride ions had the greatest efficacy in reducing demineralisation, whereas silver ions had the least effect. <sup>31</sup>P NMR results showed that silver reacts with apatite to form Ag<sub>3</sub>PO<sub>4</sub>. This was observed following application of SDF, AgF and AgNO<sub>3</sub> but not NaF. <sup>19</sup>F data showed formation of CaF<sub>2</sub> in samples treated with SDF, NaF and AgF.

**Conclusions:** SDF application inhibits the demineralisation process of enamel, which might be attributed to the establishment of a barrier consisting of Ag<sub>3</sub>PO<sub>4</sub> and CaF<sub>2</sub> on the surface. The fluoride ions play the major role of the cariostatic function.

<b>Table 1. – Four groups of cariostatic agents</b>		
<b>Cariostatic agents</b>	<b>Concentration</b>	<b>Sample size</b>
<b>SDF</b>	50.9 wt% (341280 ppm Ag, 60000 ppm F)	2
<b>AgF</b>	40.1 wt% (341280 ppm Ag, 60000 ppm F)	2
<b>NaF</b>	13.3 wt% (60000 ppm F)	2
<b>AgNO<sub>3</sub></b>	53.7 wt% (341280 ppm Ag)	2

<b>Table 2. – Inhibition ability based on calcium ion release</b>	
<b>Group names</b>	<b>Inhibition efficacy (% decrease in Ca<sup>2+</sup> release)</b>
<b>SDF</b>	45.3±4.6 %
<b>AgF</b>	52.8±5.2 %
<b>NaF</b>	55.6±3.3 %
<b>AgNO<sub>3</sub></b>	11.9±3.7 %



2017 BSODR in Plymouth, UK (poster presentation #83):

W. Huang\*, P. Anderson, S. Shahid "Cariostatic Effect of Riva Star vs Conventional Silver Diammine Fluoride"





**#83**

## Cariostatic Effect of Riva Star vs Conventional Silver Diammine Fluoride

W. Huang\*, P. Anderson, S. Shahid

### Introduction

SDF has been used in dentistry since 1970s, and numerous studies have proven its abilities in arresting dental caries<sup>1</sup>. However, the blackening of the treated teeth is a severe disadvantage, which refrains its application.

In contrast to conventional silver diammine fluoride (SDF), Riva Star (SDI, Australia) contains saturated potassium iodide solution (SSKI) to prevent black staining due to photo-reduction of silver<sup>2</sup>.



Fig 1. – Riva Star (SDI, Ltd). Silver capsule = SDF; Green capsule = SSKI.

### Aims and Objectives

This study compared the effects of applications of SSKI following SDF applications on demineralisation of human enamel, dentine and cementum.

### Methods

A human permanent molar was sectioned to provide enamel, dentine and cementum samples (n = 2), which were allocated into SDF Tx (3.16 M SDF) and Riva Star Tx groups (SDF + SSKI). Each sample was coated with nail varnish, leaving 3 mm X 4 mm window exposed. Protocol of each group was same as follows. Firstly, sample was immersed into 50 mL, pH 4.0, 0.1 M buffered acetic acid at 37 °C for 4 h demineralisation. Next, sample was taken out to be topically treated with SDF Tx or Riva Star Tx using a micro-brush. Thereafter, treated sample was put back into pH 4.0 solution for further 4 h demineralisation. Throughout 8 h demineralisation, Ca<sup>2+</sup> ion selective electrodes (ISE) was used to monitor changes of ion concentrations at 1 min intervals. Cariostatic effects of treatments were based on decrease of Ca<sup>2+</sup> releases before and after Tx.

### Results

The percentages of reduction in the rates of mineral loss (PRML) of treatments were shown in Fig 3. Relative to conventional SDF, Riva Star Tx showed enhanced cariostatic effect on enamel and cementum, but not dentine. Furthermore, there was less staining of samples treated with Riva Star as compared to conventional SDF.

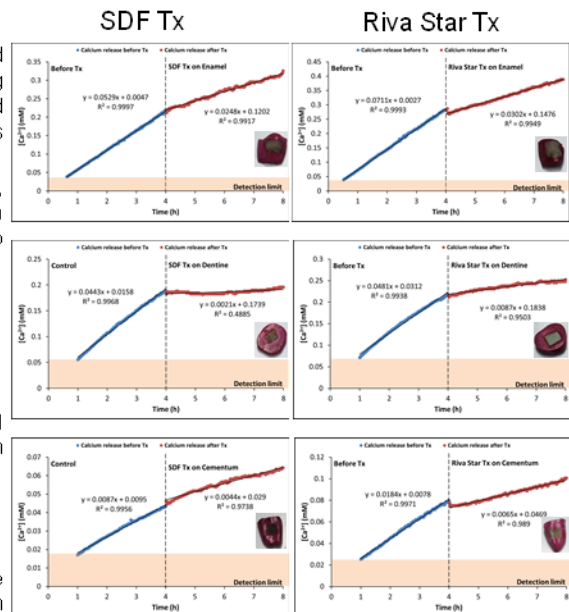


Fig 2. – Typical plots of calcium ion release before and after treatment of Riva Star on human enamel, dentine and cementum.

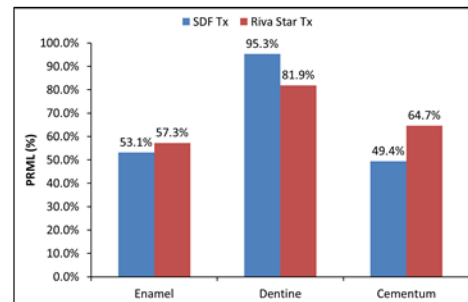


Fig 3. – PRML of SDF & Riva Star on different human dental tissues.

### Conclusion

SDF treatments (with and without SSKI) have significant cariostatic properties. Addition of SSKI application enhances the cariostatic effects on enamel and cementum, but not dentine. SSKI application eliminates black staining to some extent.

1. YAMAGA, R., NISHINO, M., YOSHIDA, S. & YOKOMIZO, I. 1972. Diammine silver fluoride and its clinical application. *J Osaka Univ Dent Sci*, 12, 1-30.  
 2. MURPHY, G. M., MONTI-RE, J. M., CRAG, G. G., MALYANI, Z.I.M, P. S. & GULLY, N. J. 2007. Differences between normal and demineralised dentine pretreated with silver fluoride and potassium iodide after an in vitro challenge by *Streptococcus mutans*. *Aust Dent J*, 52, 18-21.

2018 IADR in London, USA (oral presentation #0454):

W. Huang\*, P. Anderson, S. Shahid "Dose-dependent Inhibitory Effects of Silver Compounds on Enamel Demineralisation"

### **Abstract**

**Objectives:** To investigate the effects of different concentrations of AgNO<sub>3</sub>, AgF and Ag[NH<sub>3</sub>]<sub>2</sub>F (silver diamine fluoride, SDF) on enamel demineralisation.

**Methods:** Fifty-four enamel samples were sectioned from caries-free permanent molars and polished using 600 grit sandpapers. Thereafter, samples were nail varnished, leaving a 3 mm X 4 mm window exposed. The samples were then allocated into nine groups (n = 6). These groups were treated with 3.16 M SDF, 3.16 M AgF, 3.16 M AgNO<sub>3</sub>, 2.36 M SDF, 2.36 M AgF, 2.36 M AgNO<sub>3</sub>, 0.7453 M SDF, 0.7453 M AgF and 0.7453 M AgNO<sub>3</sub>, respectively. Initially all samples were individually demineralised by immersing into 50 mL, buffered pH 4.0 acetic acids for 4 h at 37 °C. Next, the samples were topically treated with their assigned application agents with micro-brush for 1 min and then return to the acids for further 4 h demineralisation. Calcium ion selective electrodes (ISEs) were used to monitor the ion concentrations at 1-min intervals during the demineralisation. The percentage reduction in the rate of calcium loss of enamel (PRCL<sub>enamel</sub>) was calculated, based on the change of Ca<sup>2+</sup> release rate. Afterwards, enamel from each group was powdered and scanned with <sup>19</sup>F and <sup>31</sup>P magic angle spinning-nuclear magnetic resonance (MAS-NMR).

**Results:** The mean PRCL<sub>enamel</sub> of all groups is shown in **Table 1**. The PRCL<sub>enamel</sub> increased with concentration in the groups treated with SDF and AgF, while decreased in the groups treated with AgNO<sub>3</sub>. In the spectrums of MASNMR, CaF<sub>2</sub> and fluorapatite (FAP) were detected in the groups treated with SDF and AgF. Also, formation of CaF<sub>2</sub> was predominant over FAP for every group except that treated with 0.7453 M SDF, for which FAP was predominant.

**Conclusions:** Silver compounds have dose-dependent inhibitory effects on enamel demineralisation. The inhibitory mechanisms of SDF and AgF are associated with the formations of CaF<sub>2</sub> and FAP.

<b>Table 1. – PRCL<sub>enamel</sub> of the silver compounds in different concentrations</b>			
<b>Silver compound concentrations (M)</b>	3.16	2.36	0.7453
<b>SDF</b>	65.2+3.3 %	60.9±4.5 %	41.6±2.2 %
<b>AgF</b>	65.6±6.2 %	61.0±5.5 %	61.7±3.7 %
<b>AgNO<sub>3</sub></b>	0.0±5.3 %	4.5±5.9 %	21.9±3.2 %

**Appendix E: Published paper and papers in preparation**

“Validation of a Real-Time ISE Methodology to Quantify the Influence of Inhibitors of Demineralisation Kinetics in vitro Using a Hydroxyapatite Model System”: Caries Res. 2018 May 25;52(6):598-603.

Papers in preparation:

“Inhibitory mechanisms of Silver Compounds on Hydroxyapatite Demineralisation”: Aimed to submit to JDR. (Drafting)

“Dose-dependent Inhibitory Effects of Silver Compounds on Enamel Demineralisation”: Aimed to submit to JDR. (Drafting)